The University of Birmingham

TRACKSIDE MEASUREMENT OF CRITICAL ZONES IN RAILWAY TRACKS

By

Hongsin Kim

A thesis submitted to the
University of Birmingham
for the degree of
DOCTOR OF PHILOSOPHY

The Birmingham Centre for Railway Research and Education
School of Electronic, Electrical and Systems Engineering
College of Engineering and Physical Sciences
The University of Birmingham
May 2016

Abstract

Classic railway track can be viewed as an elastic system that consists of rails, supported by sleepers on ballast that rests on the subgrade. In this case, the track stiffness is a function of the ballast depth and the nature of the subgrade or foundation. Abrupt changes in track stiffness can occur where the ballasted track transitions from soft foundations onto bridges and viaducts, onto hard foundations and into tunnels, or at the interface between ballasted track and slab track. Stiffness changes can also be found at the transitions from plain line into switch and crossing areas. Such interfaces between areas of different track stiffness are defined as critical zones and can cause passenger discomfort, unpredictable track degradation and, potentially, track support failures. Given their nature, maintaining critical zones is more expensive than maintaining plain line track and measuring and assessing the variations in track stiffness are critical activities in track maintenance and in ascertaining the quality of newly designed and built railways.

Existing methods of track stiffness measurement are not sufficiently accurate and dependable and, in addition, they require track access and productivity is low. Therefore, the aim of this research was to develop an innovative but rapid method of assessing track stiffness, so as to identify problems in transition zones. During her doctoral research, the author designed and built a sleeper deflection measurement system as a means of quickly assessing track stiffness. The laser-based digital system developed uses position sensitive detectors (PSDs) and a line laser. It can monitor up to 18 consecutive sleepers.

The performance of the new measurement system was verified in the laboratory by comparing it with the output from a geophone and from a commercial laser based optical displacement sensor. A good agreement was found between the geophone and the laser-based measurement system, with a resolution of around 10 μm and an accuracy of better than 0.1 mm. Field trials were conducted on a private railway at Long Marston, which showed that the system was able to capture the displacement data of individual sleepers and thus the continuous movement of rails supported by 18 sleepers.

Dynamic Cone Penetrometer (DCP) testing was also conducted to investigate the subgrade characteristics of the test track at Long Marston and to obtain the value of subgrade stiffness Ks (N/mm^3). By applying the DCP test result and real displacement data to the Beam on Elastic Foundation (BOEF), the relationship between the stiffness and subgrade condition was established both quantitatively and qualitatively. As shown in Section6.6, the results obtained with the two methods correlate very well.

The researcher concludes that a line-laser based system can be used to measure and assess dynamically the track stiffness in transition zones by monitoring the continuous vertical movement of multiple sleepers, with good productivity and at an acceptable cost. Observing the train-induced dynamic deflection patterns across multiple sleepers allows a rapid assessment of the track stiffness and provides the information that is necessary to manage the stiffness variation around transition zones. The system is suitable for in-service monitoring of operational railways.

Acknowledgements

I would like to express my deepest appreciation to those who have contributed to this thesis and supported me in one way or another during this precious journey. Foremost, I would like to express my sincere gratitude to my supervisors, Professor Clive Roberts and Professor Felix Schmid for their continuous support of my PhD study and research, for their patience, motivation, enthusiasm, and immense knowledge. Their guidance helped me during the research and writing of the thesis. I especially want to thank my academic advisor, Dr Paul Weston, whose support and guidance made my thesis work possible. He has actively supported my work and has always been available to advise me. I am very grateful for his patience, motivation, enthusiasm, kindness, warmth and immense knowledge. All these qualities make him a great mentor.

Very special thanks to the Track 21 research project team and the department of EESE for giving me the opportunity to carry out my doctoral research and for the financial support. It would have been impossible for me to even start my study had they not given me a scholarship for the research.

Piotr Konopka has been a good friend and I thank him for his continuous support of my work all these years. Piotr has tried to be available to do his best in giving me feedback on my work, whenever I required help. His critical view has always been helpful in improving my work.

My sincere gratitude is reserved for Dr Tatiana-Ioanna Gialama for her invaluable insights and suggestions for the civil engineering works. I remain amazed that despite her busy schedule, she was able to support my field test and met me very often with comments and suggestions to improve the work. In addition, I sincerely cherish our friendship.

The thesis would not have come to a successful completion, without the help I received from the staff of the BCRRE. Louis Saade was kind enough to support the field test and I acknowledge the meticulous work he has done. Adnan helped setting-up the test equipment in the lab and the test track in Long Marston, and I thank and appreciate his efforts. I remember Joy Grey, Mary Winkles and Charles Watson for their continuous encouragement. Thank you to Katherine Slater. Through your help my English has improved. A further thank you to all of my colleagues in the research group, who provided inspiration and guidance in resolving various issues.

I would also like to take this opportunity to thank Dr David Hughes from Queen's University, Belfast and Dr. Michael Burrow in the Civil Engineering Department at the University of Birmingham - my viva examiners, for their very helpful comments and suggestions. These have been invaluable in improving the thesis.

PhD students often talk about loneliness during the course of their study but this is something which I never experienced at Birmingham. A heartfelt thanks to the really supportive Schmid- Eickhoff family-Emilie, Bridget and Thomas, the Moses family, the Soo family and all my friends who made the UK experience something special, in particular, Ziyi Yang, Say leng Tan, Gloria, Liz Stordahl, Reza Zolfaghari, Gemma Nicholson, Dave Kirkwood, Zhenhe, Tosaphol, Masaki, Tingyu Xin, Xindi Chen, Ning Zaho, Doctor Ham , Minjeong Kim, Jungsoo Choi and Sunjoong Kim family.

I am very much indebted to my family, father, mother, mother-in-law and father-in-law, who encouraged me in every possible way to see the completion of this work. I thank my sister, Doctor Sunmi Kim and brother-in-law Christopher for their wonderful support and love all these years. The Fonseca-Shim family has been a great support ever since I started my PhD study and I owe them so much for their care, prayer, love and support. I also thank my brother-in-law, Hyun Sung and sister-in-law, Young Ji and my brother Hong In for their good wishes.

Thanks to Felicity, the best daughter I could ever have, for her smiles that made easily overcome the difficulties encountered in my pursuit of the PhD degree.

Finally, I would like to acknowledge the most important person in my life – my husband Yong Sung. Yong Sung has been a constant source of strength and inspiration. There were times during the past five years when everything seemed impossible and I did not have any hope. I can honestly say that it was only his determination and constant encouragement that ultimately made it possible for me to see this project through to the end.

Preliminaries

Table of Contents

List of Figures

List of Tables

Glossary of Terms

Term	Meaning / Definition
ABS	Automatic Ballast Sampler
BB	Benkelman Beam
BOEF	Beam On Elastic Foundation
CAN	Controller Area Network
CBR	California Bearing Ratio
DBT	Displacement Basin Test
DCPT	Dynamic Cone Penetrometer Test
FD	Functional Decomposition
FEA	Finite Element Analysis
FEM	Finite Element Method
FFT	Fast Fourier Transform
FPS	Frames per Second
FRA	The Federal Railroad Administration
FWD	Falling Weight Deflectometer
GCR	Great Central Railway
GPR	Ground Penetrating Radar
HSD	High Speed Deflectograph
ID	Identification Code
IDC	Insulation-Displacement Connector
I^2C	Inter Integrated Circuit
IMV	Infranord Measurement Vehicle
LCC	Life Cycle Cost

Term	Meaning / Definition
NMT	New Measurement Train
PBT	Plate Bearing Test
PCA	Portland Cement Association
PCB	Printed Circuit Board
PD	Physical Decomposition
PIV	Particle Image Velocimetry
PSD	Position Sensitive Detectors
RDD	Rolling Dynamic Deflectometer
RMS	Root Mean Square
RSMV	Swedish Rolling Stiffness Measurement Vehicle
RSSB	Rail Safety and Standards Board
RTST	Rail Trackform Stiffness Tester
RTRI	Railway Technical Research Institute (Japan)
S&C	Switch and Crossing
SR	System Requirement
TLV	Track Loading Vehicle
tph	Trains Per Hour
TRV	Track Recording Vehicle
TSD	Traffic Speed Deflectometer
TTCI	Transportation Technology Center, Inc.

1 Introduction

The present thesis has been written to summarise research carried out on the measurement of railway track stiffness in so-called critical zones, where differences in the track structure or the material properties change the elasticity to a higher or lower level.

1.1 Background

1.1.1 Life-Cycle Costs (LCC) and Optimal Maintenance

Railways were developed in the period following the industrial revolution, expanded rapidly from about 1810 and had become the main form of land transport by about 1900. After the end of World War II, road transport grew quickly until, by the end of the 1960s, the railways were being marginalised. However, oil price rises and congestion have given railways a new lease of life. As the railway industry continues to grow, there is a requirement for heavier axle-loads and higher speed operation. The railway was originally designed and built to run in an environment with relatively low speeds (70-100 km/h), light axle-loads (8-10 tonnes) and low train service frequencies (1-2 tph).

Given the current axle loads and train service frequencies, the line speed has to be restricted in certain areas. The limits are imposed to try to prevent an increase in track degradation, which would lead to delays due to poor track quality (Hendry *et al*., 2010) and the need for more periodic maintenance (Zoeteman, 2001). Temporary speed reductions, imposed due to malfunctions or the poor state of the infrastructure, cause reductions in service performance through, e.g., reduced punctuality. Conversely, in order to maintain a good level of track quality, maintenance work is required, often with long possession times, safety issues and the cost of maintenance workers and equipment. In addition, long possession times are likely to affect quality of service. Where the scheduled maintenance work cannot be completed on time, extended possessions result in unplanned service disruption. On the basis of satisfying the demand for more capacity and better reliability, there has been growing interest from the railway industry in reducing system LCC. There is thus a need to find a balance between passenger demands and LCC (Ward *et al*., 2010).

Typically, maintenance work and remedial work has been done at fixed periodic intervals (Silmon and Roberts, 2010) based on either empirical or analytical data. This can sometimes cause excessive spending due to unnecessary work being carried out. Railways must be maintained with fewer staff and smaller budgets to ensure an optimised LCC. This means that there is a requirement to employ an optimal maintenance strategy, which

provides for less expenditure. Optimal maintenance requires the implementation of the right measures at the right time to satisfy safety, comfort and availability levels, whilst considering LCC. Condition-based maintenance is seen as a significant contributory factor in achieving an optimal maintenance strategy and in reducing unnecessary work (Ward *et al*., 2010). In order to adopt condition based maintenance, there are some important parameters that should be monitored continually.

1.1.2 Track Quality and Condition of Trackbed

The quality of the track, i.e., its ability to support the level of traffic while retaining good geometry, is directly related to the design and condition of the trackbed and earthworks (NR/SP/TRK/9039, 2005). The trackbed consists of two parts, namely, the ballast and the formation (subgrade). Failures of the trackbed can occur due to ballast deterioration, pumping, loss of subgrade strength or poor stiffness characteristics. Track geometry measurement systems are nowadays standardised and are used on a regular basis (BSI, 2008). When track geometry is poor, maintenance activities such as tamping and re-ballasting are conducted in order to keep track geometry within acceptable limits, thus increasing the effectiveness of the ballast. However, they are not optimal solutions, as these methods of enhancing track geometry are purely superstructure focused (Priest and Powrie, 2009), rather than addressing substructure issues, which could eliminate the source of the superstructure problems. The root problems which make track geometry poor cannot be solved by such maintenance activities, as track geometry defects tend to reappear after conducting these corrective measures. In order to assess track quality and obtain information on the performance of a track on the basis of a substructure focused system, various methods are available to measure the value of track stiffness. Track stiffness is one of the indicator of the subgrade condition, which affects vehicle ride comfort, wheel/rail forces and the rate of deterioration of track geometry. Dynamic sleeper stiffness has been used on Britain's National Rail network as an important parameter to describe trackbed stiffness. The dynamic sleeper support stiffness (K), expressed in kN/mm/sleeper end, is the ratio between the peak load divided by the peak deflection of the rail seat area of an unclipped sleeper. It is measured by a Falling Weight Deflectometer (FWD). A specially developed stiffness measurement vehicle and trackside sensors have also been used to obtain track stiffness data. However, the stiffness measurement techniques are not standardised (Li and Berggren, 2010) and the measurements are not performed regularly. In addition, there are some problems with the existing methods, for example, investigations

can only be performed at low speeds, requiring significant track possession time (Priest and Powrie, 2009), which results in low productivity. The level of accuracy of the measurements is also limited. In addition, to date, measurements have not been taken on a regular basis, since there is no standard agreed measurement regulation.

1.1.3 Track Stiffness and Transition Zones

While the geometry is within the acceptable limits, the condition of the subgrade is neglected. However, the root causes of problems which are identified by recording the track geometry cannot be found by the analysis of the geometry data alone. Track stiffness data supports the identification and finding of the root cause of track geometry deterioration problems (Puzavac *et al*., 2012) (Berggren, 2009).

The concept of track stiffness does not have a universal definition. The most common definition is that track stiffness is the relation between the applied force and the displacement response of the track. According to a Rail Safety and Standards Board (RSSB) report (Hunt, 2005), track stiffness is influenced by the following factors:

- The rail and resilient pads;
- The sleeper and its condition;
- The ballast and sub-ballast and their settlement condition;
- The subgrade and environmental factors such as water logging, draught, freezing temperatures.

A further discussion of track stiffness is included in section 2.1.1.

The following diagram, Figure 1-1, presents the elements of track stiffness and illustrates the process that results in the variations in track stiffness and the influences on track geometry deterioration due to poor condition of the subgrade.

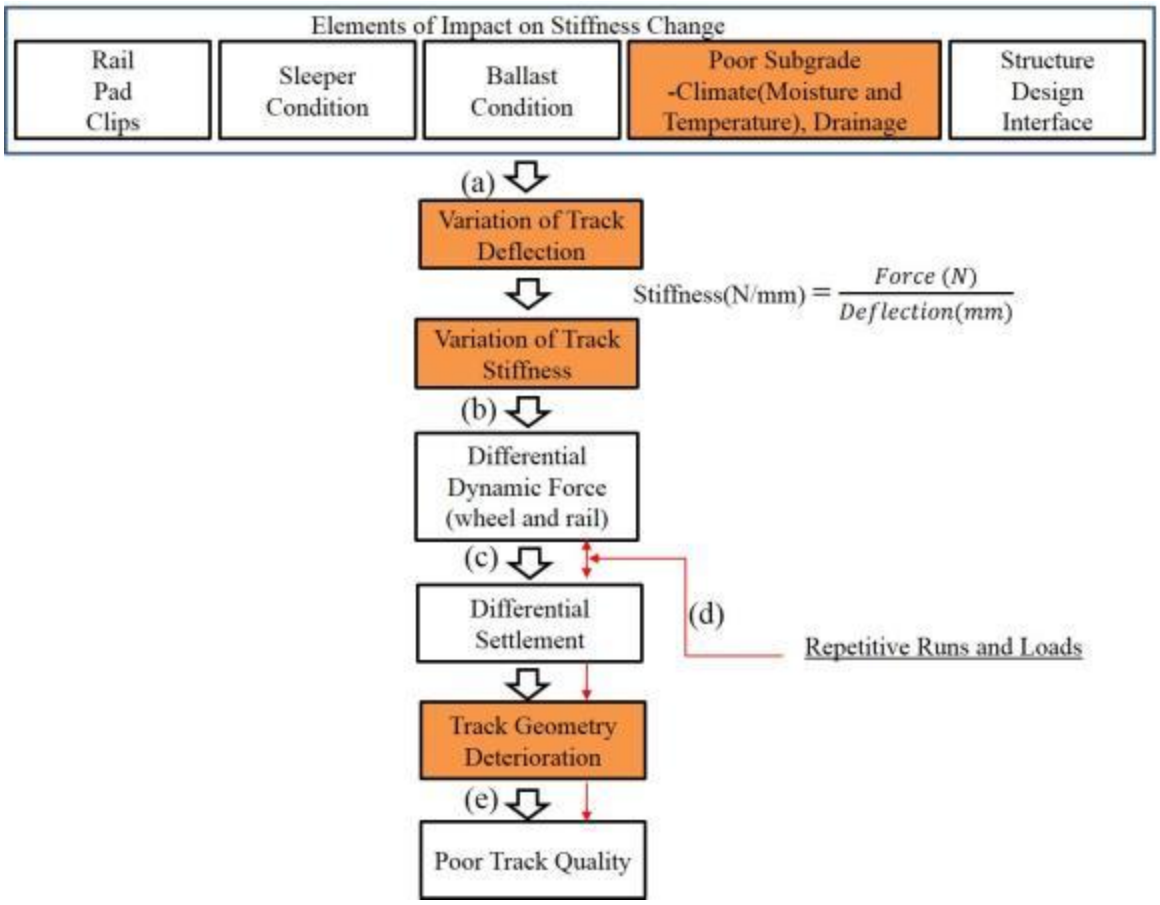

Figure 1-1: Diagram of the link between the track deterioration process and track deflection (stiffness)

At the very early stages of track construction, the structure and foundation is designed and built and it is then expected to allow maintaining a track with optimal track stiffness during operation. However, as a train runs on the track, the design of the components, and the running environment to which they are subjected, have the potential to increase or decrease track stiffness. The characteristics of the particular tack section can change due to changes in the mutual interface between all relevant elements. The non-linear degradation process of each track component or the poor condition of the subgrade can result in track deflection and stiffness changes (Figure 1-1, a). For example, fouled and dirty ballast can result in poor drainage performance so that the sleeper cannot support the load resiliently as intended. This may cause greater deflections and a decrease in track stiffness.

Reasonably high stiffness resulting from adequate track support is good since it leads to low track deflection. However, very high stiffness increases the dynamic forces at the wheel and rail interface, which in turn decreases component life and, hence, increases the LCC. On the other hand, very low track stiffness, resulting in higher more deflection, leads

to increased rail displacement and an increase in bending moment, which influences long-term fatigue conditions (Berggren, 2009).

A rapid discrete change in track stiffness is a critical problem for the safe and efficient operation of a railway. When the train runs across an area between low and high stiffness, and vice versa, the dynamic force varies (Figure 1-1, b), which causes differential track deterioration. Changes in settlement due to the level of the groundwater table and weather effects can also increase the differential dynamic load and dynamic force between the wheel and rail, which increases differential settlement (Figure 1-1, c), particularly under high axle-load conditions at high operating speeds.

In the long term, the processes of differential settlement and different dynamic forces are repetitive (Giner and Chaves, 2012), which accelerates the track deterioration rate, leading to track component damage and ballast breakdown. This results in poor track performance, requiring more maintenance activity and significant expenditure (Figure 1-1, e) in preventative maintenance due to the perceived risks. Therefore, the early detection of differential settlement and monitoring of the variation in track deflection are important for the assessment of the state and the identification of the preventive actions necessary to maintain a good level of track quality. Early preventive action will serve to prevent the negative effects mentioned in Section 1.1.1, such as temporary speed restrictions and extended track possession with low productivity.

1.1.4 Critical Zones

Given the above discussion we define as critical zones the areas of the infrastructure which demand extensive maintenance work due to the variation in track stiffness between different structure and substructure types. The following examples are typical critical zones in railways:

Figure 1-2: (a, b, c, d): Examples of critical zones in railways (Watson, 2014)

Figure 1-2 (a) is a transition between ballasted and slab track near Wanzwil, Switzerland, on the Mattstetten–Rothrist line during its construction in 2004. Figure 1-2 (b) shows an example of the double sleeper installation of Insulated Block Joints typical in continental Europe. Figure 1-2 (c) shows a transition between an embankment and the bridge over the Rio Chanchas in Huancayo, Peru. The line is poorly maintained, and both ballast and track fastenings are subject to theft, as these materials are commonly used in construction. Figure 1-2 (d) shows a transition between ballasted track and a through girder bridge with longitudinal way beams at Vauxhall in London.

The maintenance cost in these types of areas is four or five times higher than the cost of normal open track, and the number of work occurrences is 2 to 4 times greater than for standard embankments (Kang *et al*., 2002), (Coelho *et al*., 2011). Track passing over fixed structures, such as culverts or over-bridges, is also subject to changes in stiffness. Varying support in the vicinity of Switches and Crossings (S&C) also creates changing stiffness. It is critical to reduce the difference in track stiffness and to increase track stability in the area of structures such as tunnel entrances and exits, bridges and level crossings. The abrupt change in track stiffness in these critical areas increases dynamic loads and passenger discomfort. Change in dynamic load causes differential settlement, which causes track geometry changes. If the phenomenon could be better understood, it would be possible to minimise risk and reduce LCC.

There are some methodologies that can be used to decrease the magnitude of track stiffness variation, see Section 2.1.2, by improving the design of the structure. One solution is to design and build a transition zone that is specifically designed for these areas in order to provide a continuous change in stiffness between rigid substructures and open track (Coelho *et al,* 2010).

Figure 1-3: Example of the transition design using two extra rails at the transition between slab track and ballasted track (Michas, 2012)

Figure 1-3 shows an example of the design of a transition zone between slab track and ballasted track. Since slab track has a higher stiffness than ballasted track, the transition zone is designed to provide a gradual increase in stiffness between the two arrangements by placing two auxiliary rails and using different types of pads, sleepers and ballast gluing.

When the condition of the transition zone is well maintained, track performance will be good and it will fulfil its design purpose. However, if the performance of the transition zone is poor, it will worsen the track geometry conditions.

A large amount of research has taken place in recent years to assess the quality of straight sections of track, whereas there has been relatively little research to assess transition zone performance (Lee *et al*., 2005) (Coelho *et al*., 2009) (Innotrack, 2009) (Kang and Yang, 2010) (Jing *et al*., 2010) (Li *et al*., 2010) (Coelho *et al*., 2011). As a result, it is not yet possible to understand fully the mechanism of track geometry deterioration in transition zones. A better understanding of the existing state of the substructure (i.e., through measurement of track quality in some form) will support predictable maintenance decisions and result in less expenditure being required to avoid unknown risks. In addition, a detailed understanding of the condition of the existing state of the substructure can lead to better designs to improve performance in transition zones.

1.2 Aims and Objectives

As discussed in Section 1.1, an adequate level of trackbed stiffness is a key determinant for the ability to maintain a good track geometry (Section 1.1.2) with track deflection providing an indication of this trackbed stiffness (Section 1.1.3). However, the current measurement methods for track deflection have some challenges, such as high operation costs, long track occupancy time during operation and low productivity. Consequently, the aim of this research is to develop an innovative, productive and accurate means of identifying changes in track stiffness over time, which can be effectively used on sites during normal train operation, thereby avoiding some of the weaknesses of the current system. The change in stiffness can be established by comparing the stiffness of the support of each individual sleeper with that of the adjacent sleeper over the section of track. Measuring the change in stiffness over time means comparing the indication of relative stiffness, which is calculated by the axle load divided by the maximum displacement of each sleeper, continuously, in real time.

The overall aim will be achieved by meeting the following objectives:

1. Review the concept of track stiffness, transition zones and the relevant theory;
2. Investigate and evaluate the current techniques of both railway trackbed and road structure stiffness measurement, to find the strengths and drawbacks of each;
3. Through the analysis of the necessary functionalities and characteristics develop a functional specification for the measurement device.
4. Design and construct a measurement system in accordance with the specification.
5. Validate the measurement system by carrying out field tests: taking into account the known conditions of the test environment, such as vehicle dimensions, axle loads and sleeper spacing, the shape of the deflection bowl can be estimated. This deflection will show how the stiffness can change sharply by comparing the theoretical calculation and with the data from the real measurement. In order to check the accuracy of the measurement system, different types of trackside sensors, such as geophones and a video recording system, shall be compared with the laser measurement system developed as part of the research.
6. In addition, the results of a dynamic cone penetration (DCP) test, one of the traditional techniques for measuring trackbed stiffness, will be compared with the

deflection measurement system to show how the measurement data can be co-related to the condition of the subgrade and stiffness.

7. Analyse the effectiveness of the measurement system and draw conclusions.

The work presented in this thesis has been undertaken as part of the Track 21 collaboration project between the Universities of Birmingham, Southampton and Nottingham, the aim of which was to find sources of uncertainty in the performance of railway track systems and to improve railway track for the 21st Century (www.track21.org.uk). In order to contribute to providing a qualitative measurement of track stiffness, which is thought to be possible using continuous in-service measurements from both vehicles and trackside, the author's research work was undertaken to measure the changing track stiffness using sensors for comparison with the data from train-based in-service measurement.

1.3 Contributions

In the academic research field that addresses track subgrade issues, various measurement systems have been developed to produce track deflection data that can be used to evaluate track stiffness. The idea is to create a system that is quick and easy to install and autonomous to operate. Some track occupancy during the measurement procedures is inevitable, since the measurement vehicle usually runs on the track. The operation speed of these special purpose trains is increasing, currently up to 130 km/h, however, there are still speed restriction issues where the line speed is high.

Recent research shows that trackside sensors can measure the deflection of individual sleepers during the passage of trains, enabling track deflection to be measured without affecting the train timetable or requiring track possession. However, there are some issues to be addressed regarding accuracy and productivity before the trackside sensor system can be an off-the-shelf product. In this context, the research described in this thesis is aimed at developing an easy to use trackside measurement system that requires minimal labour resources and track access. The measurement system will produce continuous deflection data for multiple sleepers rather than providing the maximum deflection data for individual sleeper – which is what the current trackside sensors produce – so that it can be used to monitor the abrupt change of stiffness in critical zones. The laser based measurement system discussed in this thesis has been developed through some significant upgrades of hardware and software that were aimed at producing the shape of a deflection bowl for multiple sleepers. The measurement system consists of up to 20 newly designed sets of

displacement sensor nodes with an auto-calibration function, two sets of specially developed power controllers for reliable data communication, a railway-safe focused infra-red laser sensor node and user interface software developed using C# that enables laser setting, data measurement and processing with minimum human interaction. The following list represents the innovative contributions achieved through the the research:

1. The algorithms which utilise equation (20) in Section 4.2.1 to analayse the two output channels from the displacement sensor were developed for easier detection of the infrared-laser on the surface of the displacement sensor on the multiple sleepers.This had not been implemented for the prototype system.
2. A visual screen which shows the alignment of the invisible laser source has been implemented, thus not only minimising the human interaction by allowing adjustment of the laser source rather than requiring the re-positioning of multiple displacement sensors on sleepers, but also allowing the acquisition of a deflection bowl over multiple sleepers in real time. Studying the change in track stiffness over a reasonable length (deflection and stiffness over 18 sleepers can be shown), can improve maintenance decisions. (Section 4.2.2.1 and Section 6.3.5)
3. As different propagation distances from the laser source to each sensor node resulted in variations of the laser power, it was expected that the calibration work would be difficult. In order to try and find an optimal frequency and gain, a binary-search algorithm was proposed, which enables a steady value of deflection to be obtained. This allows the laser sensor nodes, positioned at distances of 8-10 m, to be calibrated remotely and to produce a close to steady output. (Section 4.2.2.1)
4. For the real time data logging function, a Controller Area Network (CAN), originally developed for use in the automotive industry, has been adopted as a low cost data-logger network in this research to produce a continuous and real time data transmission across multiple nodes (Section 4.2.1).
5. The concept of the versine has been applied to the raw deflection data in order to remove the common pattern of vibration of the laser source that would be found from the deflection sensors over multiple sleepers, thus, only the relative movement of multiple sleepers is included in the data, thereby removing any effect of the movement of the laser source due to ground vibration or wind effects (Section 6.4.4).

6. The real measurement data has been collected and compared to the theoretical deflection curve that was accomplished by the DCP test and the application of Zimmerman's theory. The outcome of the work demonstrates a clear link between the stiffness value and the subgrade condition.

In summary, the condition of the subgrade over the short section of track near the transition zone can be assessed preliminarily by looking at the shape of the deflection bowl. As a result of this research, less labour intensive measurement procedures can be implemented by adopting the measures described above.

1.4 Thesis Structure

The thesis is divided into eight main chapters and the structure of each chapter is outlined below:

Chapter 1: Background and research objective

This chapter introduces the background, research motivation, research approach, aims, objectives and thesis structure.

Chapter 2: Literature review of track stiffness transition zones and the relevant theory

This chapter provides a review of track stiffness being used in the railway industry. It also presents a detailed review of the Beam On Elastic Foundation (BOEF) theory that can be used to calculate theoretical track deflection and thus track stiffness. Research on track stiffness measurement at various transition zones is also discussed. The mechanism of a transition zone is described with the results from previous research. Overall, this chapter provides the civil engineering background of the track system and the performance of transition zones by reviewing different research results.

Chapter 3: Literature review of current practice in track quality measurement

This chapter provides a review of relevant current practices and techniques discussed in recent literature for measuring track geometry, track stiffness, track displacement and pavement stiffness. After comparing and discussing various methodologies to measure track quality, the conclusions of this chapter led to the establishment of the system requirements to build a trackside continuous measurement system, which was developed as described in Chapter 4.

Chapter 4: The process of the system development

This chapter introduces the whole process from conducting the research and the research methods used to develop a measurement system in an efficient way. During the research process, system engineering is applied and the Vee-model is adopted as a tool. The system requirements were extracted from the review and pros and cons of current practices and actual operational needs, which were discussed in Chapter 3. Following requirement identification, the functional and physical decomposition process was completed to the lowest possible level in order to design and build a whole system.

Chapter 5: Verification test and results in a laboratory

After the development of the measurement system in Chapter 4, this chapter shows the verification process for the new measurement system. The purpose of this chapter is the analysis of a laboratory based comparison test with other measurement techniques. Some issues were found and improvements made before the field test.

Chapter 6: Field trial for deflection measurement of series of sleepers

This chapter presents the first field test at the Long Marston Test Facility. The field test was aimed at testing the equipment and observing the moving shape taken up by a sequence of sleepers around a transition during continuous train passage. First, the theoretical deflection curve was calculated on the basis of the BOEF theory in order to establish the difference between the theoretical data and actual measurement data. Second, a Dynamic Cone Penetration (DCP) test was conducted to investigate the in situ strength of the subgrade. Third, the results from the laser based system were compared with video recording data and geophone data as part of a further validation test. The data was compared and analysed; some issues were identified and a new experimental set up with system improvements was then used to obtain supplementary experimental data. This chapter shows the feasibilities and capabilities of the measurement system including a discussion of the effects of the variation in train speed, loads, and different types of substructure and subgrade condition on the displacement.

Chapter 7: Conclusions

In this chapter, the author summarises the findings of the research and then presents the conclusions of her work. In addition, she reviews her outputs against her research objectives and validates the newly developed system against the requirements. The limitations of the research are presented and further work is recommended.

2 A Review of Track Stiffness and the Transition Zone

In this chapter the author introduces background knowledge based upon her research into track stiffness and transition zones. She summarises the up to date research work on track stiffness and current practices used to monitor and improve the performance of the transition zone in two chapters of the thesis, as shown in Figure 2-1.

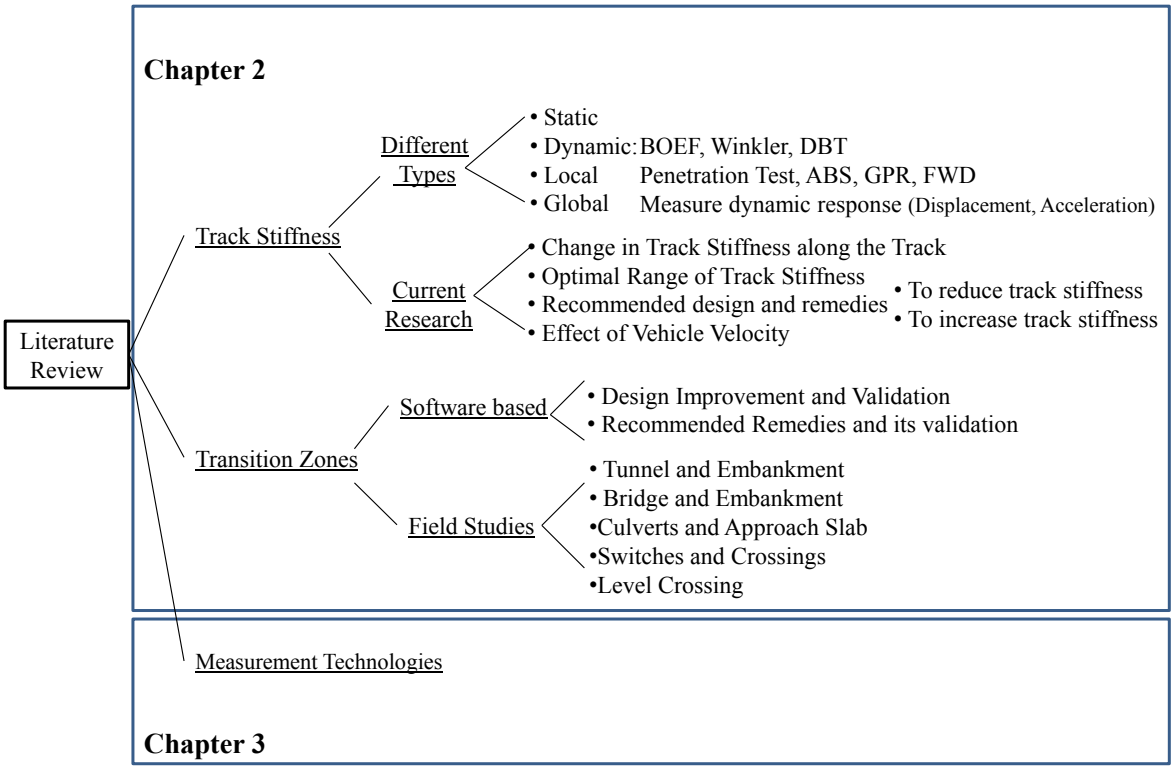

Figure 2-1: Scope of Literature Review

In the first section of Chapter 2, the author presents definitions of track stiffness and relevant research and literature. Significant work in the area of track stiffness has been undertaken in recent years, such as theoretical calculations, design solutions for the track, evaluations of the influence of high speed traffic on track stiffness, etc. As the main aim of this research is to develop an innovative, productive and accurate means of measuring changes in track stiffness over time, see Section 1.2, the Beam on Elastic Foundation (BOEF) theory will be introduced to provide a theoretical foundation to the prediction of track deflection.

In the second section of Chapter 2, relevant research work and literature regarding design, remedies and monitoring of the transition zones is provided. The chapter ends with a brief review of recent research studies on track stiffness and a discussion as to which approach

is the most relevant and effective for the purpose of this research, in the light of other research into the transition zone. This justifies the need for measuring sleeper deflection. Relevant technologies are not discussed in this chapter, but are included separately in the next chapter.

2.1 Track Stiffness

Track stiffness is a critical parameter in that it is an indicator of the root cause of problematic railway sites. In addition, when railway lines are upgraded for high speed trains and heavier axle loads, substructure information can be found from monitoring track stiffness. When railway track is newly built, the track stiffness is very important, as the values obtained can be used to verify the track quality (Berggren *et al*., 2006). This section is intended to assist the understanding of the importance of track stiffness. The author provides some of the theoretical background and discusses research trends and finds the most suitable concept of track stiffness to address the research objectives.

2.1.1 Track Stiffness and Theoretical Background

Various research documents and papers present a definition of track stiffness, (Puzavac *et al*., 2012), (Colorado *et al*., 2006), (Berggren, 2009), (Hunt, 2005), (Li and Berggren, 2010), however, there is no clear international or European agreement on a definition of track stiffness, see Section 1.1.3. In general, track stiffness is a function of the structural properties of rail, pad, sleepers, ballast, sub-ballast and subgrade soil (Hunt, 2005). Similar to the concept of track stiffness, track modulus is also an important parameter in track quality and performance. Track modulus is defined as the supporting force per unit length of rail. In order to obtain the value of track modulus, a number of sleeper deflections are measured (Priest and Powrie, 2009). The difference between track stiffness (Nm^{-1}) and track modulus (Nm^{-2}) is that track stiffness includes the behaviour of all track components, including the bending of the rails, whereas the track modulus defines the deflection of part of the track (i.e., ballast and sleepers and subgrade) rather than the rail, thus it considers the support condition under the rails (Colorado *et al*., 2006), (Burrow et al., 2010).

The simplest form of vertical track stiffness k is defined as the ratio between the vertical force Q exerted on top of one rail and its vertical displacement w.

$$k = \frac{Q}{w} \qquad (1)$$

The stiffness is influenced by the rate of application of the load Q and the resulting excitation frequency, which is generated by the condition of the foundation, running speed, bogie spacing, and the wheel-rail interface. It is a dynamic parameter that also depends on the type of measurement system. Further details regarding the measurement system will be discussed in Chapter 3.

There are theoretical methods to calculate the track stiffness and modulus, such as Deflection-Area, Pyramid Load Distribution, Beam on Elastic Foundation (BOEF) and the Winkler model (Norman *et al*., 2004). A number of researchers (Hunt, 2005) (Priest and Powrie, 2009) suggest that track stiffness and modulus can be analysed by using a mathematical model, which is known as the Beam on Elastic Foundation (BOEF), which is one of the most useful theoretical models. The BOEF model was initially proposed by Winkler in 1867 and this theory has been widely adopted by track engineers, since it is straightforward to use in analysing railway track systems. The method assumes the rail to be infinitely long and continuously supported by an elastic subgrade and foundation, with a coefficient k, and loaded by a wheel load at x=0, as described in Figure 2-2.

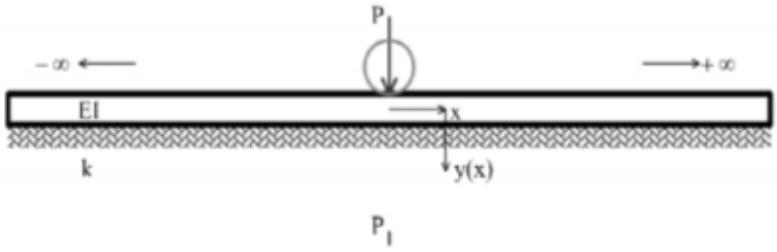

Figure 2-2: Beam on elastic foundation model (Esveld, 2007)

Where
P= wheel load [N]
EI = bending stiffness rail [N·m^2]
k = foundation coefficient [N/m/m]
W(x) = rail deflection at x[m]

On the basis of Winkler's theory, a calculation method for the deflection curve was developed by Zimmermann in 1888. It assumed that the rail is supported by an ideal sleeper (dimension: a×b2) and that it is supported continuously, not with discrete supports. This method was improved again by Eisenmann in 2007. The idea is to transform the single supported beam by transferring the bearing areas into a continuously supported beam, as described in Figure 2-3.

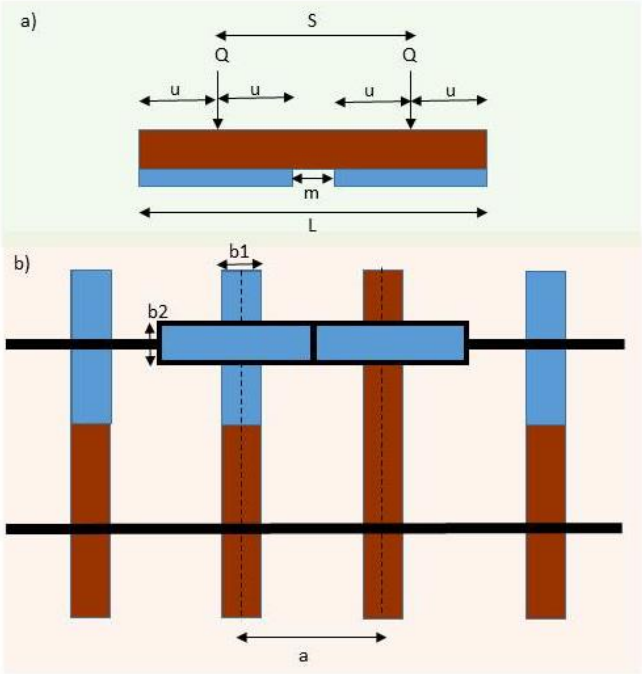

Figure 2-3: The concept of Zimmermann's theory developed by Eisenmann (N.F. Doyle, 1980)

where:

L = length of sleeper (mm)

a= sleeper space (mm)

m = length of area without support (mm)

b1 = width of the actual sleeper (mm)

b2=the width of the converted area (mm)

The actual support areas of half the sleeper (2u), as shown in Figure 2-3, (a) are converted into the connecting areas between two adjacent sleepers in order to create the continuous support for the rails (Figure 2-3 (b)). The dimensions of the converted (a×b2) area are calculated as below.

$$\text{Effective length (2u)} = \frac{\text{Sleeper length(L)} - \text{Sleeper unloaded length(m)}}{2} \quad (2)$$

$$\text{A} = \frac{\text{Sleeper length(L)} - \text{Sleeper unloaded length(m)}}{2} \times \text{original sleeper width(b1)} \quad (3)$$

$$\text{Width of ideal sleeper (b2)} = \frac{\text{effective length(2u)} \times \text{sleeper width(b1)}}{\text{sleeper space(a)}} \quad (4)$$

Where the quantity L known as characteristic length is represented by:

$$L=\sqrt[4]{\frac{4EI}{k}} = L=\sqrt[4]{\frac{4EI}{C\times b2}} \quad (5)$$

- Where C is the value of the foundation modulus in the contact area between sleeper and ballast bed [N/m^3].

The value of C value is simplified in the Zimmermann method. For real operation on a ballasted railway, the value of C can be identified by combining the relevant modulus values of each component or layer, as shown:

$$\frac{1}{C\ total} = \frac{1}{C\ rail-pad} + \frac{1}{C\ ballast} + \frac{1}{C\ subgrade} + \frac{1}{C\ foundation} \quad (6)$$

Esveld refers to C (K_s) as the modulus of subgrade reaction, which ranges between 0.02 and 0.2 N/mm^3 (Esveld, 2001), as shown in Table 2-1.

Table 2-1: Order of magnitude of elasticity constants (Esveld, 2001)

Quality of track support	Unit	Poor	Good
Foundation modulus C (K_s)	[N/mm^3]	0.02	0.2
Spring constant k_d	[N/mm]	5.5	55
Foundation coefficient k	[N/mm^2]	9	90
Characteristic length L	[m]	1.30	0.70

On the basis of equations (2), (3), (4) and (5) above, the maximum deflection (W_{max}) is found as follows.

$$W_{max} = \frac{Q}{2CbL} \quad (7)$$

In the Zimmermann method, multiple deflections from continuous sleepers are calculated using an influence factor of deflection (η). The function η(x) determines the relative deflection for x=0 resulting from nearby wheel loads.

$$\eta(x) = e^{-x/L}[\cos\frac{x}{L} + sin\frac{x}{L}] \quad (8)$$

and x is the distance from the wheel load to the point of interest to be measured. Thus, when there are multiple axles, the deflection from the multiple axles is

$$W(x) = \frac{1}{2CbL}\sum P(x) * \eta(x) \quad (9)$$

For example, the deflection shape of the sleeper that is affected by two axles is calculated as follows. The first element is the deflection which results from the load P1 directly, thus η (0) is 1, and the second element is the result of load P2 that is, for example, 2000 mm away.

$$W=\frac{P1}{2\cdot b\cdot C\cdot L}\cdot 1+\frac{P2}{2\cdot b\cdot C\cdot L}\cdot \eta_{2000} \quad (10)$$

Equation (9) can be applied to calculate the deflection from sleepers located at different distances under multiple axle loads. The dynamic deflection (W_{max}) is calculated on the basis of applying the Dynamic Amplification Factor (DAF) formula against train speed, track condition and the probability of failures, in order to reflect reality as below.

$$DAF = 1+t\Phi \quad \text{if } V< 60 \text{ km/h} \quad (11)$$

$$DAF= 1+ t\Phi \left(1+\frac{V-60}{140}\right) \quad \text{if } 60 < V < 200 \text{ km/h} \quad (12)$$

$$W_{max}= W\times DAF \quad (13)$$

Depending on whether the line speed is restricted to 60 km/h or not, equations (11) and (12) apply. Table 2-2 shows the elements of the DAF to insert into equations (11) and (12).

Table 2-2: DAF elements (Esveld, 2001)

Probability	t	Application	Track Condition	Φ
68.40%	1	Contact stress, subgrade	Very good	0.1
95.40%	2	Later load, ballast bed	Good	0.2
99.70%	3	Rail stresses, fastenings, supports	Bad	0.3

In Winkler's hypothesis, it is assumed that the elastic foundation is a system of identical, independent, closely spaced, discrete and linearly elastic springs. Accordingly, the ratio is constant between the load and deflection at every point of the contact surface (Puzavac *et al*., 2012). A number of researchers have applied this hypothesis, e.g., (Norman *et al*., 2004) and (Hendry *et al*., 2010), to investigate the relationship between absolute deflection and track modulus, as shown in Figure 2-4.

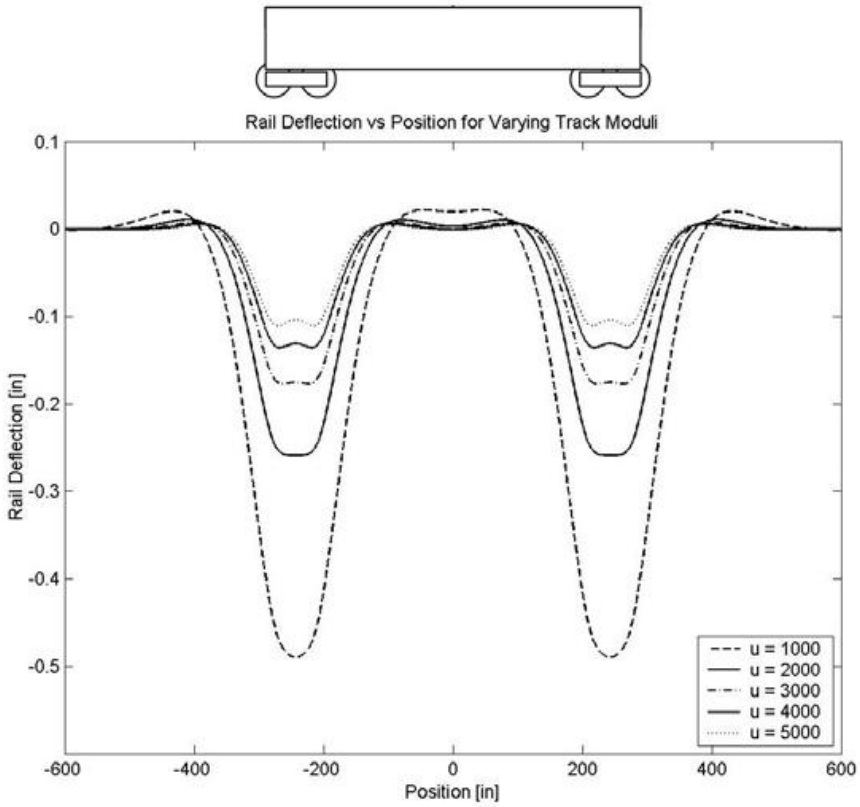

Figure 2-4: Winkler model of rail deflection (Norman *et al*., 2004)

In order to calculate the dynamic track modulus, two different techniques, BOEF and Displacement Basin Test (DBT), are applied comparatively (Priest and Powrie, 2009) and show that the sleeper response is a good measure of stiffness. Table 2-3 shows how each different equation has been applied. The DBT method requires the measurement of a number of sleeper deflections under the application of a static load, as in Equation (14).

Table 2-3: Comparison between DBT and modified BOEF techniques

DBT Method Equation	Modified BOEF Equation
$\sum_{j=1}^{N} Pj = kS \sum_{i=1}^{M} Pi$ (14)	$\delta_0 = \frac{P}{2kL}\left(\sum_{i=1}^{n} r_i \, e^{-x/L}[\cos\frac{x}{L} + sin\frac{x}{L}]\right)$ (15)
Where:	Where:
P: wheel load (N)	x_i: distance from the i^{th} wheel to the measurement point
S: distance between the sleepers (m)	δ_0: maximum displacement under the first axle load
δ: displacement of the rail (m)	r_i: P_i/P
M: number of sleepers deflected under the load	P_i: i^{th} wheel load
N: number of loads applied (e.g., the number of wheels)	P: Leading wheel load
	$L = \sqrt[4]{(EI/k)}(m)$
	EI = bending stiffness of rail (Nm^2)

As a result, the whole displacement basin is captured, with the assumption that the track modulus is constant over a short section of track, as shown in Figure 2-5.

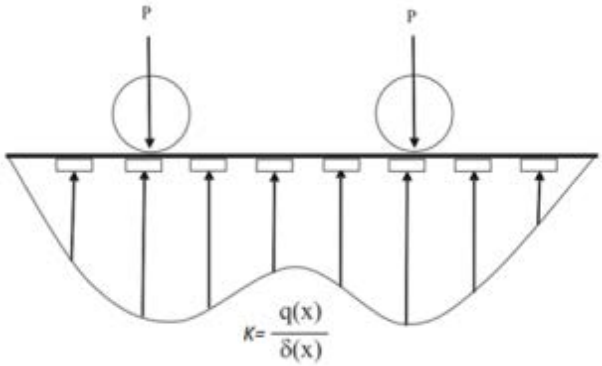

Figure 2-5: DBT Method (track modulus k equals to supporting force per unit of rail, q(x) divided by vertical displacement of rail) (Priest and Powrie, 2009)

From the DBT equation on the left hand side in Table 2-3, the calculated modulus k actually represents the average value from the number of sleepers under static load. The shape of the graph between the real displacement of individual sleepers over a certain time, see Figure 2-6 and the theoretical response from the static load over a certain length of rail with a certain number of supports (sleepers), see Figure 2-5, is quite similar. From their study, Priest and Powrie found that a dynamic track modulus can be calculated by measuring the displacement of individual sleepers over time for the DBT technique, but the DBT gives a lower value of track modulus due to the elastic response, so the BOEF method is preferable, according to their study.

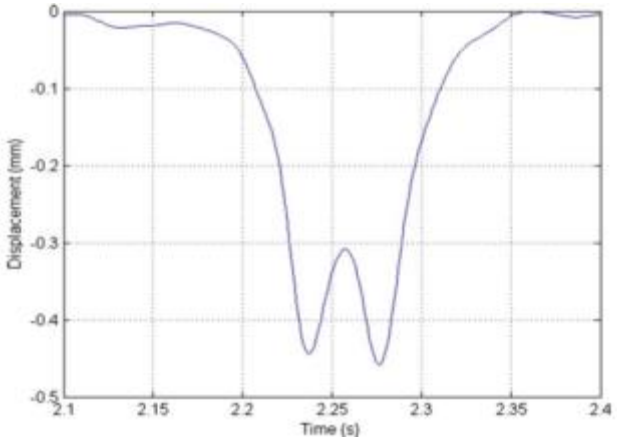

Figure 2-6: Sleeper displacement during train passage (Priest and Powrie, 2009)

Although the Winkler and Zimmermann method is still widely used, it helps the understanding of track behaviour that shows elastic and linear characteristics, however, the theories do not reflect the real condition of railway tracks. In reality, track behaviour is inelastic and nonlinear, as shown in Figure 2-7: For example, specific voids under sleepers will cause the stiffness to be lower than a generalised model might suggest. Research has found that the theoretical stiffness can be higher than the measured stiffness with less deflection and that stiffness is increased while excitation frequency is increased (Burrow et al., 2010). Real railway track has discrete support by cross sleepers and different thicknesses and extents of layers of subgrade and different materials which interact. Sometimes, the sleepers are loosely attached to the rail or too tightly fastened, resulting in more or less deflection of the track.

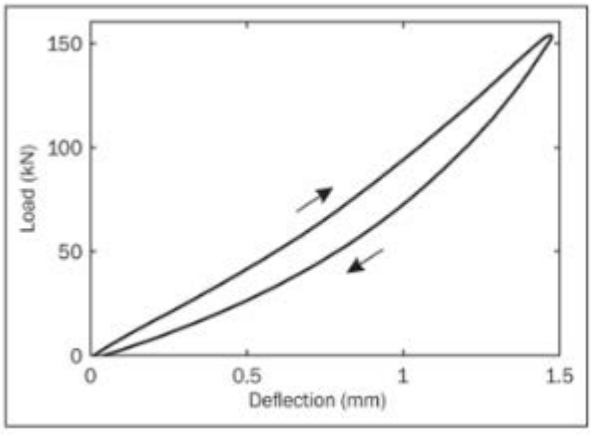

Figure 2-7: Load and deflection diagram (Burrow et al., 2010)

There are two relevant concepts to illustrate local stiffness. Firstly, local stiffness indicates the stiffness of an individual track component, which is quantified from laboratory tests by the component's manufacturer (Ekberg and Paulsson, 2010). Secondly, local stiffness can

be obtained on-site from a penetration test applied to different layers, which consist of soils and granular materials, at ground level, with a combination of Automatic Ballast Sampler (ABS) and Falling Weight Deflectometers (FWD). A comparison of these methods will be discussed in Chapter 3. From local stiffness data precise information concerning the characteristics of the granular material resistance can be obtained and the behaviour of the material can be estimated. The analysis of local stiffness gives information on geometry and mechanical data of the track structure (Berggren *et al*., 2006).

The amalgamation of individual local stiffnesses results in the global track stiffness, which considers overall track stiffness rather than the individual stiffness of each different component or layer, as stated in equation (6) above. In the BOEF theory, the deflection is calculated with the concept of global stiffness and expressed in kN/mm/sleeper end. Global track stiffness is defined as the ratio between the vertical force combination value from the local stiffness of each rail, rail pad, sleeper and foundation (Berggren, 2009). This global stiffness plays an important role in indicating overall trackbed performance, although it does not present an accurate value of the elastic properties of each layer.

2.1.2 Unevenness of Track Stiffness Issue

As presented in Chapter 1 (Section 1.1.2), there are studies that have been carried out in order to get a good understanding of stiffness along the track and find the cause of uneven track stiffness. There are two approaches to the research, one is to measure the stiffness of a long length of railway track and the other is to focus on a variation of track stiffness within a short section of track. Track stiffness and its variation have been measured and analysed on a typical Swedish track along a 100 km length, which is a relatively long section of track (Li and Berggren, 2010). They found a relationship between the global track stiffness and the response of the rail displacement, which is influenced predominantly by the condition of the ballast and subgrade. The small deflection of hanging sleepers and partly supported sleepers was monitored by research work conducted on a relatively small section of track where abrupt change in track stiffness was an issue (Coelho *et al*., 2011).

2.1.3 Optimal Track Stiffness

As discussed in Section 1.1.2, a very low value of track stiffness is an indication of a weak subgrade or dirty ballast, which causes excessive displacement and increases the track deterioration rate. On the other hand, very high track stiffness can lead to faster deterioration of the track and track components because of inefficient support for the train load (Burrow

et al, 2009), (Berggren, 2009). As a result, it is important to find an optimised track stiffness value and make an effort to maintain it. Figure 2-8 illustrates that the optimum range of track stiffness is important to decrease track geometry deterioration.

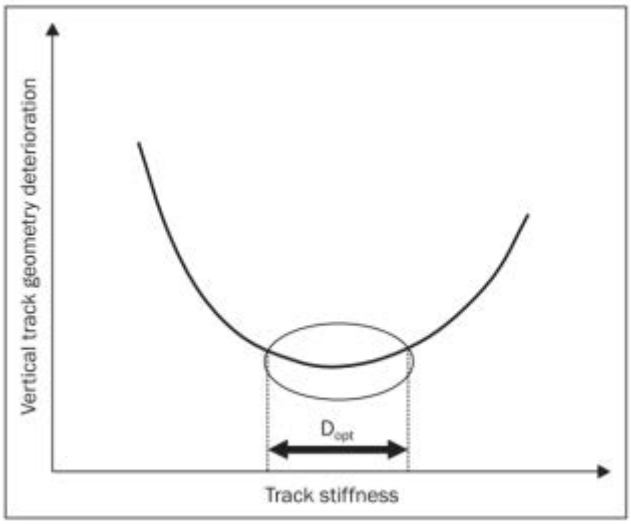

Figure 2-8: Optimum track stiffness (Puzavac *et al*., 2012)

Previous research has considered how to determine an acceptable track stiffness to help with maintenance decisions and extending rail fatigue life. The empirical results of identifying an optimum value of the vertical stiffness of the track are as follows:

- 75 kN/mm typical British railways (Hunt, 2005);
- 70-80 kN/mm for high speed lines (LoApez et al., 2004);
- 78 kN/mm for normal track, 31.6 kN/mm for soft track and 171.5 kN/mm for stiff track (Li and Berggren, 2010) ;

The structural design of railway track in the UK is based on required FWD track stiffness values obtained from a FWD measurement method, as below.

- 60 kN/mm for mainline without reinforcement (NR standard 039, 2005)
- 60 kN/mm for new track up to 100 mph and 100 kN/mm for new track above 100 mph (NR standard 039, 2005)

Burrow *et al* presented permissible rail deflection (x) under a 200 kN axle load (Burrow *et al*., 2009).

- $1 \text{ mm} \leq x \leq 2.2 \text{ mm}$ for train speed ≤ 160 km/h;
- $1.5 \text{ mm} \leq x \leq 2.0 \text{ mm}$ for train speed ≥ 160 km/h.

In addition, the research (Burrow *et al*., 2009) suggests that variations in the stiffness of the subgrade should be less than 10% of the mean value of track stiffness.

2.1.4 Design Recommendations and Remedies for Better Performance

In order to maintain track stiffness within an appropriate range and mitigate problems due to variations in stiffness, several designs have been recommended and implemented to decrease and increase track stiffness. In the literature, a number of ways to improve track performance at transitions by reinforcement are described and presented, which are as follows:

- Stone Columns: As discussed, the track foundation has a major influence on the variability in track stiffness. The installation of stone columns is designed to strengthen and improve the drainage of weak subgrade (Colorado *et al*., 2006);
- Geogrid reinforcement: In order to compensate for variable stiffness, geogrid reinforcement has been used (Colorado *et al*., 2006);
- Resilient components: In order to decrease track stiffness where stiffness is relatively high, concrete sleepers with rubber pads, plastic sleepers, wooden sleepers and ballast mats under the ballast layer are all used (Li *et al*., 2010), (Colorado *et al*., 2006), (Paixao *et al*., 2013);
- Installation of additional rails between running rails to reduce variation of wheel load and increase stiffness where it is low (Kang *et al*., 2006), (Colorado *et al*., 2006);
- Approach slab between an embankment and a structure to smooth out the track stiffness (Coelho *et al*., 2009), (Lee and Kang, 2010);
- Gluing ballast to increase track stiffness (Lakušic *et al*., 2010);
- Reduce sleeper spacing and use longer or wider sleepers to increase stiffness (Iwnicki, 2006).

In general, these reinforcement methods have been validated before implementation in the field to assess the resulting track response and to ascertain their effectiveness through simulation models.

2.1.5 Effect of Train Speed on Track Stiffness and Deflection

There are railway tracks where it is necessary to have train speed restrictions over soft ground in order to reduce the dynamic response from running high speed trains (Iwnicki and Dahlberg, 2006). Research has been conducted to find the relationship between the

effects of vehicle speed and dynamic effects on ballasted track. The critical velocity is that where the track response or resonance is maximum (Hendry *et al*., 2010). More description of critical velocity can be found in the literature (Yang *et al*., 2009).

Yang *et al.* found that the reduction in track stiffness and increase in track displacement with increasing train speed is apparent (Yang *et al*., 2009). The research concluded that when train operation speed is below 0.1 × critical velocity, the track performs in a quasi-static manner. More than 0.1 × critical velocity, the train influences the track dynamically and when it approaches the critical speed, the soil is likely to fail. Similarly, Priest and Powrie (Priest and Powrie, 2009) found that an increase in track displacement with increasing train speed is apparent through a comparison of the displacement data between the running speed at 99-129 km/h and at 260 km/h. Kang *et al* found that the variation of dynamic load is increased significantly when the train speed is higher than 75 km/h (Kang *et al*., 2002).

Hendry *et al*. pointed out that, rather than dynamic excitation, static deformation due to poor foundation is the lead cause of embankment deformation (Hendry *et al*., 2010). The researchers found that train speed does not significantly affect displacement of track even when a train runs at a maximum line speed, which is much less than critical velocity.

In summary, track displacement could increase with train speed but it is not linear and it has a limited effect on the deflection as long as the speed is under the critical speed.

2.2 Research on Transition and Critical Zones

In Section 2.1, the issue of unevenness of track stiffness was discussed. The variation of stiffness, in particular, leads to sudden changes in track support are often associated with track geometry and component degradation, high maintenance demand and poor ride quality. Therefore, there are many different methods of design which can be recommended in order to improve track stiffness, as discussed in Section 2.1.4. Transition zones are designed to equalise the stiffness, dynamic force and rail deflection between structures, e.g. tunnel, bridge, culverts and embankments and to provide a gradual increase in the stiffness, as described in Figure 2-9.

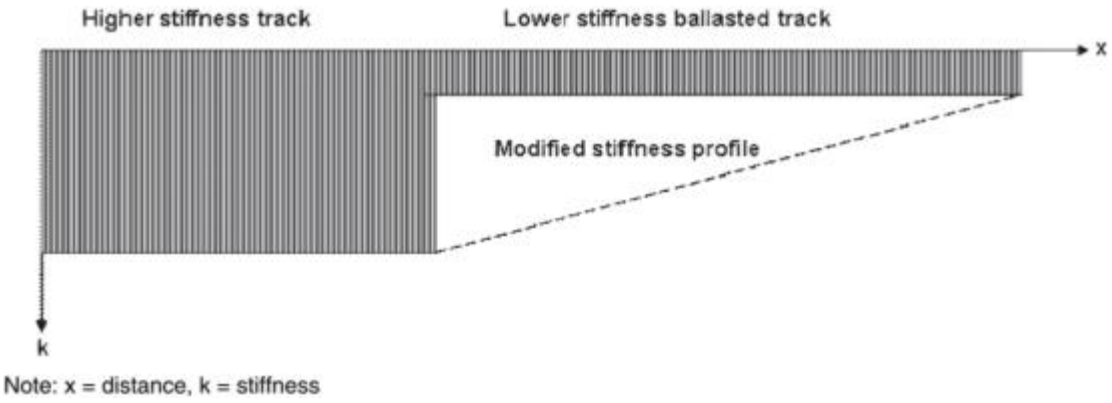

Figure 2-9: Transition remedy for gradual stiffness change (Colorado *et al*., 2006)

Although the transition zone is designed and operated to provide a smooth (seamless) transition between track sections of different stiffness, there are often some problems after repetitive traffic loading. Therefore, adequate countermeasures are required to satisfy the original design purpose. There has been some research regarding track performance at the transition zone that is based on monitoring track performance and which recommends new designs or remedies.

This section gives a short overview of recent studies in the area of the transition zone design and other critical areas in terms of abrupt changes in track stiffness, such as the turnout, which is regarded as having high stiffness, and an insulated rail joint area. In order to understand how to achieve better track performance in the transition zone and critical areas, Section 2.2.2 and Section 2.2.3 will be used to present reviews of modelling (FEM) and simulation based studies and field based research.

2.2.1 Management of Transition Zones

Two major problems at the transition zone were identified by Paixao *et al*., 2013. One is abrupt changes in track stiffness and the second is differential settlement in the foundation. In order to manage and maintain an optimal range of track stiffness values in transition zones, from the design stage, railways must monitor and manage the specific parameters. For instance, the Railway Technical Research Institute (RTRI) in Japan uses a variation ratio *between dynamic and static axle loads* ($\triangle P$) between dynamic axle loads and static axle loads such that it is an acceptable value for track stiffness management when $\triangle P$ is less than 0.13 (Lee *et al*., 2005).

$$\triangle P = \frac{P_d - P_s}{P_s} \quad (16)$$

Where,

△h: Variation of dynamic and static load rate

P_d: Dynamic Axle Loads

P_s: Static Axle Loads

Similarly, the Korean railway uses △P with the acceleration of the car body and uplift force of fasteners being measured to manage and maintain transition zones (Kang *et al*., 2002), (Yang *et al*, 2007).

2.2.2 Modelling Based Research

There is some modelling research which employs vehicle-track dynamic models to identify the vehicle-track-subgrade dynamic response. Finite Element Method (FEM) or Finite Element Analysis (FEA) are tools for material and structure analysis and are being applied to the analysis of railway structures using a computer simulator. There are multiple sub-elements that are included in the problem domain and the relevant physical laws are applied to each element. Each element and the associated physical laws are included in the matrix equation and solving this equation is enabled by the software.

The following studies have been carried out by employing the FEM and FEA modelling methods in order to anticipate the efficiency of remedies and to have a more effective design of the transition zone.

2.2.2.1 Design Consideration

Research carried out by Lei and Zhang (2010) studies the influence of different transition patterns of track stiffness on the dynamic behaviour of vehicles by utilising the FEM method. The wheel and rail forces and rail acceleration are simulated on the basis of four different designs, see Figure 2-10.

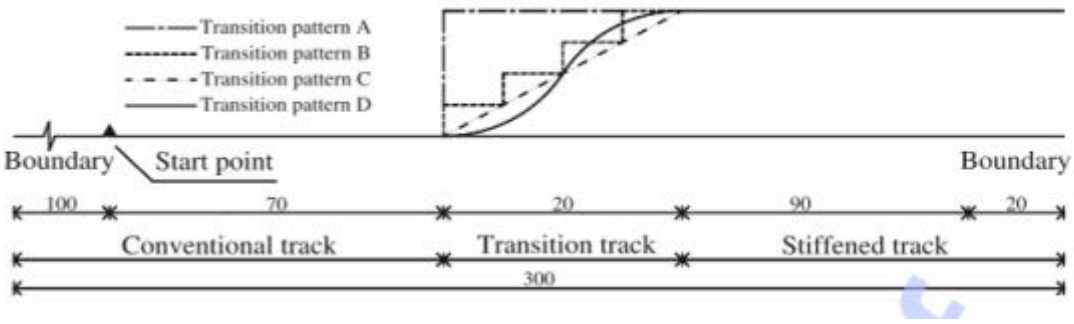

Figure 2-10: Four different patterns of transition zone (Lei and Zhang, 2010)

The result shows the dynamic behaviour of the wheel and rail, see Figure 2-11. The right hand graph shows an obvious reduction of the wheel/rail force with the application of Transition pattern D.

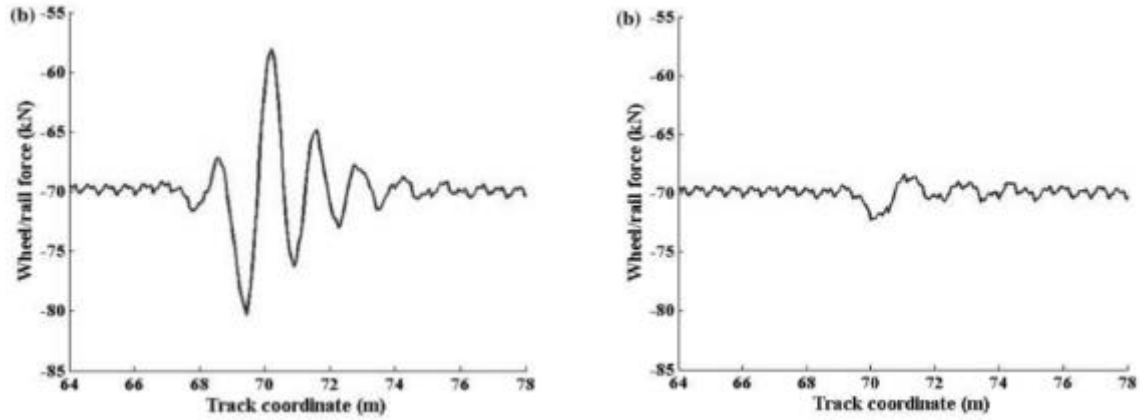

Figure 2-11: Simulation result, Left side: Pattern A and Right side: Pattern D

2.2.2.2 Design Improvement between Bridge and Embankment

Giner and Chaves (2012), who also use the finite-element method to explain a typical behaviour exhibited by embankment–structure transitions, recommend placing the granular material properly in order to avoid an excessive increase in stiffness close to the abutment, as shown in Figure 2-12.

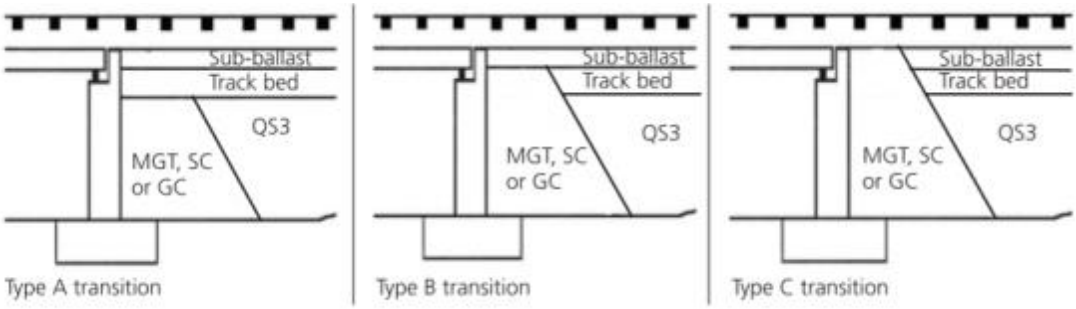

Figure 2-12: Three different types of design for placing materials (Giner and Chaves, 2012).

Lee *et al* (2010) developed a FEM to simulate the dynamic behaviour according to different lengths of approach block (Figure 2-13), and the effects of four different cases which are: no reinforcement, only using approach block, implementing approach block and slab, and approach block, slab and sub-slab all together (Figure 2-14). From the case study, the reinforcement obviously has an influence on a smooth change in stiffness when the approach block is longer, see Figure 2-15a, and when there is more reinforcement, as shown in Figure 2-15 b.

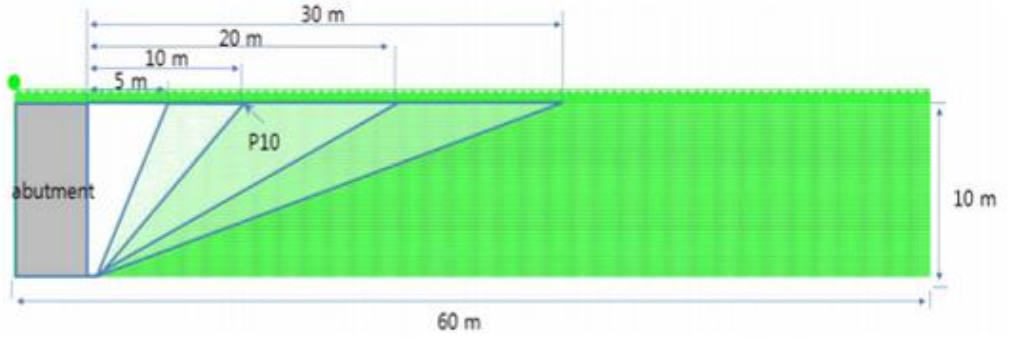

Figure 2-13: Different lengths of approach block (Lee and Kang, 2010)

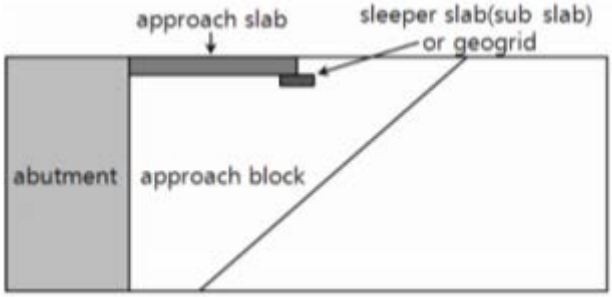

Figure 2-14: Reinforcement methods at bridge to earthwork transition (Lee and Kang, 2010)

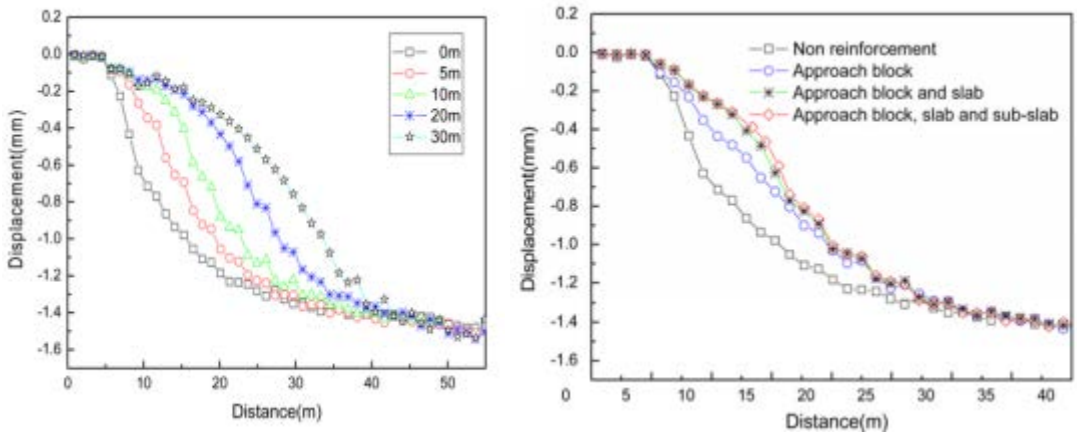

Figure 2-15 (a and b): Comparison of maximum displacement of each design application (Lee and Kang, 2010)

2.2.2.3 Design Improvement at Turnouts

Changes in support in the vicinity of switches and crossings also create changing stiffness. Abrupt changes in track stiffness around turnouts are critical since they can result in damage to the nose due to high dynamic forces, as shown in Figure 2-16. In order to reduce the dynamic force on the crossing nose, a numerical, software based study has been undertaken which recommends optimising the design of crossing noses by increasing the height and width of the beginning part of the nose (Wan *et al*., 2013).

Figure 2-16: Crossing nose and damage (Wan et al., 2013)

The simulation results show that the optimised design results in a reduction of the vertical and lateral forces on the crossing, as shown in Figure 2-17. However, the recommended design has not yet been implemented, so there will be a need to assess its performance after implementation.

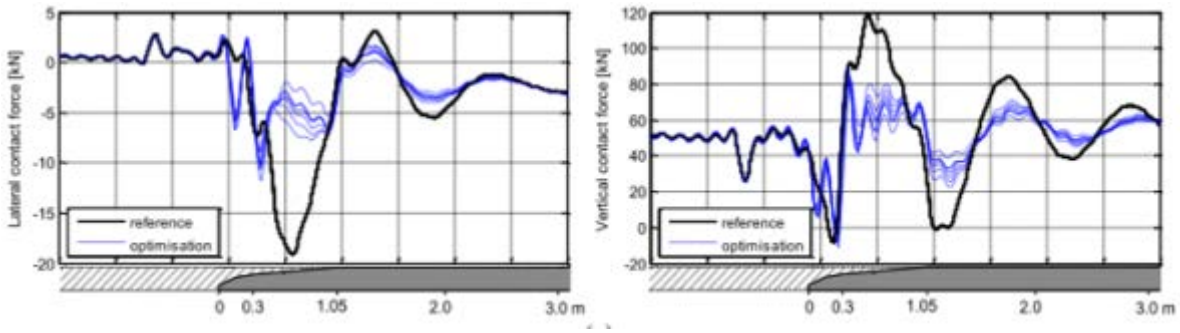

Figure 2-17: Lateral and vertical forces at the crossing (Wan *et al*., 2013)

2.2.2.4 Prediction of the Performance on Insulated Joints

An insulated joint is used to electrically separate track circuit sections, in particular between signalling blocks or around crossovers. The joint presents a track discontinuity, therefore, if it is not properly maintained, vehicles running over the insulated joint introduce dynamic interaction and forces, resulting in rail damage and dynamic loading on the sleeper. The vertical strain over the insulated joint has been simulated and tested in the field in order to predict impact loading (Zong *et al*., 2013) as shown in Figure 2-18.

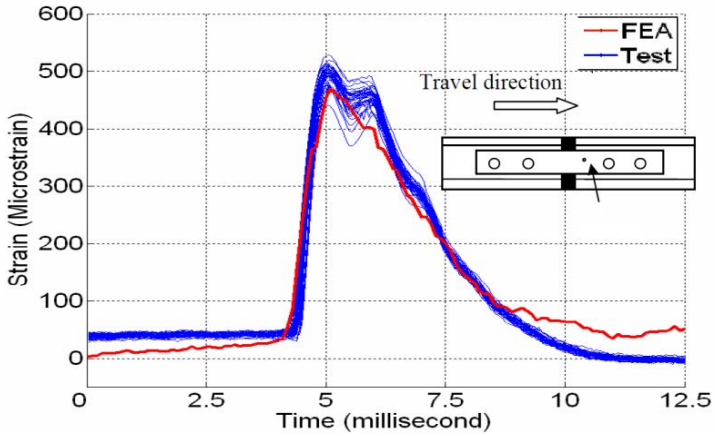

Figure 2-18: Measurement of vertical strains and simulation result

2.2.2.5 Effectiveness of Remedies between Two Different Types of Track Form

Kang *et al* developed a simulation programme to help understand the transition zone between a concrete slab track and ballasted track (Kang *et al*., 2006). In order to improve performance at the transition zone between the slab track and ballasted track, simulation and a validation test were conducted to evaluate the effectiveness of remedies on the newly built Jeolla-line of Korean Railways. Auxiliary rails were installed between the running rails at transition zones to attempt to create a smooth transition between two different types of track form, as shown in Figure 2-19.

Figure 2-19: Installation of additional rails (Kang *et al*., 2006)

Rail pads were also installed in order to create a gradual change in track stiffness. The graph shows the effectiveness of the gradual change in track stiffness by installing the auxiliary rails and placing the pads as shown in Figure 2-20.

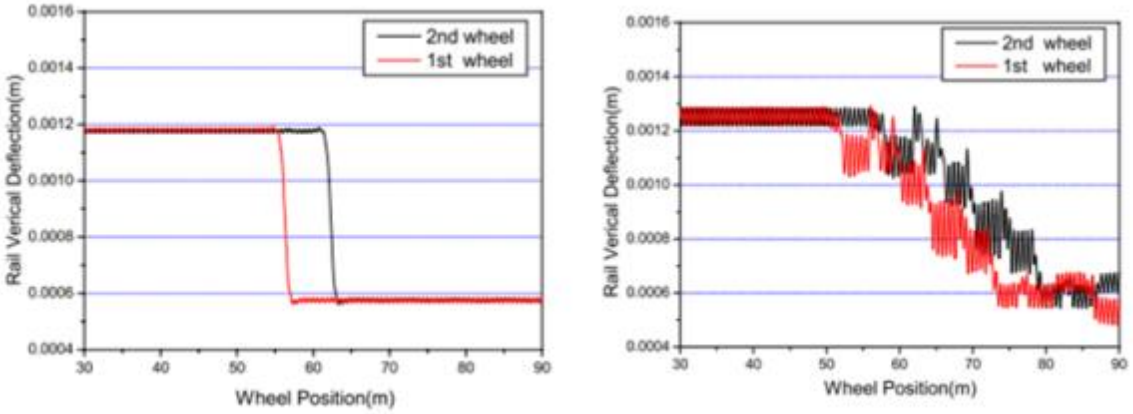

Figure 2-20: Rail vertical displacement before and after improvement (Kang et al., 2006)

Similarly, Xin *et al* also conducted a simulation study to see how the performance of two types of adjacent track forms can increase the change in track stiffness between two different types of tracks and recommend countermeasures (Xin *et al*., 2014).

2.2.3 Field Assessment of Performance at Transition Zones

Section 2.2.2 described research that uses numerical technique (FEM) to simulate the dynamic performance of vehicle and track to investigate the impact of a better design or remedial solution. To date, a relatively small volume of field research has been carried out in transition zones such as at tunnels, bridges, culverts and zones between slab track and ballast track to observe dynamic track performance. In this section, identified mechanisms from other research on the transition zone are introduced. However, the detailed information regarding technologies and methods adopted will be introduced in the next chapter.

2.2.3.1 Field Test between Tunnel and Embankment

Research has been carried out to monitor the performance of transition zones between embankments and tunnels in South Korea (Lee *et al*, 2005). The work studied tunnels which are single track, therefore trains run bi-directionally, as shown in Figure 2-21.

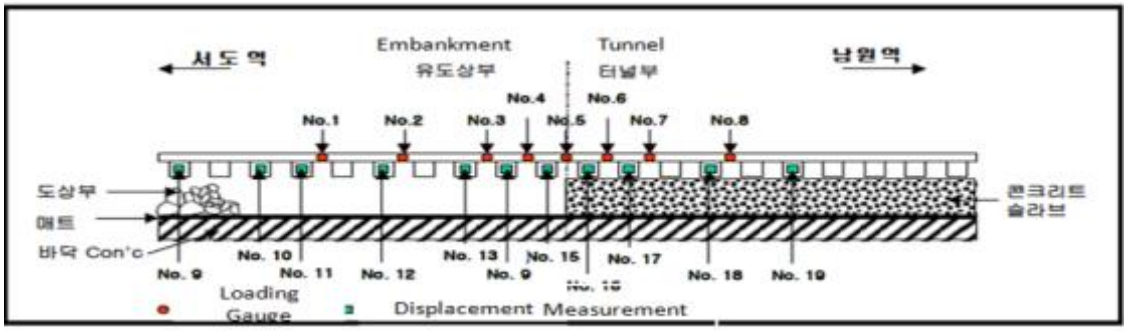

Figure 2-21: Layout for the experimental site (Lee et al, 2005)

The sleeper vertical displacement and axle-loads were measured and the bi-directional running effects between a tunnel and embankment were monitored, e.g. high stiffness to low stiffness and vice versa.

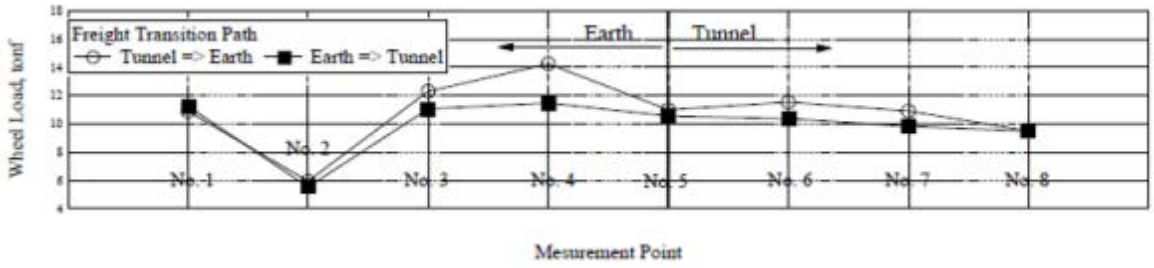

Figure 2-22: Dynamic wheel loads for two directions (Lee et al, 2005)

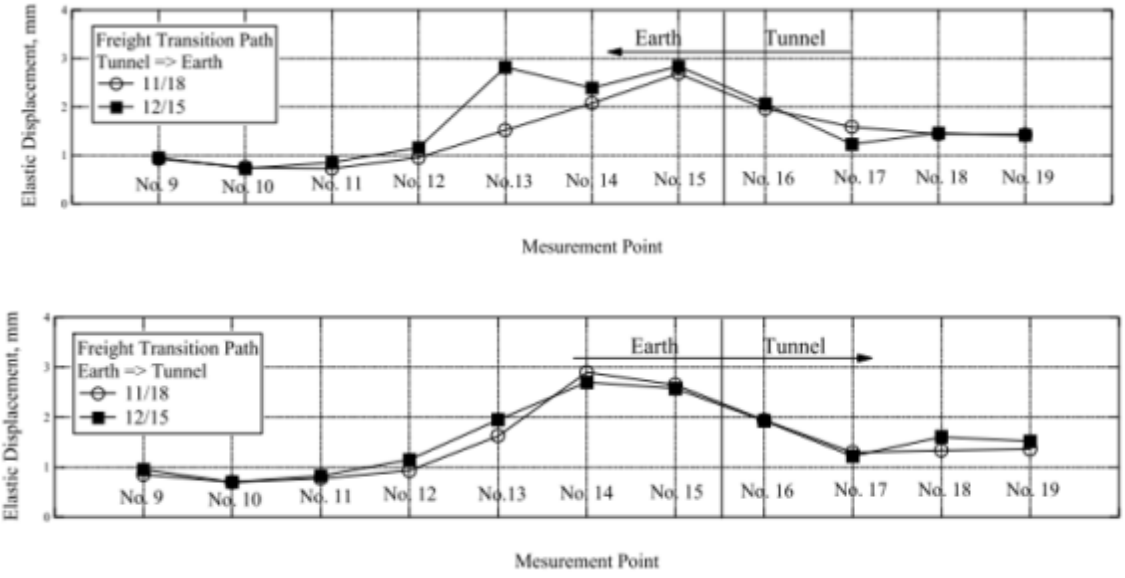

Figure 2-23 Displacement data when train moves in two directions (Lee et al, 2005)

Overall research shows that the variation of dynamic loads of each sleeper is higher on an embankment compared to a tunnel when the train moves from the high tunnel stiffness to the low embankment stiffness. However, when the train moves from the embankment to the tunnel the dynamic load of each sleeper is kept relatively constant, see Figure 2-22.

Figure 2-23 shows the displacement data for a train running in both directions after a time gap (one month). More displacement was found on the embankment when the train runs from the tunnel to the embankment (Figure 2-22). However, the variation of the displacement at the tunnel end (Sleeper No 16.) is relatively small.

This study shows the performance of a localised track in a tunnel. However, the constraint of this study is that the root cause of the problem is not specified in the research paper.

2.2.3.2 Field Test between Bridges and Embankment

It is known that the variation in stiffness between bridge and embankment is relatively high compared with that between a tunnel and an embankment. Therefore, more studies have been conducted on the transition zone of bridges (Lee *et al*., 2005). Li *et al* present research into the problems associated with railway bridges and approaches, discuss their root causes and effective solutions. Problems on railway bridges include rapid track degradation, mud pumping and track component damage (Li *et al*., 2010). These problems are caused by geotechnical issues, track drainage conditions, inadequate track resilience and inconsistent lateral track strength. The Federal Railroad Authority (FRA) track transition study (Plotkin *et al*., 2006) also shows the large change in stiffness between open track and a bridge, which is measured by the Track Loading Vehicle (TLV). Dynamic wheel loads and track stiffness are measured. As shown in Figure 2-24, the modulus at the approach block is 30-50 (N/mm/mm) and 60-80 (N/mm/mm) at the bridge.

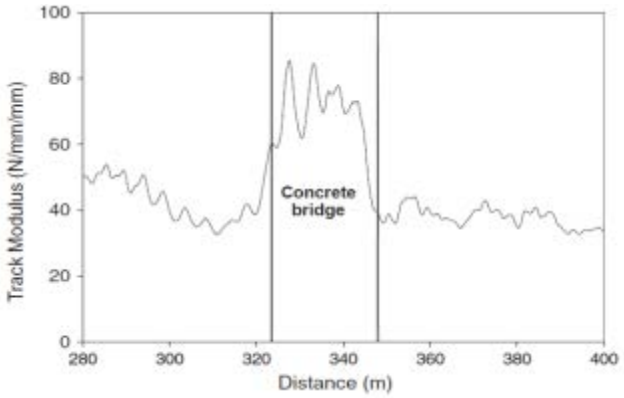

Figure 2-24: Change of vertical track modulus (Li *et al*., 2010)

After these field experimental studies, the use of ballast mats and rubber pads were recommended and implemented to reduce track stiffness on bridges. In addition, stone columns were recommended to strengthen the weak subgrade soil on the approach section.

2.2.3.3 Field Test at Culverts and Approach Slab

A railway culvert is a small structure under a railway line, usually made from brick or concrete, that allows water to flow under the railway line. Culverts are commonly buried shallowly under the railway, which can lead to abrupt changes in stiffness. Commonly an approach slab is implemented to help smooth the difference in track stiffness, as shown in Figure 2-25 (a).

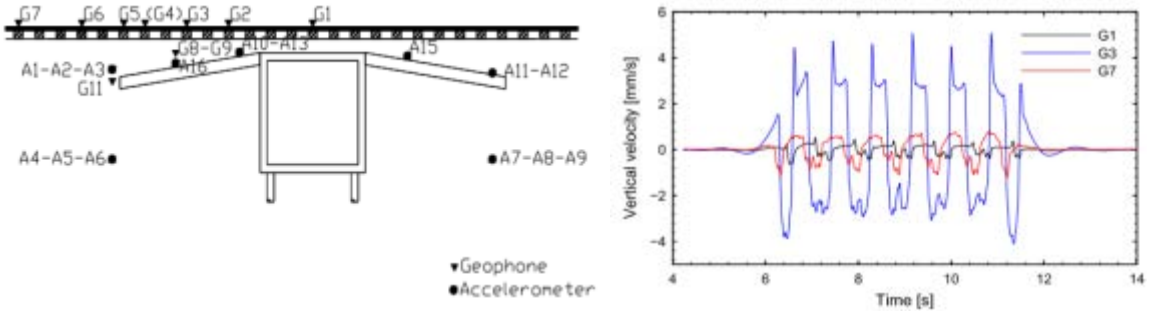

Figure 2-25 (a / b): Performance of approach slab, Dutch Railway (Coelho et al., 2011)

Research aimed at monitoring culverts and corresponding approach slabs concluded poor performance of transition zones. Research by Coelho *et al*., 2009 monitored the transition zones at culverts and found poor performance. The research presents data on the dynamic behaviour of the track between the open track and a concrete culvert on the Dutch Railways. The displacement measurement was carried out at different depths, for different types of scheduled trains. A long term investigation was also conducted to monitor the track settlement and the change in pore water pressure for over a year (Coelho *et al*., 2011). This research found that the approach slab has lower stiffness compared to open track and culverts. The vertical displacement over the approach slab was 8 times higher than open track, as shown in Figure 2-25(b). The research found that there was large settlement over transition zones, so the design purpose of the transition zone was not accomplished, which is due to the unsupported sleeper on the approach slab. This resulted from the different ballast compaction due to the dynamic train loading and the following amplified differential ballast settlement, which is a repetitive process.

Coelho *et al* concluded that a clear understanding of the ground conditions at the track site is important when the transition zone is designed. Also, the permanent and dynamic movement and possible intervention from other behaviours of relevant structures must be understood.

2.2.3.4 Sleeper Displacement Measurement at Switches and Crossings

As mentioned in Section 2.2.2, dynamic wheel/rail force over the crossing area can cause damage to a turnout and its components. A number of researchers have considered the dynamic response of the turnout and crossing area (Kaewunruen, 2014), (Liu *et al*., 2014). Liu *et al* monitored the dynamic movement of a sleeper under the stock rail before and after tamping and after the crossing nose frog renewal, as shown in Figure 2-26.

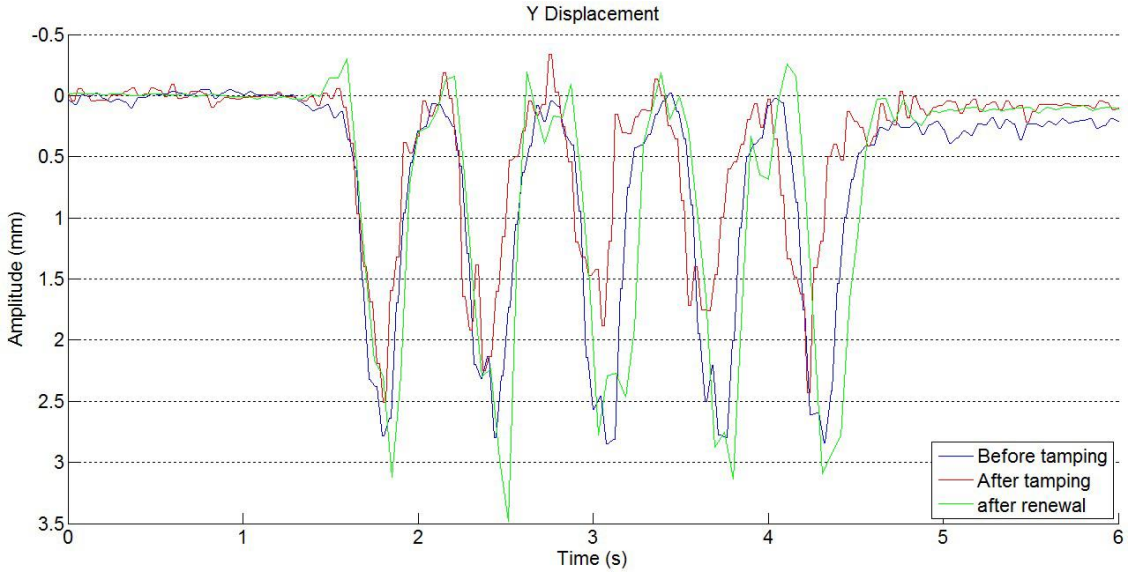

Figure 2-26: Vertical displacement before and after tamping and crossing renewal

The research found that optimising the geometry in the crossing zone results in reducing the dynamic forces in the crossing area and relatively increases the dynamic force on the stock rail due to equalising the force between them.

2.2.3.5 Level Crossings

Insufficient research has been conducted on level crossings to measure track stiffness compared to other structures. The behaviour of transition zones onto a level crossing was monitored using a geophone and remote video recording system (Le Pen *et al*., 2014) as shown in Figure 2-27. This research found that maintenance work and tamping has not been effective for many unsupported sleepers, as the nature of the structure of level crossings makes them difficult to access in order to carry out maintenance work.

Figure 2-27: Monitoring of level crossings (a: Geophone, b: Video recording system) (Le Pen *et al*., 2014)

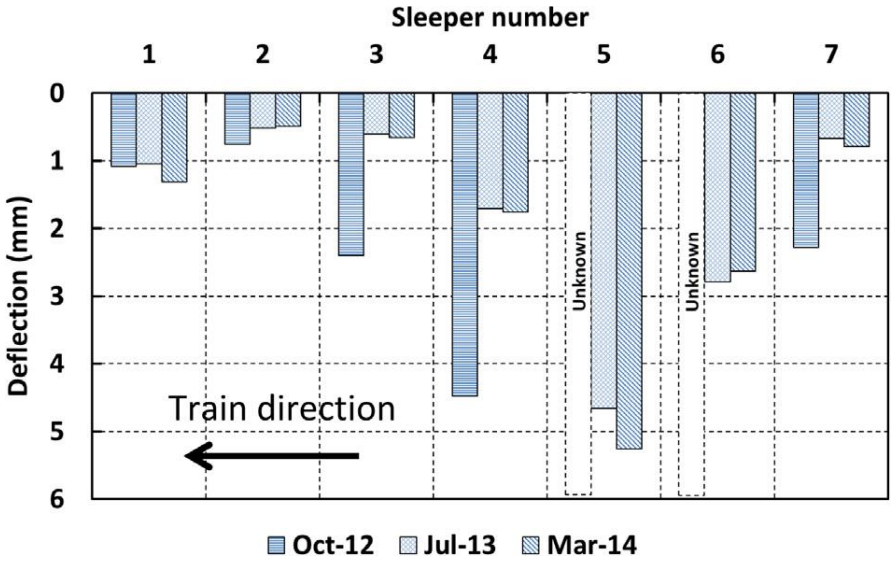

Figure 2-28: Sleeper movements for three measurements (Le Pen *et al*., 2014)

As plotted in Figure 2-28, data from sleepers 5 and 6 shows poor performance with a large range of deflection, up to 5 mm. Tamping had been conducted before the second measurement, therefore it was found that tamping was not very effective in improving the track near the level crossing.

2.3 Summary for Chapter 2

Track stiffness and modulus are important parameters to help understand the track condition, particularly the substructure. Theoretically, stiffness is defined as the ratio between the vertical force on top of one rail and the vertical track displacement. It is essential to measure the track deflection to assess its stiffness. Winkler's theory and Zimmermann's method is a classical tool to calculate the deflection of multiple points where a number of loads are applied, however, it is not entirely realistic since some factors which have an influence on the dynamic performance are neglected due to the hypotheses on which the theories are based. For instance, discrete support is neglected in this approach. Nonetheless, the BOEF theory still enables an assessment of the track stiffness that can be used as an indicator of the condition of the subgrade and that shows the approximate level of deflection that can be expected because of by the variation in track and vehicle condition. In reality, stiffness is a dynamic parameter, which is assessed best by a rolling measurement that reflects reality, such as track geometry, the wheel and rail interface, running speed and, most importantly, foundation condition. Local stiffness considers each different layer of the track, which is relatively complicated to measure, e.g. undertaking a destructive penetration test, whereas global stiffness gives an overall integrated stiffness of

all relevant components of the track, can be achieved for rapid assessment of subgrade condition, and is relatively simple to assess by monitoring vertical displacement and velocity or acceleration of track movement.

Although the transition zone is a critical area in terms of maintenance cost and requires more maintenance interventions compared to a straight section of track, insufficient research has been carried out to find an understandable mechanism for the transition zone. Two and three dimensional FEM is a powerful method that can be applied to estimate the deflection relatively precisely, so most research to date has been in the area of software based track/vehicle modelling methods to validate recommended designs or remedies. In the literature recommended designs which aim to improve track stiffness or modulus are introduced. In order to validate the modelling methods, dynamic based field tests should be conducted before and after the new design application. Different remedies are also presented in the literature. After implementing the recommended measures on the track, the efficiency of the remedies should be assessed. Some field case studies have been conducted to understand the mechanism of the transition zone behaviour, however, most of the studies have monitored the bridge and embankment transition areas and a relatively small amount of research has been conducted in the tunnel to embankment, S&C, ballasted track to ballast-less track and level crossings areas. Therefore, it appears that more research is required in these areas.

The research by Priest & Powrie (2009), Lee et al (2005), Li et al (2010) clearly shows that observing dynamic response over sleepers caused by the application of axle loads is useful to assess dynamic stiffness or modulus. This suggests that it is appropriate to find a simpler and more rapid method of subgrade assessment by monitoring the sleeper response by means of physical measurements. In addition, different methods and technologies were applied to assess the subgrade condition. In the next chapter, the author describes current practices used in the measurement of track stiffness or modulus and how each parameter can be reproduced from the different types of systems. Then, the author will summarise technologies which may be practically applied in this research. In Chapter 4 a design plan is established to develop a deflection measurement system by summarising recent trends for evaluating the performance of the transition zone from Chapters 2 and 3.

3 A Review of Current Practices and Techniques

In Chapter 2, the author noted the importance of assessing track stiffness in order to obtain a better understanding of the condition of the substructure, since this knowledge is necessary to support improved design and more effective maintenance work. In Chapter 3 the author summarises the tools used to date to assess track quality for railways and relevant techniques, as shown in Figure 3-1.

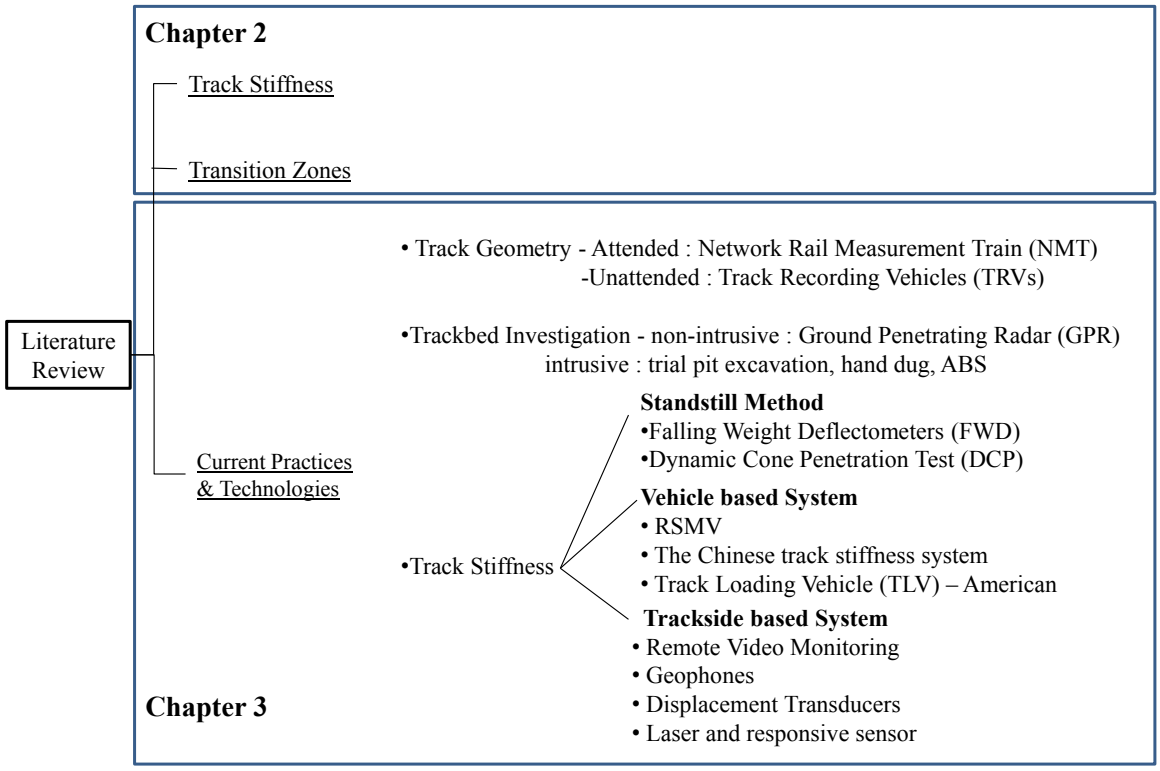

Figure 3-1: Scope of literature review for Chapter 3

Figure 3-2 shows the correlation between track deflection and track quality.

As found in Chapter 2, the deflection response of the track is a good indicator for the condition of substructure. In this chapter, in order to investigate and evaluate appropriate methods to measure track stiffness in transition zones and in critical zones, current practices and relevant parameters and techniques will be reviewed, with a discussion of their advantages and drawbacks.

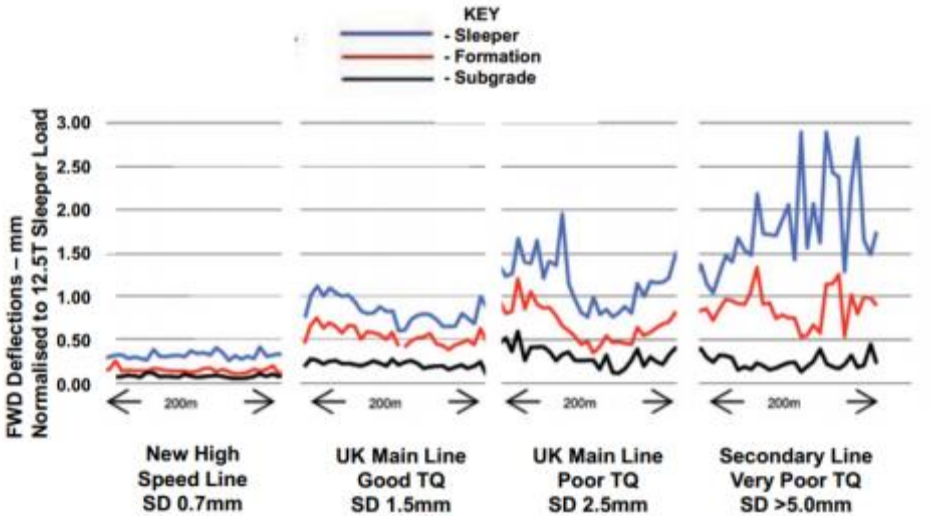

Figure 3-2: The relationship between track stiffness and track quality (Hakim, 2013)

The chapter will conclude with a discussion and decision as to which technologies shall be adopted or approached for this research in order to develop a measurement system to measure track stiffness more efficiently. By utilising current techniques and methods available to measure displacement of track, trackbed condition and track geometry, track quality has been identified. In general, the methods are divided into two categories depending on the location of the monitoring position, being either vehicle based or trackside measurement systems.

3.1 Track Quality Measurement

The railway track system consists of substructure and superstructure, as shown in Figure 3-3. In general, the focus of recent track maintenance work has been on the performance of superstructure rather than the condition of substructure, such as subgrade and soil layers. Traditionally, the condition of track superstructure has been assessed by measuring track geometry. The geometry measurement system will be reviewed in Subsection 3.1.1.

The substructure condition should be assessed to find the root cause of problems. Track settlement can be a factor in track geometry deterioration since it induces long wavelength irregularities of the track both vertically and laterally (Iwnicki and Dahlberg, 2006). More importantly, track stiffness information should be obtained, as it is more relevant to the condition of the structure and it complements track quality information, together with track geometry (Section 3.1.1), track settlement and trackbed strength data (Section 3.1.2). Therefore, in order to assist track quality management, which already measures the change in track geometry on a routine basis, track settlement and strength and track stiffness

should also be monitored to evaluate the deterioration rate of track geometry over a period of time.

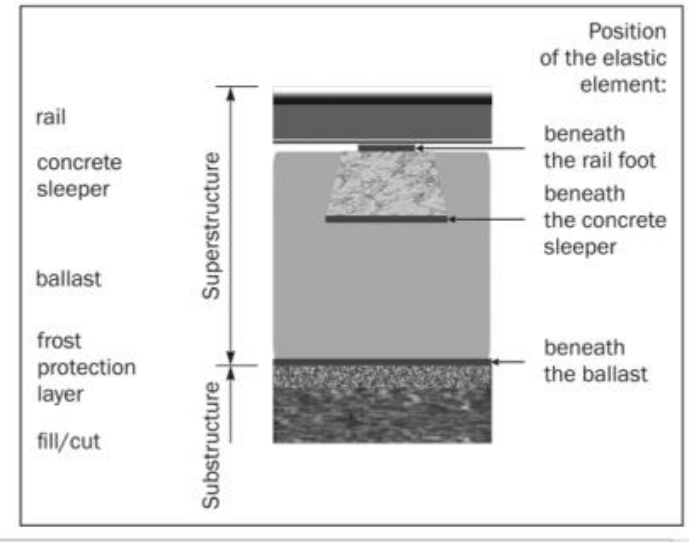

Figure 3-3: Substructure and superstructure (Puzavac *et al*., 2012)

3.1.1 Measurement System of Track Geometry

It is mandatory to measure track geometry in most countries. Depending on the measurement of loading or non-loading track geometry, there are two types of system. Non loaded track geometry is measured using a trolley based system. Loaded track geometry measurement systems are categorised into two groups, which are attended and unattended systems, as below.

For the attended routine inspection of railway track, infrastructure managers in different countries developed their own bespoke Track Recording Vehicles (TRVs), e.g., Doctor Yellow for the Japanese railways, the Infranord Measurement Vehicle (IMV) for Sweden's railways, the New Measurement Train (NMT) for Network Rail, see Figure 3-4, etc.

Figure 3-4: The NMT, a typical track recording vehicle (Charles Watson, 2013)

Over the mainline railway network in the UK, the running speed of the NMT is up to 125 mph and it runs every two weeks on main routes while the inspection of slower speed lines is scheduled at 8,12,16 and 24 weeks (Lewis, 2011). In order to analyse the track geometry quality, the TRVs measure primary parameters, such as track gauge, vertical profile (longitudinal level), cross level, horizontal profile (alignment) and twist. For data processing, the long wavelengths are removed by filtering the data for these parameters. The processed data are analysed by mean value, extreme value and standard deviation over a certain distance, normally 200 m or one eighth of a mile, to describe the track geometry quality (British Standard, 2010). The result is reported to the engineers to aid their maintenance decision. Figure 3-5 shows an example of a chart report that provides the profile of track data.

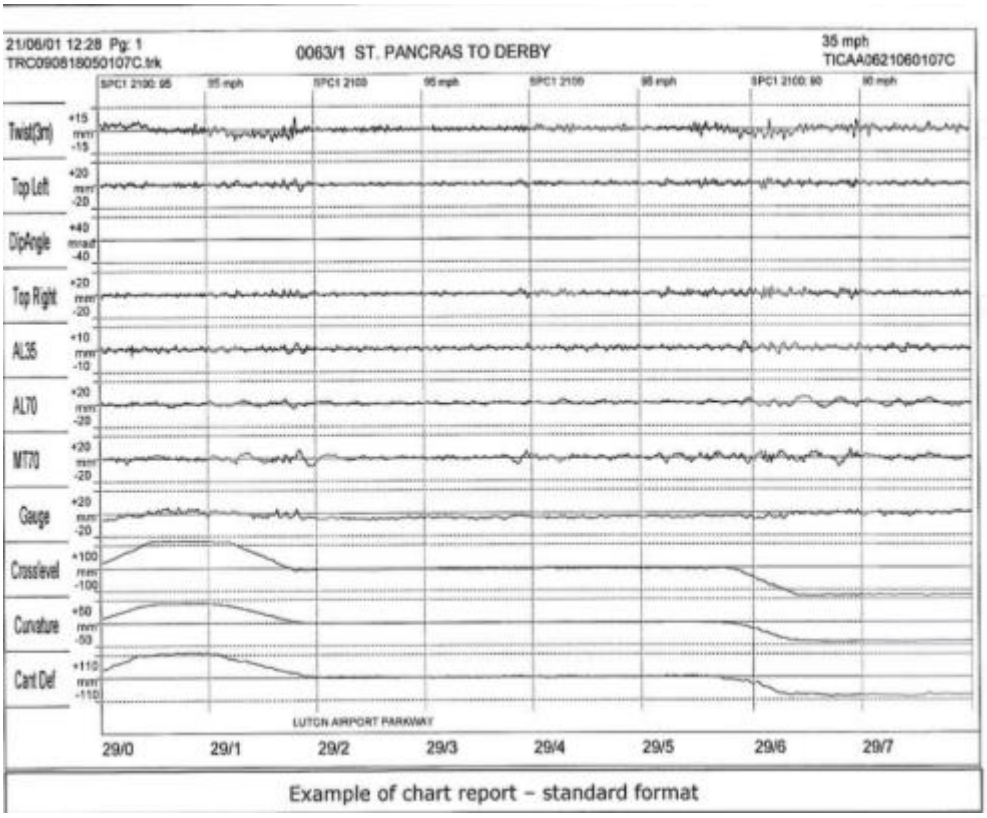

Figure 3-5: Example of NMT report (Lewis, 2011)

The report shows the variation of each parameter and the respective thresholds, based on the line speed. It also reports on the urgency of the required interventions, depending on the scale of variation. If the pattern of a graph is displayed in an unusual way, this could give an indication of the root cause of the poor track quality. For example, if a reported twist is sharp, with a large dip angle spike, then it could be a broken rail or fishplate. If it

manifests itself over some distance, then it is more likely to be a wet spot or a set of voided sleepers (Lewis, 2011).

Two different techniques are used to measure these parameters, which are referred to as the chord offset and inertial measurement. The chord offset has been widely used in the past and it is still used in railway systems. The principle is that three points are measured along a track; the chord offset can then be drawn, as shown in Figure 3-6.

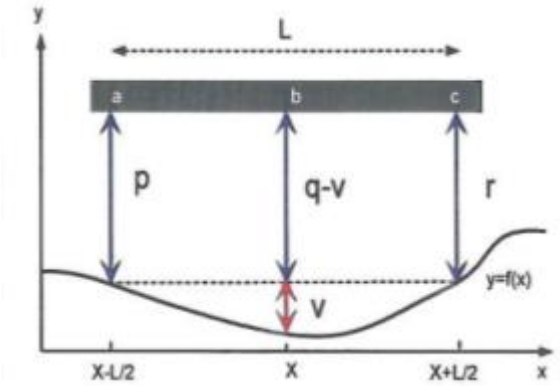

Figure 3-6: Chord offset measurement (Lewis, 2011)

The advantage of this method is that it works at zero speed. However, it is not easy to use in a vehicle based system, so an inertial system has to be created. Various types of sensors, such as gyroscopes and accelerometers, are used to sense the displacement of a mass. For example, the accelerometer signal is double integrated with respect to time and it produces the shape of the track surface. The typical system is as shown in Figure 3-7. Equally, gyroscopes can be used to measure twist and curves.

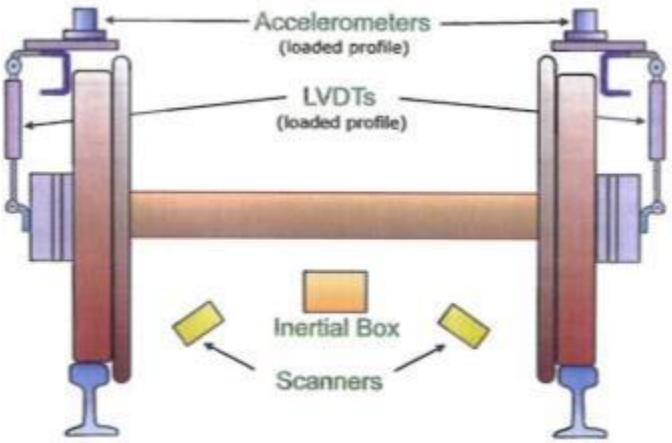

Figure 3-7: Typical layout of inertial system (Lewis, 2011)

Nowadays, as a cost-effective approach using the inertial method, sensors are fitted on passenger trains to measure track geometry, which is an unattended method. Some systems

use gyroscopes and accelerometers, which are mounted on the bogie or axle-box, to monitor the vertical irregularity (Weston *et al*., 2007b), lateral irregularly (Weston *et al*., 2007a), train speed and track defects. In some other cases, the monitoring system is situated in the car (Nielsen *et al*., 2013). The advantage of this method is that there is no traffic disruption during the measurement of track geometry, as service trains are used, and there is the capability for the continuous monitoring of track. Therefore, track geometry can be monitored more often than by using a special purpose vehicle. By enclosing triaxial sensors in an inertial box and using non-contact optical sensors, the vertical profile can be measured. The linear variable differential transformer (LVDT) produces a vertical profile during the loaded and unloaded state. The difference between the two profiles could give an indication of voided sleepers, but this has not yet been proved (Lewis, 2011). The inertial method has not been widely introduced on rail networks, as it has been viewed by maintainers and operators as an unnecessary complexity. Table 3-1 summarises the two types of track geometry measurement system.

Table 3-1: A summary of track geometry measurement systems

Type of devices	Operation	Parameters/Units	Comments
Attended method : Track geometry vehicle(e.g., NMT)	Regular operation using the chord offset method or the inertial measurement method	Measure of variation standard deviation (SD), lower and upper limit for each parameters	An effective tool that has been introduced on a network widely.
Unattended sensor mounted vehicle	Daily running operation using inertial measurement, more frequency data collection	Measure of variation standard deviation (SD), lower and upper limit for each parameters	The loaded profile could give an indication of voided sleepers but this has not been proven yet (Lewis, 2011).

3.1.2 Measurement System for Trackbed Investigation

A Trackbed in poor condition can fail to retain a good geometry. Therefore, various approaches are adopted to investigate the trackbed interface to find the root causes the rapid deterioration of track geometry. The approaches are categorised into two groups; intrusive methods and non-intrusive methods. Ground Penetrating Radar (GPR) is an effective method which can be used to give information on layering, material type, moisture content and variation. It is a non-destructive inspection method that uses a radio wave source to transmit a series of very short electromagnetic pulses (generally 10 MHz to 1,000 MHz) into the inspected structure, which last a maximum of 10 ns each. The

reflected energy is received by an antenna and recorded for data analysis (Silvast *et al*, 2010). Figure 3-8 shows that it is possible to obtain information about different layers and depth without excessive digging work by using GPR inspection.

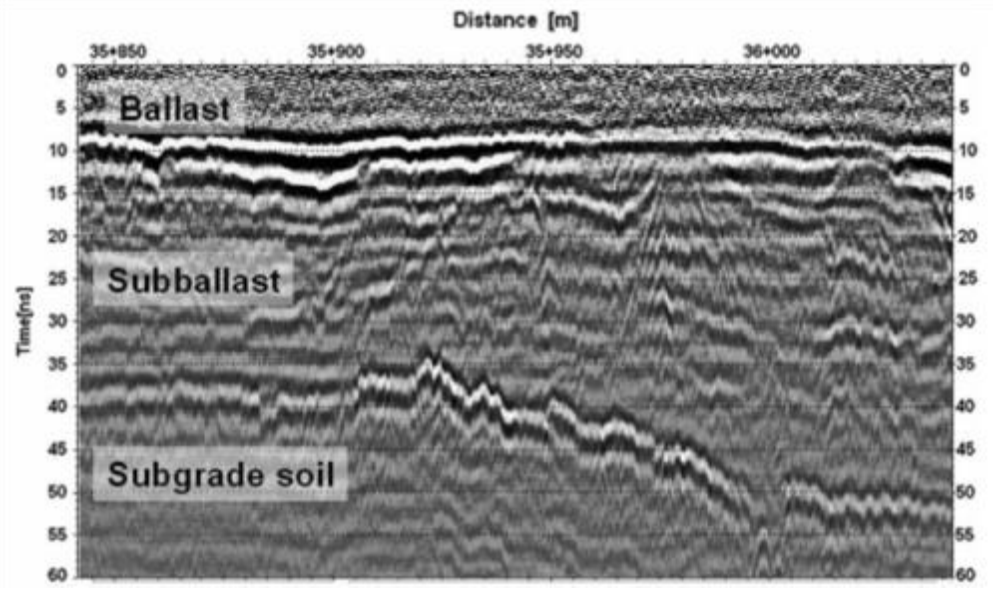

Figure 3-8: Example of GPR processing data (Silvast et al., 2010)

GPR technology is employed with different types of GPR systems, such as train mounted systems, lightweight road trucks (see Figure 3-9) or carried by hand.

Figure 3-9: Railway truck with GPR system attached front (Silvast *et al*., 2010)

GPR technology has been extensively adopted to carry out substructure inspection. GPR has been used to detect fouled ballast, classify ballast degradation (Silvast *et al*., 2010) and water content (Berggren, 2010). The GPR survey results help to develop preventative maintenance planning. GPR is also adopted to measure the variation in depth of ballast and monitor the position of the approach slab (Coelho *et al*., 2009).

The major limitations of GPR have been identified by Sorge (Sorge, 2008). The difficulty of estimation of the ground dielectric property with standard GPR antennae is identified. The inaccuracy of positioning of the collected data is also a problem due to fast moving platforms. In addition, the lack of both automatic data interpretation tools and an integrated software approach for long-term monitoring of large railway infrastructures have been identified as limitations of this technology. Furthermore, the GPR method can be sensitive to noise from vehicles, buildings, fences, power lines and trees, all of which can cause unwanted reflections or scattering. The interpretation of data collected through GPR methods can be subjective, especially if interference is not attributed correctly (Beres & Haeni, 1991).

Recent improvements in GPR systems which are mounted under passenger trains have enabled these systems to acquire good quality data at line speeds of 100 km/h (Eriksen *et al.*, 2006). The cost of the track possession process is also eliminated.

Table 3-2: Strengths and weaknesses of using GPR

Strengths	Weaknesses
• It is possible to make a link between poor quality track geometry and the data from the GPR trace. • The identification of changes in the interface of track substructure is accurate, so it supports the efficient planning of a intrusive investigation.	• Cost of hiring a device and the requirement for a specially trained engineer • Terrain must be flat and even • Sensitive operation in clay due to signal loss

In general, the GPR trace can be used to find a link between track the geometry data and the GPR data, but intrusive methods are normally added for the design of remedial work. A trial pit excavation or a dynamic cone penetrometer, both intrusive methods, are used to investigate the condition of the substructure, and are sometimes adopted to validate the results of the GPR method. Trial pit excavation, or trial holes, is a typical method to obtain a sample of the structure of the subgrade by excavation of the ground. Similarly, hand dug trial holes are used to investigate trackbed conditions, with a typical depth of 0.5 m. In recent years, the Automatic Ballast Sampler (ABS) has been used widely to obtain samples of the ballast and the underlying layers using 1 m long heavy duty steel tubes driven into the ground, typically to depths of 1 m or up to 2 m below the base of the ballast. The following table shows a comparison of the productivity of the two intrusive methods.

Table 3-3: Comparison of hand dug trial pits and Automatic Ballast Sampling

Attribute	Hand Dug Trial Holes	ABS
Description	Excavated using hand digging and spoon shovels under the ballast layer	Percussive coring device that takes a continuous sample through the trackbed using a hydraulically powered hammer.
Challenges	In situ sampling is time consuming and obstructions can seriously reduce productivity.	Only a small sample can be collected and lateral variations cannot be investigated.
Engineer on site	Required	Not required
Productivity	15 No. Shallow (< 0.5 m) 10 No. Deep (< 1 m)	40 No. to 1 m 15 No to 2 m

Overall, the major benefit of the application of the GPR system to the railway is the assessment of trackbed condition using a non-intrusive site investigation method which acquires continuous information on the layering of the trackbed, while further information from a trial dig or ABS will be required to get a real sample and better information on the stiffness of the materials. Therefore, these techniques are useful where track stiffness is investigated in the field (Berggren, 2010), (Coelho *et al*., 2011), (Hendry *et al*., 2010).

3.2 Measurement Systems for Track Stiffness and Pavement Deflection

Current trends and concepts which have been adopted by the railway to measure track geometry and to investigate trackbed condition are reviewed in the first section of this chapter. Over the past two decades, track stiffness measurement systems have been researched, developed and are starting to be commercialised, with the aim of finding the root cause of the following issues:

1) Variation in track stiffness along the railway track;
2) Abrupt changes in track stiffness at the transition zone and critical zones;
3) Overhanging sleeper issues and insufficient support from the foundation.

In order to include current trends and concepts which can be adopted by the railway, technologies and methods of investigating road pavement condition are briefly reviewed in the first part of this section, since significant research has been done in this area since the 1950s and 1960s. Standstill, semi-standstill and dynamic measurement systems will be reviewed in the last part of this section, including both laboratory and field-site test methods.

3.2.1 Pavement Deflection Measurement System

The Benkelman Beam (BB) Deflection technique, see Figure 3-10, is a method of evaluating the structural condition of the pavement using a portable device. It measures a discrete part of a certain length of pavement and has been in use since the 1950s. It is a low cost and cheap device, approximately 1/30th of the FWD cost (Molenaar, 2006), however, it is a labour intensive device.

Figure 3-10: The Benkelman Beam (Molenaar, 2006),

Internationally, FWD is the most extensively used method to measure pavement deflection. It evaluates the pavement condition by dropping a pre-defined load at a range of 30 kN and 250 kN to the pavement, then the deflections are measured directly under the load from several geophones at set distances from the loading and the deflection bowl is recorded, see Figure 3-11.

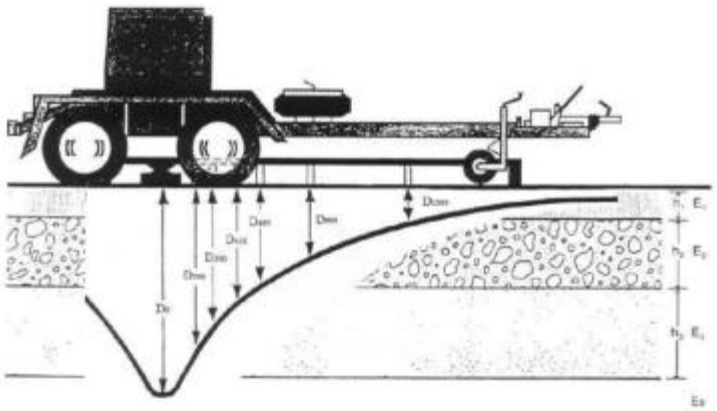

Figure 3-11: Principle of the Falling Weight Deflectometer operation (Molenaar, 2006)

An accuracy of 0.1 mm can be achieved with an FWD (Arnold et al., 2009).

The challenge is that FWD operation causes traffic disruption due to its slow movement along the track. In addition, it uses geophones, so a sensitivity issue should be considered due to the nature of the sensor. Furthermore, the stiffeness of the rubber pad used is dependent on the ambient temperature (Molenaar, 2006), therefore the values vary with the temperature. This will be discussed in Section 3.2.4.

The Deflectograph (see Figure 3-12) has been applied since the late 1960s and has been used to measure the deflection of the pavement under prescribed loads for routine maintenance work for 30 years. It originated from the French system, referred to as the Lacroix deflectograph. Both FWD and the Deflectograph are currently in use for the measurement of the structural condition of the pavement. The operating speed of the Deflectograph is up to 2.5 km/h and it measures the deflection of the pavement at a spacing of every 3 to 4 m. The Deflectograph operates automatically following the principle of the Benkelman Beam Deflection technique. Thus more measurements can be taken with the Deflectograph compared to the BB in the same time period.

Figure 3-12: Deflectograph beam to measure deflection of pavement

These systems are expensive to operate in terms of running speed and the possible disturbance to road users. These issues have motivated research into a better continuous measurement method which can be used at normal road speeds. A Traffic Speed Deflectometer (TSD) is being developed by the English Highways Agency, on the basis of a prototype of the Danish TSD, to provide an improved method of measuring deflection velocity rather than velocity to assess pavement condition. The TSD is designed to use four non-contact laser sensors using the Doppler Effect to measure the vertical velocity of the road pavement. The research (Ferne *et al*., 2009), (Jenkins, 2009) proves that the TSD can

be used to assess the pavement condition at speeds up to 100 km/h. The tools used for the assessment of the structural condition of pavement systems have been developed so that they are capable of measuring faster and automatically, with better accuracy. Now the challenge is to improve the procedure of assessing the condition of track or road so that it is less labour intensive and does not require occupancy of the track or road. It is necessary to find an effective method which does not occupy the track during the assessment process.

3.2.2 Measurement of Trackbed Stiffness

The value of the trackbed stiffness is a major element in ensuring satisfactory track geometry and it gives an excellent indicator of trackbed performance. Standstill measurement devices are used to measure the vertical track stiffness at discrete intervals. The impact hammer, the FWD and track loading vehicles are categorised as standstill methods. Internationally, the FWD is the most frequently used method to measure pavement deflection, although the FWD operation causes traffic disruption due to its slow movement. It evaluates the pavement condition by dropping a pre-defined load in a range from 30 kN to 250 kN onto the pavement. The deflections (mm) are then measured directly under the load by several geophones at set distances from the load impact, and the deflection bowl is recorded, see Figure 3-13.

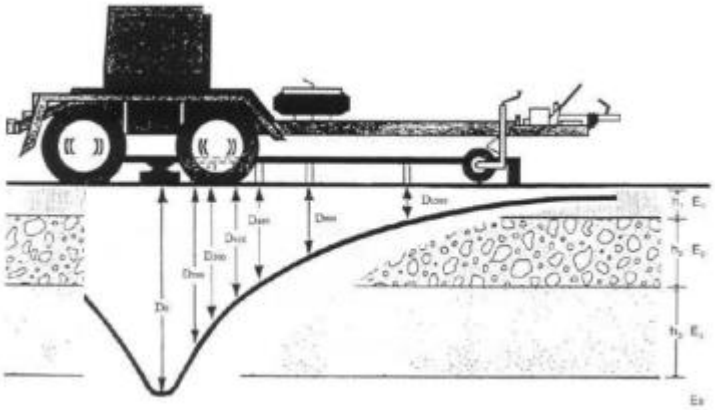

Figure 3-13: The principle of FWD operation (Molenaar, 2006)

FWD has been used for measuring the dynamic sleeper support stiffness of the railway track structure since 1992 (Burrow et al., 2010). After disconnecting the rails, the device drops a pre-defined mass (e.g., in the range of 30 to 120 kN) three times from specific heights onto rubber buffers mounted on a plate. The impact force is measured by a load cell and the resulting load pulse behaves in a similar way to axle passing. A velocity

transducer and geophones are positioned at different distances from the centre of the impact load, as shown in Figure 3-14.

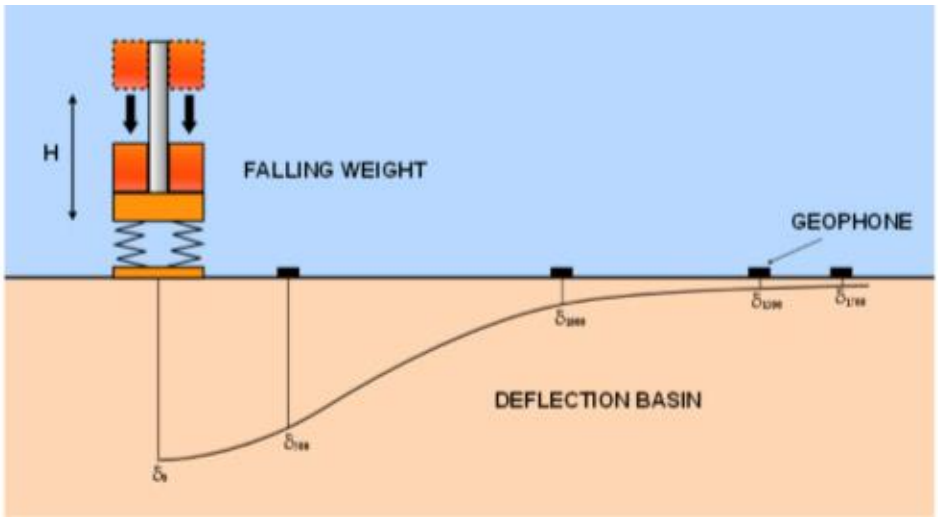

Figure 3-14 : Schematic of the FWD (Burrow et al., 2010)

The following graph, Figure 3-15, shows how the surface deflection is displayed after the integration process from the obtained velocities by geophones from the centre of the loading point which are at 300 mm, 1000 mm and 1500 mm. The obtained velocities are integrated into displacements. The FWD provides a dynamic sleeper stiffness (KN/mm/sleeper end) that is derived from the calculated displacement and the measured load.

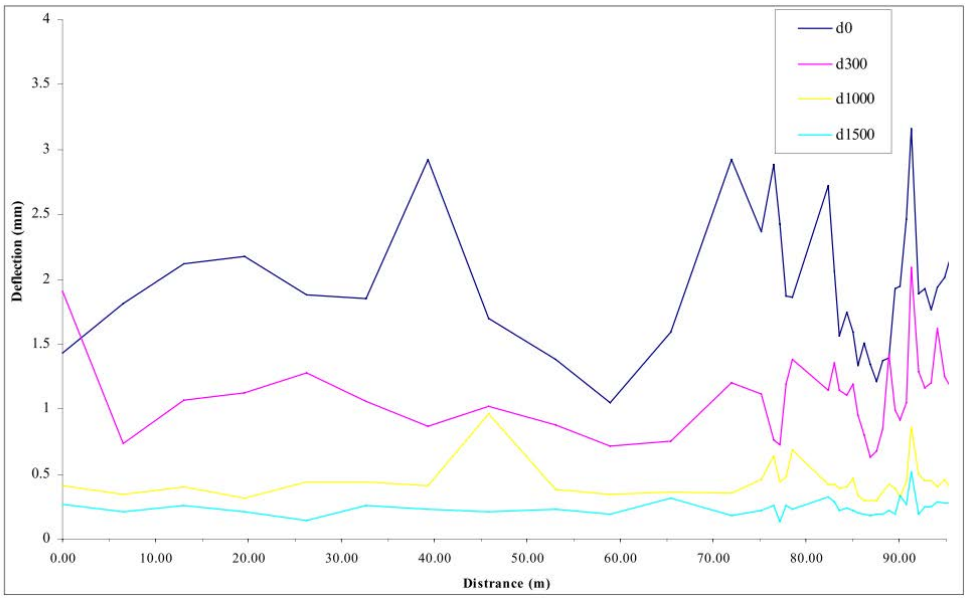

Figure 3-15: Example of results produced by the FWD (Burrow et al., 2010)

Although the slow motion is a constraint, FWD has been used for many years in railways to take measurements. Whilst it is very effective at assessing trackbed foundation, since it gives a direct measure of trackbed stiffness by looking at the displacement of the end-sleeper, the major drawback of this method is that it requires the rails to be unclipped from the sleepers, which is a very intrusive and expensive approach. In addition, it only gives track stiffness data at the specific point where the sensors are positioned, rather than the overall track stiffness in the vicinity. This approach may not be practical for a busy railway track or in a situation which requires rapid assessment of the track.

Table 3-4: Benefits and drawbacks of using the FWD

Benefits	Drawbacks
• It gives dynamic support stiffness of the sleeper, which is useful in a model	• Slow motion, track occupancy issue, high operation cost • Time to take FWD on the track • Mostly used for the research of specific areas (Burrow et al., 2010) • It is not suitable for measuring track stiffness during the service life.

The dynamic sleeper support stiffness only provides an overall indication of the trackbed performance and does not give the stiffness of the individual layers. There are different tools available to measure the stiffnesses of each individual layer. The Dynamic Cone Penetrometer (DCP) test is a method that allows a rapid measurement of the in situ strength of the trackbed layer. The principle is that a penetrating rod is inserted into the base layers and subgrade, on which is dropped a pre-determined load (8 kg). The stiffness of the layer materials at different depths is assessed by measuring the penetrating depth of the load (mm) for each impact. The Plate Bearing Test (PBT) is another way of evaluating the foundation bearing capacity and settlement under loading. In the BOEF theory, the modulus of the subgrade reaction is originally obtained from the PBT and the value is used for designing rigid (concrete) pavements. Since this method is expensive and time consuming, costing from $1,000 to $5,000 per test in 1981, there are studies which attempt to establish the modulus of the subgrade reaction (C-value) with more economical and less time consuming laboratory tests, such as the California Bearing Ratio (CBR) and others. The CBR was developed by the California State Highways Department in order to evaluate the strength of pavement subgrades. The CBR is the percentage of the soil load required to produce a 0.1 inch deflection, compared to a standard crushed stone. CBR is an index of

the strength and deflection characteristics of soil that has been correlated with pavement performance (Sowers & Sowers, 1970, p. 249). There are approximate relationsships between these values that were published by the Portland Cement Association (PCA) as below.

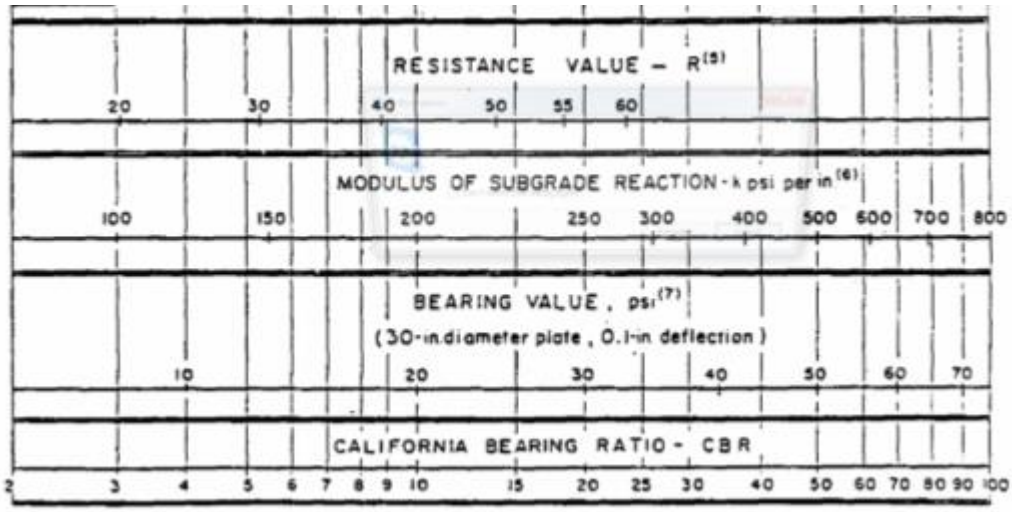

Figure 3-16: Correlation Chart (PCA)

Equations (17) and (18) were drawn up by the PCA as below.

$$Ks\ [kg/cm^3] = \frac{CBR}{5} + 3 \quad (17)$$

$$Ks\ [N/mm^3] = (\frac{CBR}{5} + 3) \times 10^{-2} \quad (18)$$

Studies have also been conducted to show the correlation between the DCP index (DPI) and CBR in order to estimate the California Bearing Ratio (CBR). The CBR values can be estimated based on equation (19) that was proposed by Livneh et al (1994), bsed on his study that had included both field and laboratory based tests and where the materials tested were both granular and cohesive. A higher CBR reading, presented as a percentage, means a stiffer foundation and a lower reading means a softer foundation.

$$\log (CBR) = 2.46 - 1.12(\log DPI) \quad (19)$$

Table 3-5: Typical CBR and DPI ranges for various soils (H.Sullivan, 2015)

Soil type	CBR range	DPI range (mm)
Clay	2-17	127-15
Sand	17-45	15-6
Gravel	53-100	5-2.7

Table 3-5 shows the classification of soil type on the basis of the empirical correlation between CBR and DPI. Using the subgrade resistance, the soil type of the layer can be

assumed. Table 3-6 summarises the different methods of subgrade performance measurement as below.

Table 3-6: Summary of methods of determination of various stiffness parameters (NR standard, 2007)

Type of method	Phase of trackbed treatment	Application	Parameter measured and units	Remarks
FWD on sleepers	Investigation/design/ diagnostic Tool	Track	Dynamic support stiffness kN/mm per sleeper end	High mobilisation cost
DCP	Construction control, efficiency of compaction, stabilized layers, subgrade moisture content	Subgrade	Blow/mm	Rapid measurement to evaluate the properties of subgrade. In some cases, it is very difficult to retract the corn from the ground.
Plate Bearing Test	Construction	Subgrade/ formation	kN/m²	Expensive, time consuming, only appropriate for major projects.
CBR	Subgrade/formation	Subgrade/ formation	CBR, %	Initially used in pavement. Can be used to derive an approximate value of stiffness.
Triaxial Test	Design	Trackbed	E, MN/m2	Requiring highly specialised technique.

3.2.3 Vehicle Based Dynamic Measurement System – Rolling Measurement System

Several attempts have been made to develop a vehicle based measurement system that can run at close to line speed, however, to date only prototype systems are available. All the same, in the last decade such measurement solutions have attracted much attention from the railway research industry. The proposed systems are based on an approach with continuous assessment of stiffness of track at line speed, rather than measuring at discrete intervals. The first example is the Rolling Stiffness Measurement Vehicle (RSMV) system, which was developed by Banverket for the Swedish railway (Berggren, 2009). This vehicle is modified from a two-axle freight vehicle with oscillating mass and static loading of 180 kN, plus dynamic load up to 60 kN, as shown in Figure 3-17. While the FWD or other methods measure the stiffness of subgrade at discrete intervals, the vehicle based measurement system measures dynamic stiffness continuously along a track. Track stiffness is calculated from measuring the axle-box force and using accelerometer data. Measurements can be taken at speeds of up to 40-50 km/h, whereas more detailed investigation can be conducted at 10 km/h (Berggren *et al*., 2006).

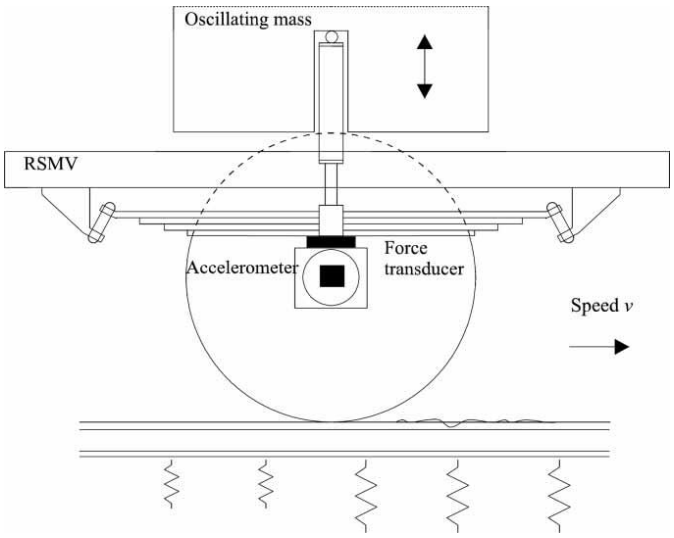

Figure 3-17: Measurement principle of RSMV (Berggren, 2010)

Other dynamic measurement systems include:

- The Chinese track stiffness measurement system, which has a running speed of up to 60 km/h (Burrow et al., 2010);
- The High Speed Deflectograph (HSD) developed by Technical University of Delft, which uses a laser Doppler sensor and can travel up to 130 km/h (Berggren, 2009);
- An American vehicle developed by the Transportation Technology Center, Inc (TTCI) called the Track Loading Vehicle (TLV), which can be used to measure both vertical and lateral stiffness, which has a maximum speed of 16 km/h (Li *et al*., 2004);
- A measurement system using a line laser by the University of Nebraska (Lu, 2008);
- The French Portancemeter (Robinet *et al*., 2008);
- Swiss track stiffness measurement vehicle (Berggren, 2009).

However, the limitations of the rolling measurement system are pointed out by (Berggren *et al*., 2006) and (Hosseingholian *et al*., 2009). The track stiffness measurements by the vehicle based systems developed to date result in different values because of different operating conditions, such as differences in static loading, exciting frequency, speed, resolution of the system, different measuring points from the wheel set, and different degrees of influence due to track irregularity.

Table 3-7: Pros and cons of vehicle based dynamic measurement system

Pros	Cons
• More realistic measurement system compared to static measurement system considering, for example excitation frequency. • Continuous stiffness measurement of the entire track system, whereas FWD produces discrete points of stiffness	• Many organisations invented rolling measurement systems which have adopted different methods (Different resolution, different running speeds).

3.2.4 Trackside Sensor Based Measurement System

In recent years there has been a growing interest in measuring dynamic track deflection on a real time basis during train passage without track possession. As continuous measurement is necessary to monitor transition zones or critical zones, such measurements should be undertaken with only minimal disturbance to traffic operation or preferably without disturbance at all. Therefore, for the most part, work on the transition zone has been approached by using trackside measurement systems, as illustrated in the previous chapter (Section 2.2.3). The sleeper response was experimentally measured using different techniques since the magnitude of sleeper response is a good measure of track stiffness or track modulus (Section 2.1.1). Each different technique can be categorised into three groups, depending on what the system measures, as follows.

1) Vertical displacement : Laser sensor, Video Recording
2) Vertical velocity : Geophone
3) Acceleration of response of track : Accelerometer

Remote video monitoring is one of the methods used to measure track displacement from the trackside, as shown in Figure 3-18. Particle Image Velocimetry (PIV) is a method used to visualise fluid flow, and it is applied for analysis of recording data.

Figure 3-18: The installation of a video recording system at Long Marston

Research to monitor the dynamic movement of track has been carried out using video recording at the track side (Bowness *et al*., 2007), (Ward *et al*., 2010), (Li and Berggren, 2010). Bowness *et al* carried out a comparison test between data obtained from the video camera, which captures 30 frames per second (FPS) and data from the geophone. A webcam mounted on a telescope was positioned at 6 m from the track to reduce the influence of vibration of the ground. It captures an image of the target, which is mounted on the sleeper for the measurement of peak to peak displacement, and enables the measurement of horizontal movement. The results from the measurement using PIV analysis with video recording and geophone measurement match closely, as shown in Figure 3-19.

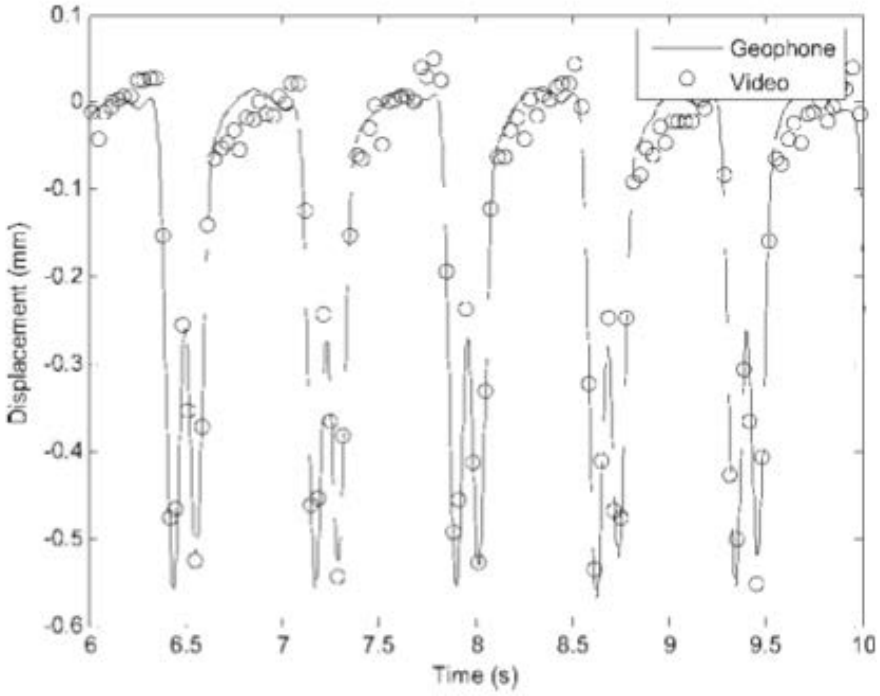

Figure 3-19:Data comparison between PIV and Geophone (Bowness *et al*., 2007)

However, a key limitation of this method is that a video recording system is able to monitor the displacement of only one or two sleepers. Also, this measurement can be inaccurate depending on train speed. The dominant frequency during the passage of trains varies depending on the bogie spacing and train speed. Thus, when the domain frequency is over a certain value (2 Hz), which is calculated from the bogie spacing and train speed (for example, when the train speed is 100 km/h with a 13 m of bogie spacing, the domain frequency is 2 Hz) the result can be underestimated due to the low acquisition rate of the camera. For running under high speed train operation, a higher FPS is required, such as 150 Hz frame rate (Bowness *et al*., 2007).

Table 3-8: Pros and cons of video recording system

Pros	Cons
• No requirement for data logger or electrical connection along the track • Measurement of both directions (vertical and horizontal)	• Vibration effect of tripod • Monitors only a small localised point along the track (e.g.: 1 or 2 sleepers), thus low productivity • Requires higher frames per second (FPS) for high speed train running – can be suitable for use during lower speed running.

Over the past decade most research in monitoring critical zones has utilised trackside sensors, in particular, geophones, see (Bowness *et al*., 2007), (Priest and Powrie, 2009), (Coelho *et al*., 2011) and the Innotrack technical report (Ekberg and Paulsson, 2010). A geophone is a velocity transducer. In particular, low frequency geophones have been used for seismic measurement and site engineering. They output a voltage proportional to the relative velocity of the object, thus they measure velocity. The output voltage is integrated to indicate the displacement of movement. However, the problem with using a geophone is that the linear frequency range is limited to frequencies above the natural frequency. For example, if the dominant frequency is lower than or close to the geophone's natural frequency, which this research has shown to be typically 1 or 2 Hz, the velocity data must consider the sensitivity response (V/ms^{-1}) and phase lag (See Figure 3-20) when it is calculated from the voltage output through digital processing (Burrow M. *et al*., 2007). Otherwise, it could underestimate the output of velocity. From the test results with the geophone, it was found that the frequency should be higher than 0.5 Hz to obtain good geophone performance, whilst line speed is faster than 25 km/h with bogie spacing of 13 m (Bowness *et al*., 2007).

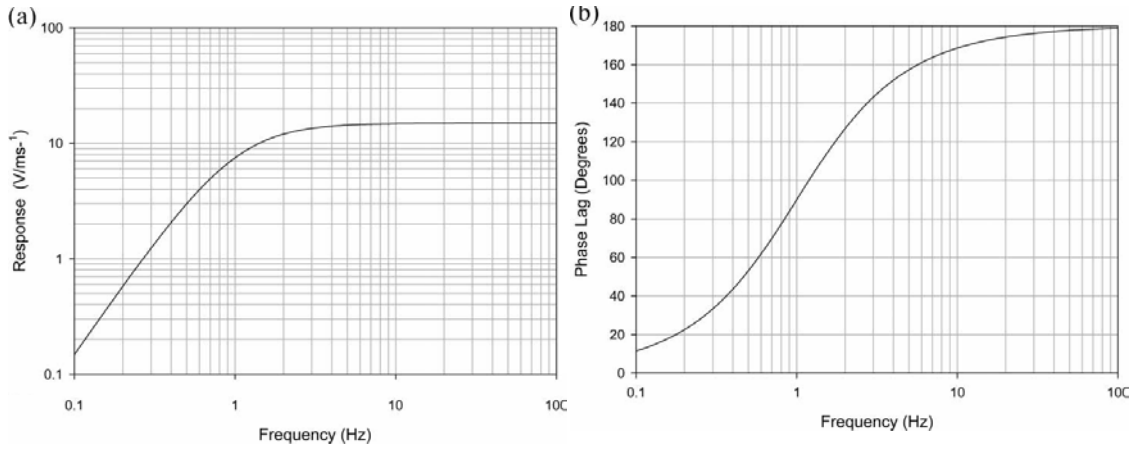

Figure 3-20: Sensitivity and phase response of LF-24 Geophone (Bowness *et al*., 2007)

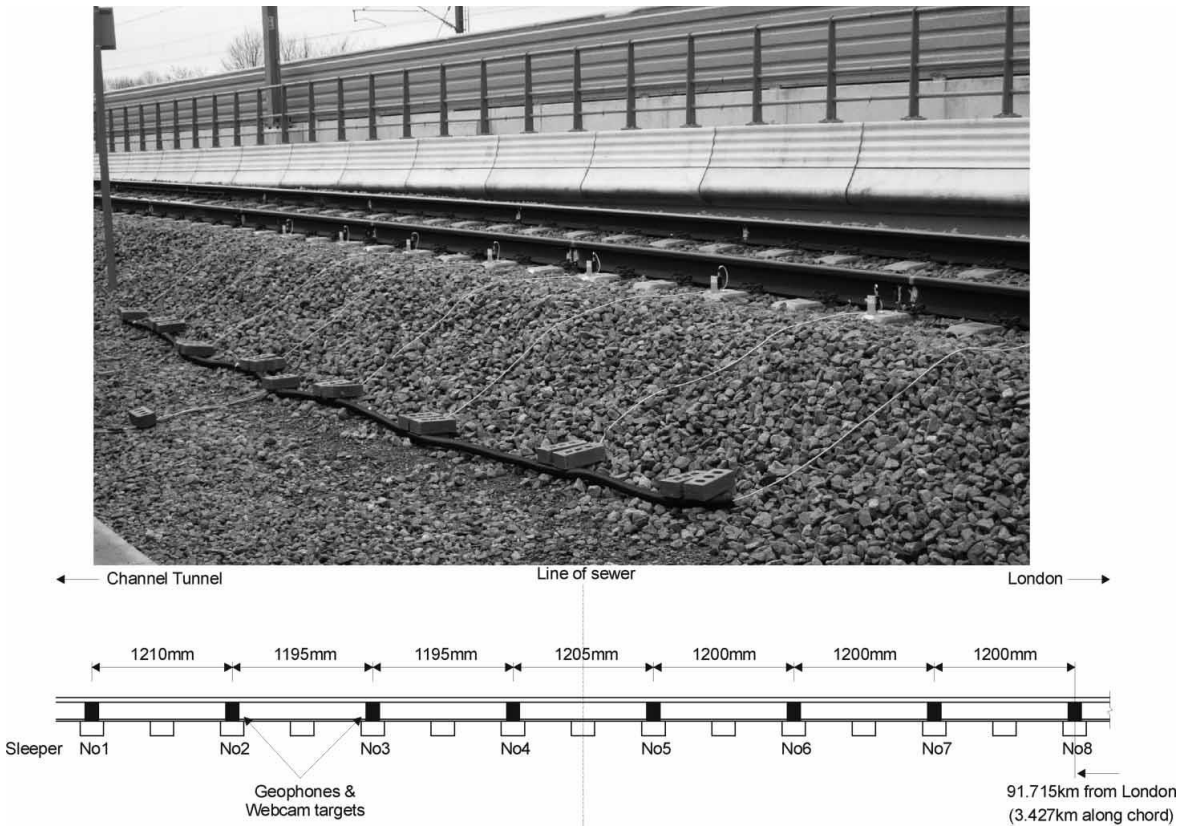

Figure 3-21: Geophone installation site (Bowness *et al*., 2007)

Figure 3-21 shows a number of geophones which were installed along the track over multiple sleepers at a site. Technology using a video recording with PIV does not require electrical connections along a track, whereas geophones need to connect to a data logger or computer to store and analyse the data. Laser based systems, which will be reviewed in the next section, also require an electrical connection along the track. Therefore, track access is required for the instrumentation process. The benefit of using a geophone is that it can be positioned underneath the ground, so that it measures the vertical displacement of each different layer, as shown in Figure 3-22. A geophone is also able to monitor not only vertical movement of the track, but also horizontal motion (Burrow M. *et al*., 2007).

However, the cost of the geophone increases exponentially with a decrease in geophone frequencies, therefore, this can be an expensive option.

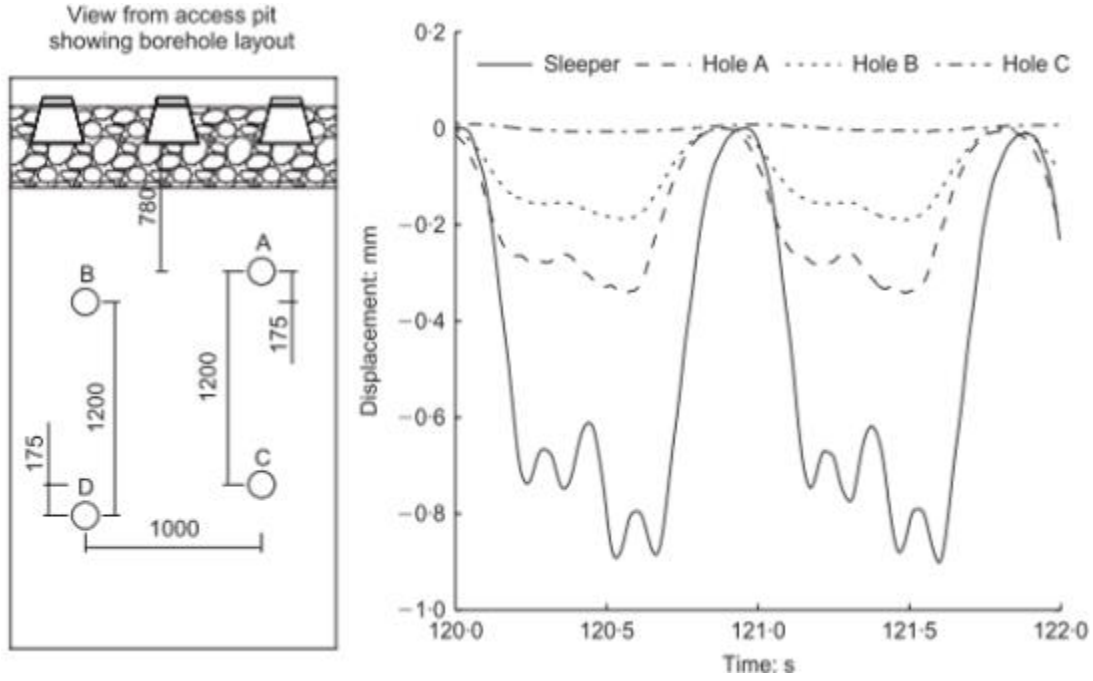

Figure 3-22: Schematic of borehole and vertical displacement during train passage (Priest *et al*., 2010)

Table 3-9: Pros and cons of Geophone monitoring system

Pros	Cons
• Fairly easy to place on track • Can measure underground or inside ballast • Vertical or horizontal measurements • Good performance on high speed lines • A geophone works in the rain	• Sensitivity is reduced with decreasing frequency, thus, it does not work during the passage of very low speed trains • Cost of geophone : LF-24, 1 Hz geophone price - £ 383 unit price (date : June 2011) • Requirement for data logger or electrical connection along the track • Not allowed next to third rail (safety issue)

Figure 3-23: Laser based measurement system on GCR (Track 21 presentation, 2010)

To date, laser based systems have only been used to measure track stiffness for research purposes. Several field tests have been conducted in recent years (Berggren *et al*., 2006), (Hendry *et al*., 2010), (Burrow M. *et al*., 2007) and (CEDEX/ADIF, 2009). These were undertaken using a novel sensor which was developed using an infrared laser and Positional Sensitive Detector (PSD), which is a light sensing device. The laser source was positioned 3 m to 6 m away from the track and it produced a line laser beam which is detected from the laser sensors on the sleepers, as shown in Figure 3-23. Until now, field tests using a laser based system have only considered a single sleeper, with one sensor mounted on a single sleeper end, as shown in Figure 3-24. Therefore, the system delivered low productivity, which was the same as using a video recording system.

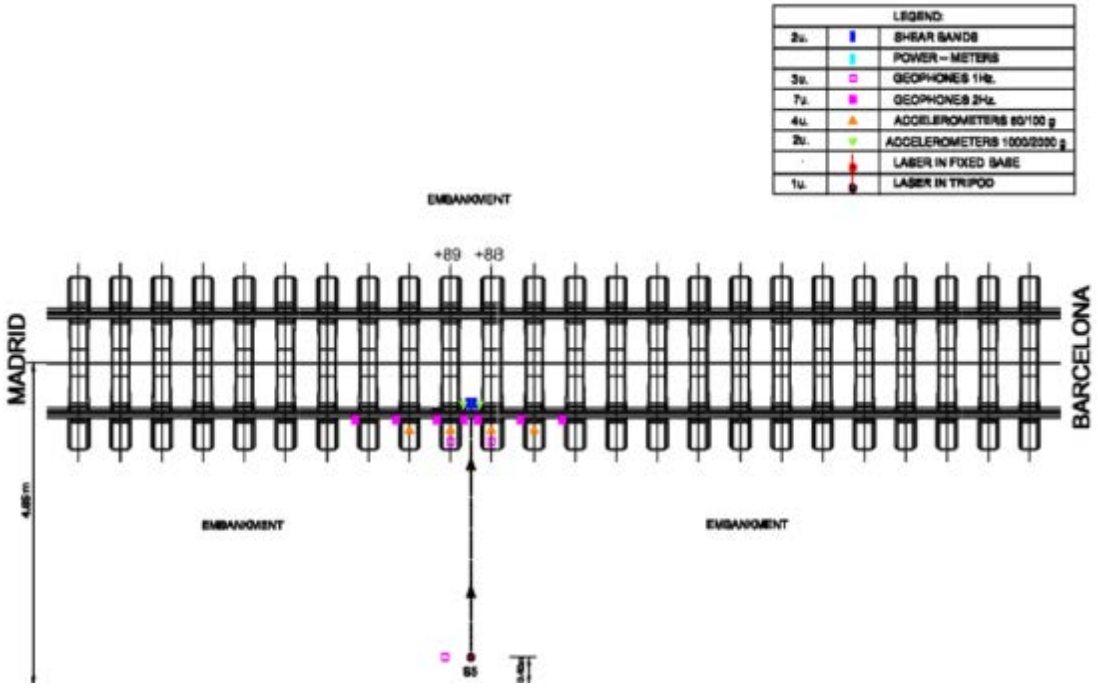

Figure 3-24: Layout of measurement with various trackside sensors (CEDEX/ADIF, 2009)

Three prototyped laser sensors were trialled on three sleepers on the Great Central Railway (GCR) to measure sleeper displacement (Burrow M. *et al*., 2007). The results obtained by the laser sensor were compared to those obtained by the PIV method and showed reasonable agreement, as shown in Figure 3-25. However, both methods rely on a tripod set-up, sensitive to ground vibration. Weston P. (2007) monitored the vertical movement of three sleepers using a single laser source, which was mounted on a tripod. The results of this trial prove that there is a possible advantage monitoring multiple sleepers in a short section with a single laser source, as there is potential to filter the effect of laser movement out of the results.

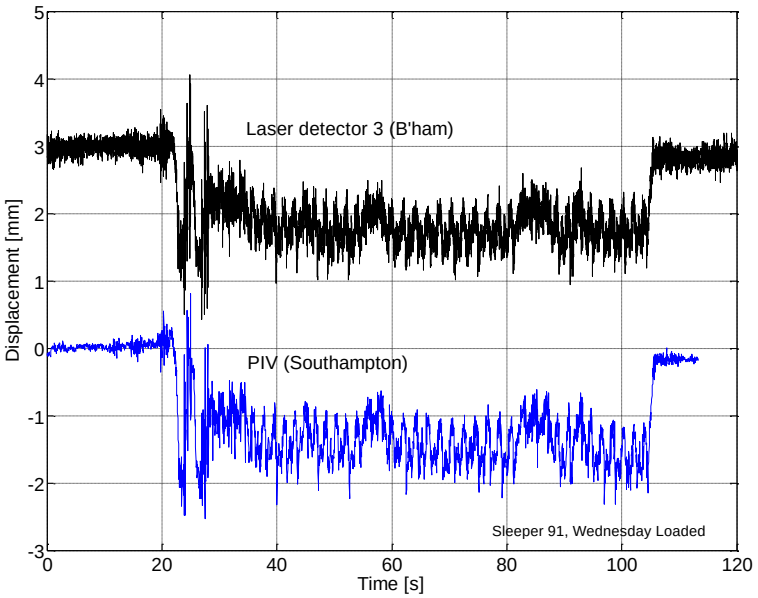

Figure 3-25: Comparison of laser sensor and PIV method (Burrow M. *et al*., 2007)

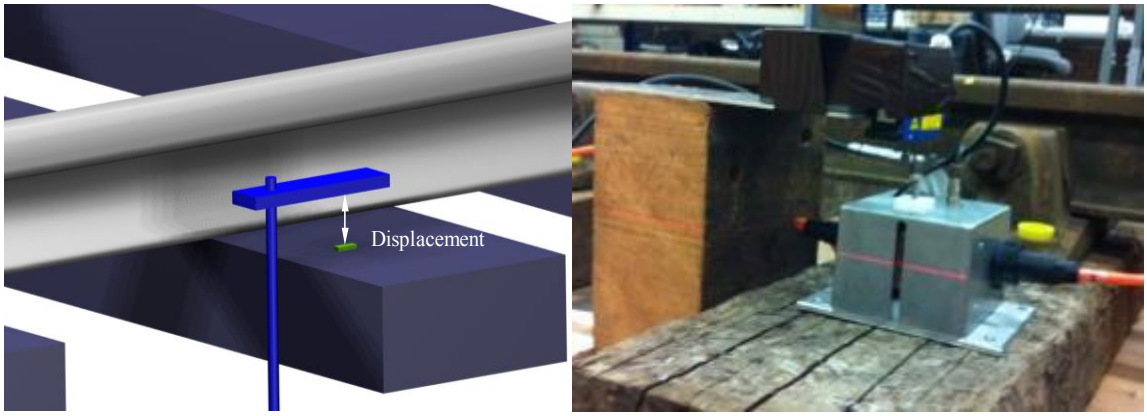

Figure 3-26: (a) Schematic of displacement transducer (Burrow M. *et al*., 2007) *(b) Instrumentation constructed by the author in the lab using a Micro-Epsilon Laser*

A non-contact infra-red displacement sensor (see Figure 3-26) was used to measure the displacement of the target point of the fixture. Weston *et al*., (2007) conducted a field trial at the GCR site. The result, displayed in Figure 3-27, shows that a low resolution displacement transducer is only suitable when displacements are greater than the resolution of the sensing device.

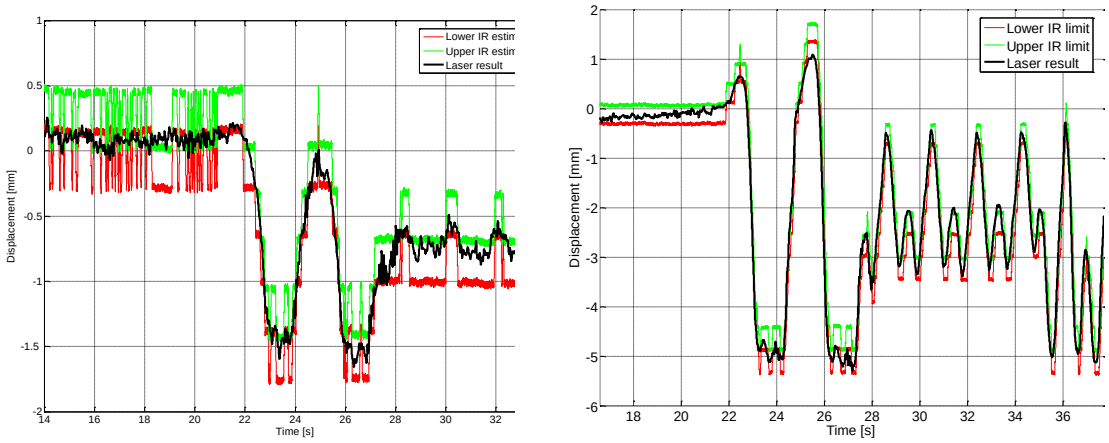

Figure 3-27: Comparison of IR Sensor and line laser test result (Burrow M. *et al*., 2007)

Although the laser based system has the potential to monitor multiple sleepers at once, the operational issues need to be addressed before an off the shelf product can be developed. Using the earlier system to measure sleeper deflection required a significant amount of manual work and many working hours. The setting-up procedures were difficult due to the requirement for the manual alignment with the laser source from the individual sleepers. In addition, manual calibration work had to be done inside the sensor box to adjust the analogue potentiometer. Thus, using the laser based prototype system, the work had to be conducted near to the track which could compromise safety. The cables between the three sensor nodes on the sleepers and the computer had to be connected individually, therefore they required a space along the track. Also, the data logger connected to the three sleepers, using the PC, was very basic. The data transmission rate was not a problem for work using three sensors, but it had to be for multiple sensors, thus it needed to be improved for further utilisation.

Table 3-10: Pros and cons of laser based system

Pros	Cons
• Potential advantage of measuring multiple sleepers over a longer section • Acceptable cost compared to geophone (£40 for the 37 mm dimensional PSD sensor and £ 488 for the line laser) • No speed restriction (can work at both high speed and low speed)	• Effect of ground vibration on tripod based equipment • Connection to the data logger and power • Line of sight issue from laser source to receiver

3.3 Summary for Chapter 3

Many different types of devices and technologies are available to identify track quality, which produce a large volume of data. It is important that the various sources of data are combined in a way which yields an accurate picture of track quality, but it is also critical that each item of obtained data should be accurate, low-cost, automatic and continuously corrected. Track geometry measurement (e.g., by means of the NMT) provides an understanding of the functional condition of the track, however, the root cause of problems cannot be found by looking at track geometry data alone. It has been assumed that the vertical data from a track geometry measurement vehicle under loaded and unloaded conditions provides an indication of under-sleeper voids or similar relevant information, which could produce track stiffness information, however, this has not yet been proved. GPR is useful for obtaining information to evaluate the substructure condition with in terms of the different substrate layers, to assess track stiffness data. Intrusive investigations are necessary, however, to supplement the GPR trace.

Finding a method of condition monitoring without traffic disturbance is significant for both railways and roads. While FWDs are mainly used to investigate structure conditions for research purposes for both railways and roads, they require a significant amount of track or road occupancy due to their slow motion, which affects both train schedules and car users. Other methods are available to evaluate substructure condition. The differences in the results obtained through different methods and, consequently, their applicability are reviewed in Table 3-6. Out of these, DCP is a rapid in-situ method to measure the strength of the trackbed layers at different depths. Although it involves intensive manual procedures during measurement, it costs less than other disruptive methods.

Newly developed vehicle based systems have been welcomed since they enable monitoring at close to or actual line speed. However, each system has different pre-setup values and the operation speed is still limited, although it is higher than for FWD operation. Therefore, the challenge is to develop an effective tool to measure track stiffness which is accurate and easy to use without causing traffic disruption. Trackside sensors would be a more effective method since they do not absorb track operational capacity.

Table 3-11 has been produced to compare different trackside sensors. It shows the advantages and disadvantages of each method and the suitability for application at the transition zone. Although a trackside measurement system using a range of sensors does

not require operational track occupancy for measurement, track access is required for installation and the setting up of sensor instrumentation takes 1 to 2 hours, which must be done overnight or during a longer possession. The level of accuracy should also be considered when deciding the application of each different sensor. For geophone use, the accuracy relies on a sampling rate and the dominant frequency, which is dependent on train line speed, bogie spacing and the distance between the axles. Low productivity is one of the major restrictions of using a video recording system.

Table 3-11: Comparison among major trackside sensors

Major Sensors	Pros	Cons	Suitability
Video Recording System	• No requirement for data logger or electrical connection along the track • Measurement of both directions (vertical and horizontal)	• Ground Vibration effect on tripod • Monitors only one point along the track (e.g., 1 or 2 sleepers), thus low productivity • Requires greater frames per second (FPS) for high speed train running	Due to low productivity, it is not suitable to monitor transition zones
Geophone	• No restriction for the instrumentation (does not involve line of sight operation) • Measurement of both directions (vertical and horizontal)	• Sensitivity reduces with decreasing frequency, thus, it does not work during the passage of very low speed trains • Cost of geophone (e.g., LF-24, 1 Hz geophone £383) • Requirement for data logger or electrical connection along the track	In recent research, geophones have been used. There is a sensitivity issue for use at low speed which is a problem in practical operations
Laser based sensor	• Potential advantage of measuring multiple sleepers at once • Can produce a track deflection bowl that shows relative stiffness along a section of track • Cost acceptable compared to geophone (£40 for the 37 mm dimensional PSD sensor and £488 for the line laser) • No speed restriction (can work at both high speed and low speed) • Potential to monitor longer section of track	• Effect of tripod vibration • Connection to the data logger and power • Line of sight issue from laser source to receiver • The setting up procedure is laborious and time consuming.	It has the potential to deliver high productivity and the prices are reasonable, compared to using geophones

The motivation of the previous work was to assess the potential of the laser based system. One significant advantage of using a laser based system is that monitoring can be conducted at both high and low line speed without occupying the track – this is particularly relevant for measuring critical zones where speed restrictions may be in place (e.g., where a fault is known to exist), or around S&C. The second advantage is that a laser based system has the potential capability of monitoring multiple sleepers through a critical zone so that data can be produced efficiently and the track deflection bowl can be observed.

For the development of a rapid assessment system for transition zones and critical zones, it is concluded that it is reasonable to conduct a comparison test between a laser sensor based system with system upgrades and a geophone in order to validate the system and check the accuracy of the data. One of the elements of the BOEF theory, the modulus of subgrade reaction (Chapter 2, page 17), can be achieved by the correlation between DCP and CBR, therefore, DCP can be useful in the research since it is easier and cheaper than FWD or other destructive methods. In order to estimate the deflection of each sleeper and also to assess the subgrade strength, a DCP measurement will be also be included and the data will be explored along with the data from the trackside sensor(s). This process will give a link between deflection and subgrade condition.

A newly-developed system would fill the gap that exists among the current technologies by improving the productivity, shortening the set-up time and using a method which is non-disruptive to train operation. The development process for the proposed system, designed on the basis of a laser system, is discussed in Chapter 4.

4 Trackside Measurement System Development

In the previous chapter it was demonstrated that a laser based system is a feasible option to satisfy the objective of this research, which is to develop an easy to use monitoring system for the in-situ deflection response of the track during train passages. An analogue laser based system was prototyped and tested previously, as described in Chapter 3, mounted on three sleepers. Although the test result was successful, the system had to be manually calibrated and analogue errors were caused by changes of temperature, humidity, cleanliness and aging. It is therefore considered better to develop a system based on digital components by replacing most of the analogue parts.

In Chapters 4, 5 and 6, the author outlines the steps of system development which were undertaken, from the planning stage, through design and implementation to demonstration of the system through a verification and validation process.

4.1 Planning the Development

A system engineering approach was applied during the development process for the laser based measurement system in order to reduce unnecessary work and improve efficiency. Each step of the Vee-model was followed, from requirement analysis to functional development, software and then hardware development, as shown in Figure 4-1.

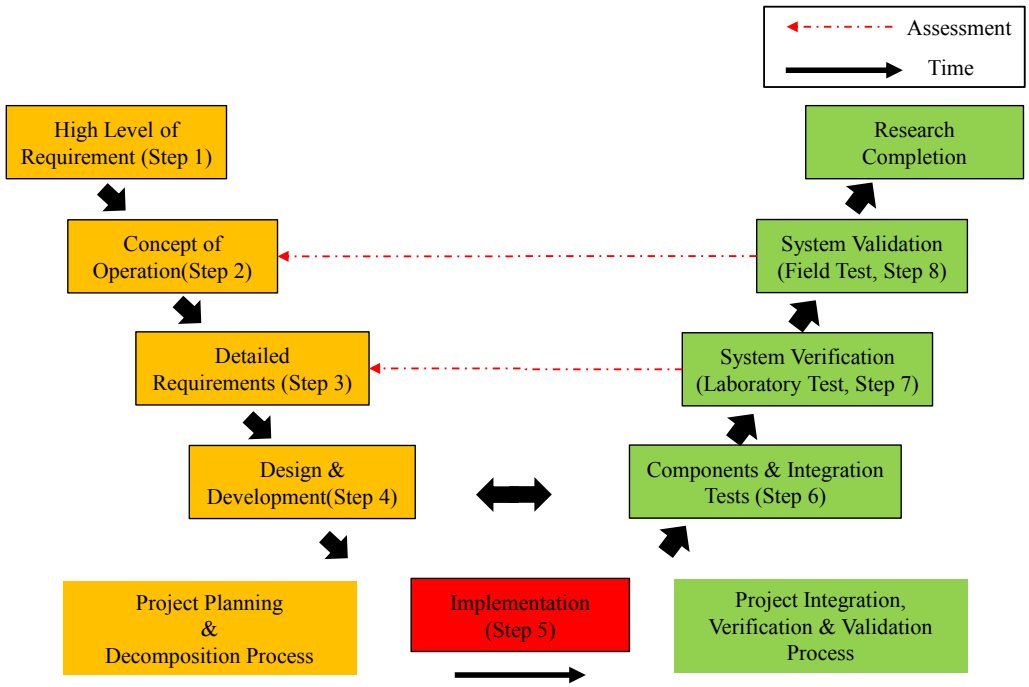

Figure 4-1: Vee-model system engineering approach

The 'Vee' model is widely used in industries that require multidisciplinary work in order to produce efficient results in a way that: (1) reduces risk, (2) controls cost and schedules, (3) improves quality, (4) reduces repetitive work throughout a development process, (5) avoids personnel resourcing difficulties and results in traceability of requirements and resources and (6) meets research needs. As there are different versions of the Vee-model, the application should match the scale and characteristics of the project. In this research, the Vee-model is applied using 7 steps, as described below.

- Step 1 High level Requirements: General direction of the research;
- Step 2 Concept of Operation: Describes the way in which the proposed system will perform in the relevant environment;
- Step 3 Detailed Requirements: Extracts the fundamental and specific requirements of the operational and technical system design, the integration and risk assessment;
- Step 4 Design and Development: Describes how the system will meet the requirements through functional and physical development and deliver a test plan which will verify if the system satisfies the requirements and validate whether the system agrees to the concept of operation;
- Step 5 Implementation: The construction and deployment of the system by way of hardware and software design;
- Step 6 Integrating Test: As each component is assembled and completed for the system, it shall be integrated to ensure that the system has been demonstrated in accordance with the design, and to see overall performance;
- Step 7 System verification: To verify the developed system to ensure that it is consistent with the detailed requirements and that it satisfies pre-defined test specifications. This process will be supported by a lab-based test;
- Step 8 System validation: To validate the overall system to see whether it meets the high level requirement and concept of operation using a field test under railway operating conditions by implementing the system on the test track.

The left-hand part of Figure 4-1, referred to as the decomposition phase, is followed in order to specify the project requirements and to deliver a high quality system through the design and build activities. The right-hand of the Vee-diagram represents the integration

phase, which is undertaken by assembling all components together and conducting an integration test by connecting multiple nodes together. Then, a laboratory based test will be carried out for system verification purposes and a field test will be executed as a validation process on the basis of the Vee-process model, in order to ensure that the final output of the project meets the high level requirements which will be set out at an early stage of the project.

4.1.1 High Level Requirements

The goal of this initial step is to define correctly the direction of the thesis project and to capture the high level requirements through requirement elicitation from diverse stake-holder perspectives. It is envisaged that more detailed information about the research will follow in the next stage. The objective of the research has been previously stated in Section 1.2 as below.

Research Objectives:

- Through the analysis of the necessary functionalities and characteristics develop a functional specification of the measurement device.
- Design and construct a measurement system in accordance with the specification.
- Validate the measurement system by carrying out field tests.

In order to fulfil the research objectives (research requirement), the top level requirement of the thesis should be clearly presented and it must capture the essence of the research purpose. The top level requirement of the research project is defined as follows.

The research project shall result in an innovative trackside measurement system to monitor the vertical displacements of multiple sleepers during train passage continuously and accurately at different transition zones.

Figure 4-2 (top left) shows where this step is in the Vee-diagram and the relevant chapters for each step are also presented.

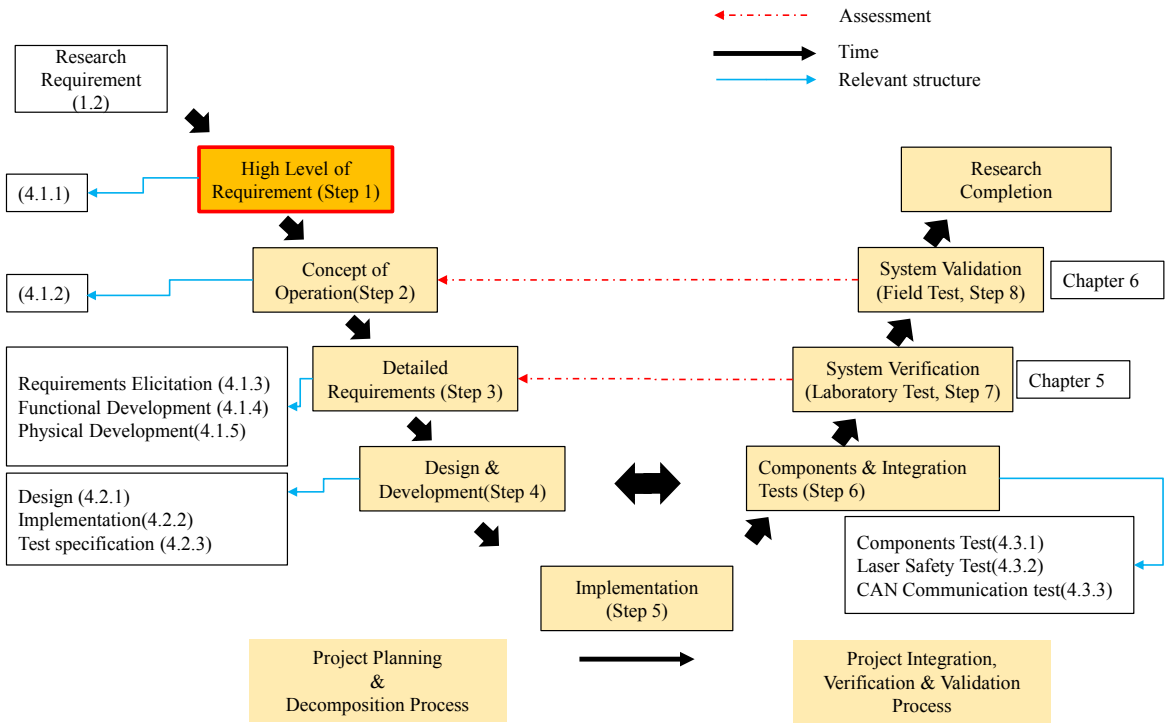

Figure 4-2: Planning stages of Vee-model diagram

4.1.2 Concept of Operations

As concluded in Section 3.3, the new system will be developed using the experience gained with the development of an earlier laser based prototype, which could measure between one and three sleepers.

In this step, in agreement with the high level requirement, the concept of operation is described in Figure 4-3. This will be the basis of requirement elicitation, which will be the next step. The system is intended to measure continuously the vertical displacement of a sequence of sleepers in response to the load during a train passage, using a laser sensor, which has been selected as the most viable option from the literature review (Chapter 3). However, in order to develop further the technology that has been shown to be capable of measuring multiple sleepers (Weston, 2007), the operational issues discussed in Section 3.2.4 need to be addressed. The issues are summarised below.

- The laser setting procedure is difficult, due to the requirement for manual alignment of the laser source to the sleepers;
- A large amount of manual work and many working hours are required;
- Manual calibration work has to be carried out inside the sensor box to adjust the analogue potentiometer, next to the track, which is not safe and takes more time;

- The cables between the sensor nodes on the sleepers and a data logging computer have to be individually connected to the sensor nodes, therefore the cables require a space along the track.

When the system is updated to resolve the issues listed above, the dynamic movement of each sleeper will be observed in real time (see Figure *4-4*), with good resolution and reasonable accuracy, using a laser and sensor combination.

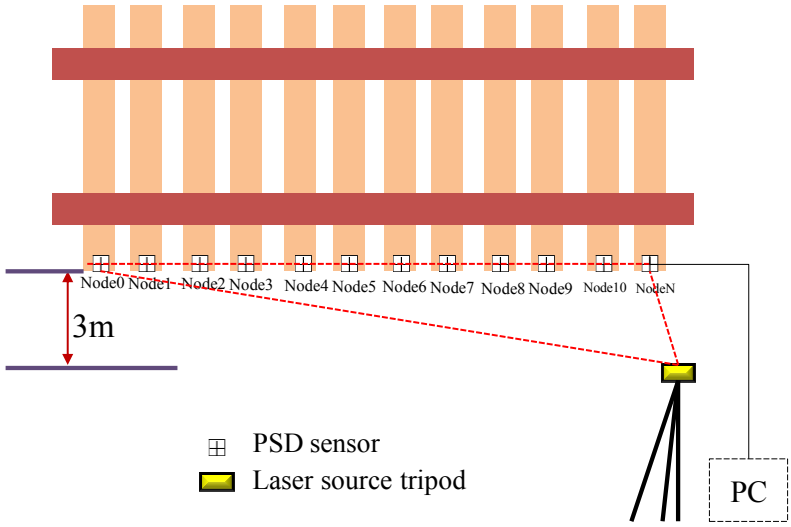

Figure 4-3: Concept of Operations (high level view) of the laser measurement system

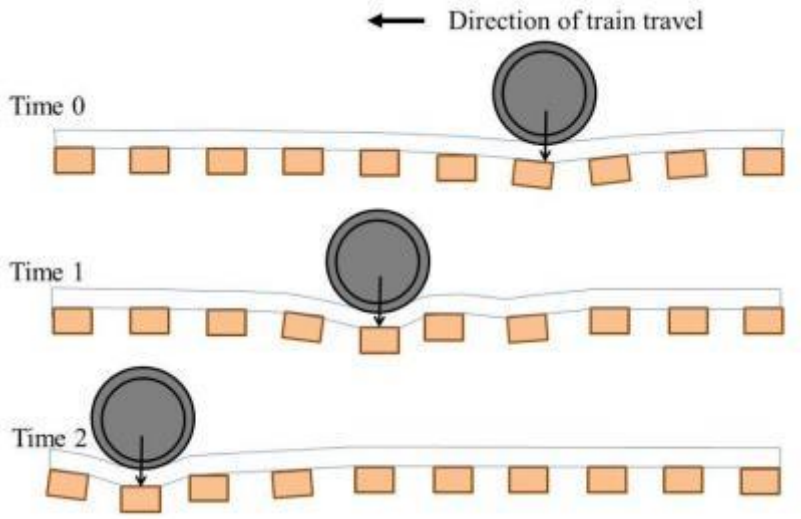

Figure 4-4: Concept of measurement system which shows the positions taken up by sequential sleepers over time

As shown in Figure 4-5, the proposed system has the potential to observe the moving shape taken up by a sequence of sleepers around a transition zone and record how this looks

before maintenance or renewal, after maintenance or renewal work, and then later on to see if the maintenance or renewal was successful.

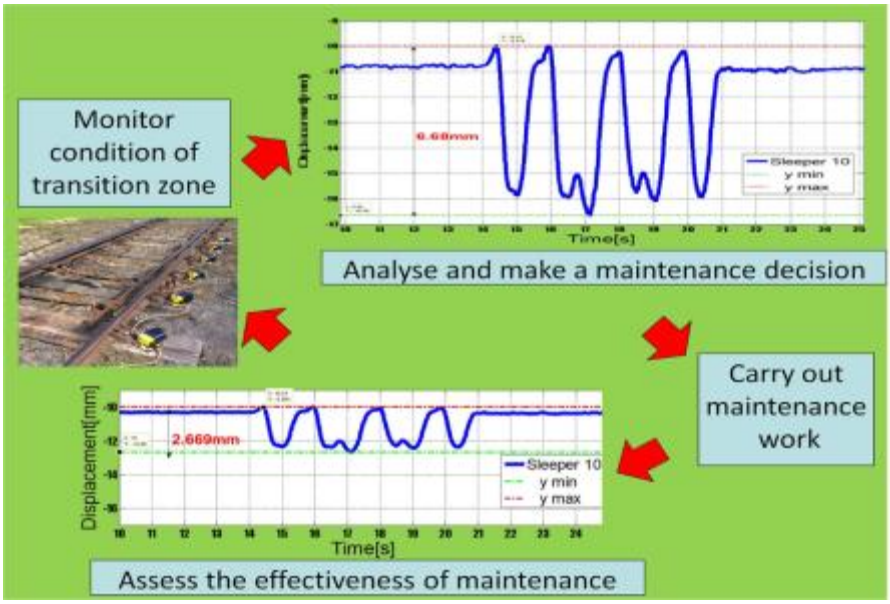

Figure 4-5: The concept of future operation

In addition, the proposed system shall be operated under a safe and reliable environment for system users and train operation during the measurement process. In terms of cost effectiveness, the system should be reasonably priced compared to the existing system. Throughout the operation process, the system should be approached with a user-friendly concept for feasibility.

The keywords for the concept of operation are summarised as follows.

- Main objectives: Measurement System (M)
- Low-cost based system (L)
- Safety (S)
- Reliability (R)
- Data Accuracy (A)
- User-friendly (U)
- No disruption for train operation (D)

4.1.3 Requirements Elicitation

This stage is required to specify the concept of operations in Section 4.1.2 and the problems with the laser based system should be resolved by being linked to the

requirements. Thus, the relevant corresponding requirements are stated in this section. The requirement statement should be SMART, which stands for Specific, Measurable, Achievable, Realistic and Timebound. In addition, it should be traceable so that it can be used in the process of verification and validation. It must also be reviewed to asses whether it is aligned with the high level requirements (4.1.1) and operations concept (4.1.2) to ensure continuity and compatibility. All requirements should be stated in a way which is verifiable, so that they can be evaluated after the system development. The following step, which covers the function or implementation details, will be described in the next section. Each requirement shall be managed using identification codes for traceability, as shown in Table 4-1, and each statement indicates what the system will be expected to do. They are sorted on the basis of each different keyword, such as the main functions of the system, reliability, accuracy, repeatability, safety, user-friendliness, no disruption to trains and low-cost which are stated in Section 4.1.2. The identification (ID) code has been applied for traceability, e.g., System Requirement (SR) 1-SR 14.

Table 4-1: Statement of requirements

Operations Concept	ID code	Operational/Technical/Design/System Integration Requirements
Main function	SR1	The measurement system must be a laser-based method.
	SR2	The measurement system shall monitor the condition of track continuously while a train passes the transition zones.
	SR3	The system shall quantify the amount of track displacement so that it gives specific evidence to help maintenance decisions.
Reliability	SR4	The system shall be practically applicable to be tested in both adjacent railway track and in the lab.
	SR5	The laser based system should be comparatively tested with one of the existing systems.
	SR6	The power for the system shall be sufficient for it to be operated either for the laboratory based or field based test.
	SR7	Data shall be obtained during measurement and easily readable in the right format.
Accuracy	SR8	The required level of accuracy of measurement shall be managed within the error of 0.1 mm. The level of accuracy shall be demonstrated considering two elements of accuracy, which are repeatability and reproducibility. (-0.1 mm < true value - measured value < +0.1 mm)
Safety	SR9	The system shall not cause any harm or risk to users. (Since it is laser based system, which was concluded in Chapter 3, the power level of the laser will be considered with regard to health and safety matters.)

Operations Concept	ID code	Operational/Technical/Design/System Integration Requirements
No disruption for trains	SR10	The system shall not disturb train operations, e.g. it shall not require track occupancy during measurement.
User-Friendliness	SR11	The system should be remote controlled.
	SR12	The measurement system should be easy and simple to install and remove so that the process takes less than two hours.
	SR13	The measurement system should be as light as possible to carry.
Low cost	SR14	The market price must be reasonably affordable and competitive compared to other measurement systems. It should be priced at a similar level as current systems, or lower.

The issues listed in Section 4.1.2 have been applied to the requirements (SR11, SR12 and SR 13).

4.1.4 Functional Decomposition

On the basis of the requirement statements (Table 4-1), the functional and physical decomposition process has been implemented. The functional decomposition process delivers statements that show the functions which the system must have in order to satisfy the concept of the operation. It is important to ensure that all relevant requirements are allocated into functional decomposition statements and physical decomposition statements. The system design must follow the requirements, provided that they correspond to each system function and each physical decomposition. To meet the system requirements defined in Section 4.1.3, detailed functional statements are presented in this step. It is important to ensure that most system requirements are mapped to each function for traceability, i.e., some of the requirements may require neither functional nor physical development.

Table 4-2: Statement of functional decomposition development

ID code	Functional Decomposition (FD) Statement
FD1	Interface between laser and sensor.
FD2	The measurement system produces stable values over time during the measurement. It should not break down easily during measurement.
FD3	The operating software produces relevant graphs and data.
FD4	The measurement system must be protective.
FD5	An additional sensor (geophone) is used to measure and compare the data.

ID code	Functional Decomposition (FD) Statement
FD6	The system operation should be reliable in terms of power supply for a one day trial. (24 V/ 1.5 A)
FD7	Storing the data on a PC.
FD8-1	The system should achieve a reasonable degree of accuracy (0.1 mm).
FD8-2	The measurement data should be linear. The deflection data should be proportional to the amount of the real movement of the object.
FD9	Laser emissions should be controlled in a way to ensure eye safety.
FD10	After the implementation, the whole measurement system must maintain a minimum clearance from the track to ensure safety.
FD11	The user interface provides graphical user interface (GUI) with control button for user inputs.
FD12-1	The process of assembling and dissembling is simple and easy
FD12-2	The set up process for the sensor node and laser should be easy.
FD13	The measurement system must be portable and easy to carry for users.
FD14	Price comparison.

Although it is easy to see how some of the statements can be fulfilled, all stated functional decomposition statements must be considered by conducting further tests and reviewing the data results. For example, in order to check if these statements (Table 4-2) are fulfilled through the follow-up process of test specification in Section 4.2.2.3, tests are required after the prototype is built and data should be collected and analysed. Therefore, these statements require test specifications for the purpose of system verification.

4.1.5 Physical Decomposition

The physical decomposition step is presented in Table 4-3. It states the appropriate physical solution by mapping each functional description (Section 4.1.4) to the definite physical components (Section 4.1.6) with parallel lines.

Table 4-3: Statement of physical requirements development

ID code	Physical Decomposition (PD) Statement
PD1	Hardware implementation using laser and PSD sensor.
PD2	Build a robust firmware system for stability during measurement.
PD3	Software implementation 1 (Displacement data).
PD4	The sensor node material and cable connections are completely enclosed in a waterproof box.
PD5	Installation with a geophone

ID code	Physical Decomposition (PD) Statement
PD6	Using a battery for a power supply operating multiple nodes and a laptop for the field test. Alternatively, a generator can be used.
PD7	PC and software implementation 2 (Data Storage).
PD9	Sufficient level of laser power with safety.
PD10	The dimensions of the enclosed node box should be considered and the positioning of the laser source should keep the clearance.
PD11	Software implementation 3 (automatic calibration hardware/software). Hardware implementation (main hub for remote control).
PD12-1	Individual nodes and cables which are easily assembled and dissembled (cable connector).
PD12-2	Software implementation 4 (laser detection function)
PD13	Light material for nodes box.

Figure 4-6 provides a graphical view of the physical developments from the statements. This physical decomposition diagram will be further divided into relevant components in the next step, which is the design development process (Section 4.2). The red arrows show the interface issues between the components, software and hardware. After the design development, they will be specified in more detail in the test plan (test specification). Then, the design will be tested through the integration process (Section 4.3).

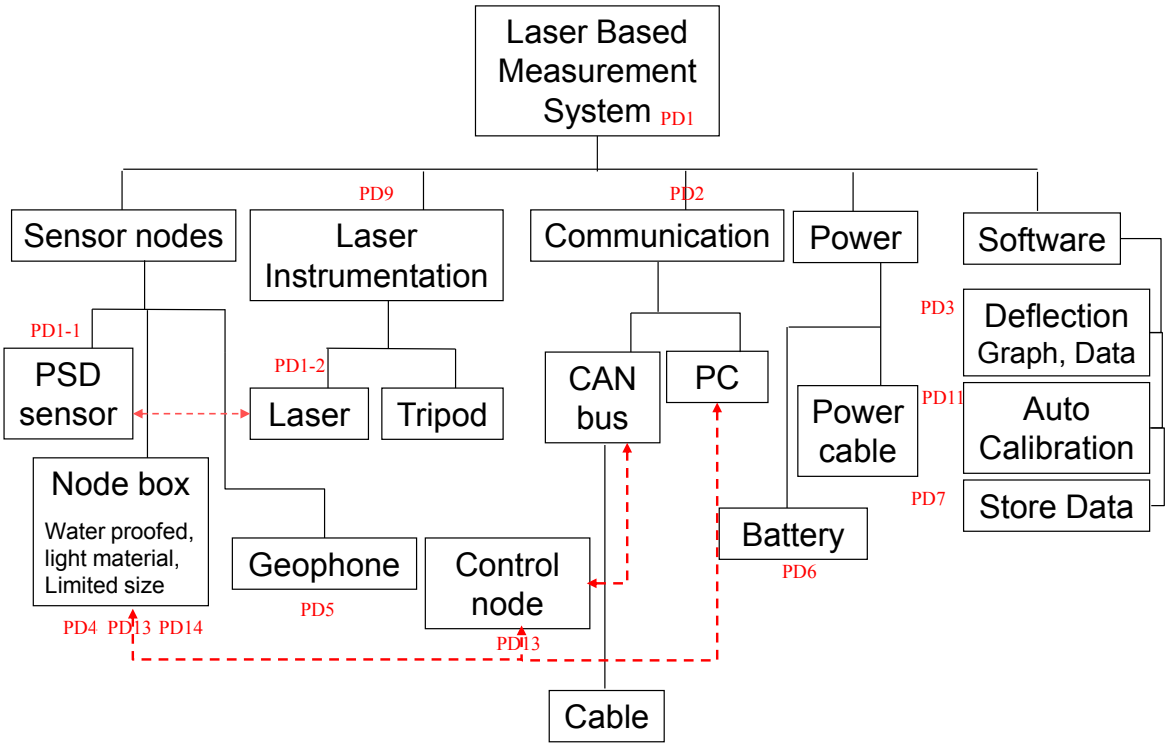

Figure 4-6: Physical development of laser based measurement system

4.2 Design Development and Implementation

As the overall requirements have been established and stated in the previous stages, as per the Vee-process set out in Section 4.1, the design and development aspects of the research are initiated in this section. By completing this stage, the architecture of the detailed design will be drawn. Figure 4-7 below shows where this section belongs in the Vee-diagram. In Section 3.1.2, the concept of operation issues was discussed in terms of the current operational and technical issues of the laser-based prototype that has been developed (Weston, 2007). The issues are applied to the requirement elicitation and the requirements have been developed into the functional and physical decomposition stage in Section 4.1.

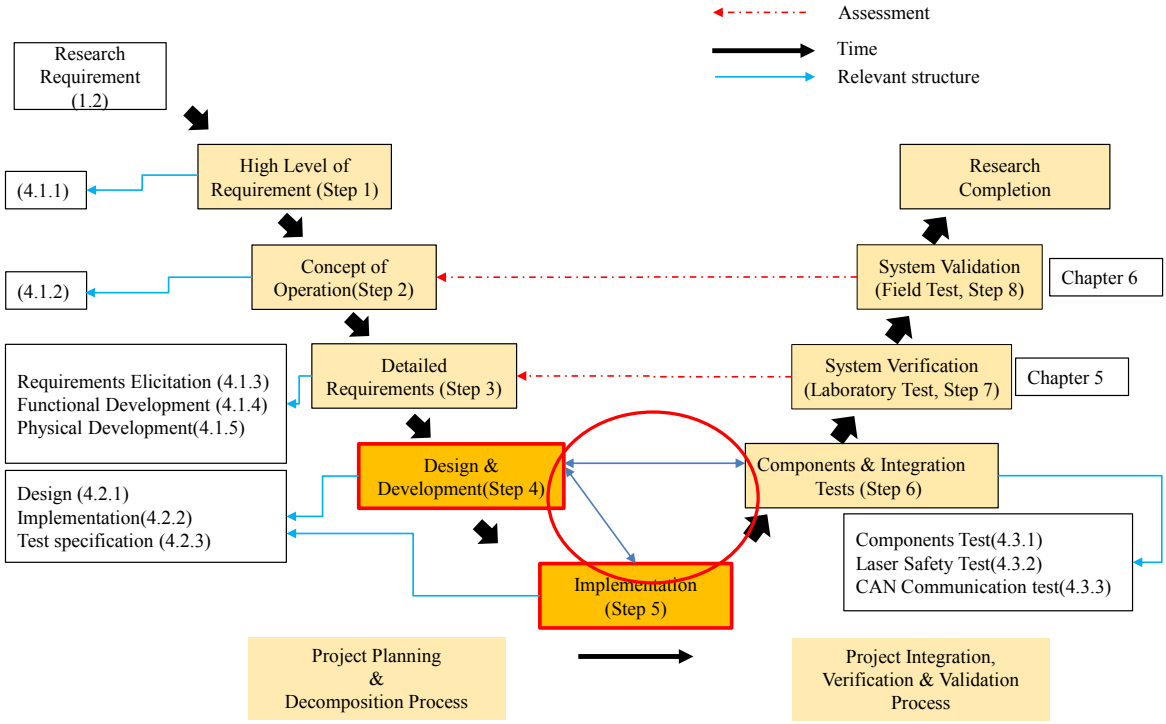

Figure 4-7: Design and implementation stages of the Vee-model diagram

In this step, the development of the hardware and software will be presented on the basis of upgrading the previous system and each new component and test will be considered. The system development works have been continuously modified and upgraded through the project as needed to meet the detailed requirements, or to find a missing part, as noted by a red circle in Figure 4-7. During the update process, each ID code (SR, FD and PD) was used to manage the requirements more effectively.

4.2.1 Design and Development Process

From the high level view of the measurement system in Section 4.1.2 (Concept of Operations) and the requirements process, the system described in this section was developed. An amplitude modulated fan laser is directed towards the ends of multiple consecutive sleepers. Sensor nodes attached to the ends of these sleepers detect the vertical position of the laser line, responding only to the modulation frequency and not to ambient light. The relative motion between the consecutive sleepers can be determined because the reference line is fixed. Even if the reference laser line moves up and down, or rotates a small amount in response to ground-borne vibration, as long as the line remains on the sensors, the shape taken up by the sleepers can still be correctly determined. The vertical position measurement shall have a bandwidth of over 100 Hz.

Resolution shall be better than 10 μm, with accuracy which is closer to 100 μm. The designed system enables geophones to be included with any node to allow for an extension of the frequency response if required and to employ it for system verification purposes.

The sensor nodes and laptop are connected to a Controller Area Network (CAN) bus, so the nodes can be 'chained together' and are connected via one cable to a laptop, as presented in Figure 4-8. The laser node also communicates with the CAN so it can be operated at a distance using a remote control. CAN operates a serial communications protocol which efficiently supports distributed real-time control with a very high level of security; the protocol was developed by BOSCH (Gmbh, 1991). Multiple nodes communicate with each other without having a master node. The CAN bus has a distance limitation, e.g., a CAN bus can connect up to 250 m with the baud rate of 250 kbit/s and the shortest maximised data rate with 1 Mbit/s is 40 m.

The power control node, or 'master node', is a main hub for the CAN network and is intended to control a 24 V power supply, a 5 V laser power supply and to interface the CAN network by using a PCAN-USB connector in order to connect to the PC, as shown in Figure 4-8. When this master node is connected into a 24 V power supply, all other connected nodes (Figure 4-9) are notified and displayed on the software.

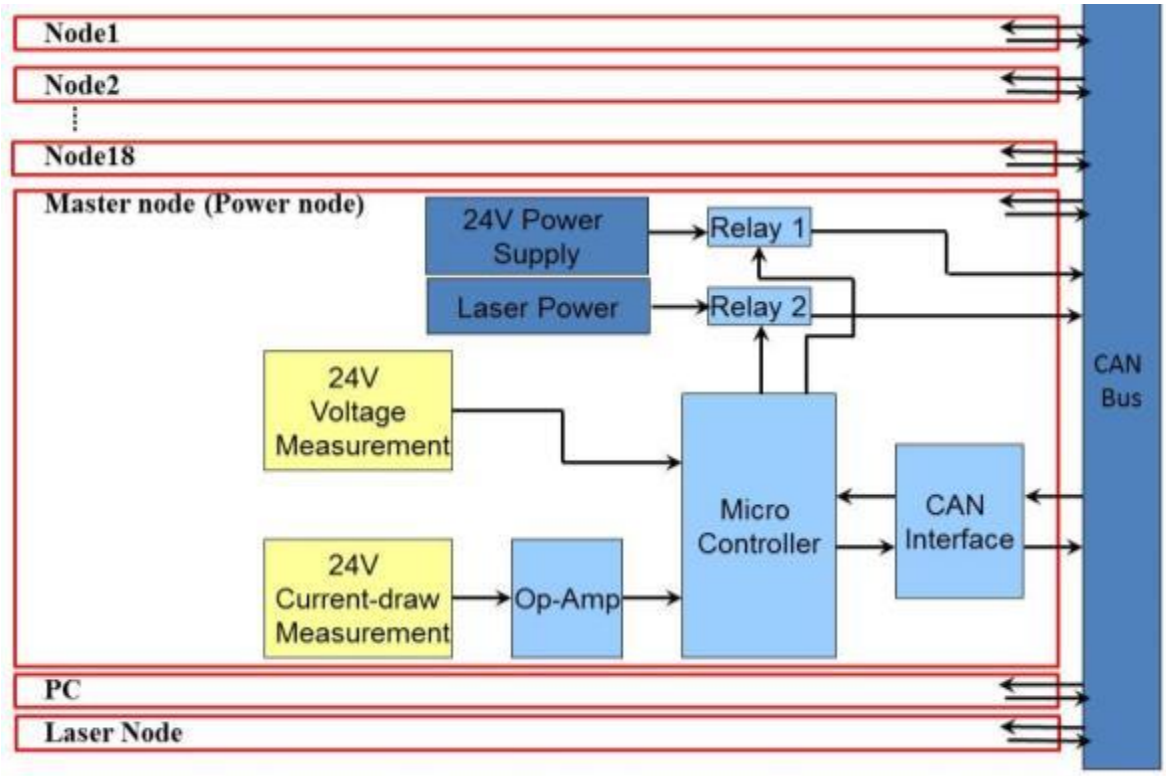

Figure 4-8 : Master (power control) node system block diagram

Three analogue sensor nodes have previously been tested in the field. Now, it is intended that a new digital system will be developed that can measure up to 18 consecutive sleepers concurrently. To allow this to happen, the analogue components have to be replaced by digital components that are suited to auto-calibration and remote control, as shown in Figure 4-9. Trackside measurement of the deflection shape of a sequence of sleepers is designed using PSDs and a line laser. Multiple nodes on a bus will be connected to a laptop where data is logged. Each sensor node performs measurement of the transmitter output voltage of the Root Mean Square (RMS) converter. The node will be implemented with an automatic calibrating method to use a digital potentiometer to reduce manual work, thereby enabling an operator to control remotely the calibration corresponding to the laser power level, which is influenced by the distance from the laser source.

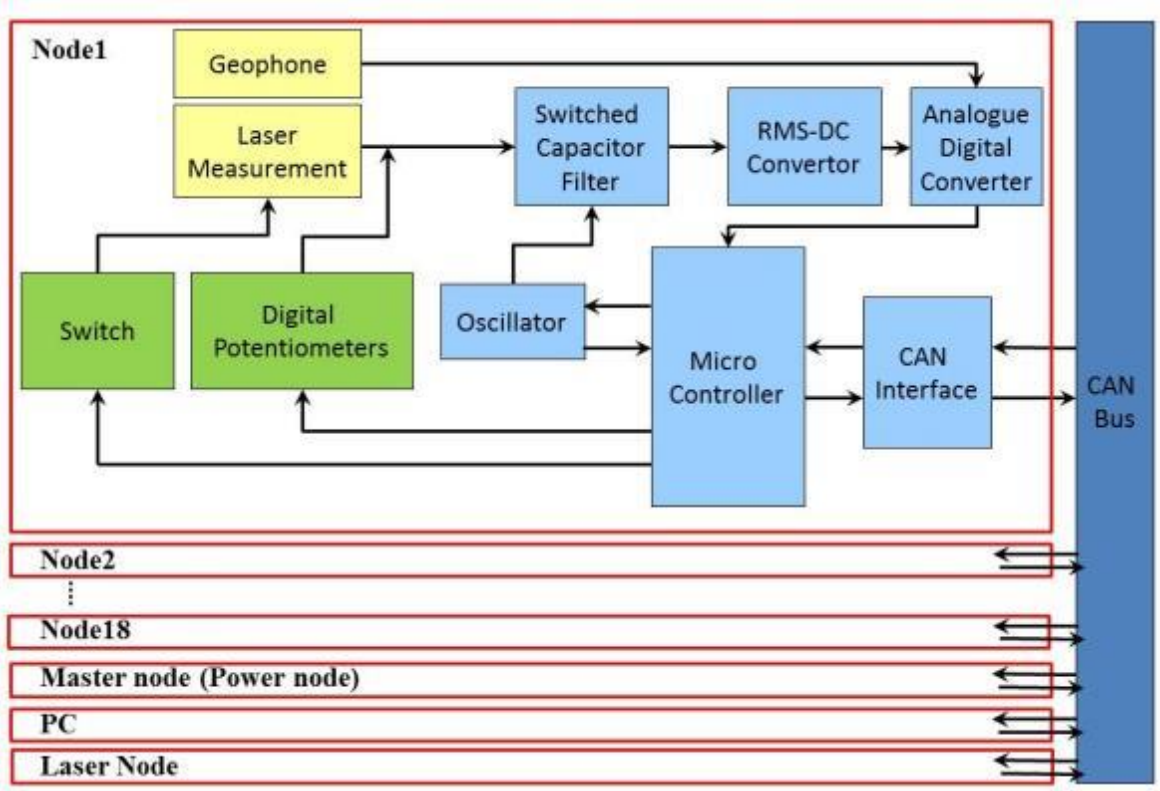

Figure 4-9: Sensor node system block diagram

The selection of individual components has been carefully proposed for the development of each sensor node prototype to prevent compatibility issues and each component has been initially tested on the breadboard.

Microcontroller PIC18F2680

The microchip PIC18F2680 shall be used for system design integration for the following purposes:

- I^2C communication between digital potentiometers and programmable oscillator;
- CAN bus protocol;
- Input control for channel selection for AD636;
- Digital positive 5 V supply for digital chips;
- Serial communication for RS-232 operation to display on the screen;
- Initial AD conversion of 10 bit Analogue to Digital (AD) converter for two channels.

The microchip enables Inter Integrated Circuit (I^2C) communication for fine tuning of the central frequency using a digital potentiometer (AD5282) and CAN bus control for data transmission between nodes.

Digital potentiometer AD5282

Two mechanical potentiometers from the analogue prototype system can be replaced with a digital potentiometer, which is smaller and stable with age and vibration, and which can be calibrated and recalibrated remotely and automatically. As noted above, I^2C operated digital potentiometers (50 kΩ) have been used in order to control the gain and the central frequency at the first trial of the circuit. AD5282 enables dual channels and each channel has 256 positions.

Bandpass Filter LMF-100

Due to weather changes and changes in temperature in particular, the central frequency needs to be optimised for the bandpass filter. In order to attain an automatic tuning process, an automatic system for central frequency control needs to be achieved. The LMF -100 dual switch capacitor filter was used with a signal generator for processing the data. In order to find the optimal central frequency, the magnitude of the waveform was reviewed. The central frequency was supplied by a signal generator (Sine Square Oscillator LFM3). The output signals from the bandpass filter were overviewed depending on different frequencies from the signal generator.

Programmable Oscillator

The LTC6904 uses an I^2C interface. The frequency setting can be done by a programme within the PIC 18F2680. The oscillator performed well when tested on a range of frequencies and the data was observed under various frequencies over two specified frequency ranges. In the next part of the software implementation work, the optimised central frequency will be automatically set up through the PIC and LTC6904 I^2C interface.

RMS-DC Converter

For data processing, the RMS-DC converter can be used. The LTC1966 and AD736 were tested. For using a LTC1966, an external capacitor, called an average capacitor, was placed inside the circuit to ensure an undistorted RMS waveform. However, using a larger value capacitor also resulted in a slower response time. This is not suitable for use in a continuous condition monitoring system in terms of precision. AD736 was used as an alternative to obtain a short response time, and it is therefore preferred.

PSD Sensor

PSDs are optical position-sensitive detectors which are simple photodiodes capable of detecting the position of a light spot projected onto their surface. They are suitable to apply in industrial tracking and displacement sensing applications (Si, 2000).

A one dimensional PSD sensor is shown in Figure 4-10.

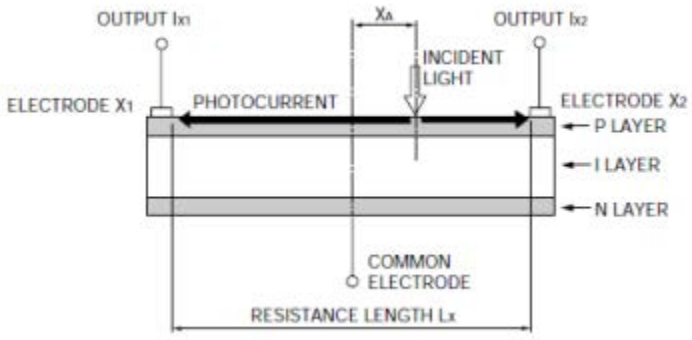

Figure 4-10: The principle of operation of a PSD sensor (Hamamatsu, 2011)

By producing two output photocurrents I_{x1} and I_{x2} from electrodes X_1 and X_2 on the basis of the intensity of light with resistance length Lx, the sensor shows the light spot position (X_A) on the active area of the sensor with the following equation:

$$\frac{IX2-IX2}{IX2+IX1}=\frac{2XA}{LX} \qquad (20)$$

For the preliminary prototype system, a 24 mm long PSD sensor was used, which senses wavelengths between 350 nm and 1100 nm. A 37 mm long PSD sensor, which senses wavelengths between 700 nm and 1100 nm, was considered and built into the measurement system at a later stage.

Laser Source

While using the 24 mm PSD sensor, a red laser with a wavelength of around 650 nm was used. It was later replaced by an invisible infrared laser with a wavelength of 905 nm, in compliance with the 37 mm PSD sensor (Section 0).

Geophone

In order to extend the frequency bandwidth of the measurement data, the use of a low-frequency sensor, which has a 1 Hz natural frequency (model: LF-24), has been considered, so that it can collect data extending down to 1 Hz.

The function of individual components was tested and all wiring components were transformed into a schematic design, which represents all components and wires linked to

the components. Then, the schematic design was converted into a Printed Circuit Board (PCB) design using DipTrace, which is a software application for schematic design and PCB design, on the basis of the prototype system of the analogue based device which was previously tested.

In order to accommodate the PCB in a limited size node box, all components must be placed in the right position. This process is iterative in order to connect all components easily. The larger and critical components should be placed first. The size of PCB is restricted to be as small as possible in accordance with PD10 (see Table 4-3), which states, "The enclosed node box size should be considered and positioning of the laser source should keep the clearance." For the sensor node, the analogue and digital circuits were produced for the digital and analogue parts by being partitioned on a PCB layout with separation to prevent interference between the two signals.

After the PCB design and manufacture process, the design of the sensor enclosed box and laser box was considered. Some modifications were made from the preliminary analogue based prototype system.

The design of the node box considered the following issues.

- It is better to ensure sufficient space for the combination including the geophone measurement, with limitations in the dimensions of the box in order to maintain clearance from the track;
- The sensor node should be a light and easy to carry device with limited dimensions and weight;
- The node box can be tested on either a concrete sleeper or a wooden sleeper;
- The sensor electronics are enclosed in a node box, so that the performance of the measurement system is not be influenced by temperature, humidity, or exposure to wind and sun;
- For moisture and corrosion protection of the printed circuit boards, it is essential that no fluids enter the box.

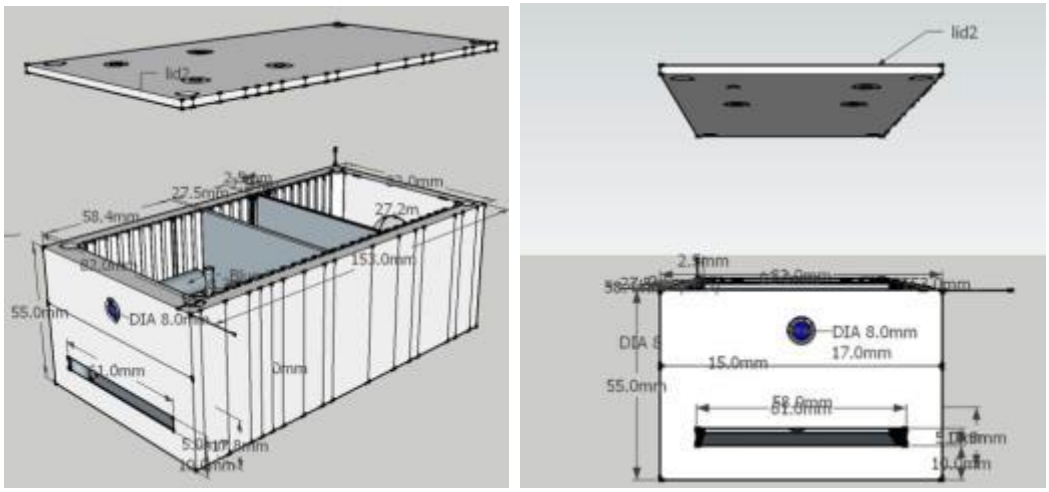

Figure 4-11: Laser box design (ISO and Front)

A laser source will be mounted on the tripod and a line-laser will be enclosed in the box, as shown in Figure 4-11. A blue LED indicates when the laser is on.

4.2.2 Implementation of the Prototype Laser Based System

The new implementation is to resolve the operational challenges of the earlier technology, which were summarised in Section 4.1.2.

4.2.2.1 Software Implementation

The measurement system was built following the design and development stage of the Vee-process. The extracted software requirements are summarised as below.

Table 4-4: Software requirements

Relevant ID code	Software requirements
PD2	Send a message over the CAN bus from PC to sensor node
	Ensure the synchronisation to record and store data
PD3	Display displacement result(mm)
PD6	Display continuous voltage and current draw
PD7	Recording data (csv files)
PD11	Allow for setting of parameters
	Calibration of each node individually (gain, central frequency)
	Display gain/central frequency
PD12-2	Software implementation 4 (laser detection function)

In order to meet all functionality requirements, the system was implemented in software, which was developed in C#. To allow for the continuous monitoring of sleeper movement and remote control for each PSD node, the software is interfaced with new digital sensors. The data logging functionality is also implemented so that all data received from the CAN

nodes are saved onto the computer and written into an Excel file. A screenshot of the application is shown in Figure 4-12. The software presents all connected nodes which will be mounted on multiple sleepers, the deflection level (mm) of multiple nodes using either a geophone or laser system, it displays the power used by the system and the status of the laser beam, CAN network, and allows calibration for PSD sensitivities.

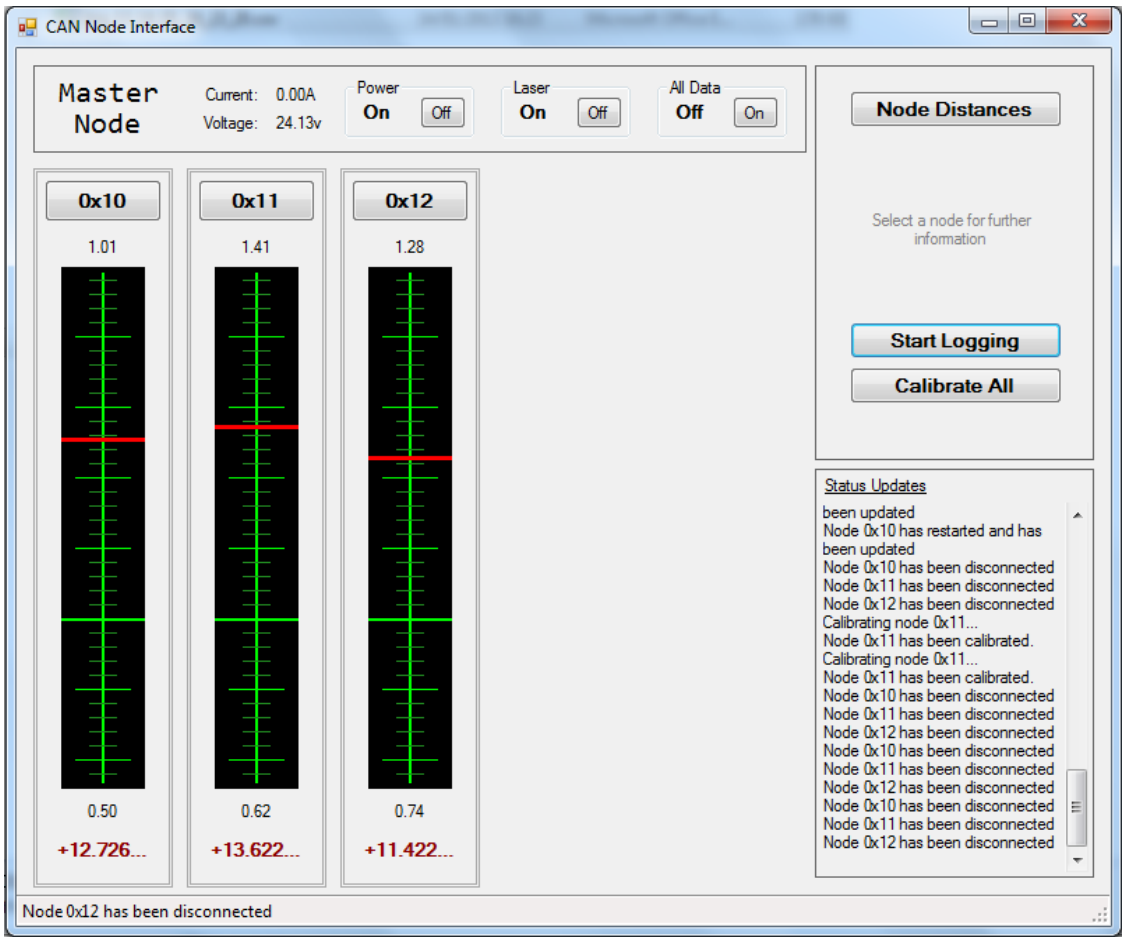

Figure 4-12: Screenshot of software used for real time monitoring of sleeper deflection

Additionally, in order to visualise the moving shape of multiple sleepers in a section of track as a train runs through that section, is visualised with a Matlab programme to produce the animation file to see the deflection data after the measurements are taken, as shown in Figure 4-13.

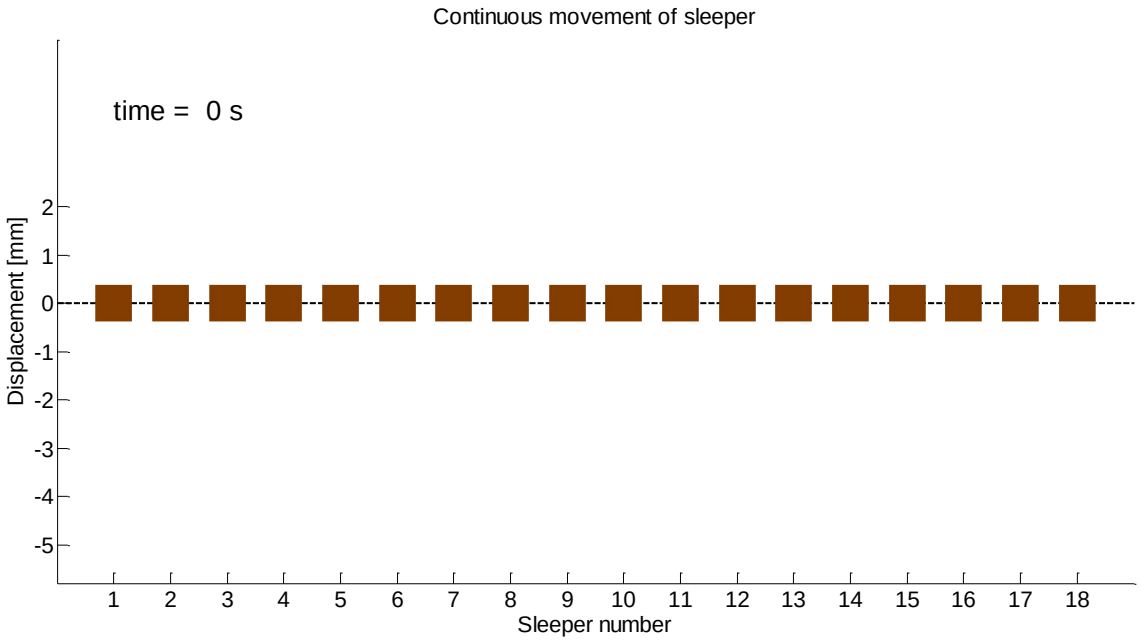

Figure 4-13: The screen shot of a movie file for deflection data after measurement

This is the screenshot of the movie recording file of Matlab and the measurement time is shown on the left top of the figure. The x-axis is the number of sleepers along the track and the y-axis is a range of displacement (mm). The example will be presented in the field trial in Section 6.4.6.

4.2.2.2 Hardware Implementation

Once the three PCBs and the node boxes had been manufactured and the software design had been completed, as described in Chapter 4.2.1, all components were assembled and enclosed into the node box as a complete system as shown in Figure 4-14 for the verification process, which will be presented in Chapter 5.

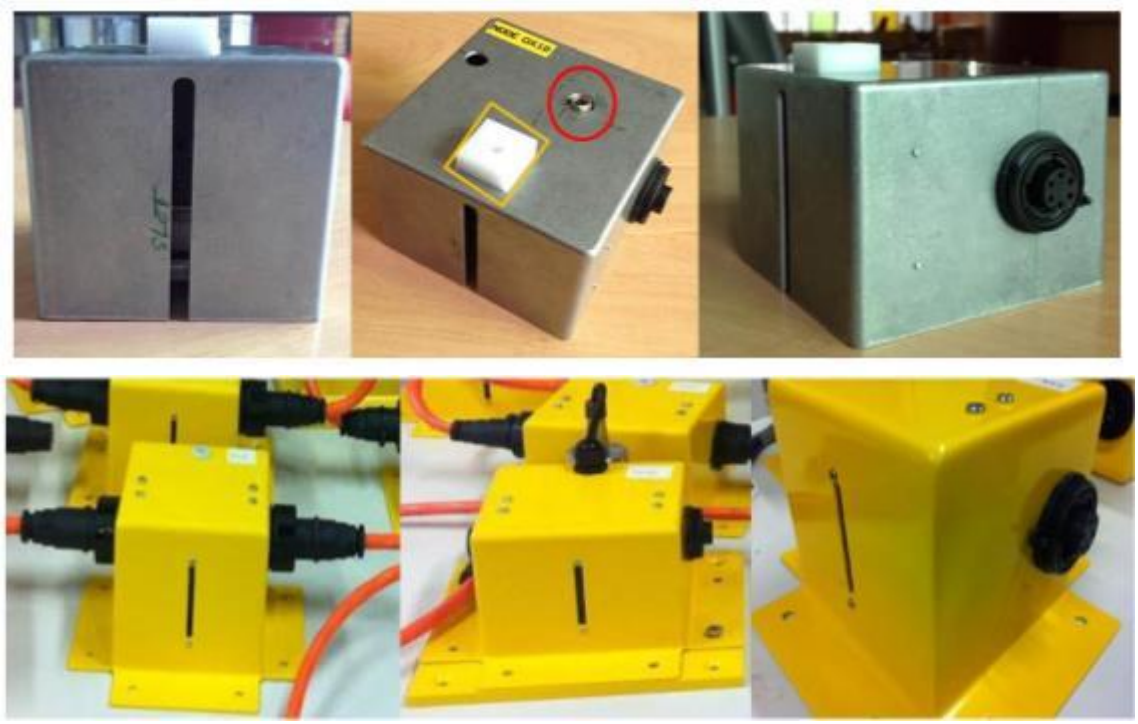

Figure 4-14: (a) First prototype of the sensor node box (box front, slot for geophone and PSD sensor, cable connecter), (b) The second prototype of the sensor node box (node which does not have a geophone, node with geophone and side photo)

Three sets of prototype sensor boxes were built, as some design flaws were found with the prototype, therefore it required design upgrades and modification as follows:

- It was not easy to accommodate the geophone together with the laser sensor inside the sensor box. For the second version of the node box, the geophone has to be positioned outside the box as shown in Figure 4-14 (b);
- It was not easy to position the PSD sensor exactly in the middle of the box using a structure as shown in Figure 4-15 (a) with the first design. Thus a method of finding a simple and easy way of positioning the sensor was considered (b).

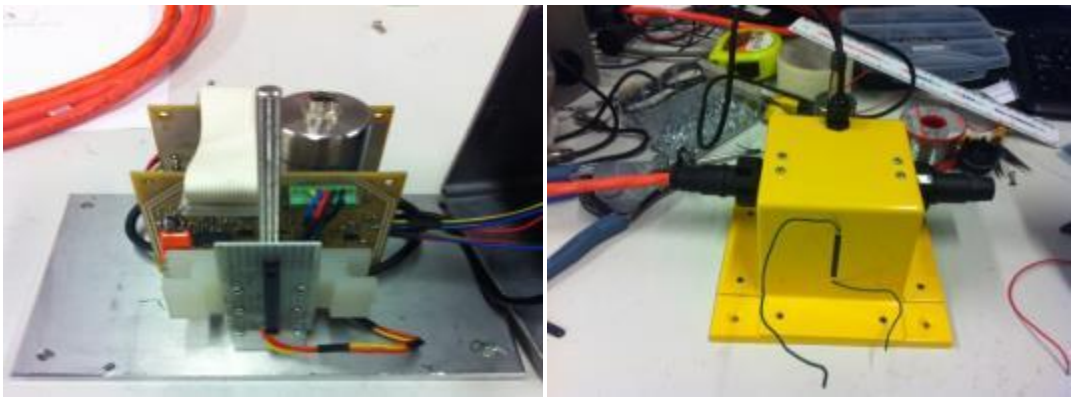

Figure 4-15: (a) Old, (b) new version of node box showing PSD sensor position in middle

- It was decided that the box should be of a bright colour so that it is easily visible;

- Matching the direction in which the laser is pointing to the sensor node is not easy to set up.

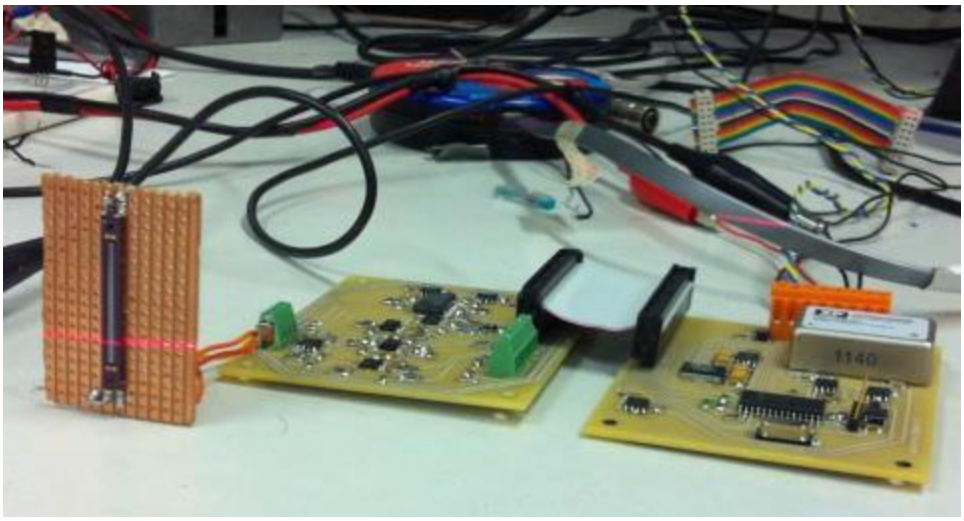

Figure 4-16: Prototype PCB with PSD sensor

The previously used 24 mm PSD sensor was connected into a newly designed PCB board. As part of the verification process, which will be presented in the following chapter, it had to be replaced later with a 37 mm PSD sensor. As shown in Figure 4-16, the Insulation-Displacement Connector (IDC) 24 pin ribbon cable connecting the two boards is too big to fit in the box, so it requires a modification of the PCB board. This has been replaced with 2×8 16 pin dual row sockets, as shown in Figure 4-17.

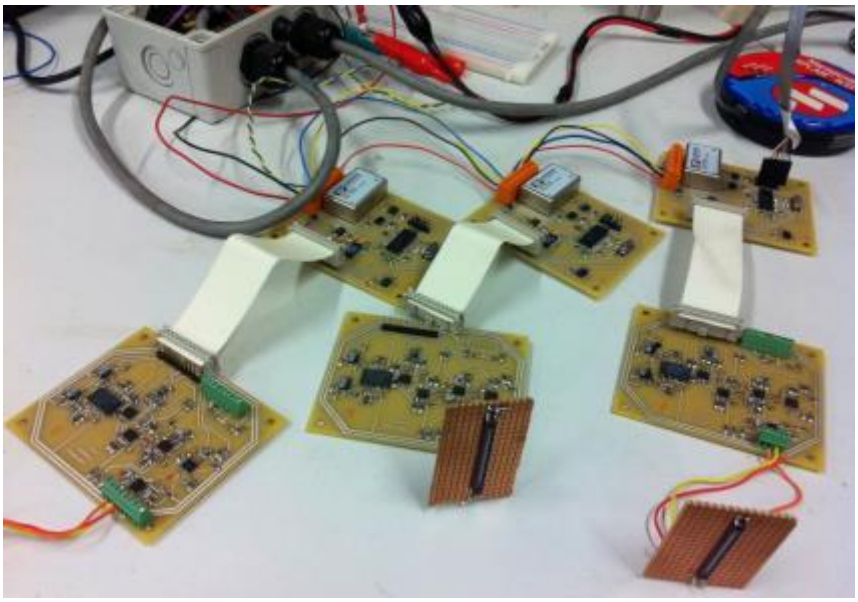

Figure 4-17: Three sets of prototypes

4.2.2.3 Laser Detecting and Auto-Calibration Algorithm

While building and testing the measurement system across multiple sleepers, the distance from the laser source to the individual sensor nodes that sit on the sleepers along the track will be different and, thus, the gain of each signal must be optimised. Figure 4-18 is an example of an installation of 14 sensor nodes along the track with a single laser source. The power density at node 14 would be weaker than at the other nodes that are closer to the source, thus the function of automatic calibration is required to find the optimised gain.

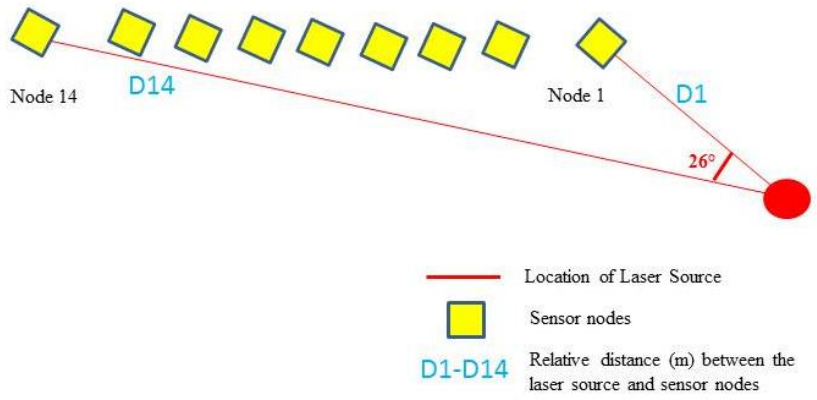

Figure 4-18: The relative distance between a sensor source and the responding sensors

The central frequency of the bandpass filter must be optimised also since it changes due to temperature changes and so on. This process was conducted manually for the earlier prototype. In order to automate the system, the measurement system can calibrate to find the optimised gain and frequency by remote control and help improve the laser setting by implementing PD11 (Calibration function) and PD 12-2 (laser detection function) in Table 4-3. The following diagram, Figure 4-19, shows the implemented data calibration algorithm and laser detection work.

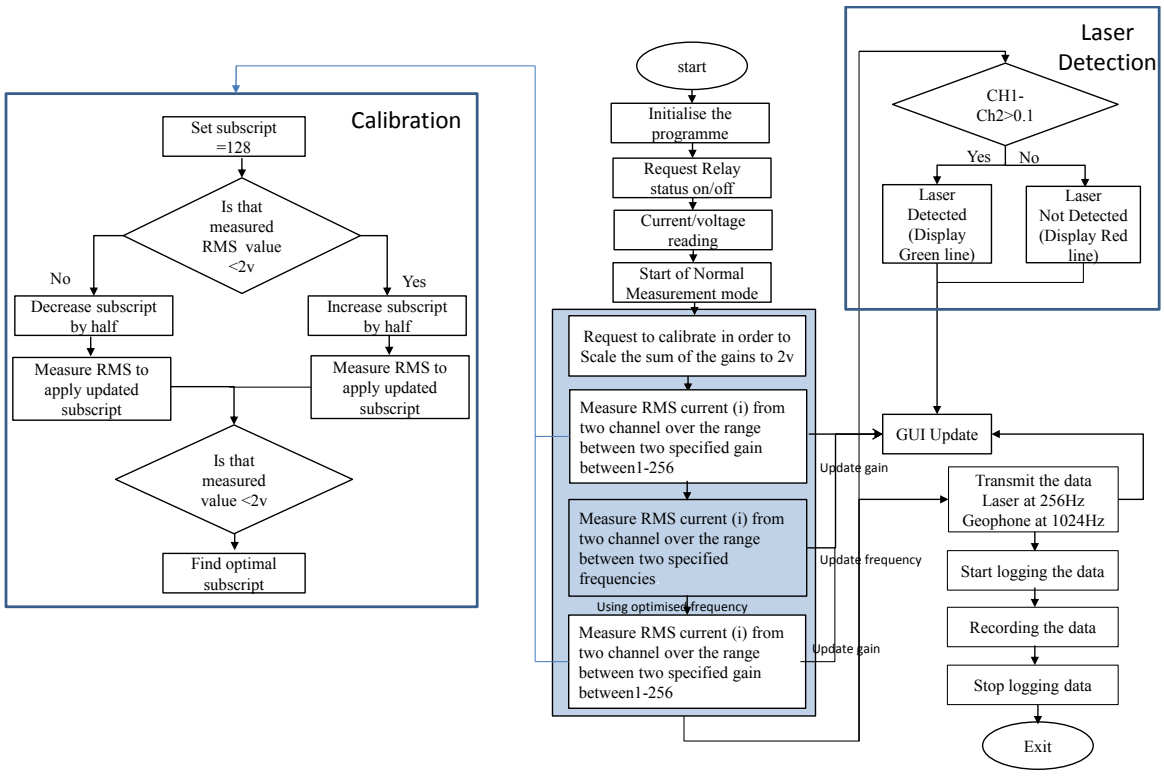

Figure 4-19: Flow chart of the calibration and laser detection algorithm implementation

For the auto-calibration function, a binary search algorithm, which is generally used in computer programming, is used to find the optimised position of the updated value of the gain within a range between 1 and 256, depending on the strength variation of the laser source, corresponding to the distance from the laser source or the angle. Firstly, electrical current and electric voltage data are converted to Root Mean Square (RMS) format. Then, the binary search process is repeated until the result of the iteration finds an optimised gain value that produces a rescaled RMS value that is closest to 2 V, which is the maximum working voltage of an RMS-DC converter (ADG636). For the laser detection of each sensor node, the laser strength is measured from the optimised gain and a differential value is taken between Ch1 and Ch2, whether the laser is detected within the fixed length of the sensor or not. When the laser strength is above the minimum level and detected, a green line is displayed, which indicates that the laser is detected, otherwise the line is red while the laser is not detected.

4.2.3 Test Specifications

After the prototype had been implemented, the test plan was considered for the purpose of system verification. Table 4-5 sets out how the functional specifications, which correspond

to Figure 4-20, were checked. The test plan will be used in Section 4.3 for the integrated components test and Chapter 5 for the laboratory experiment.

Table 4-5: Test specification in accordance with requirements

ID code	Test Specification	Acceptance Criteria
TS1	Interface test between laser and PSD sensor and see the maximised optimum distance with calibration.	• Maximum distance to be monitored should be decided, for example, 18 m. • The number of sleepers that can be assessed by the laser measurement system
TS2	• Test continuous measurement for 35 s, assuming that a very slow train passes. • Each test will be repeated 40 times (5 trains × 8 hours) • Test in order to find an optimum number of connecting nodes.	• The CAN network and measurement recording should be stable during the measurement • Maximum number of connecting nodes (12-18 nodes)
TS3	Check if the screen shows the displacement clearly.	Displacement (mm) is monitored in real time.
TS4	Test under adverse weather conditions to check waterproof function and see the effects of the wind.	Normal operation during adverse weather.
TS5	Comparative test with geophone and data agreement with geophone, in particular, consider testing at different frequency (train speed).	A variation in the measurements will be examined with a range of different frequencies.
TS6	The battery should last for at least one day. Current Consumption calculation.	Normal operation during using a battery for one day experiment. 1.5A/90AH = Last 60 hours
TS7	Test data storage function if data is stored in right format.	Data has stored in excel format during system measurement.
TS8-1	The system accuracy will be examined.	The system accuracy is closer to 100 μm (0.1mm).
TS8-2	Take a displacement measurement at a range of different distances of the laser source and see the result.	The variability in the characteristics of a laser source could be examined depending on the distance, e.g., the intensity of the laser source and the distance between the source and sensor and beam divergence.
TS8-3	Test the resolution of the system.	The resolution is better than 10 μm.
TS9	Check the laser power level and make sure the count is measured for safety protection, in case it is required.	Possibility of using laser level 1 so that it does not require the use of a safety device.
TS10	Check whether the dimensions of the node box are under the rail top, and that the laser source is 3.5m from the track at every measurement.	Node boxes and laser position give sufficient clearance from the railway track.
TS11	Test remote control functions:	The remote calibration works via GUI.

ID code	Test Specification	Acceptance Criteria
	• Calibration work for individual nodes • Distance Setting	
TS13	Measure time consumption to install and remove the system.	It should be less than two hours or a similar level to the geophone.
TS14	Possible to carry each node and system by hand.	It is easy to carry by hand.
TS15	Check the estimated price against an existing similar system (e.g., Geophone).	The cost of system development should be less than or the same as the Geophone.

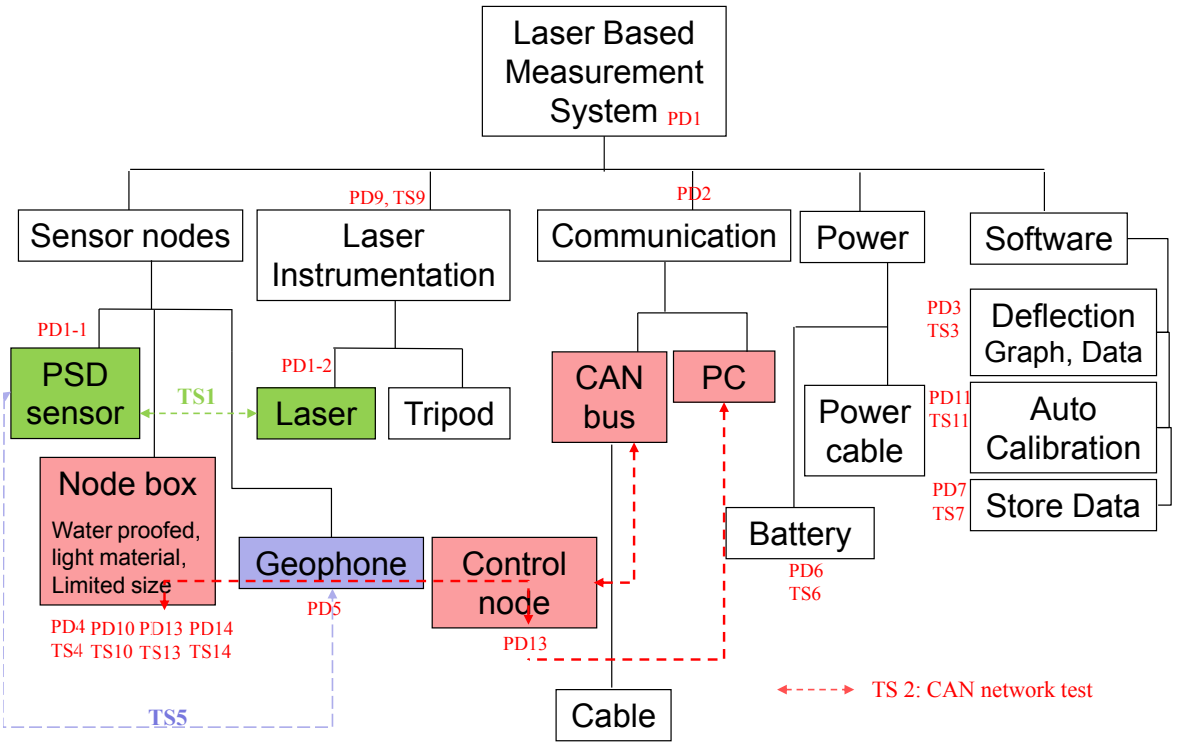

Figure 4-20: Physical development and relevant components and interface test

4.3 Integration Process

During and after the implementation of the software and hardware, the individual components and relevant interfaces should be tested and verified for the entire measurement system. This stage is shown on the Vee-diagram in Figure 4-21.

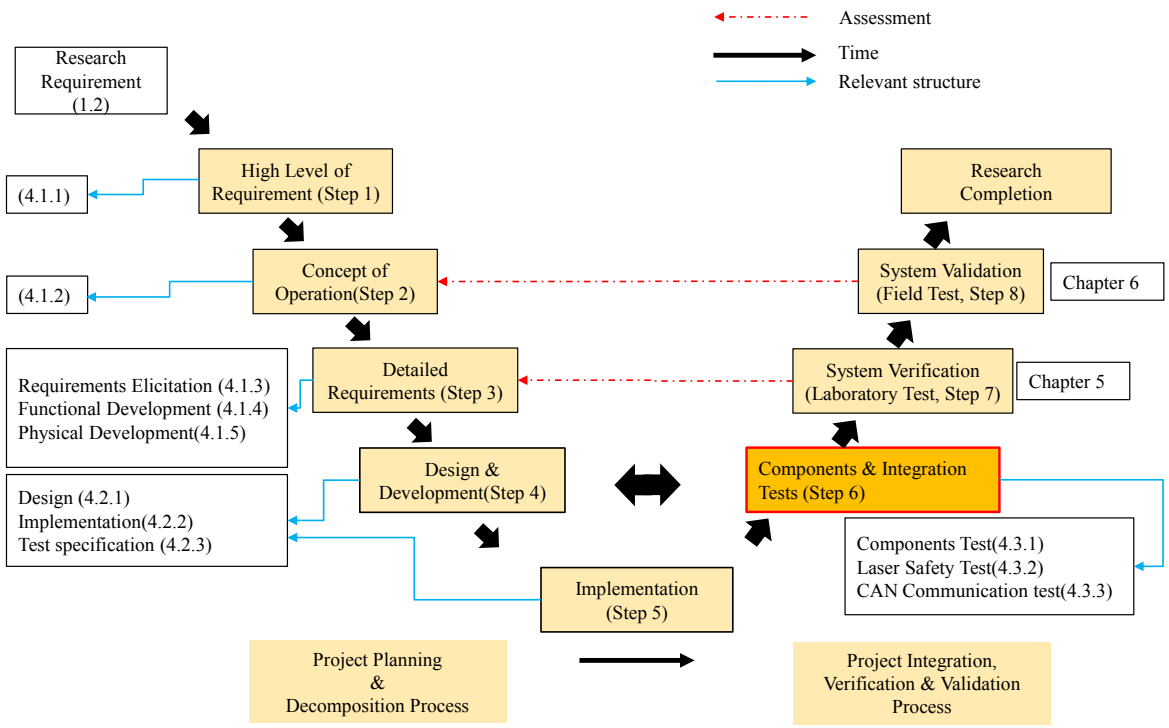

Figure 4-21: Integration test of Vee-model diagram

4.3.1 Test and Interface

The purpose of the test and this interfacing stage is to ensure all individual components work completely against the corresponding individual requirements. They must then be integrated with each other to form a complete system ready to test in the laboratory in a similar way to the field test. Therefore, once the boards were completed, the complete functionality was tested and minor issues were found that did not affect the function, but which would have to be fixed in a next revision.

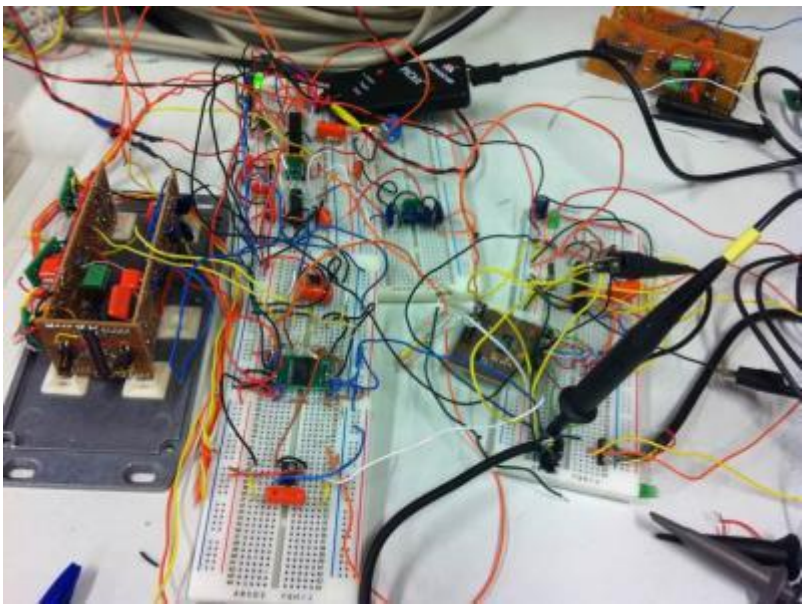

Figure 4-22: Breadboard prototyping and components test

After the process of components selection in Section 4.2.1, each digital component was individually tested on the breadboard by exploiting a previous analogue circuit, as shown in Figure 4-22, in order to replace an analogue part with digital components. The data has been presented in the 5th IET International Conference on Railway Condition Monitoring conference (Kim *et al.*, 2011), see Appendix A. In addition, an interface test was conducted for the performance of the 1 mW laser source and a 24 mm PSD sensor to ensure that a 1 mA laser source was sufficient to excite the PSD sensor when positioned at a distance of approximately 18 m, using the digital potentiometer gain control. The laser source was positioned at the corner of the laboratory and the sensor was positioned on a work bench as shown in Figure 4-23, and it showed the feasibility of the measurement system at a maximum distance of 18 m.

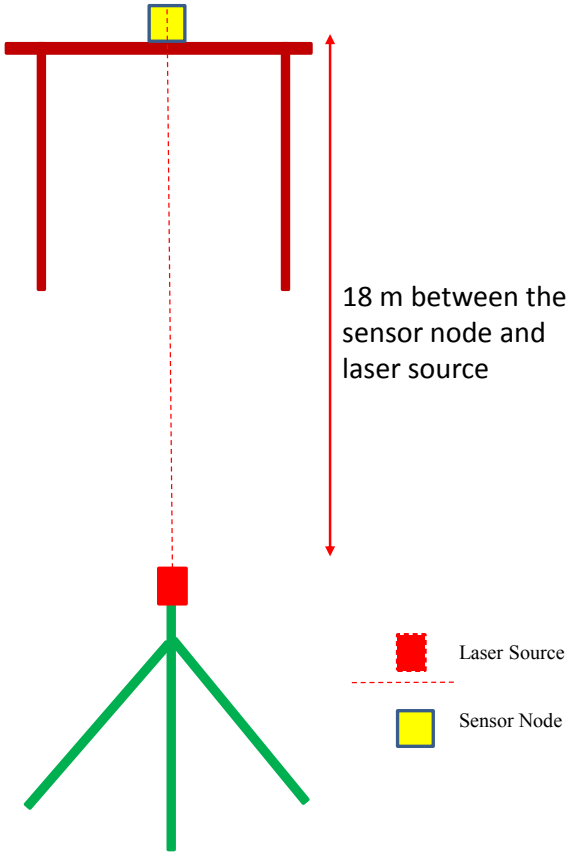

Figure 4-23: Layout for a laser source experiment set-up

4.3.2 Laser Testing

The Health and Safety unit of the University required the laser to be classified to ascertain its power level, so that safety measures could be implemented, if required. The test is conducted by using a laser power meter, as shown in Figure 4-24.

Figure 4-24: Laser power meter

Using a 1 mW infrared laser, the output power was 60-70 µW, peaking at 93 µW, which was less than the value expected, considering that the actual power output from the slot of the box was 10% of the designed output. After taking a further measurement, the laser was classified as Class 1, which is safe for all conditions without specific safety measures. When the 10 mW infrared laser was tested, it resulted in an output of less than 1 mW. Therefore, it was also classified as Class 1 when measured at the end of the slot of the node box, so it also did not require any additional safety measures.

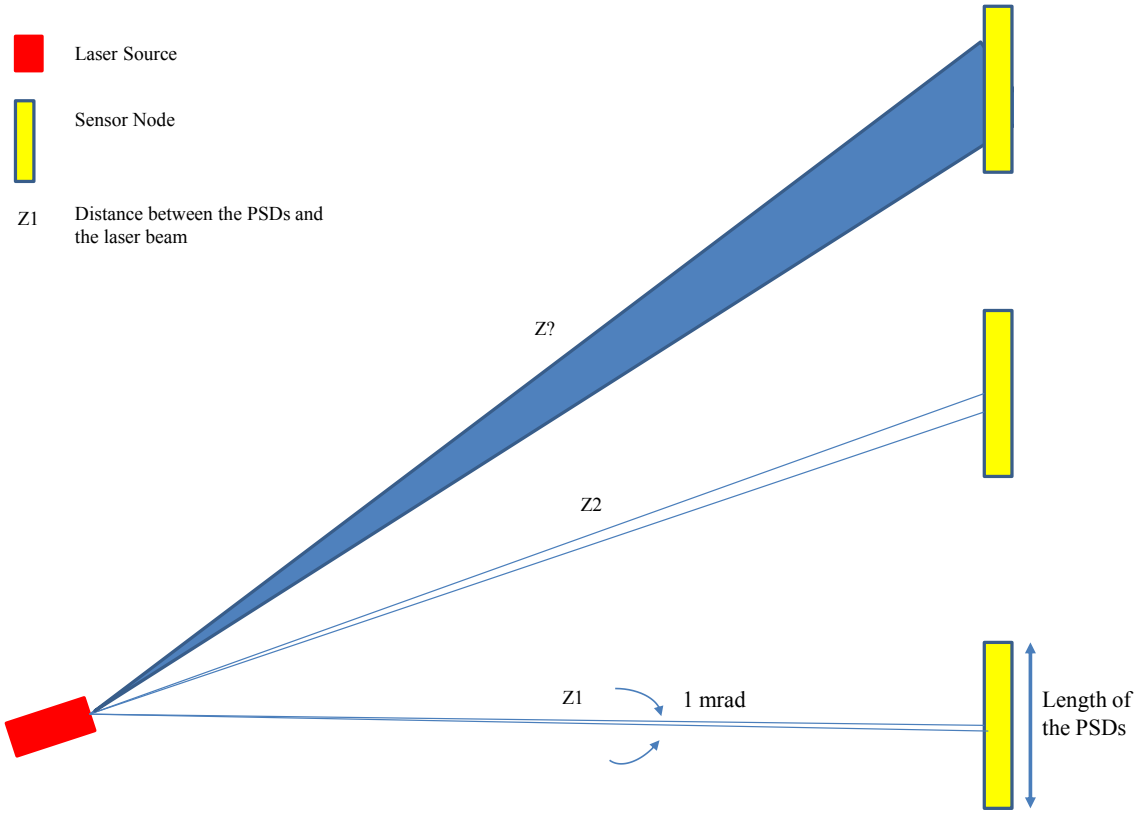

Figure 4-25: Schematic of the beam width measurement and the variation of the beam strength with distance

The beam (vertical) width is proportional to the working distance and the power density decreased from the specific working distance and line width (interview with Gus Zabierek, 2014). The variation of the beam width with vertical movement and the variation of the beam strength with different distances over 10 m have been tested using a laser power meter, as described in Figure 4-25. The laser line has some spread in the vertical direction, around 1 mrad, therefore, with a target distance of 10 m the vertical beam spread is about 10 mm. As the target moves further from the laser source, the beam spread becomes significant compared to the height of the PSD sensor, so the accuracy of the results starts to decrease.

4.3.3 CAN Communication Test

The state of the network should be stable running with multiple nodes. In this test, the ideal number of nodes was identified. Figure 4-26 shows a schematic of the CAN network. CAN master nodes are connected to the laptop via PCAN-USB, which is a USB adapter for the CAN interface, and the first adjacent nodes are connected to the next nodes.

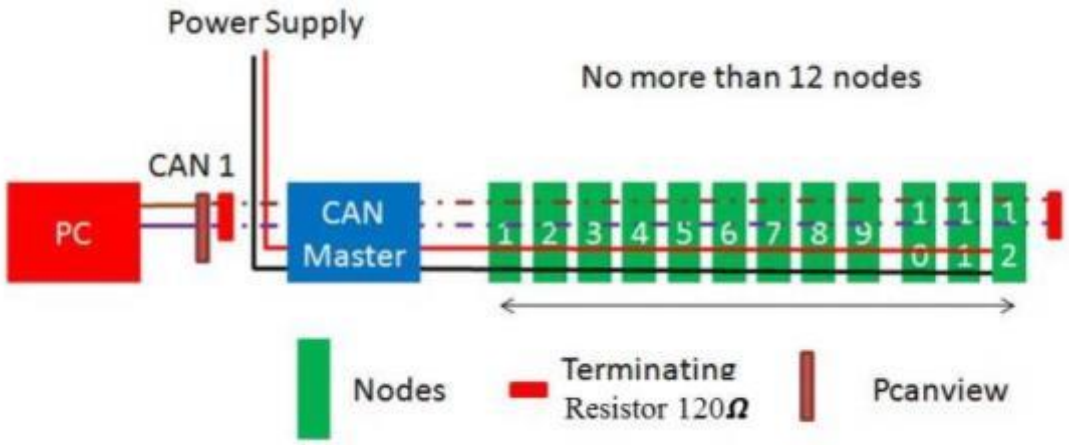

Figure 4-26: Schematic view of the initial CAN Bus connection for 12 deployed nodes

Figure 4-27: Sensor nodes layout

Before undertaking a field test at the test track at Long Marston, multiple nodes were laid out in line, as shown in Figure 4-27. It was found that the sensors were affected by sunlight, which caused a high level of noise. Therefore, it was necessary to shade the slot using a black cover so that the sensor detector was positioned in a shaded environment and not affected by direct sunlight. Considering the stability of data transmission through a CAN bus, it was identified that it is reliable to connect 12 sensor nodes mounted on the sleepers for the first field test. The CAN communication distance for 12 nodes is approximately 8.5 m.

4.4 Summary for Chapter 4

Chapter 4 has been used to show how the laser-based measurement system was developed using a system engineering approach that was aimed at upgrading the work of the prototype laser system. The selection and application of the systems-development approach using the Vee-process saves time and minimises repetitive work through a well-planned process from the initial concept to the building of three prototypes of the laser-based measurement system. At the beginning of this chapter, the high level requirement was presented and it has been decomposed further into functional and physical requirements which have a single, applicable concept set out in statements in Section 4.1.1. These statements are applied practically through the implementation of software and hardware and conclude with three sets of digital component-based prototype systems. Through component and integration testing, the author found the maximum feasible distance that can be monitored to be 18 m, which implies a number of sleepers can be measured using an optimised number of sensor nodes, ensuring stable CAN data communication.

The final two steps of the Vee-process, system verification and system validation procedures, have not been discussed in this chapter. These two steps must be performed on the basis of laboratory tests, recording the results of the measurement system and field tests against the test specifications. These procedures will be described in the next two chapters.

5 Laboratory Validation Test and Result Analysis

In the previous chapter, three nodes of a prototype system were designed and implemented and each step has moved forward on the left side of the Vee. In Chapter 5, system verification, also referred to as an acceptance test, will be carried out, see Section 0, and the result will be described to verify the developed system to ensure that it is consistent with the detailed requirements, which are stated in Section 4.1.

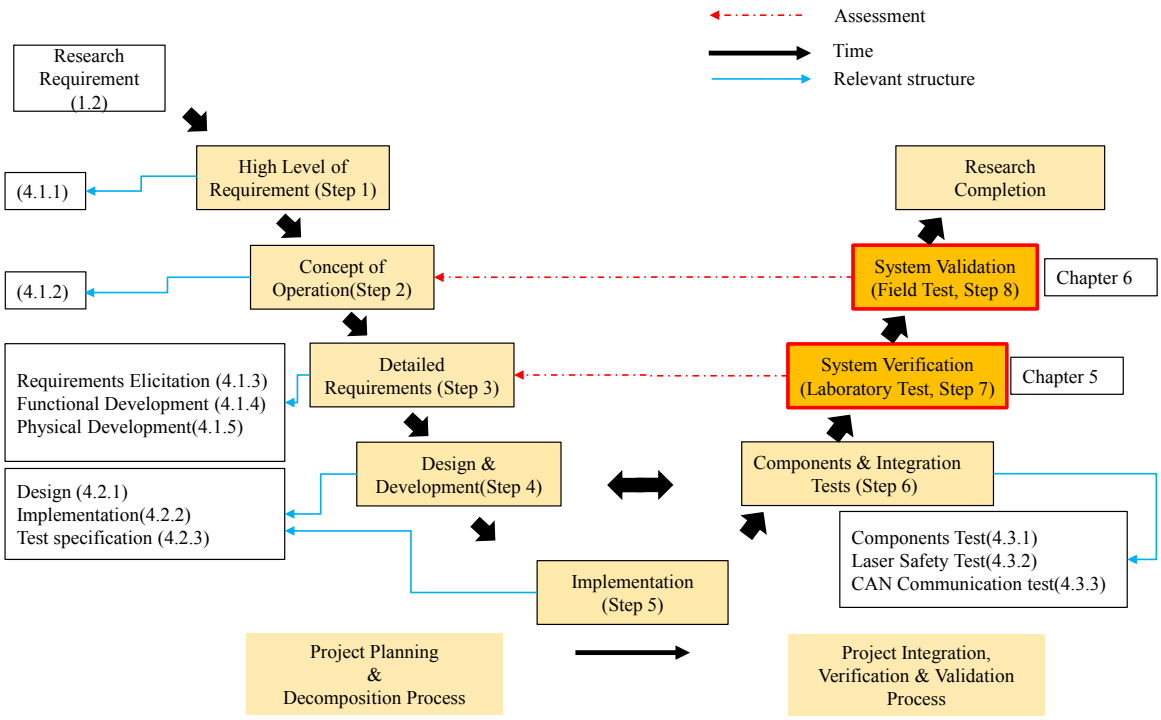

Figure 5-1: Last two stages of Vee-model diagram

The laboratory test must be carried out before the field test to ensure the required performance will successfully meet the desired level of reliability. This process is required to estimate the degree of expected error due to inaccuracy and imprecision and to confirm that the degree of error is within the accepted levels, in particular, in order to check the test specification (TS 8-1, TS 8-2 and TS 8-3) in Section 4.2.2.3 to satisfy SR 8 (System accuracy) in Section □.

For the first part of the laboratory test, the measurement system will be tested by placing different depth plates under a sensor node, taking measurements and comparing the actual displacement and the data results.

In the second section, the test will verify the laser based system, including a comparison with the geophone sensor, which is widely used for track displacement measurement

system research. In addition, the usable bandwidth for the geophone data will be verified by a comparison test between the sensor node developed and the geophone sensor.

In the third section, the level of accuracy will be verified by a comparison test between one of the prototype nodes and a Micro-Epsilon laser, on the basis of the experiment set-up plan in Figure 5-2. Part of the work that is presented here has already been published in a conference paper (Kim *et al*., 2014), see Appendix A.

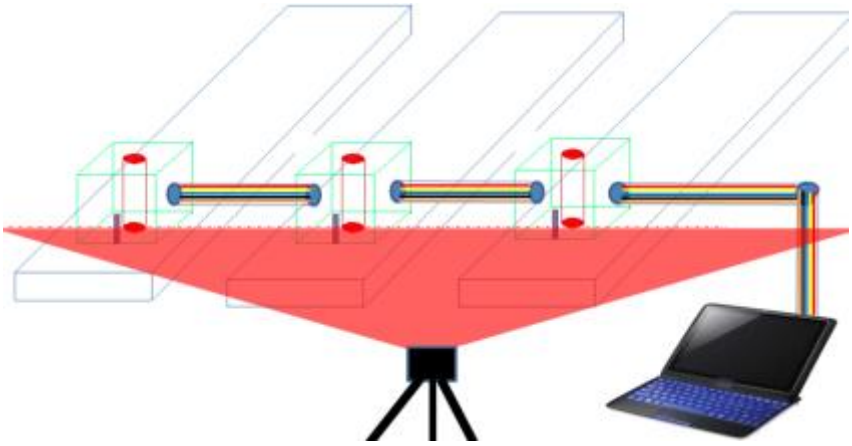

Figure 5-2: The concept of prototype experiment

5.1 Initial Tests in the lab

5.1.1 Laboratory Setup

As reviewed in the literature (Figure 3-2), the range of sleeper displacement on high speed line is less than 1 mm, it is 5 mm on poor quality track. Therefore, 2 mm and 5 mm plates were placed underneath the sensor node and measurements were taken before and after introducing the plates, as shown in Figure 5-3. The graphs and tables of repeated results and the agreement between them are shown and discussed in this section.

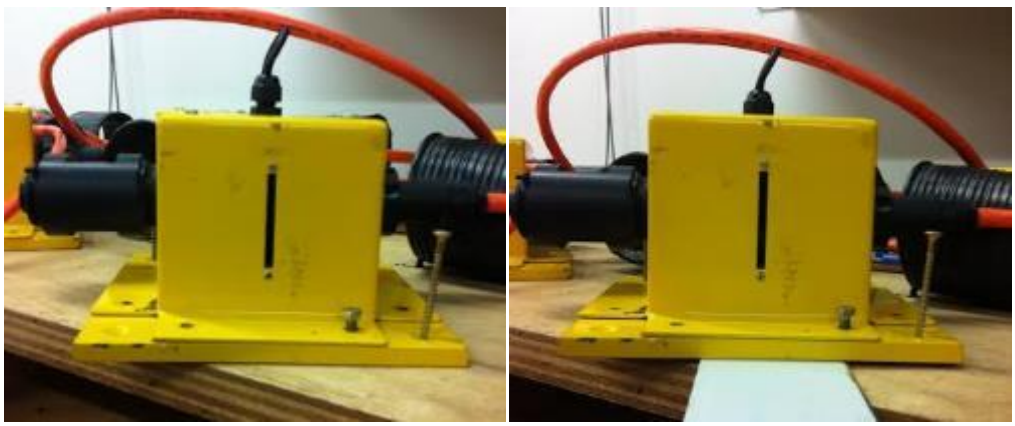

Figure 5-3: Placing different thickness plates under a sensor node box

5.1.2 Repetitive Test and Result

It was a straightforward test to simply put the plates underneath the sensor nodes, therefore any error is easily detected. Additionally, the tests were repetitively conducted with a different range of laser intensity by re-positioning the laser source, i.e., the laser source has the characteristics of a Gaussian beam, so the laser intensity from the edge of the laser source through the slot of the laser box to the PSD is not as strong as from the middle of the laser source through the slot of the source box. The system is designed to be set up with the correct gain value with a calibration function, so the value of the gain by the remote-calibration function is assumed to be proportional to the laser strength that is influenced by the distance between the sensor and source and the angle. While the controllable range is between 1 and 255, the laser strength is high when the calibrated gain is close to 1 and the laser strength is low when the resulted gain is close to 255. For the repetitive tests, a total of 100 measurements have been carried out, as shown in Table 5-1. From the range of the data, the accuracy (mm) is calculated by subtracting the processed maximum and minimum values and each width of plate between 2 mm and 5 mm; they are all within 1 mm difference, so this is the range of the data.

Table 5-1: The list of repeatability tests

Run Number	Displacement (mm)	Automatic Calibration Resulted Gain	Accuracy (mm)
1-10	2mm	7	0.035
11-20	2mm	129	0.057
21-30	3mm	7	0.057
31-40	3mm	153	0.081
41-50	3mm	7	0.059
51-60	3mm	143	0.088
61-70	4mm	7	0.041
71-80	4mm	121	0.092
81-90	5mm	9	0.051
91-100	5mm	193	0.0995

Table 5-2 shows one example of the collected data, which resulted in a 2 mm real displacement while the gain was 7, which means the sensor easily picked up the fairly high level of laser strength and, thus, the calibrated gain is relatively low. The repetitive test results (Figure 5-4) were satisfactory with less than 0.05 mm error.

Table 5-2: Displacement test (2mm)

Sleeper Measurement System Laser Data										
Power Consumption: 0.02A; 23.61v										
Node	Gain1	GR: Ch1/Ch2	Freq	Geo	DLeft	DLaser				
0x20	7	NaN	804.63 kHz	On	32					
Time	1	2	3	4	5	6	7	8	9	10
1	0.009	0.004	0.04	0	0.039	0.009	0.021	0.004	0.002	0.001
2	0.005	0.004	0.004	0.037	0.094	0.001	0.019	0.019	0.063	0.036
3	0.067	0.06	0.001	0	0	0.025	0.008	0.06	0.047	0.001
4	0.048	0.004	0.022	0.072	0.052	0.003	0.01	0.05	0.01	0.073
5	0.079	0.004	0.012	0.029	0.061	0.024	0	0.035	0.039	0.03
6	0.089	0.004	0.011	0.014	0.052	0.099	0.012	0.004	0.051	0.015
7	0.075	0.019	0.024	0.074	0.002	0.002	0.011	0.026	0.047	0.075
8	0.073	0.019	0.066	0.066	0.037	0.005	0.024	0.001	0.065	0.067
9	0.046	0.019	0.004	0	0.004	0.086	0.011	0.008	0.01	0.001
10	0.079	0.019	0.001	0.099	0.016	0.042	0.018	0.039	0.039	0.1
11	0.05	0.019	0.009	0.029	0.044	0.028	0.014	0.011	0.01	0.03
12	0.046	0.019	0.017	0.05	0.006	0.076	0.028	0.003	0.002	0.051
13	0.037	0.019	0	0.054	0.019	0.064	0.017	0.017	0.036	0.055
481	2.011	2.01	2.029	2.002	2.038	2.056	2.058	2.034	2.055	2.022
482	2.025	2.038	2.058	2.063	2.03	2.066	2.05	2.012	2.036	2.023
483	2.011	2.014	2.039	2.027	2.022	2.052	2.057	2.014	2.026	2.037
484	2.059	2.033	2.06	2.018	2.002	2.065	2.037	2.063	2.013	2.018
485	2.031	2.003	2.062	2.022	2.032	2.035	2.058	2.024	2.031	2.032
486	2.057	2.05	2.063	2.065	2.069	2.012	2.052	2.021	2.008	2.025
487	2.032	2.067	2.035	2.061	2.011	2.03	2.06	2.013	2.021	2.021
488	2.01	2.035	2.03	2.055	2.066	2.033	2.051	2.025	2.067	2.035
489	2.009	2.055	2	2	2.011	2.036	2.064	2.037	2.035	2.02
490	2.033	2.012	2.006	2.028	2.035	2.038	2.051	2.067	2.035	2.038
491	2.058	2.029	2.014	2.037	2.037	2.054	2.056	2.016	2.035	2.067
492	2.059	2.016	2.019	2.003	2.039	2.053	2.05	2.001	2.035	2.023
493	2.024	2.011	2.017	2.021	2.013	2.012	2.053	2.033	2.035	2.001
494	2.032	2.034	2.026	2.024	2.033	2.035	2.05	2.005	2.022	2.034

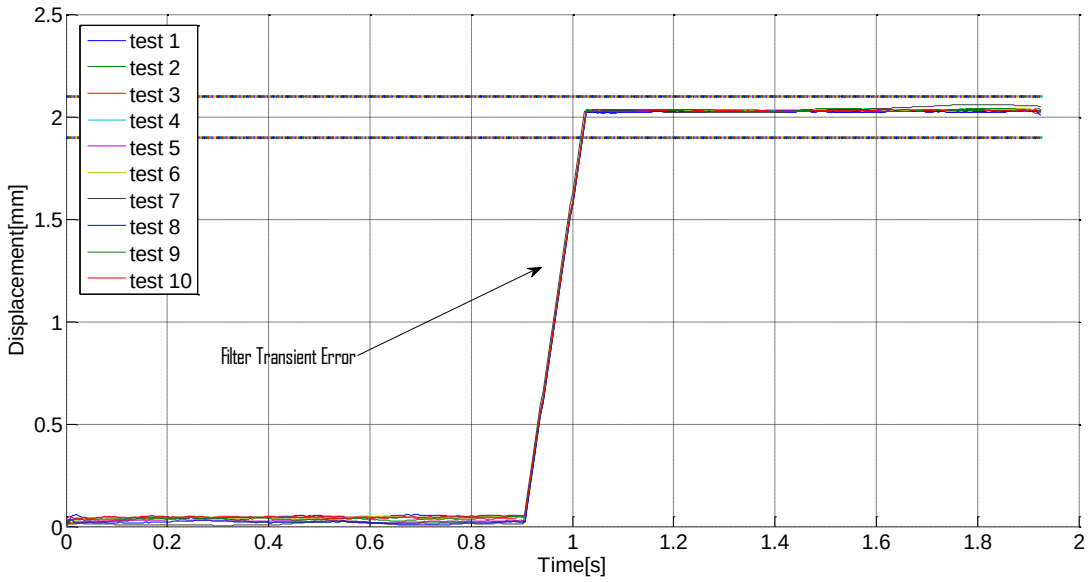

Figure 5-4: Gain of 7 with 0.04 mm error while inserting a 2 mm plate

Figure 5-5 shows the displacement which also resulted in a 2 mm real displacement while the gain is comparatively high, at 129. The result was very good with 0.1 mm error.

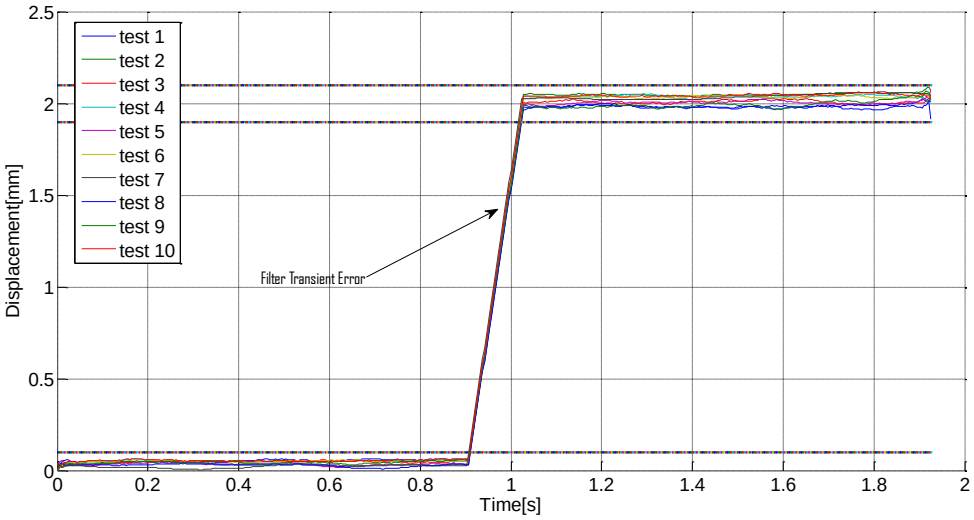

Figure 5-5: Gain of 129 with 0.057 mm error while inserting a 2 mm plate

Figure 5-6 shows that the displacement data result when placing a 5 mm plate under the sensor nodes was within 0.87 and 1 mm accuracy. It is therefore expected that a sensor node, which is positioned further away, will perform well, in agreement with the research requirement which requires 0.1 mm accuracy.

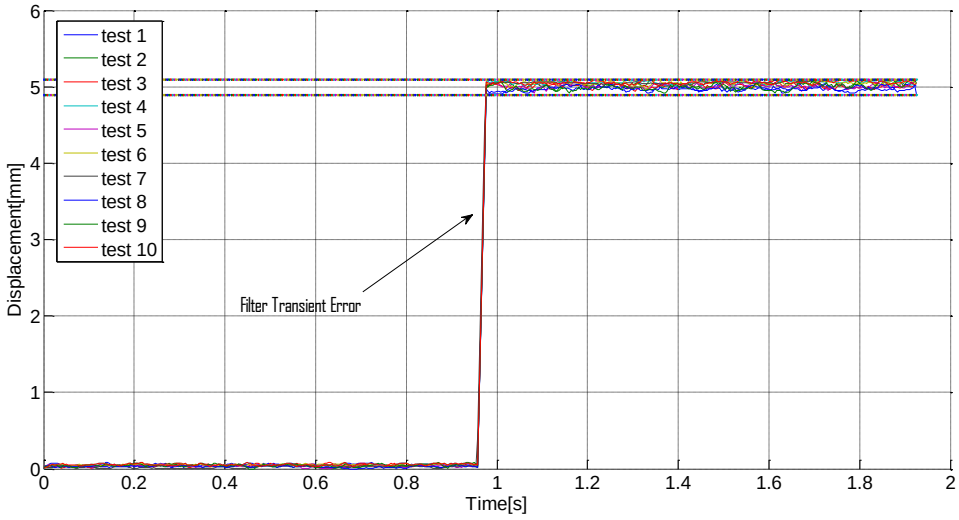

Figure 5-6 : Gain of 193 without error for 5 mm plate

5.2 Validation Test of Laser Displacement Sensor and Geophone

5.2.1 Laboratory Setup

The laser and geophone combination was tested using the workbench as a moving platform and using manual movement of the bench top, as described in Figure 5-7. The geophone

was located loose on the bench top, next to the displacement sensor, so that they both saw nearly the same vertical motion.

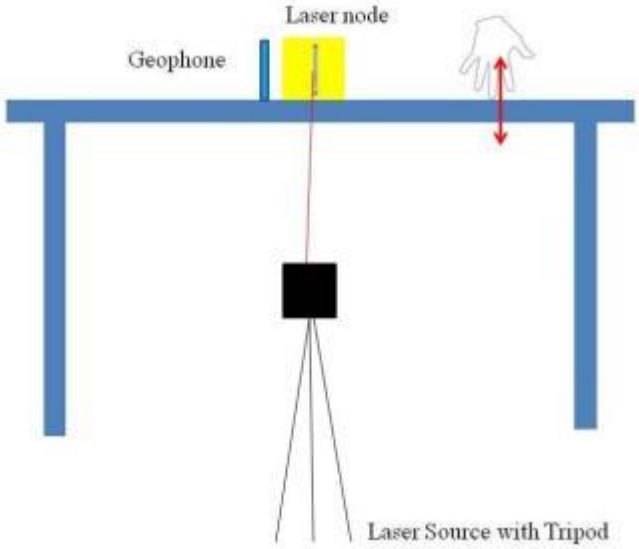

Figure 5-7: Experimental setup with a Geophone and the laser sensor box

5.2.2 Data Processing with Matlab

A geophone is a sensor which produces electrical voltages (e.g., 15 V/m/s for LF-24), which corresponds to the velocity of the object. The raw data of the geophone, which is velocity, were integrated with the laser sensor displacement data and data processing was carried out using a MATLAB programme, as shown in Figure 5-8. In order to calculate the integral to get the displacement, it was necessary to remove the mean value to adjust for unknown initial conditions.

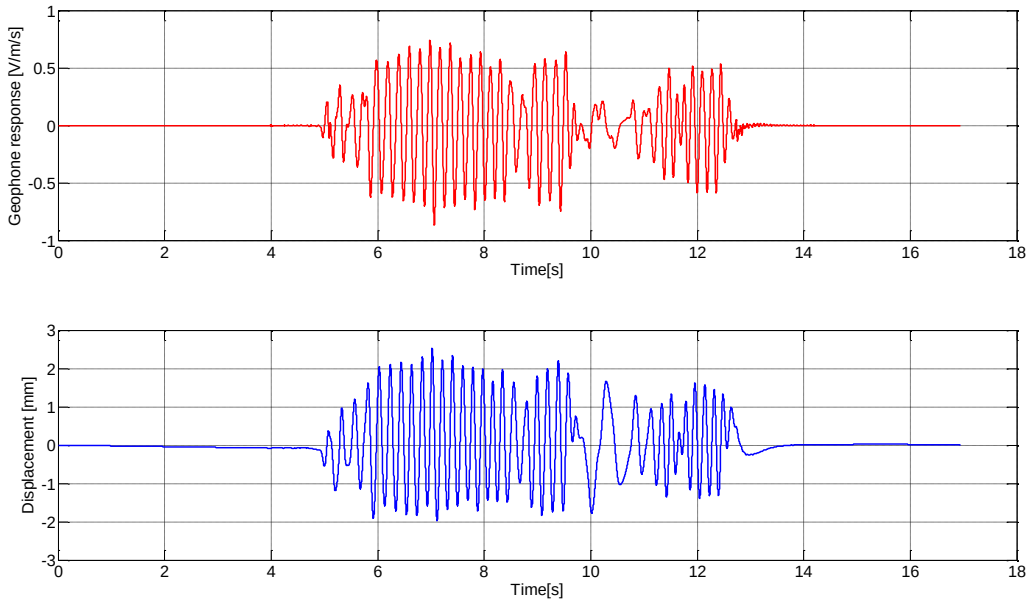

Figure 5-8: Example of Geophone data processing

The moving average filter was used for the data processing, both for the laser and geophone data. This filter is easy to use and reduces random noise while retaining a sharp step response by replacing the original input point with a neighbouring point within a predefined extent. The description of the filter is set out in Equation (21).

$$y[i] = \frac{1}{M} \sum_{j=0}^{M-1} x[i+j] \qquad (21)$$

When x [ ] is the input signal and y [ ] is the output signal, and M is the number of points used in the filter and time series related j. The following example shows that, if M is 5 and requires producing a 5th output with input x [5], the data is smoothed at the centre of the predefined scope, which is 5.

$$y[5] = \frac{x[3]+x[4]+x[5]+x[6]+x[7]}{5} \qquad (22)$$

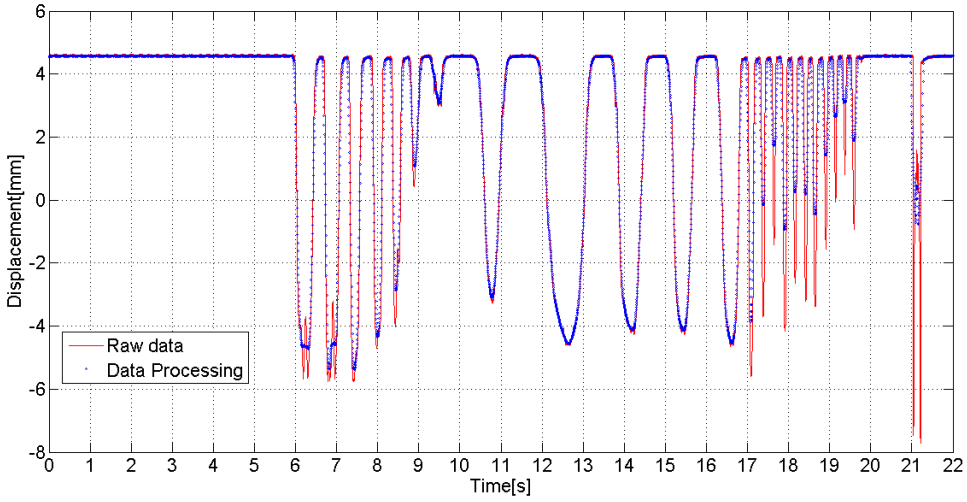

Figure 5-9: Example of the data processing of the laser system

In this research, the moving average filter has been implemented in the Matlab programme with a span of 31. As can be seen in Figure 5-9, which is one of the example files, the original values have been processed after the filtering process and smoothed values have been generated.

5.2.3 Test and Result between Geophone and Laser Prototype System

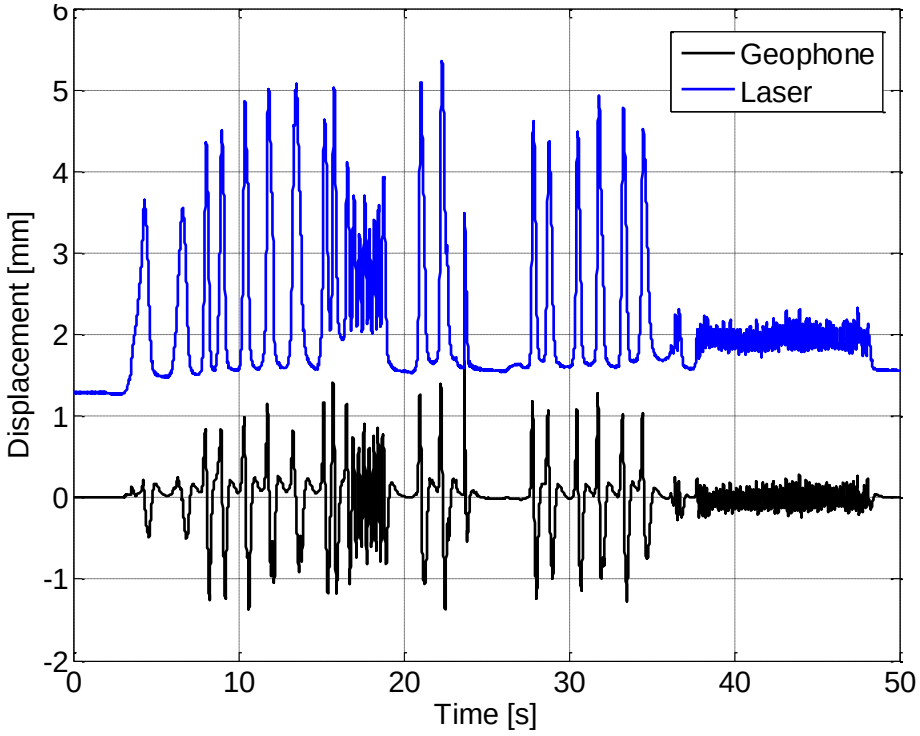

Figure 5-10: Comparison graph between Geophone and PSD sensor

Figure 5-10 shows the result of 50 seconds of manual bench top movement.

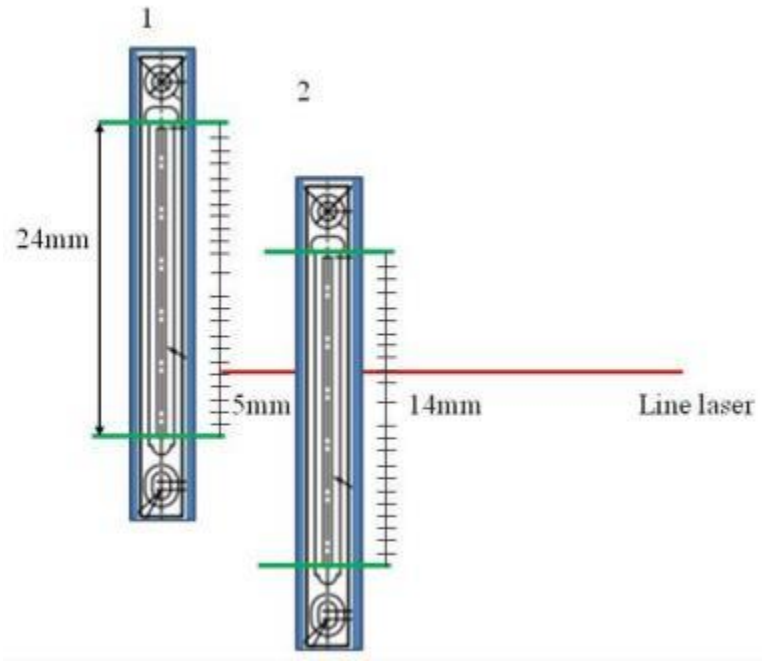

Figure 5-11: Movement of bench top (1: before, 2: after bench moving down)

As illustrated in Figure 5-11, the positive displacements make the bench top move down, which means the position of the laser on the sensor moves upwards. This can be inverted to give the movement of the target instead. The bench was initially at rest and was then pushed down by hand over a time of about 1 s and then released. After some of these tests, the bench top was vibrated by hand at about 3.3 Hz for between 17 and 19 s. After some more slow leaning action on the top, a higher frequency vibration of about 5 Hz with smaller amplitude was applied by hand, as shown on the graph between 37 and 47 s, as shown in Figure 5-10.

As described in the previous section, the geophone displacement was generated in Matlab by integrating the geophone signal, the mean having been removed to prevent linear drift. The slow movements of the bench top resulted in sensible readings from the laser displacement sensor but not much, or not enough, response from the geophone. This is expected as the geophone lower limit frequency has been stretched (by the manufacturers) to about 1 Hz. The higher frequency tests are detailed below.

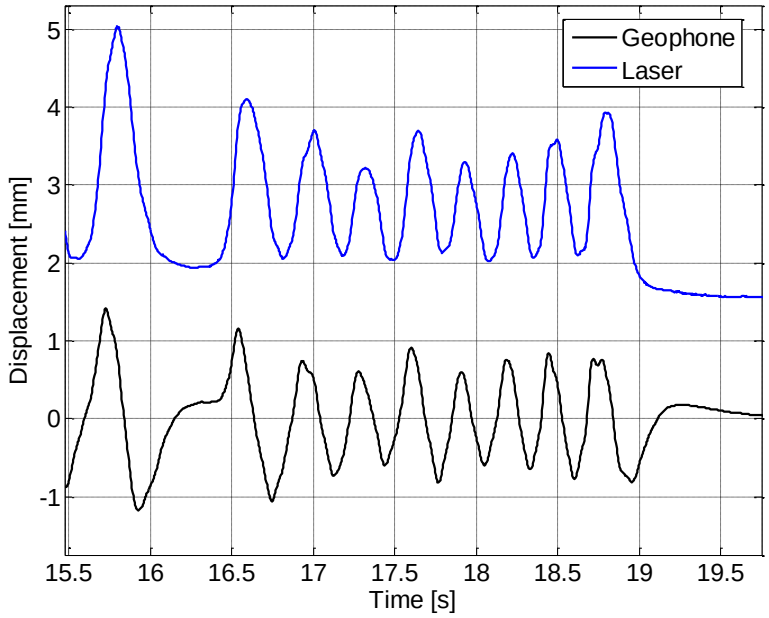

Figure 5-12: Zooming in to compare results between Geophone and PSD Sensor (3.3 Hz)

At an excitation of 3.3 Hz, the peak to peak amplitudes from the geophone are similar to those from the laser sensor, as shown in Figure 5-12, but there is a phase shift, and some distortion in the geophone signal at the start and end. The geophone has to end up with mean zero displacement (drift in the integration excepted) due to the nature of the sensor. On the other hand, the laser sensor does not force a zero mean so it resulted in the production of more realistic data.

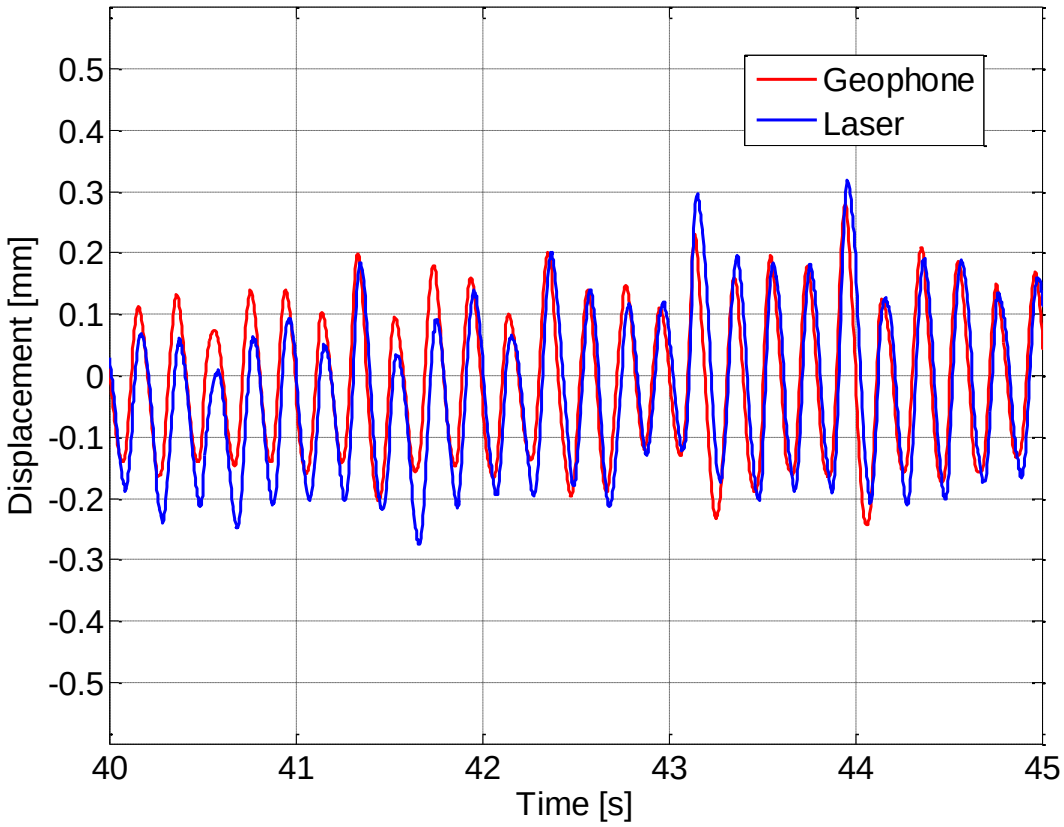

Figure 5-13: Zooming in to compare results between Geophone and PSD Sensor (5 Hz)

Figure 5-13 shows the hand induced vibration of the bench top at around 5 Hz, about 0.3 mm to 0.5 mm peak to peak movement. The red trace is the geophone signal simply scaled and integrated with respect to time (a small offset having been removed). The blue trace is from the laser sensor, shifted down 5 mm to come close to the geophone signal.

The test result for the 5 Hz generated by hand vibration movement is discussed below.

1. Peak to peak amplitudes are very similar for each cycle for the two sensor types;
2. There is a little phase shift between the results at 5 Hz;
3. The laser includes lower frequencies that the geophone loses – i.e., the geophone keeps trying to be centred around zero.

5.3 Validation Test of the Laser based Sensor Node and Micro-Epsilon Laser

5.3.1 Laboratory Setup

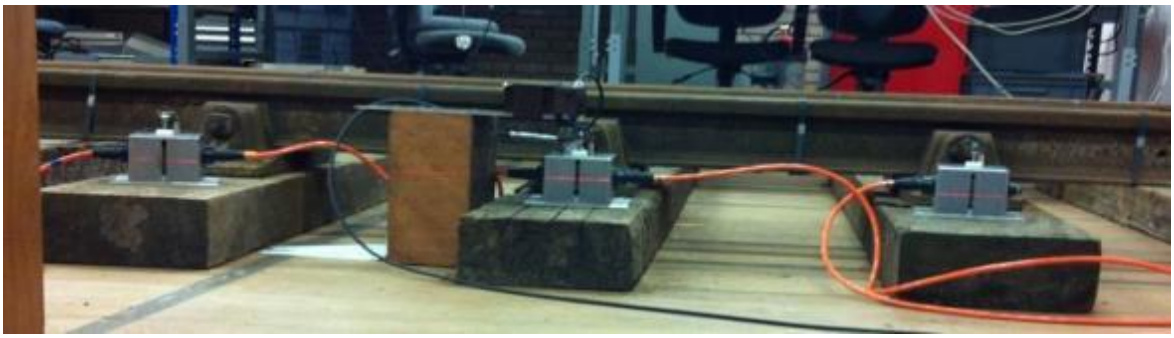

Figure 5-14: Experimental set-up for three sensor nodes

To initiate the verification process of the laser displacement system, the prototype system of three CAN connected nodes was mounted on wooden sleepers in the laboratory, as shown in Figure 5-14. Holes were drilled into the wooden sleepers and the boxes were fixed. For the purpose of validation, it was tested with a displacement sensor which pointed at the top of the box and measured the movement of displacement of the box. A laser source was positioned at a distance of 3.2 m from the track, as shown in Figure 5-15.

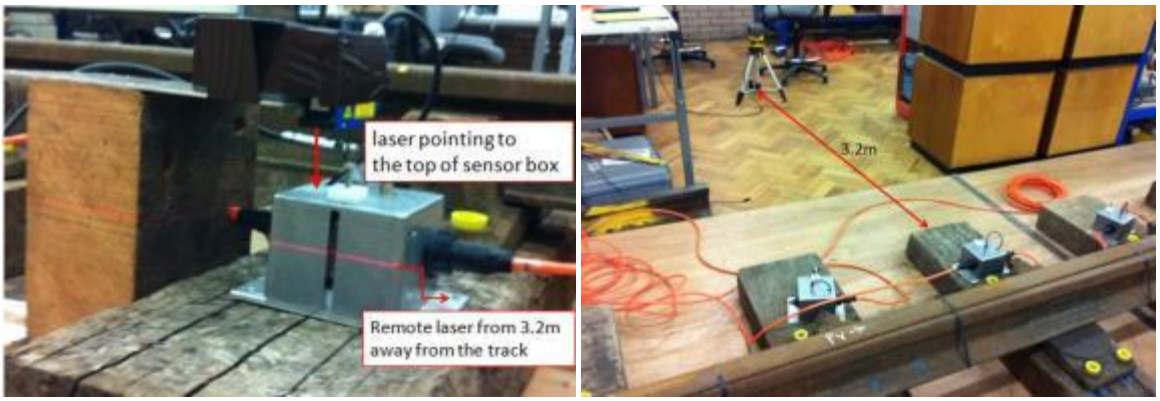

Figure 5-15: Instrumentation set-up in laboratory

5.3.2 Test and Result between Micro-Epsilon Laser and Laser Prototype System

This was the first laboratory test between the commercial displacement sensor, Micro-Epsilon laser and the laser prototype system. In order to provide a dynamic load on the rail so as to move the sleeper, a bouncing movement was performed on the rail, which produced the example data as set out below.

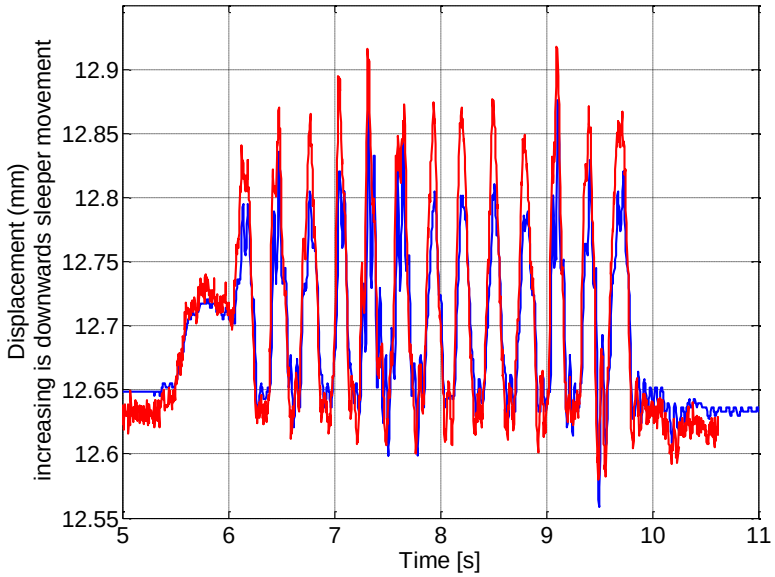

*Figure 5-16: Remote laser (Red) and Micro-*Epsilon *Laser above sleeper (Blue)*

Figure 5-16 shows that the movement which appears in the Micro-Epsilon laser is less than that seen by the sensor node. However, the movement is small, within a range of 0.3 mm.

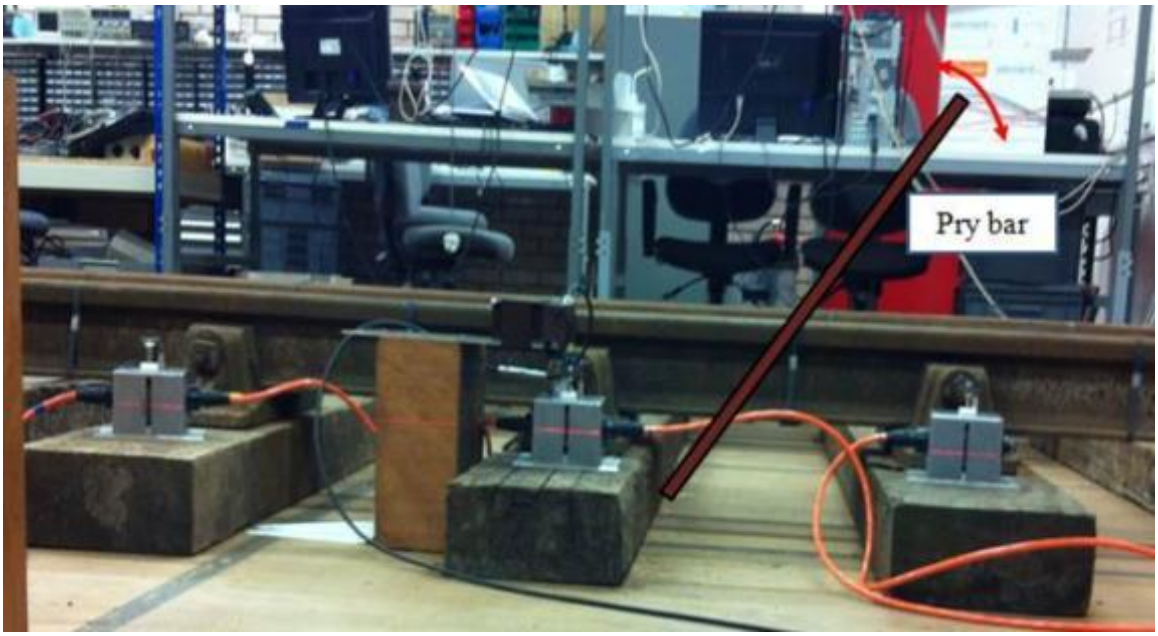

Figure 5-17: Laboratory Test using a Pry Bar

For the second laboratory test, the sensor was tested with a larger motion induced by using a pry bar as shown in Figure 5-17, which is probably a more realistic comparison than the previous test, as the plywood floor is less affected.

Even if there is an error in the test, the error is less than the 0.1 mm required accuracy, and test results with a larger displacement suggest that the errors do not increase with

increasing amplitude of movement. The result is therefore acceptable for verification against TS 8-1, which is stated in Table 4-5.

In principle, if the laser beam falls on the sensor correctly, and the auto calibration is accurate (channel gains are effectively set equal), then the displacement result from the node is automatically calibrated correctly, as it is a function of the sensor physical length, which is fixed.

When the sleeper end is touching, there is some discrepancy between the two data for the first 8 seconds. It is caused by a slight settling of the component parts, as the wooden pry bar is inserted under the end of the sleeper. Figure 5-18 shows that once the pry bar is settled in place after 8 seconds, the movements agree well, with less than 0.1 mm error.

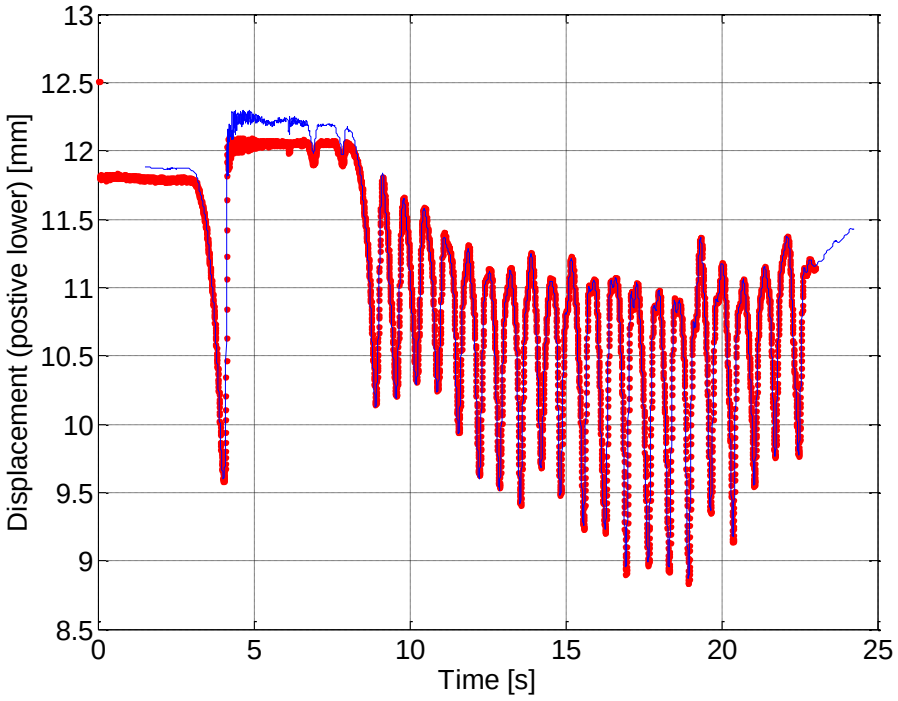

Figure 5-18: Remote Laser (Red) and Micro-Epsilon Laser above sleeper (Blue)

Focusing on the part where the sleeper end is off the floor and the sleeper is rotated slightly, the results are very similar, see Figure 5-19.

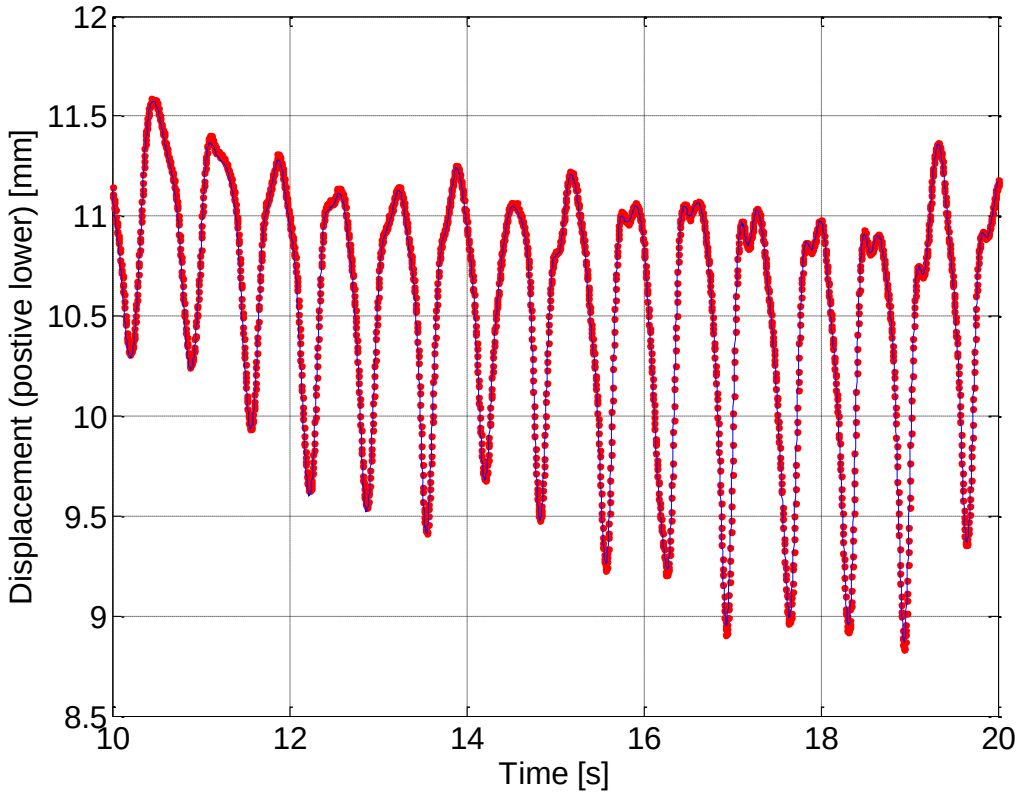

Figure 5-19: Good agreement between two sensors: Remote Laser (Red) and Micro-Epsilon Laser above sleeper (Blue)

There is a slight under-reading of the extent of displacement around 9 mm, but the error is well under 0.1 mm. This could be because the beam is now falling somewhat towards the lower portion of the sensor, where part of the beam is starting to fall off the bottom of the sensor. As described in Figure 5-20, the initial position (corresponding to about 12 mm on the graph) is where the laser beam crosses the sensor, about 8 mm up from the bottom of the sensor (which has an active length of 24 mm). At 9 mm on the graph, the laser line is about 5 mm up from the bottom of the sensor and some of the beam power which is falling off the end of the sensor is probably biasing the result slightly towards 12 mm. The results around 10 mm on the graph (6 mm from the bottom of the sensor) appear to be more accurate. In practice, the sleeper should go down, not up, so the sensor will use its linear portion better.

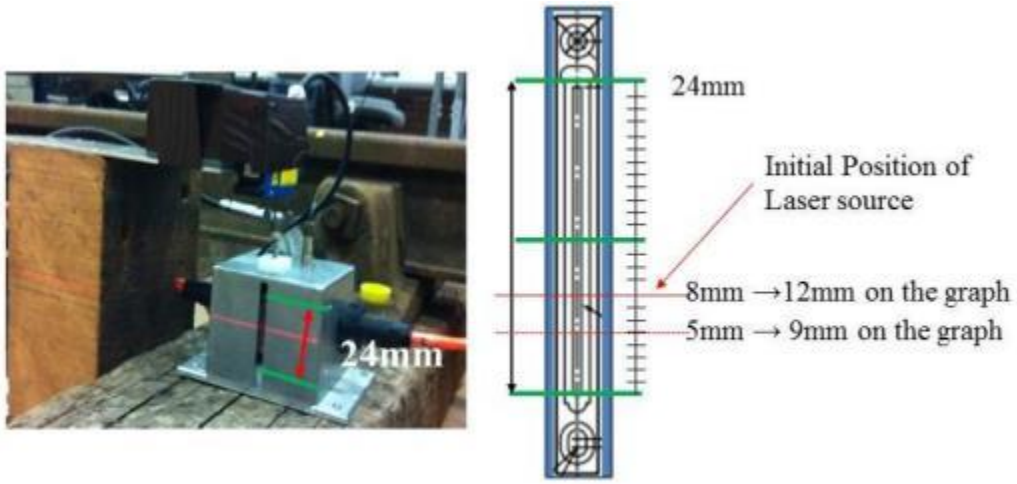

Figure 5-20: Initial position of laser source (about 8 mm from the bottom of the sensor)

When the laser source is closer to the edge of laser, the beam spread will be much larger and the linear region of operation will be reduced. Another source of error is that the sensor box was seen to be rotating as the sleeper was levered up from one side rather than from both ends of the sleeper. This makes a slight difference as the point sensed on the top of the sensor by the Micro-Epsilon laser is not exactly above the internal sensor. However, this error will not be an issue for the following field trial when it is implemented in the test track, since the load from the train will be distributed over the sleeper globally.

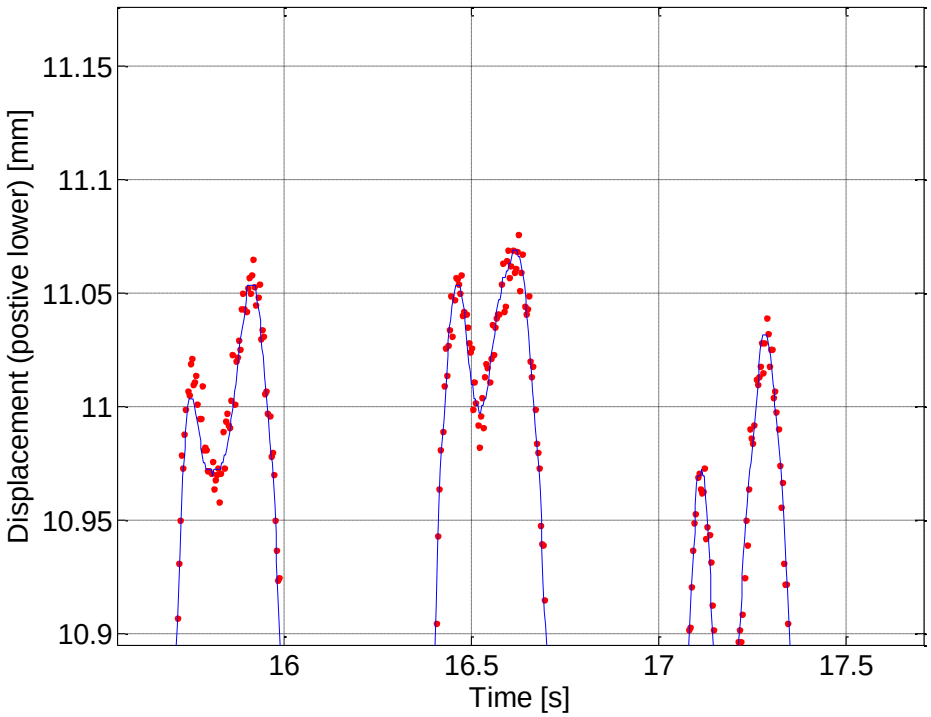

Figure 5-21: Zooming on the results for Remote Laser (red) vs. Micro Epsilon Result (blue)

Zooming in on the data result (Figure 5-19) is shown in Figure 5-21. The remote laser measurements are noisier than the Micro-Epsilon laser results. Assuming that the Micro-Epsilon laser (blue) is working accurately, the remote laser results show a peak noise of less than 20 μm, generally less than 10 μm`. The standard deviation of the noise is less than 6 μm, and probably better than this.

The results are accurate to the desired 0.1 mm, as long as the laser beam falls mainly on the sensor, and the resolution is around 10 μm, which is satisfactory for the intended application, and corresponds to the functional requirements (FD8-1, FD8-2 and FD 8-3) in Section 0 and test specifications (TS 8-1, TS 8-2, and TS 8-3) in Section 4.2.2.3. A better linear operation can be obtained by having a longer laser sensor.

5.4 Summary for Chapter 5

To carry out the system verification procedure, the laser based system was comparatively tested with a geophone and a commercialised laser displacement system, the Micro-Epsilon laser. It is found that the geophone gives similar results to the laser displacement sensor, but with some phase shift at a frequency of 5 Hz. It is expected that at frequencies higher than 10 Hz the geophone will be reliable and usable (10 times the lower frequency limit of 1 Hz, in the hope of obtaining no significant phase shift). Therefore, it has been concluded that the laser displacement measuring system is consistent with the geophone measuring system at 5 Hz and with the Micro Epsilon with agreement within 0.1 mm accuracy and 0.01 mm resolution, therefore the system seems to be generating sensible results.

During the system verification process, there were some changes and upgrades to the system. As a result of the laboratory based tests, the design was amended and components such as the laser source (1 mW red laser to 1 mW infrared) and laser sensor (24 mm to 37 mm) were replaced to deliver better performance. In addition, it was believed that increasing laser power from 1 mW to 10 mW could improve the signal to noise ratio and that it could then deliver good data measuring over 18 sleepers. After the verification process, twenty sets of sensor nodes were built for the final version of the hardware design.

In the next chapter, the developed measurement system will be demonstrated by testing in the field for system validation purposes. It will represent the developed system in use as it was fully intended, which is stated at the very first stage of the Vee-process, in an operational environment, which satisfies the concept of operation in Section 0.

6 Validation of the Laser Measurement System at Long Marston

6.1 Introduction

The laser measurement system was designed, developed and verified as described in the previous chapter, which followed the seven steps of the Vee-process. In this chapter, the performance of the system was validated by taking step 8 of the Vee-process (Figure 6-1) through the field trials which are compared against the concept of operations described in Section 4.1.2.

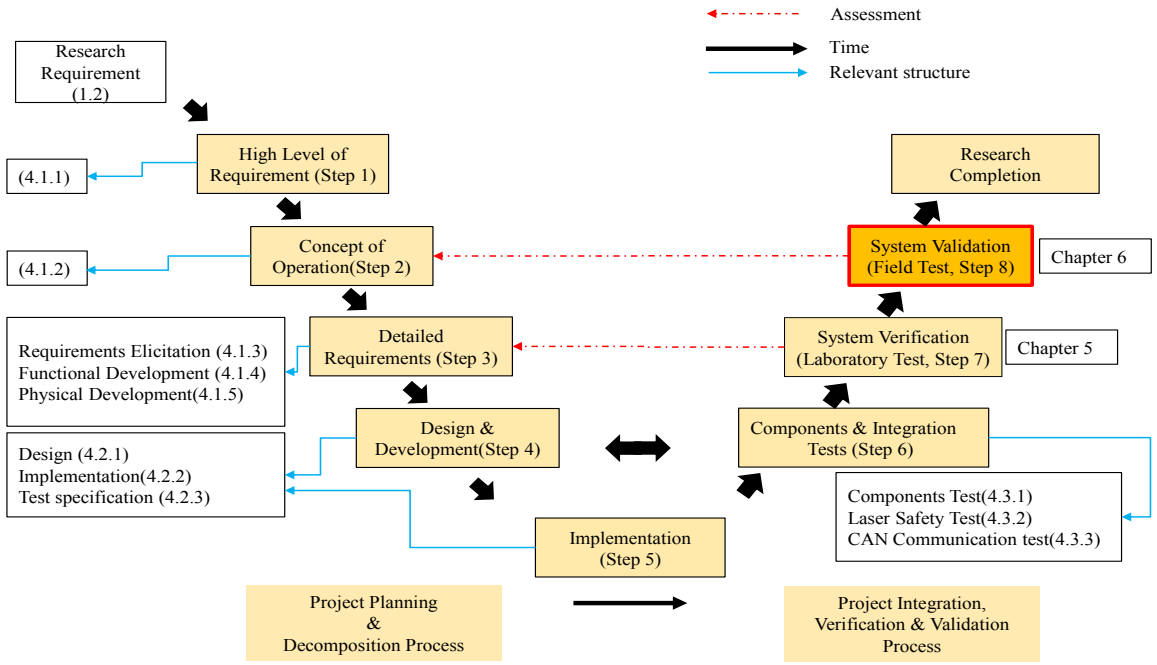

Figure 6-1: Last stage of Vee-model diagram (System Validation)

The main content of this chapter can be summarised as follows:

(1) Theoretical estimation of the deflection curve;
(2) Subgrade assessment;
(3) Data collection from the first trial and system upgrades;
(4) Data collection from the second trial and visualisation of deflection bowl;
(5) Discussion of the results.

In order to assess the usefulness of the data by comparing the calculated values and the actual response, the theoretical deflection curve will be estimated on the basis of the BOEF theory at the beginning of this section. In addition, the ground condition will be assessed by means of DCP equipment to find the relationship between the actual track stiffness and the strength of the ground condition (DCP data). Then, a description of the test site, set-up, results and data analysis for each trial will be presented, followed by a section on the

performance of the measurement system and a description of how important changes and enhancements have been made by upgrading the software and hardware. The first trial was aimed at the feasibility of employing the measurement system at critical zones. The second field trial was aimed at validating the system after making hardware improvements, that is, use of two master nodes, 10 mW laser source and stabilised CAN network) and a software upgrade. The trials section will be followed by a discussion of the data analysis through a comparison of the theoretical estimation, DCP test and real measurement, which will conclude with how the deflection measurement is used to infer the measure of the track structural performance.

6.2 Establishment of Theoretical Deflection Bowl of Multiple Sleepers

As discussed in Section 2.1.1, a typical and widely used method to establish the theoretical deflection curve or 'bowl' of multiple sleepers is based on the BOEF theory. In this section, Zimmermann's technique has been applied to estimate the maximum deflection of sleepers under load, to produce the theoretical deflection curve and analyse the influence of variations in sleeper spacing, variation in loads, the support condition of the subgrade and the train operating speed on the deflection.

6.2.1 Zimmermann's Approach and Theoretical Calculation

On the basis of equation (1) to equation (10), see 2.1.1, the parameters are calculated in Table 6-1, for the situation at Long Marston, where The University has a test site. The un-supported area is assumed to be 400 mm and the other parameters are actual values. The static axle load is 32.5 tonnes, the value for the Class 101 diesel multiple unit car that was used for the tests. Two different wagons were operated during the test, with a static axle load of 23 tonnes for the empty wagon and 26 tonnes for the partially water filled wagon. The profile of the rail installed is 132 lb/yd. The module of elasticity of the rail is 210 GPa (210,000 N/mm^2). The dimensions of the type of concrete sleeper used at Long Marston are 2440 mm long and 220 mm wide. The average distance between the sleepers is 810 mm.

Table 6-1: The parameters for the application of Zimmermann's technique

Vehicles: British Rail Class 101		tonne	32.5
Operating Wheel Load	P	N	39,812.5
Speed	v	km/h	< 60
Wagon (4 axles)		tonne	26-28
Empty Wagon Wheel Load	P	N	31.850
Loaded Wagon Wheel Load	P	N	34,300

Rail Profile: 132 lb/yd (65.5 kg/m)			
modulus of elasticity	E	N/mm^2	210,000
moment of inertia (x)	Ix	mm^4	10,979,547
elastic length	L	mm	903.3144708
Sleepers 8ft			
Sleeper length	L	mm	2440
Sleeper width	b1	mm	220
distance between sleepers	A	mm	810
unloaded length	m	mm	400
effective length	2u	mm	1020
width of idealised sleeper	b2	mm	277.04

The dimensions of the wheel spacing and the bogie spacing are 2,590 mm and 10,800 mm respectively, as described in Figure 6-2.

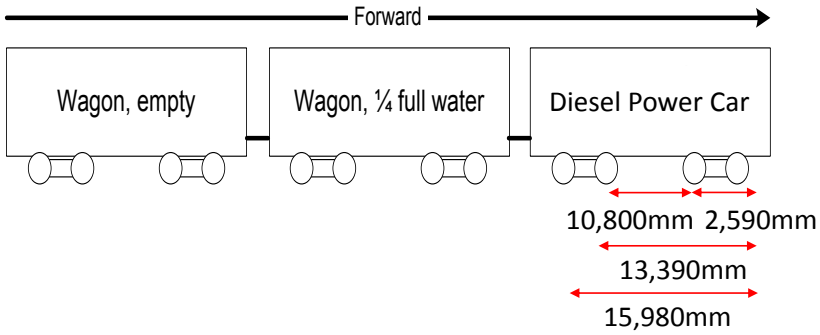

Figure 6-2: Approximate dimensions of the test train

With the four-axle power car running over the instrumented sleepers at intervals of 0 mm, 2,590 mm, 13,390 mm and 15,980 mm respectively, from the first wheel on the first sleeper along the rail over the 18 sleepers, each deflection from the individual sleepers-x, the influence factor of deflection- η(x), the static deflection (ystat) and deflection using the Dynamic Amplification Factor (ydyn) are calculated and set out in Table 6-2 to produce a theoretical deflection bowl (Figure 6-3).

Table 6-2: Example of calculation for the theoretical dynamic deflection of individual sleepers while the first axle is above sleeper 1(C=0.1)

Sleeper 1	**x**	**ξ**	**η**	**ystat**	**ydyn**	**Sleeper 2**	**x**	**ξ**	**η**	**ystat**	**ydyn**
effect of axle 1	0	0	1			effect of axle 1	810	1.066359274	0.4678		
effect of axle 2	2590	3.409717	-0.0406			effect of axle 2	1780	2.343357417	0.0017		
effect of axle 3	13390	17.62784	-1E-08			effect of axle 3	12580	16.56148107	-9E-08		
effect of axle 4	15980					effect of axle 4	15170	19.97119776	3E-09		
		Ση	**0.95936**	0.907511	1.724271			**Ση**	**0.4696**	0.4441838	0.843949
Sleeper 3	**x**	**ξ**	**η**	**ystat**	**ydyn**	**Sleeper 4**	**x**	**ξ**	**η**	**ystat**	**ydyn**
effect of axle 1	1620	2.132719	0.03715			effect of axle 1	2430	3.199077822	-0.043		
effect of axle 2	970	1.276998	0.34773			effect of axle 2	160	0.210638869	0.9616		
effect of axle 3	11770	15.49512	-1E-07			effect of axle 3	10960	14.42876252	4E-07		
effect of axle 4	15980					effect of axle 4	15170	19.97119776	3E-09		
		Ση	**0.38488**	0.36408	0.691752			**Ση**	**0.9185**	0.8688261	1.65077
Sleeper 5	**x**	**ξ**	**η**	**ystat**	**ydyn**	**Sleeper 6**	**x**	**ξ**	**η**	**ystat**	**ydyn**
effect of axle 1	3240	4.265437	-0.0187			effect of axle 1	4050	5.331796369	-0.001		
effect of axle 2	650	0.85572	0.59958			effect of axle 2	1460	1.922079679	0.087		
effect of axle 3	10150	13.3624	2.2E-06			effect of axle 3	9340	12.29604397	3E-06		
effect of axle 4	14360	18.90484	6.5E-09			effect of axle 4	13550	17.83847921	-6E-09		
		Ση	**0.58083**	0.549441	1.043939			**Ση**	**0.0859**	0.0812716	0.154416
Sleeper 7	**x**	**ξ**	**η**	**ystat**	**ydyn**	**Sleeper 8**	**x**	**ξ**	**η**	**ystat**	**ydyn**
effect of axle 1	4860	6.398156	0.00185			effect of axle 1	5670	7.464514917	0.0007		
effect of axle 2	2270	2.988439	-0.0421			effect of axle 2	3080	4.054798227	-0.024		
effect of axle 3	8530	11.22968	-1E-05			effect of axle 3	7720	10.16332543	-5E-05		
effect of axle 4	12740	16.77212	-7E-08			effect of axle 4	11930	15.70576066	-2E-07		
		Ση	**-0.0403**	-0.03809	-0.07238			**Ση**	**-0.024**	-0.0223601	-0.04248
Sleeper 9	**x**	**ξ**	**η**	**ystat**	**ydyn**	**Sleeper 10**	**x**	**ξ**	**η**	**ystat**	**ydyn**
effect of axle 1	6480	8.530874	3E-05			effect of axle 1	7290	9.597233465	-8E-05		
effect of axle 2	3890	5.121158	-0.0031			effect of axle 2	4700	6.187516774	0.0019		
effect of axle 3	6910	9.096966	-7E-05			effect of axle 3	6100	8.030606877	0.0003		
effect of axle 4	11120	14.6394	1.7E-07			effect of axle 4	10310	13.57304212	2E-06		
		Ση	**-0.0031**	-0.00298	-0.00565			**Ση**	**0.002**	0.0019268	0.003661
Sleeper 11	**x**	**ξ**	**η**	**ystat**	**ydyn**	**Sleeper 12**	**x**	**ξ**	**η**	**ystat**	**ydyn**
effect of axle 1	8100	10.66359	-3E-05			effect of axle 1	8910	11.72995201	-6E-07		
effect of axle 2	5510	7.253876	0.00098			effect of axle 2	6320	8.320235322	0.0001		
effect of axle 3	5290	6.964248	0.00133			effect of axle 3	4480	5.89788833	0.0015		
effect of axle 4	9500	12.50668	3.5E-06			effect of axle 4	8690	11.44032357	-5E-06		
		Ση	**0.00229**	0.002164	0.004112			**Ση**	**0.0016**	0.0015283	0.002904
Sleeper 13	**x**	**ξ**	**η**	**ystat**	**ydyn**	**Sleeper 14**	**x**	**ξ**	**η**	**ystat**	**ydyn**
effect of axle 1	9720	12.79631	3.3E-06			effect of axle 1	10530	13.86267056	1E-06		
effect of axle 2	7130	9.386595	-8E-05			effect of axle 2	7940	10.45295387	-4E-05		
effect of axle 3	3670	4.831529	-0.007			effect of axle 3	2860	3.765169782	-0.032		
effect of axle 4	7880	10.37396	-4E-05			effect of axle 4	7070	9.30760502	-8E-05		
		Ση	**-0.0071**	-0.00671	-0.01275			**Ση**	**-0.032**	-0.0307067	-0.05834
Sleeper 15	**x**	**ξ**	**η**	**ystat**	**ydyn**	**Sleeper 16**	**x**	**ξ**	**η**	**ystat**	**ydyn**
effect of axle 1	11340	14.92903	-3E-09			effect of axle 1	12150	15.99538911	-1E-07		
effect of axle 2	8750	11.51931	-4E-06			effect of axle 2	9560	12.58567242	3E-06		
effect of axle 3	2050	2.698811	-0.032			effect of axle 3	1240	1.632451234	0.1831		
effect of axle 4	6260	8.241246	0.00014			effect of axle 4	5450	7.174886472	0.0011		
		Ση	**-0.0318**	-0.03012	-0.05722			**Ση**	**0.1841**	0.174195	0.330971
Sleeper 17	**x**	**ξ**	**η**	**ystat**	**ydyn**	**Sleeper 18**	**x**	**ξ**	**η**	**ystat**	**ydyn**
effect of axle 1	12960	17.06175	-5E-08			effect of axle 1	13770	18.12810766	1E-09		
effect of axle 2	10370	13.65203	1.6E-06			effect of axle 2	3080	4.054798227	-0.024		
effect of axle 3	430	0.566092	0.78372			effect of axle 3	380	0.500267314	0.823		
effect of axle 4	4640	6.108527	0.0018			effect of axle 4	3830	5.042167925	-0.004		
		Ση	**0.78553**	0.743073	1.411838			**Ση**	**0.7946**	0.7516563	1.428147

With C, the modulus of subgrade reaction, assumed to be 0.1, the deflection over the first sleeper is theoretically 1.72 mm. While the first axle is over sleeper 1, the second axle is at a distance of 2590 mm away, which is equal to the distance between the two axles. In the

table, x indicates the distance between the load and the sleeper. The total sum value of η(x) over sleeper 1 is 0.95 and, thus, the static deflection (ystat) is calculated as 0.9 mm. The dynamic deflection (ydyn) is calculated as 1.72 mm on the basis of applying the Dynamic Amplification Factor (DAF) formula against train speed, track condition and the probability of failures in order to reflect reality, as described in equations (11) and (13) in Section 2.1.1. Figure 6-3 shows the resultant graph that corresponds to Table 6-2.

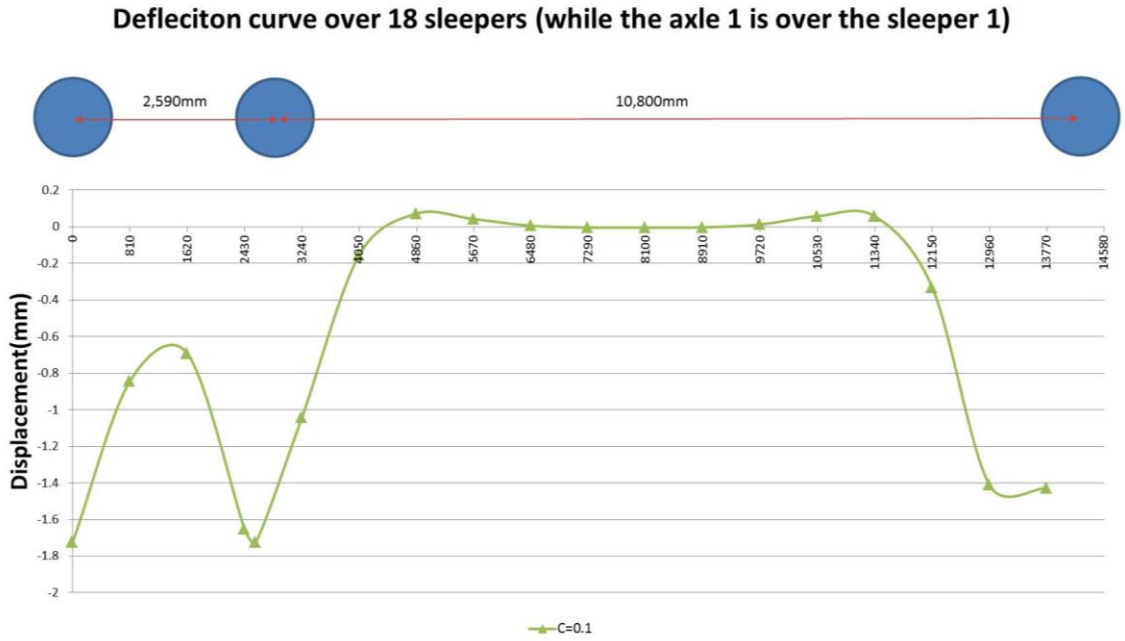

Figure 6-3: Theoretical deflection bowl shape over 18 sleepers when the first axle is running over sleeper 1

As the wheels move along the track, the resulting deflection curves are produced on the basis of the location of the loads (Appendix B).

The application of Zimmermann's approach results in the theoretical shape of the instantaneous deflection bowl over multiple sleepers, as shown in Figure 6-4. It models the entire bowl shape, as different C values (0.02, 0.05, 0.1 and 0.2, respectively) are applied. These correspond to the variation in subgrade strength, with the track stiffness is calculated as 7 kN/mm, 14 kN/mm, 23 kN/mm and 38 kN/mm, based on the operating wheel load of the diesel power car (39.8 kN).

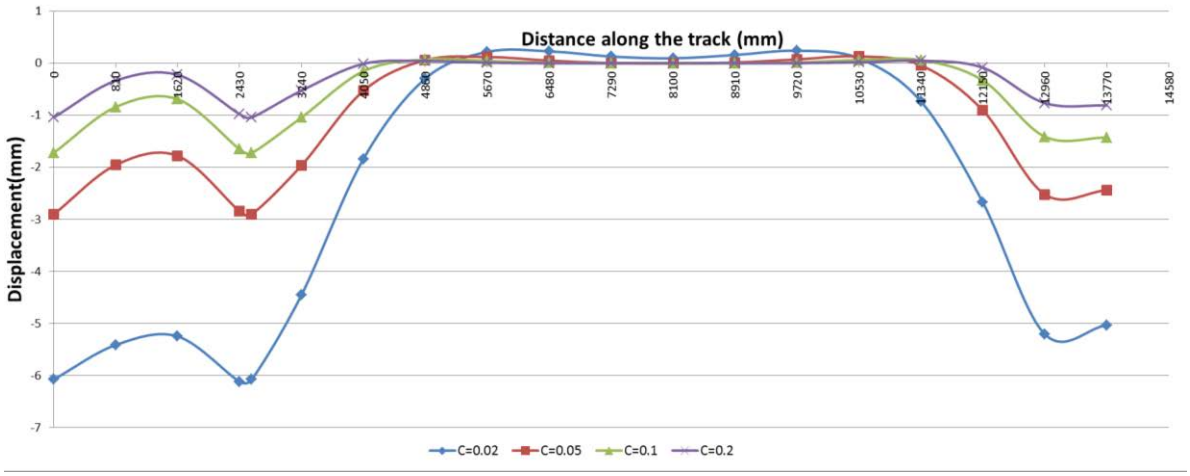

Figure 6-4: Theoretical deflection bowl shape over 18 sleepers (C = 0.02, 0.05, 0.1 and 0.2)

Figure 6-5 shows the different tangent angles (θ1- θ4) from the deflection of the unloaded sleepers (red bold line) with respect to the deflection of the load centre, with the value of C between 0.02 and 0.2. The angle is steeper (θ4) when the value of C is 0.02, meaning the level of track support is poor and the subgrade is soft, which results in larger deflection. On the other hand, the angle is shallower (θ1) as the value of C increases, which means the level of track support is better and the subgrade is stiffer.

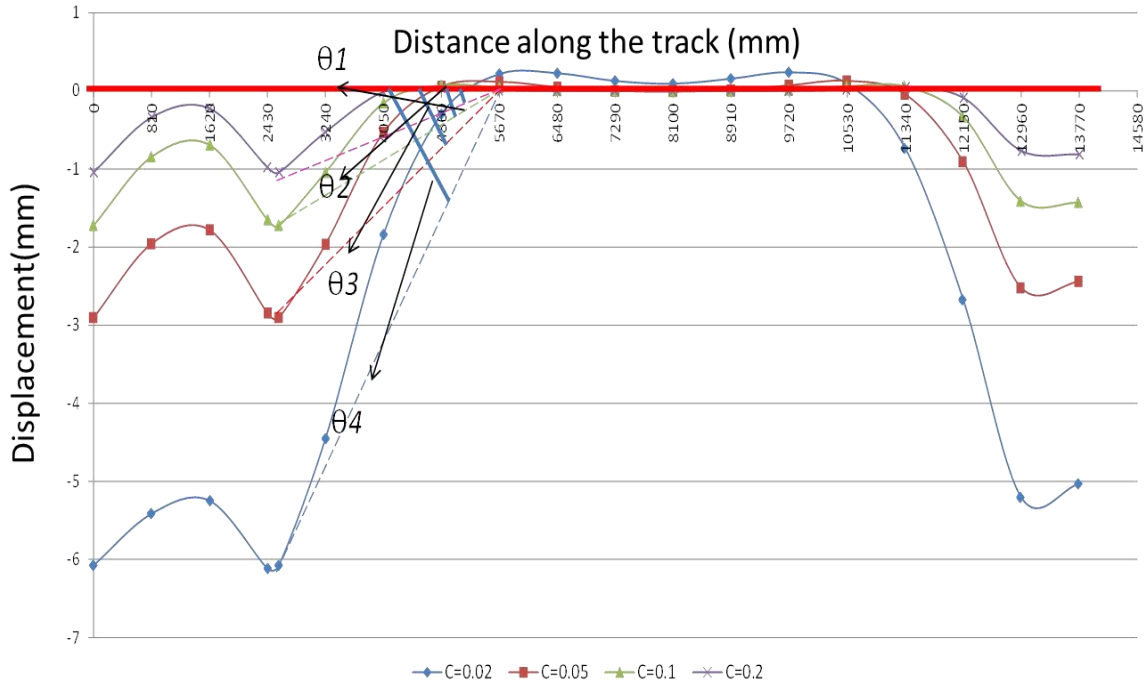

Figure 6-5: The relative angle between the x-axis and the tangent to the deflection curve for C = 0.02, 0.05, 0.1 and 0.2

In order to assess the effect of speed on the deflection, equation (12) is applied while the train speed is 60 km/h, 140 km/h and 200 km/h, as shown in Figure 6-6. The theoretical deflection at 200 km/h is 6 mm, which is two times larger than the deflection at 60 km/h, when it is 3 mm. The tangent angle is stiffer as the speed increases, in a similar manner to the behaviour shown in Figure 6-5.

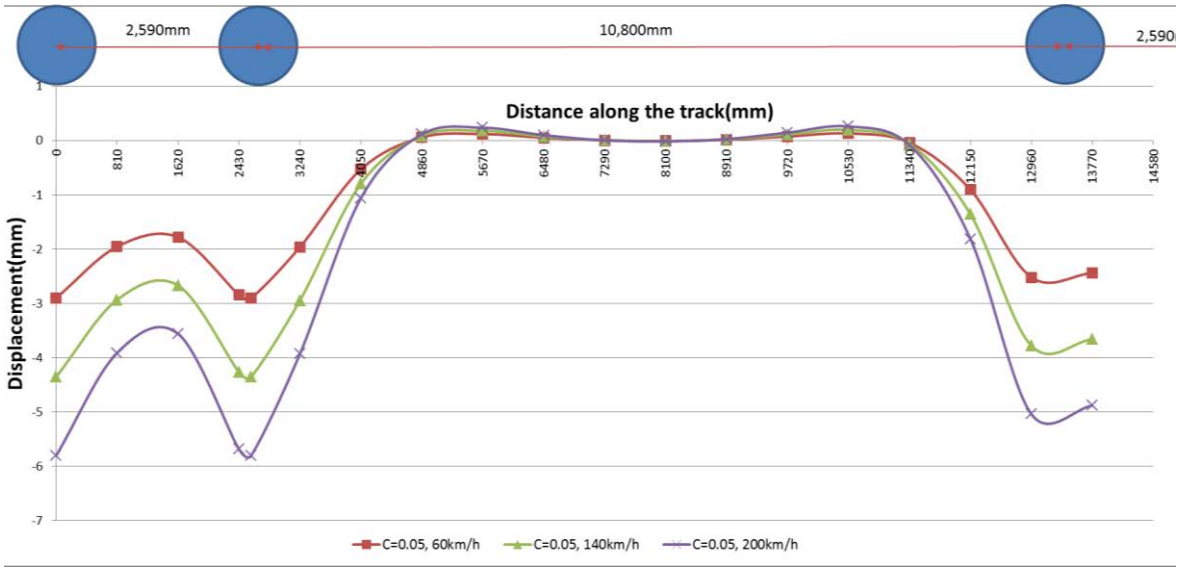

Figure 6-6: Theoretical deflection bowl with inclusion of the DAF factor (speed: 60 km/h, 140 km/h and 200 km/h) while C is 0.05

6.2.2 The Impact of Train Speed and Loads on the Theoretical Deflection

The theoretical deflection curve over 18 sleepers has been shown in Section 6.2.1. The different tangent angles of the slope indicate the relative stiffness. Values for C from a range between 0.02 N/mm^3 and 0.2 N/mm^3 have been applied to the modulus of the subgrade reaction in order to see the relationship between deflection and the effect of subgrade condition. The impact of the additional factors, such as speed and loads, has also been considered and is summarised in Table 6-3. From the table, the maximum deflection at Long Marston would be up to 6 mm where the maximum speed is less than 60 km/h.

Table 6-3: Theoretical calculation of deflection and stiffness

Speed	< 60 km/h			140 km/h			200 km/h		
C [N/mm^3]	Power Car	Water Wagon	Empty Wagon	Power Car	Water Wagon	Empty Wagon	Power Car	Water Wagon	Empty Wagon
0.02	6.07	4.86	4.3	9.11	7.29	6.45	12.1	9.72	8.6
	6.55	6.55	6.55	4.37	4.37	4.37	3.28	3.28	3.28
0.05	2.9	2.32	2.05	4.35	3.48	3.075	5.8	4.64	4.1
	13.7	13.7	13.7	9.13	9.13	9.13	6.85	6.85	6.85

Speed	< 60 km/h			140 km/h			200 km/h		
C [N/mm^3]	Power Car	Water Wagon	Empty Wagon	Power Car	Water Wagon	Empty Wagon	Power Car	Water Wagon	Empty Wagon
0.1	1.724	1.38	1.22	2.59	2.07	1.83	3.45	2.76	2.44
	23.08	23.08	23.08	15.4	15.39	15.39	11.5	11.54	11.54
0.2	1.04	0.83	0.73	1.56	1.245	1.095	2.08	1.66	1.46
	38.1	38.1	38.1	25.4	25.4	25.4	19	19.05	19.05

deflection (mm)
Stiffness (kN/mm)

One of the important dynamic factors to affect track deflection is train speed, so the deflection has also been theoretically calculated for the different train speeds. The analysis shows that a higher stiffness (C = 0.2 N/mm^3) results in 1 mm vertucak displacement and a lower stiffness (C = 0.02 N/mm^3) results in a 6 mm displacement. In addition, a speed of 200 km/h and heavier loads (power car or wagon loaded with water) cause a comparatively larger deflection of 12 mm. However, Zimmermann's approach does not provide accurate results to estimate the deflection since the support condition, the C value, varies at different discrete points. The limitation of this approach is the fundamental assumption of Zimmermann's method, namely, that track support is uniform along a track, thus the maximum deflection of each sleeper is shown to be the same. Under real operation on a ballasted track railway, the value of C can be achieved by combining the relevant modulus values of each component or layer as below.

$$\frac{1}{C\,total} = \frac{1}{C\,ral-pad} + \frac{1}{C\,ballast} + \frac{1}{C\,subgrade} + \frac{1}{C\,foundation} \quad (23)$$

Therefore, variations in the degradation of particular layers would result in a different deflection. In order to get a realistic value for C on the test track at Long Marston, a Dynamic Cone Penetration (DCP) test was conducted to assess the discrete support condition for each sleeper along a section of track. The result from the DCP method not only provide an accurate value of C but also enable the link between deflection and stiffness variations under a sleeper to be investigated by a comparison between the data from the laser based measurement system and the DCP data.

6.3 Assessment of the Track Support Condition

The Dynamic Cone Penetrometer Test (DCPT) was introduced in Section 3.2.2 (Measurement of Trackbed Stiffness) as one of the methods that can be used to measure the in situ strength of trackbed layers rapidly. As part of the research, DCPTs were conducted for an initial measurement of the in situ strength in order to get realistic C (Ks) values, so as to obtain a more accurate theoretical deflection and to assess the condition of the subgrade by looking at the penetration resistance of the foundation of the railway track. The result also supports a better understanding of how the subgrade condition affects the deflection data and track stiffness.

6.3.1 DCPT for Subgrade Assessment

DCPTs were conducted for the site investigation at the test facility at Long Marston, to support the deflection measurements near a level crossing. The penetration tests were performed in the following stages:

- Step 1: Assembling the instrument;
- Step 2: Rising and dropping a hammer from a distance of 575 mm;
- Step 3: Measuring the penetration depth per blow for each test;
- Step 4: Repeating steps 2 and 3 until the cone had been driven into the ground for the full depth of the lower shaft (900 mm) and before two extra lower shaft (500 mm) had to be added, in order to be driven through deeper than 1,900 mm;
- Step 5: Extracting the DCP by pumping the jack.

Assembling Reading and recording

Figure 6-7: The procedure of DCP measurement

Figure 6-8 shows the layout of the DCP site which is located near the level crossing area.

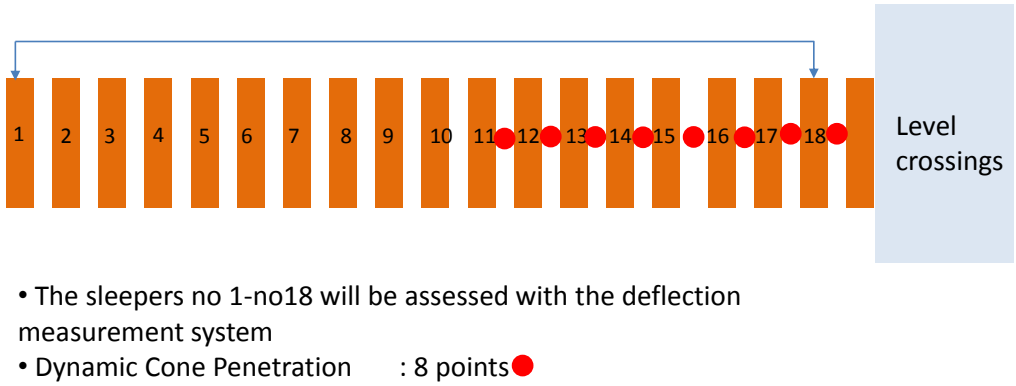

Figure 6-8: Layout of the DCP test section

6.3.2 DCPT Test Result and Analysis

Data was recorded manually in the format shown in Table 6-4. The DCPT results confirm that stiffer and stronger soil results in a lower DPI, which means more resistance while dropping the weight, and softer and weaker subgrade results in higher DPI.

Table 6-4: Example of recorded DCPT data for two locations (cribs between sleepers 16 and 17 and between sleepers 18 and 19)

Test site	Sleeper16-17				Test site	Sleeper18-19			
Blows (no)	Readings	DPI (mm/blow)	Accu depth (mm)	Estimated CBR(%)	Blows (no)	Readings	DPI (mm/blow)	Accu depth (mm)	Estimated CBR(%)
initial position	100		0		initial position	110		0	
1	135	50	-50	3.6	1	150	40	-40	4.6
2	170	50	-100	3.6	2	185	35	-75	5.4
3	195	50	-150	3.6	3	215	30	-105	6.4
4	220	50	-200	3.6	4	240	25	-130	7.8
5	240	50	-250	3.6	5	270	30	-160	6.4
6	265	50	-300	3.6	6	290	20	-180	10.1
7	285	80	-380	2.1	7	315	25	-205	7.8
8	305	80	-460	2.1	8	355	40	-245	4.6
9	325	90	-550	1.9	9	430	75	-320	2.3
10	340	100	-650	1.7	10	480	50	-370	3.6
11	355	100	-750	1.7	11	530	50	-420	3.6
12	390	100	-850	1.7	12	580	50	-470	3.6
13	410	100	-950	1.7	13	265	40	-510	4.6
14	440	100	-1050	1.7	14	305	40	-550	4.6
15	500	80	-1130	2.1	15	345	40	-590	4.6
		-					-		
51	612	5	-1670	47.6	51	750	5	-995	47.6
52	625	5	-1675	47.6	52	755	5	-1000	47.6
53	640	5	-1680	47.6	53	760	5	-1005	47.6
54	651	5	-1685	47.6	54	765	5	-1010	47.6
55	665	5	-1690	47.550337	55	770	5	-1015	47.6
56	681	5	-1695	47.6	56	775	5	-1020	47.6
					57	780	5	-1025	47.6
					58	785	5	-1030	47.6
			CBR(%)	2.5	59	793	8	-1038	28.1
			Ks(N/mm	0.037	60	798	5	-1043	47.6
							-		
					85	928	5	-1168	47.6
								CBR(%)	30.8
								Ks(N/mm	0.092

*DPI: penetration index (mm/blow)

In Table 6-4 the first column (blows) is the number of blows (dropping a weight from a certain height), the second column shows the corresponding depth of bar going into the foundation that is below the base of the sleeper at each blow (mm / blow) and the third column shows the cumulative depth (mm). As discussed in Section 3.2.2, the most common correlation of DCP data is the relative CBR value which is converted from equation (19) above, so that the average of the estimated CBR at 1165 mm is 2.5% and 30.8% respectively. The rest of the DCP data is attached in Appendix C. A plot of the DPI

versus depth is given in Figure 6-9, which shows a profile of the depth and the relative strength against the depth. The data from the DCP shows that there is a range of penetration resistances (mm) as a function of the penetrated depth.

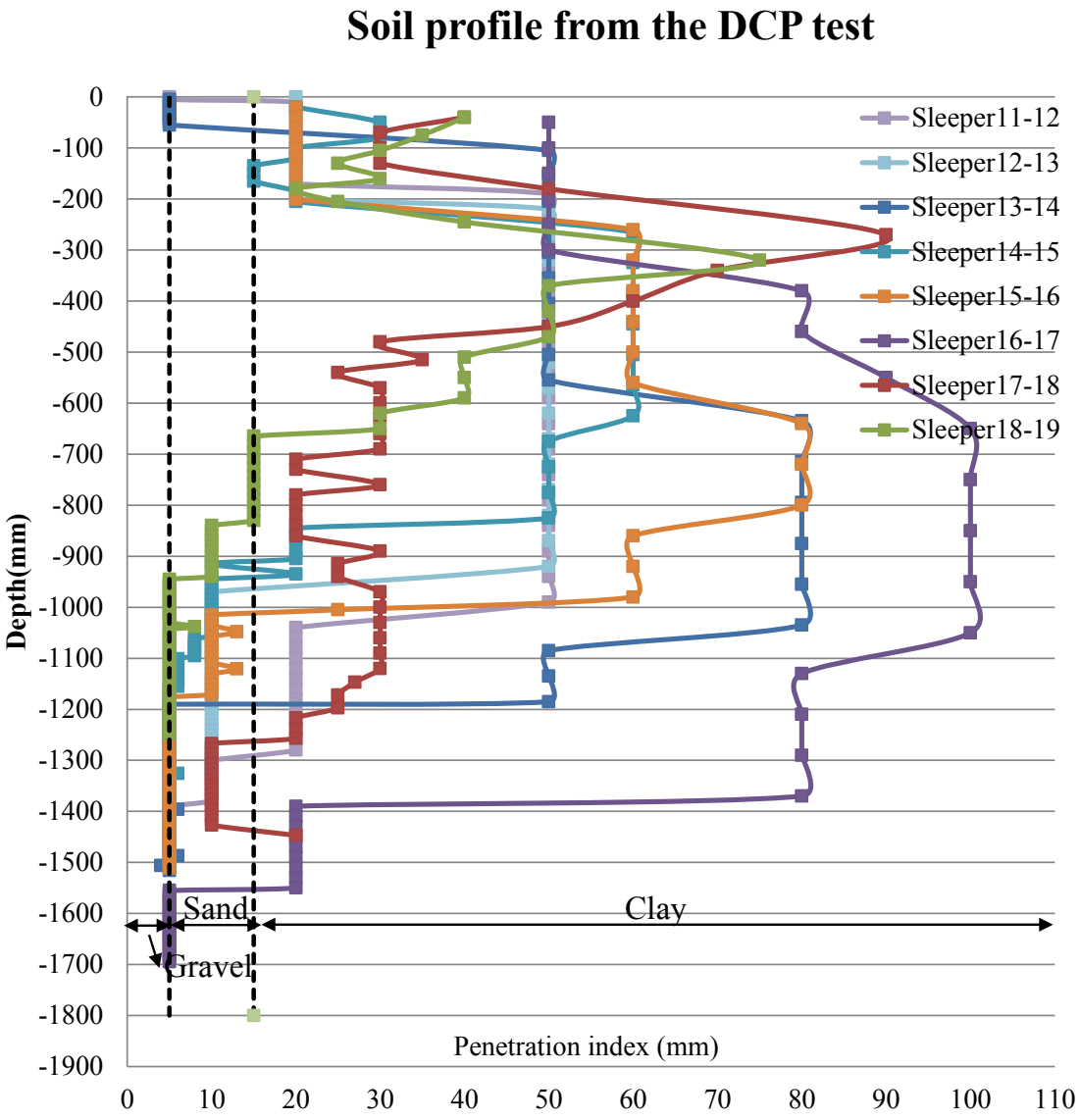

Figure 6-9: DCP profiles for eight locations

Comparing Table 3-5 (*Typical CBR and DPI ranges for various soils)* with the graphs in Figure 6-9 and Figure 6-10, the subgrade at a depth of 1,000 mm would be expected to consist of clay and below that layer there would be sand. From the visual inspection, the ballast layer is very thin. The CBR value corresponding to the DPI is calculated on the basis of the common correlation formula (equation 15) and plotted in Figure 6-10.

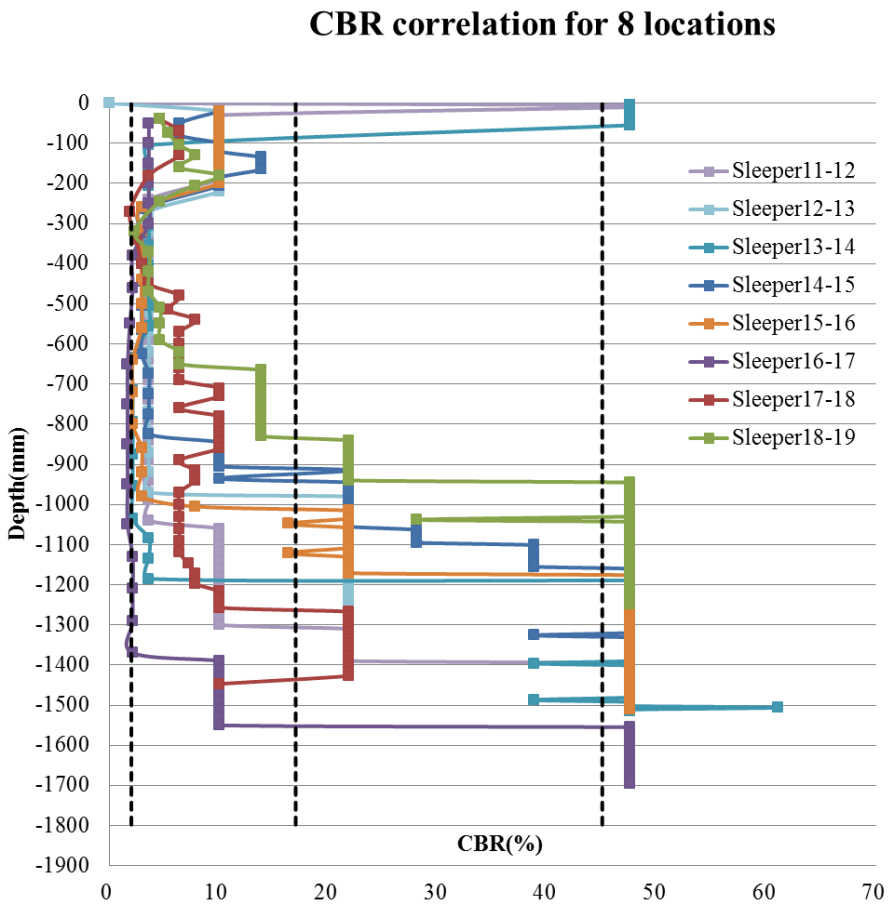

Figure 6-10: CBR correlations with the DPI for eight different locations

The penetrating depths for each DCP crib point were 1165 mm and 1619 mm, which indicates that the strength of the subgrade is different. The K_s and corresponding average CBR was calculated using equations (13) and (14), on the basis of the depth 0-1165 mm from the crib points.

Table 6-5: Average CBR and corresponding K_s (N/mm^3)

Site	Penetration depth (mm)	Total Blows	Average CBR (%)	Ks(N/mm3)
11-12	1,485	69	9.07	0.048
12-13	1,340	63	13.1	0.056
13-14	1,516	96	18.8	0.068
14-15	1,456	114	19.6	0.07
15-16	1,511	107	12.3	0.055
16-17	1,695	56	2.5	0.037
17-18	1,619	58	6.5	0.044
18-19	1,008	101	30.8	0.092

Once the rod had travelled into the ground to a depth of 1500-1600 mm it became stiffer to penetrate, so that the lower shaft and cone were stuck and further movement was no longer possible, allowing the assumption that the layer is very stiff at a depth of 1500 mm. The

values of K_s (N/mm^3) at each sleeper have been achieved by the average of the values from the two points, e.g., the K_s at sleeper 12 is 0.053 N/mm^3, which is derived from the average of 0.048 N/mm^3 and 0.056 N/mm^3) at each sleeper. The excel files used to calculate the average K_s (N/mm^3) at each sleeper are attached in Appendix C and the result is plotted in Figure 6-11.

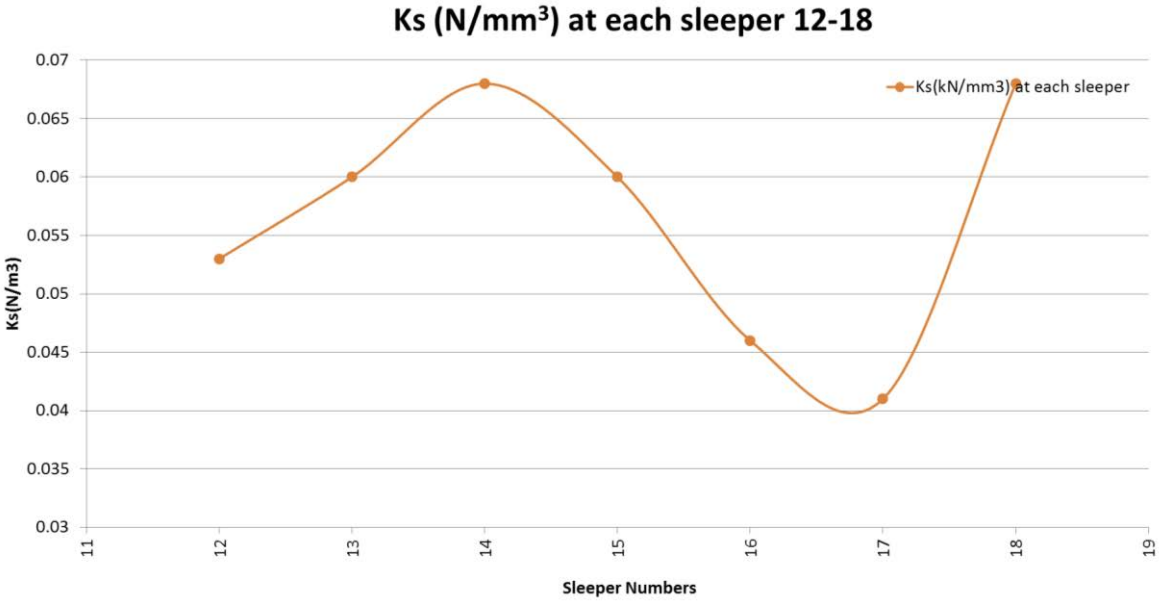

Figure 6-11: K_s (N/mm^3) along the sleeper 2 13-18

The maximum K_s (N/mm^3) of 0.068 N/mm^3 is found under sleeper 14 and 18, whereas the minimum of 0.041 N/mm^3 is found at sleeper 17.

6.4 Initial Trial of the Deflection Measurement

This initial field test was aimed at testing the equipment and measuring the vertical displacement of 12 sets of contiguous sleepers with the 1 mW infrared laser source during continuous train passage at different running speeds and axle loads. The train consisted of a 32.5 t diesel multiple unit power car with 4 axles hauling two wagons, namely, one 26 t empty wagon and one half loaded tanker wagon. As this research is focused on critical zones, it was decided to include two such transition sections, one on plain line with a level crossing and one near to a turnout. Each trial was preceded by the following tasks:

- Check the running vehicles for the specification of vehicles and axle loads;
- Choose one of the critical zones for the test site (straight section of track, S&C, level crossing);
- Measure sleeper spacing at each location;
- Levelling and stabilising a laser source at its intended position;

- Install the sets of 12-18 sensor base-plates while considering the angle towards the laser source;
- Install 12-18 sets of sensor boxes, either with geophone or laser sensor only;
- Check the calibration (gain, frequency) corresponding to the distance between the individual sleeper and laser source;
- Check individual sensor nodes while responding to the laser source and geophone work using a hammer;
- Store data of the initial value of the sleeper spacing and gain of each node;
- Take a measurement at the location while 5-10 trains run at various speeds;
- Data processing and recording the data from the laser measurement and geophone;
- Dismantling the boxes, detaching base-plates and clearing up the site.

By carrying out the test in the field, it was expected that the effect of fast and slow trains and deflection would be seen, as well as the effect of different axle loads (achieved by changes in the tanker water levels) and deflection. Minor variations will be found in measurement under the same running conditions and correlations between measurements from the geophones and laser sensors. Additionally, a video recording system which was tested by the University of Southampton was comparatively tested with one of the sensor nodes on a section of the switch.

6.4.1 Description of the First Field Trial Set-Up

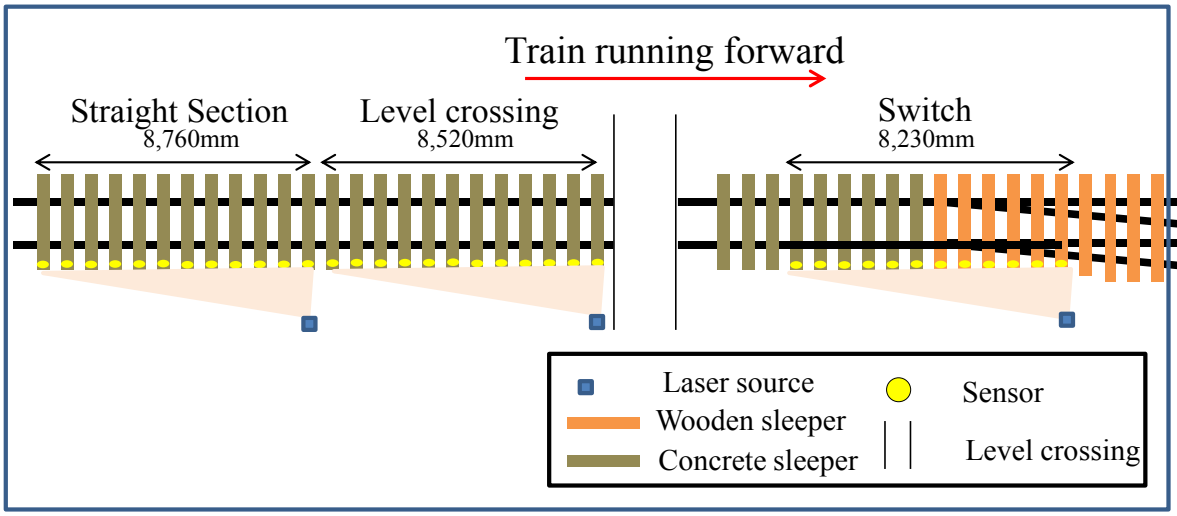

Figure 6-12: Layout of sensor instrumentation over critical zones

The trial was carried out at the Motorail test track at Long Marston, which is near to Stratford-upon-Avon, which has a 50 km/h maximum train speed restriction over the critical zones. The first measurements were taken in June 2013. The research purpose was to develop an innovative and useable system which enables the assessing of the performance of railway critical zones, where it is expected that there will be a change in support stiffness adjacent to infrastructures, by means of observing the vertical movement of sleepers in response to the passing loads. The test track does not feature any properly designed transition zones where the connection area between the embankment and structures is specially designed to reduce sudden changes in stiffness. However, specific sites were chosen in order to see the feasibility of the developed laser measurement system to test real transition zones and critical zones. For this reason three critical sites have been selected as shown in *Figure 6-12*. The maximum line speed was 25 mph (40 km/h) on the test track during the measurement of the first trial. Since this test track is not a serviceable mainline track, it was expected to have comparatively larger dynamic deflection of track than a mainline track, which is presented in Figure 3-2.

On the first day of the field trial, 5th of June 2013, the base plates for sensor boxes were placed on the sleepers at three sections. Twenty four sets of base plates were placed on twelve concrete sleepers (marked red) adjacent to the level crossing and twelve concrete sleepers on straight track (marked blue) as shown in Figure 6-13.

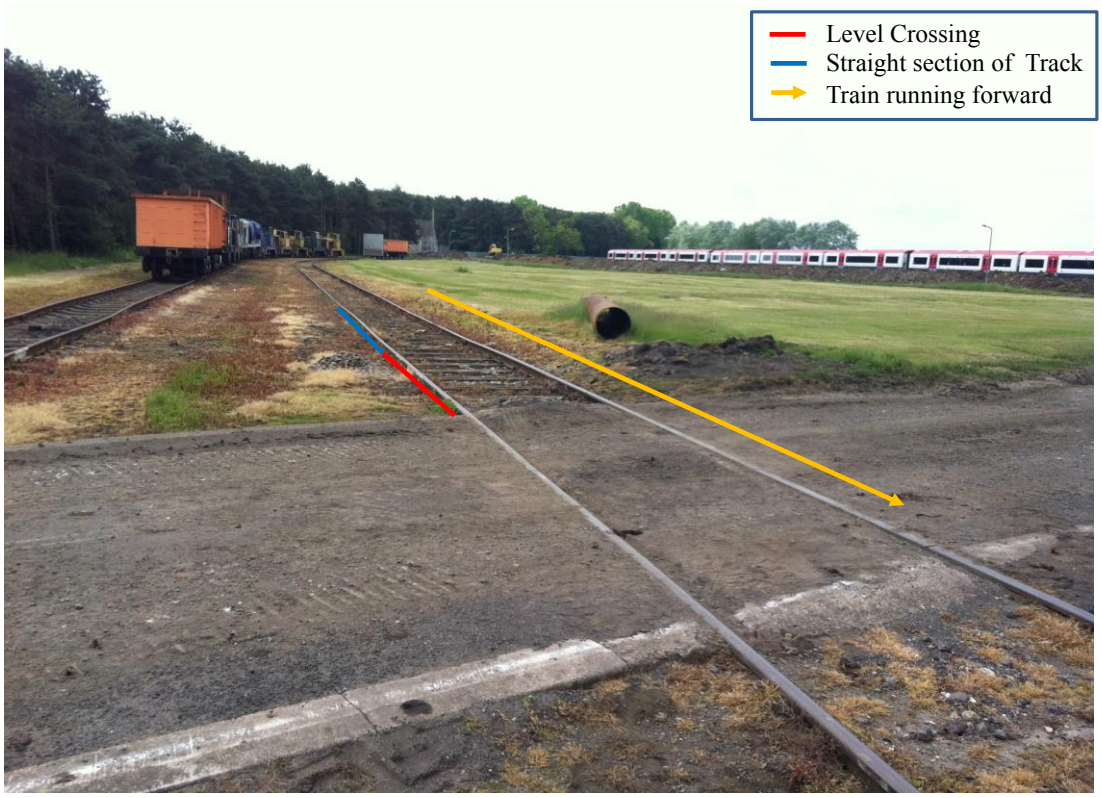

Figure 6-13: Photo of area near level crossing and straight section of track

Alongside the switch, six sets of base plates were installed on the wooden sleepers and six sets of base plates were installed on the concrete sleepers, as shown in *Figure* 6-14.

Sensors were installed right before the measurement on the second day.

Figure *6-14 : (a) View of sensor installation with hard cover on sensor node on switch between wooden bearers and concrete bearers (b) Track Adjacent to Point between wooden bearers and concrete bearers*

In order to achieve clearance from the track, the tripod laser source is spaced 3,000 mm away from the outer rail and 1,900 mm away from the closest sensor box, which was positioned to the far right along the track, as shown in Figure 6-15. The sensor box which

was positioned at the furthest distance was placed on sleeper 12; the distance was planned at 10.8 m with an angle of 42 degrees.

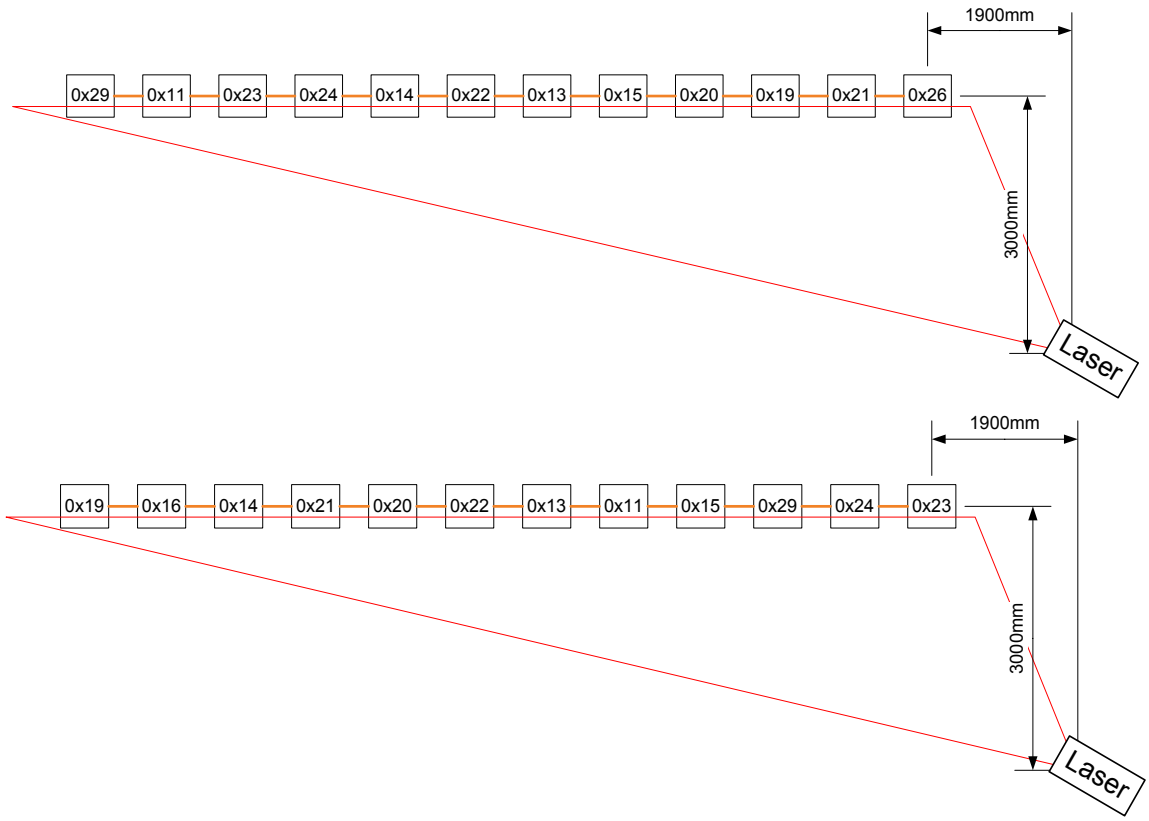

Figure 6-15: Arrangement of the initial position of laser source for the first trial (a) on the straight section of track and level crossing and (b) a switch

While setting up the position of the tripod, the effects of ground vibrations from passing trains and wind were considered. It was advised to lower the tripod to the ground to reduce the effect of wind, therefore the tripod was lowered as much as possible in this trial (Le Pen *et al*., 2014). In addition, the maximum speed at the test track in Long Marston was under 30 mph (50 km/h), therefore, it was assumed that the noise from these two factors would not be significant enough to distort the data result. However, if there was an error which is not acceptable after data processing, further improvements to mitigate the effects of these factors would be considered after the first trial and a way to eliminate the vibration of the laser source would be considered.

The following tables show each sleeper space over a level crossing, straight section and S&C on the track at Long Marston. The average sleeper spacing is 775 mm to the level crossing. Approximately 8,520 mm of track was monitored near the level crossing, where all light weight sleepers were made of concrete.

Table 6-6: Sleeper spacing on level crossing (from left to right)

Node number (left-right)	Node id	Node between	Distance (mm)	Gain	Sleeper
node1(far left)	0x19	node1-2	760	253	Concrete
node2	0x16	node2-3	650	200	Concrete
node3	0x14	node3-4	660	184	Concrete
node4	0x21	node4-5	820	146	Concrete
node5	0x20	node5-6	810	117	Concrete
node6	0x22	node6-7	770	121	Concrete
node7	0x13	node7-8	800	95	Concrete
node8	0x11	node8-9	800	90	Concrete
node9	0x15	node9-10	890	88	Concrete
node10	0x29	node10-11	790	120	Concrete
node11	0x24	node11-12	770	201	Concrete
node12 (far right)	0x23	Total Track	8,520		Concrete

Table 6-7: Bearer spacing on switch (from left to right)

Node number (left-right)	Node id	Node between	Distance (mm)	Gain	Sleeper
node1(far left)	0x19	node1-2	860	253	Concrete
node2	0x16	node2-3	750	90	Concrete
node3	0x14	node3-4	800	90	Concrete
node4	0x21	node4-5	790	90	Concrete
node5	0x20	node5-6	550	90	Concrete
node6	0x22	node6-7	690	90	Concrete
node7	0x13	node7-8	740	120	Wood
node8	0x11	node8-9	760	90	Wood
node9	0x15	node9-10	770	90	Wood
node10	0x29	node10-11	760	90	Wood
node11	0x24	node11-12	760	90	Wood
node12 (far right)	0x23	Total Track	8,230		Wood

Approximately 8,230 mm of track was monitored near to the switch section and half of the bearers were light-weight concrete and the other half were wooden sleepers. The average sleeper spacing is 748 mm in this section.

Table 6-8: Sleeper spacing on the straight section of track

Node number (left-right)	Node id	Node between	Distance (mm)	Gain	Sleeper
node1(far left)	0x19	node1-2	720	253	Concrete
node2	0x16	node2-3	790	90	Concrete
node3	0x14	node3-4	830	90	Concrete
node4	0x21	node4-5	770	90	Concrete
node5	0x20	node5-6	790	90	Concrete
node6	0x2**2**	node6-7	810	90	Concrete
node7	0x13	node7-8	800	120	Concrete
node8	0x11	node8-9	850	90	Concrete
node9	0x15	node9-10	830	90	Concrete
node10	0x29	node10-11	700	90	Concrete
node11	0x24	node11-12	870	90	Concrete
node12 (far right)	0x23	Total Track	8,760		Concrete

Approximately 8,760 mm of track was monitored near to the straight section of track and all sleepers were light-weight concrete sleepers. The average sleeper spacing is 775 mm on the straight section. In order to calculate the velocity of the train, the dimensions of the train, e.g., bogie space, axle space and deflection and speed graph were used as described in Figure 6-2. As shown in Table 6-9, the vehicle running speed was 8 to 39 km/h (kilometres per hour), which was not optimal to compare the data from the laser sensor to the geophone, since the application of a 1 Hz natural frequency geophone can produce reliable data when the train runs at near to 45 km/h (30 mph) in the case of having a 10.8 m bogie space (Le Pen *et al*., 2014).

Table 6-9: Vehicle Running Schedule during the Measurement

Run Number	Time	Speed (mph)	Speed (km/h)	Speed (m/s)	Direction	Location
1	12:29	19	30	8.3	Forward	Points
2	12:41	22	35	9.8	Forward	
3	13:20	24	39	10.8	Forward	
4	13:34	22	35	9.8	Forward	
5	14:30	10	16	4.4	Forward	Level Crossings
6	14:34	5	8	2.2	Backward	
7	14:40	10	16	4.4	Forward	
8	14:48	15	24	6.7	Forward	
9	15:17	5	8	2.2	Backward	Straight Section of Track
10	15:21	15	24	6.7	Forward	
11	15:25	5	8	2.2	Backward	
12	15:30	14.3	23	6.4	Forward	

6.4.2 Test Results

6.4.2.1 Results from the Area adjacent to the Track on the Switch

After the first trial, data was processed to show the deflection of each single sleeper. One of the examples (Figure 6-16) shows that the maximum deflection during the passing of the power car and wagons is 4.0 mm for the power car, 4.4 mm for the water-wagon and 3.6 mm for the empty wagon, where track stiffness is 8.4 kN/mm.

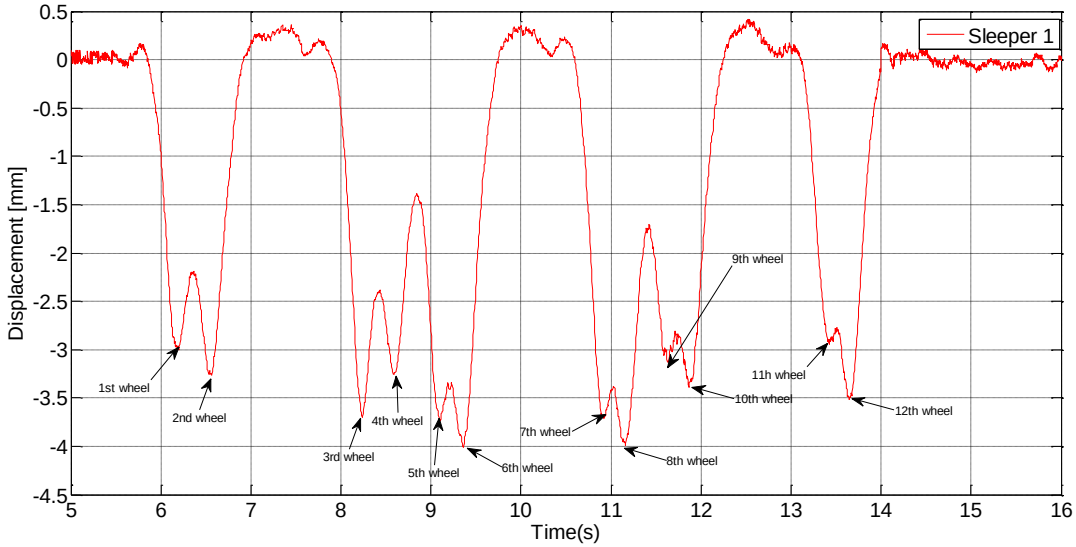

Figure 6-16: Example of data (sleeper4_0x21) to show deflection of individual sleeper

The largest deflection occurred while the loaded second vehicle (the 5th wheel to the 8th wheel) was passing over sleeper 4. This was due to the combined effect of the 4th, 5th and 6th wheels on the track near sleeper 4.

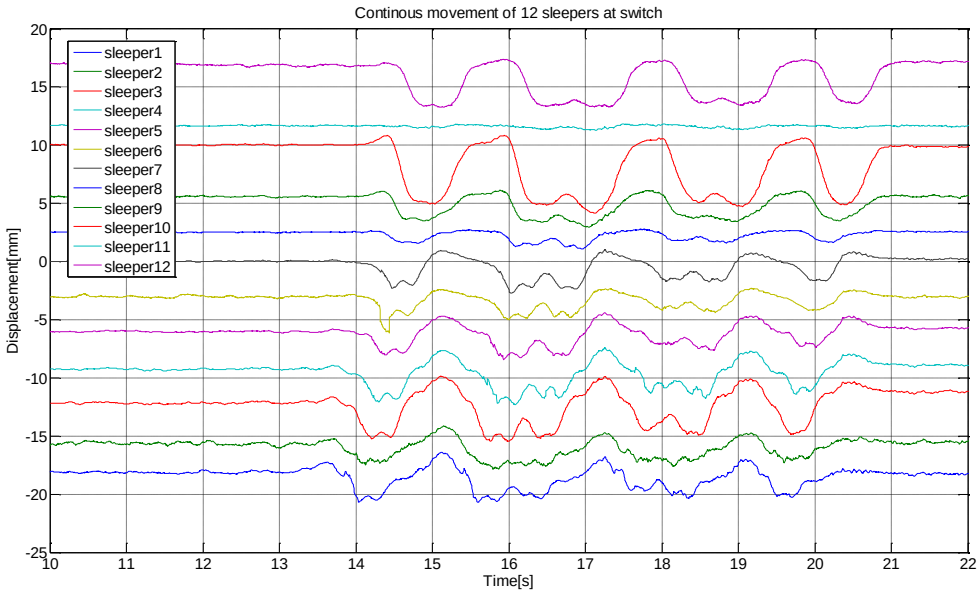

Figure 6-17: Deflection of 12 nodes on a switch (30 km/h, forward)

Figure 6-17 shows the deflection of 12 consecutive sleepers adjacent to the switch. The data from sleeper 1 is the furthest one from the laser source. The graph shows a different reference line for the individual sleepers after data processing on Matlab and the reference line of each data point is different after the data processing in order to show the movement of individual sleepers more clearly within one graph. The train runs from the sleeper 1 to sleeper 12, and backwards it is vice-versa. The data result shows one of the sensor nodes (0x21) on sleeper 11 was faulty. It is assumed that the connection was loose between the digital and analogue PCB board and the difference in the height of the adjacent sleeper is different, so the laser source was outside the limits of the active range of the PSD in the sensor node.

There are some sleepers which were observed to have upward spikes in the displacement-time histories in Figure 6-17. The maximum deflection of individual sleepers has been monitored, as shown in Table 6-10 and Figure 6-18. Data from the sensor node 0x21 which was positioned on sleeper 11 has been removed, since the data was faulty. The range of vertical defection was between 2 mm and 7 mm and the range of track stiffnesses was 5.8 kN/mm and 19 kN/mm.

Table 6-10: The magnitude of displacement of the switch

sleeper number	1	2	3	4	5	6	7	8	9	10	11	12	Avg
Average deflection(mm)	4.30	4.25	6.21	5.06	4.12	2.97	3.70	2.12	3.54	6.82	-	5.05	4.38
Stiffness(kN/mm	9.26	9.37	6.41	7.87	9.66	13.40	10.76	18.78	11.25	5.84	-	7.88	9.10
Std													3.62
VAR													13.11

Compared with typical results from the mainline, the measurements show that the track quality at Long Marston is rather poor, since the NR standard (NR standard 039, 2005) requires the optimised track stiffness to be 30 kN/mm. Here, the mean value of the track stiffness is 9.1 kN/mm and the variation in the stiffness of the subgrade is definitely more than 13.11%. Thus, the subgrade condition must be viewed as very poor, since the literature (Burrow *et al*., 2009) suggests that the stiffness variation should be less than 10% of the stiffness of the subgrade.

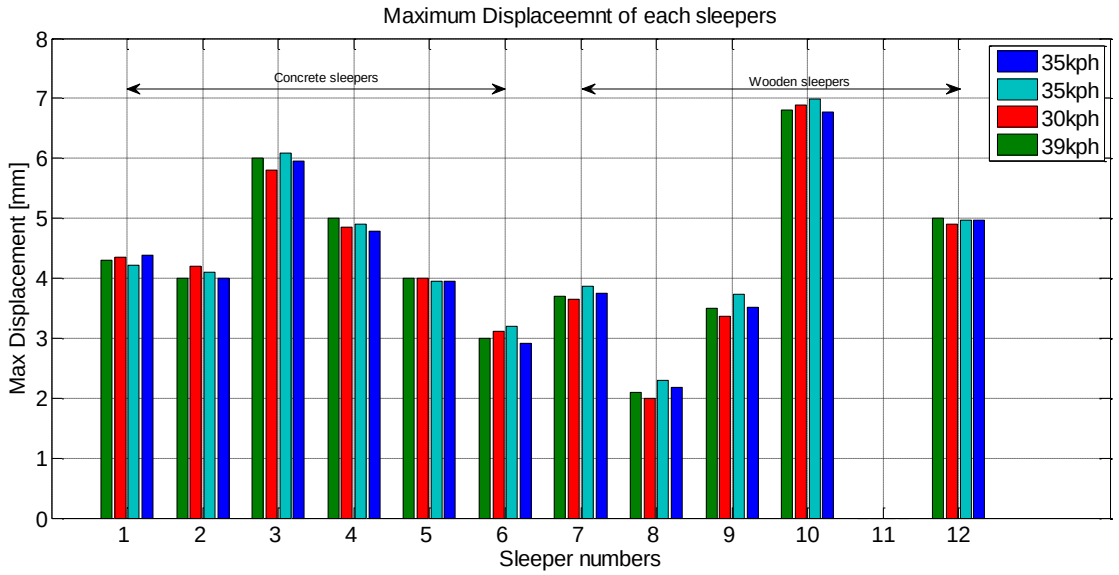

Figure 6-18: The magnitude of maximum displacement of 12 sleepers on switch (all speeds)

Figure 6-18 also shows the displacement of sleeper 4 adjacent to the switch while the different speeds of train are running. It does not show a proportional relationship between them when the peak to peak displacement is compared.

6.4.2.2 Results Data from the Area near the Level Crossing

The field data collected from the level crossing is shown in Table 6-11. The standard deviation (std) value is relatively lower than the standard deviation on the switch.

Table 6-11: Magnitude of the displacement of the level crossing

sleeper number	3	4	5	6	7	8	9	10	11	12	Avg
Average deflection(mm)	3.81	2.43	1.93	1.65	1.58	2.08	2.12	1.91	2.45	2.01	2.20
Stiffness(kN/mm	10.45	16.38	20.63	24.13	19.14	18.78	18.78	20.84	19.81	19.81	18.12
Std											3.55
VAR											12.62

In order to reproduce the data under the same running conditions, tests at the same speed were carried out at 16 km/h forward, as shown in Figure 6-19. The maximum displacement of each test was 3.81 mm and the track stiffness was calculated as 10.45 kN/mm.

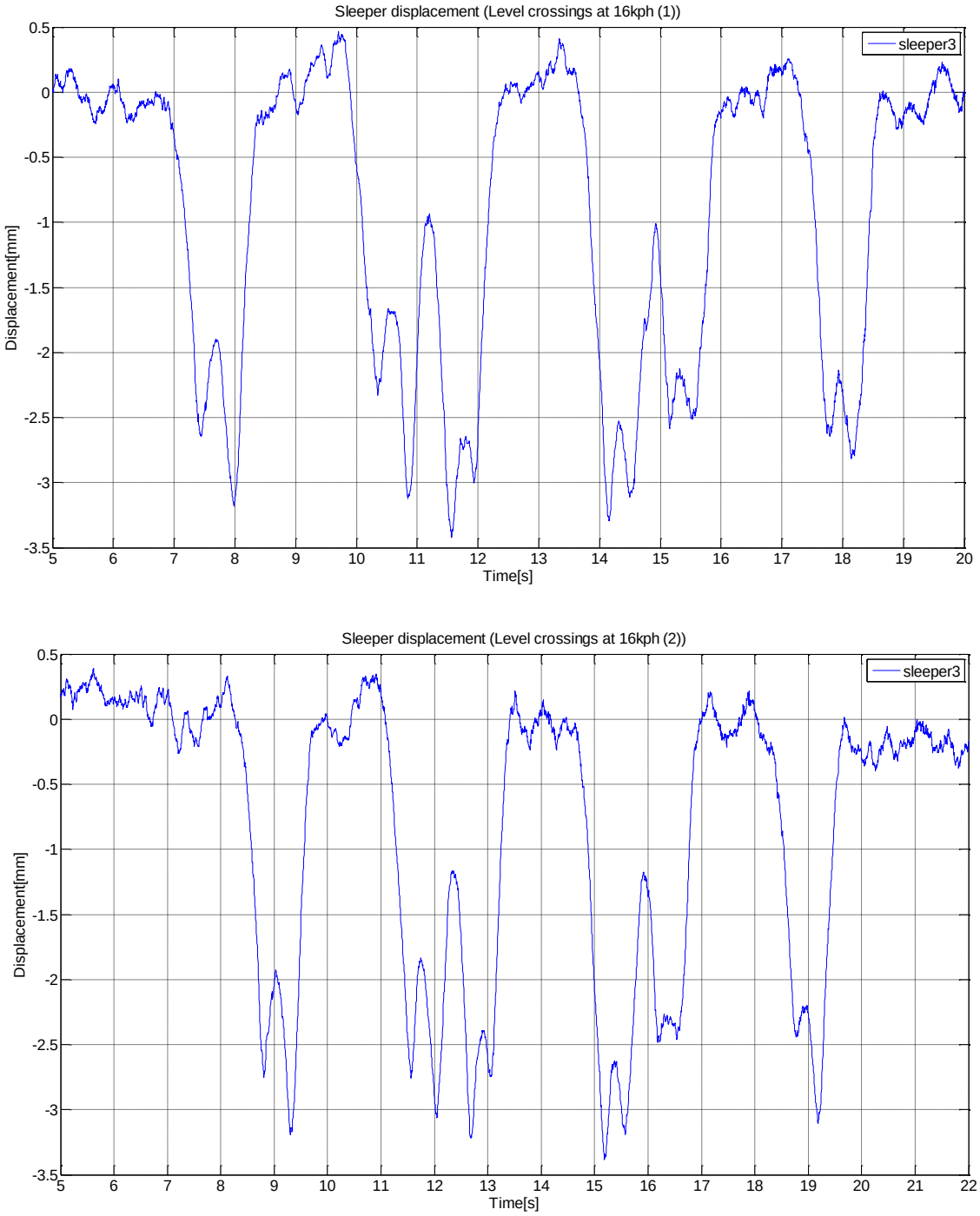

Figure 6-19 : Sleeper displacement (a) 16 km/h (test1) (b) 16km/h (test2)

Figure 6-20 shows the movement of ten out of twelve sleepers in one graph. Two sensor nodes were not operational.

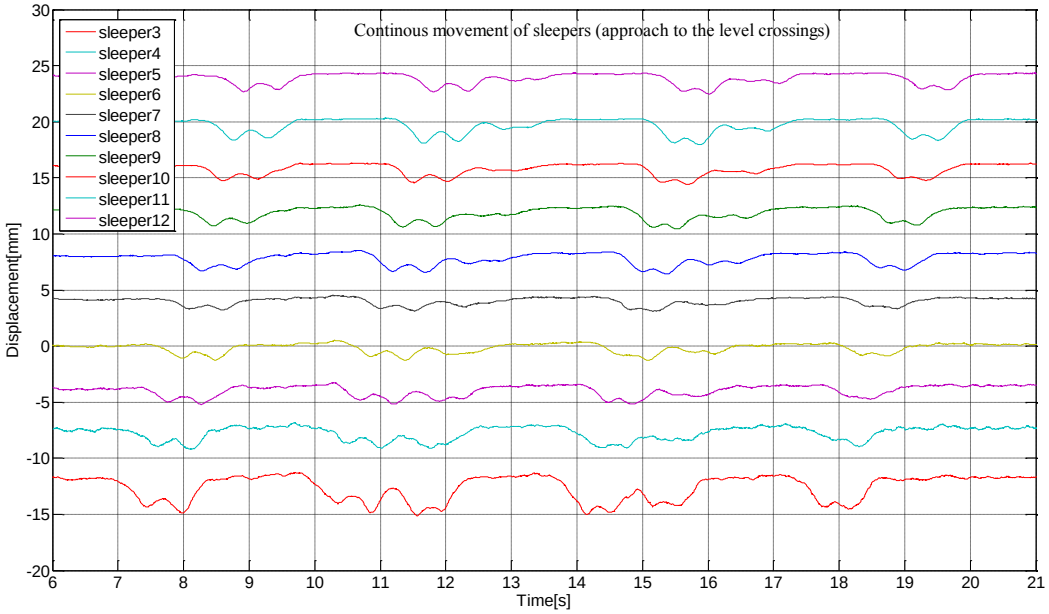

Figure 6-20: Displacement of 10 nodes on the approach to the level crossing (16 km/h, forward)

Figure 6-21 shows the maximum deflection of ten individual sleepers. The range of values is between 1.6 mm (stiffness: 19 kN/mm) and 3.8 mm (stiffness: 10.5 kN/mm).

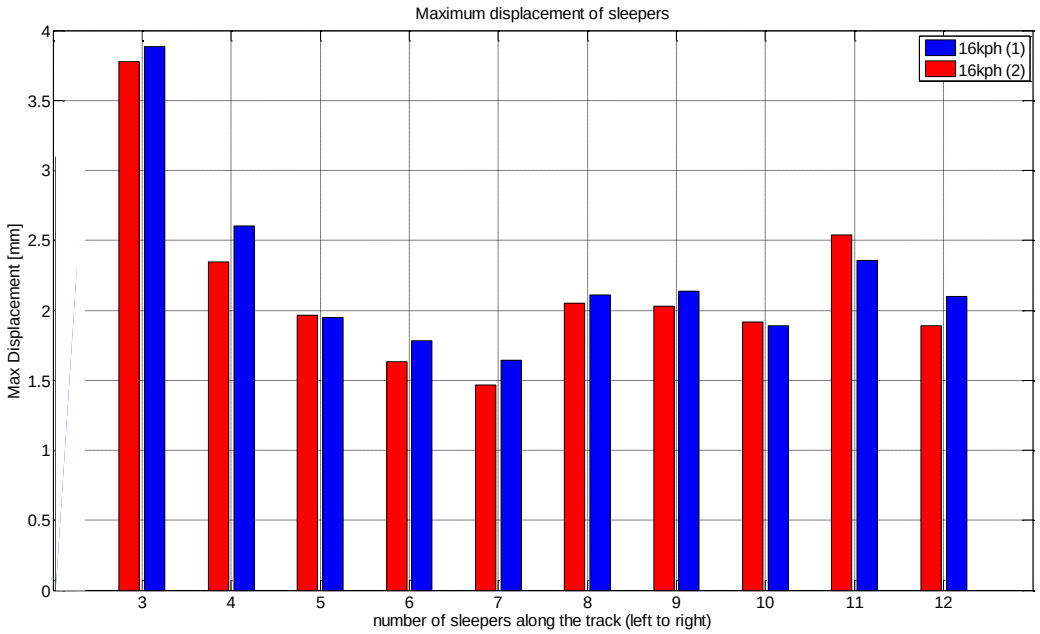

Figure 6-21: Maximum displacements of 12 sleepers on the approach to the level crossing for two moves at 16 km/h

6.4.2.3 Results on Straight Plain Line Section of Track

The field-collected data for a straight section of plain line track is shown in Table 6-12. The standard deviation is 2.28 on this section, which is lower than the standard deviation

on the switch (3.62) and the level crossing (3.55), indicating that the variation in stiffness over this section is smaller.

Table 6-12: The magnitude of displacement on a straight section of plain line track

sleeper number	3	4	5	6	7	8	9	10	11	12	Avg
Average deflection(mm)	5.08	5.51	5.12	4.15	2.72	3.31	3.10	3.21	4.23	4.56	4.10
Stiffness(kN/mm	7.84	7.23	7.78	9.59	12.03	12.84	12.84	12.40	8.73	8.73	10.00
Std											2.28
VAR											5.20

In order to see the data result for the direction of the train, tests while the train was running at 24 km/h forward and 8 km/h backward (the maximum permitted in propelling mode) were undertaken. Figure 6-22 shows that the maximum deflection is 5.5 mm while the overall displacement is roughly similar in both directions.

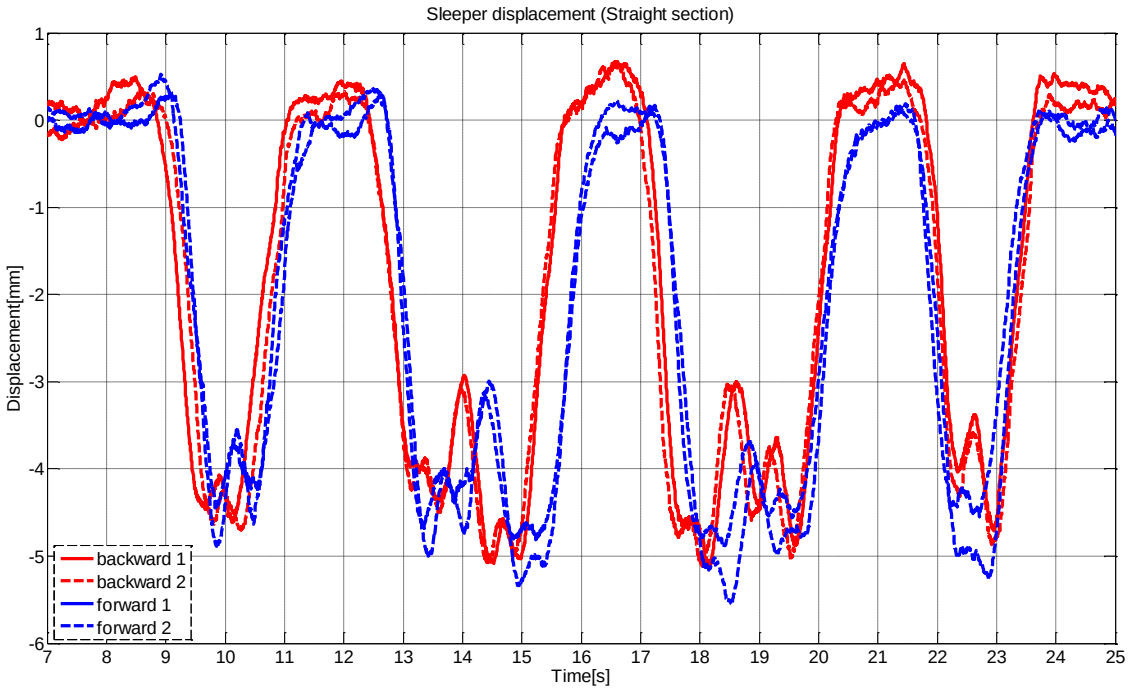

Figure 6-22: Sleeper 4 data to show deflection pattern of sleeper and direction of train

Two sensor nodes (0x29 and 0x11) were faulty, affecting the measurements on sleeper 1 and sleeper 2. Figure 6-23 shows the movement of ten sleepers in one graph.

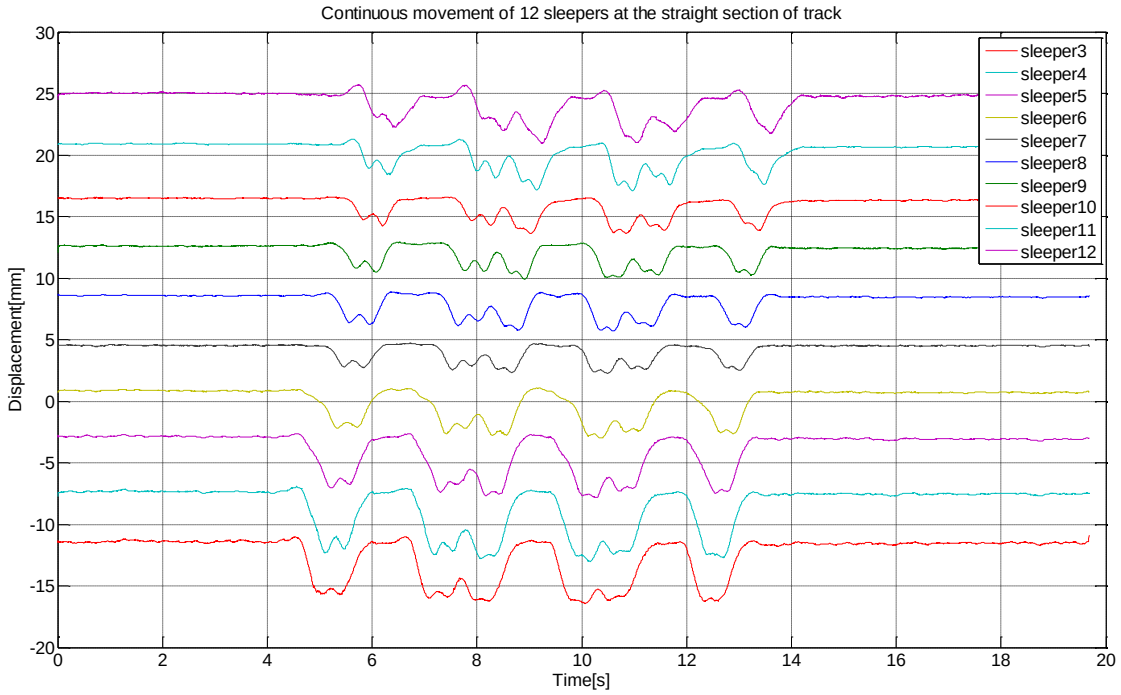

Figure 6-23: Deflection of 10 nodes on the section of the straight section of the track (24 km/h, forward)

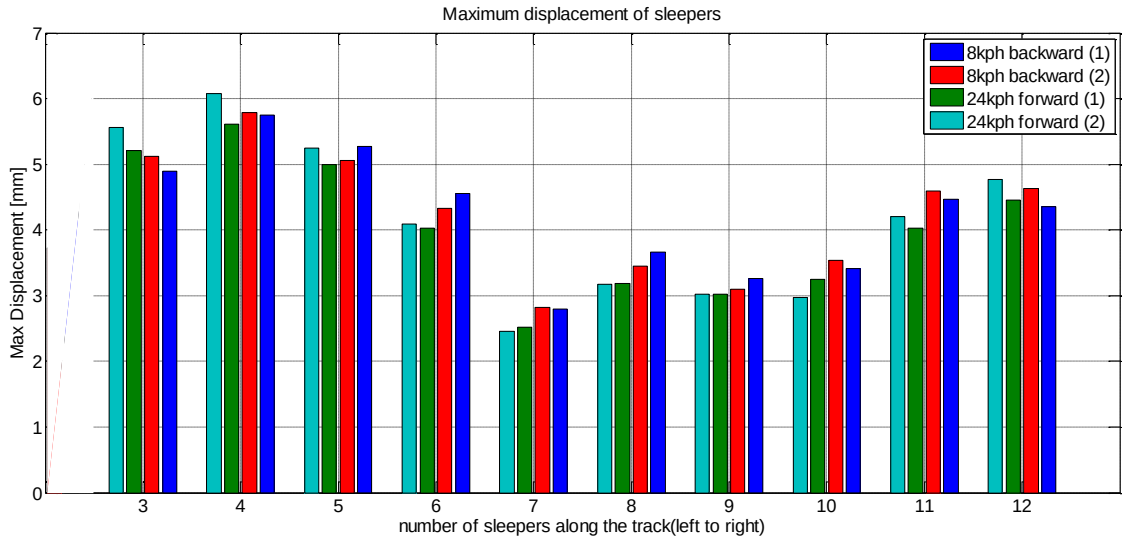

Figure 6-24: Maximum displacements of 12 sleepers on straight plain line track, all speeds

6.4.2.4 Comparison between PIV and Laser Sensor

The results from the laser measurement system were compared with those obtained by the remote video recording system. The layout for the instrumentation of two the sensors is described in Figure 6-25. The tripod of the video recording system is positioned to face straight to the monitored sleeper but the laser source was on the 10th node from the laser source, which is the 3rd from the left.

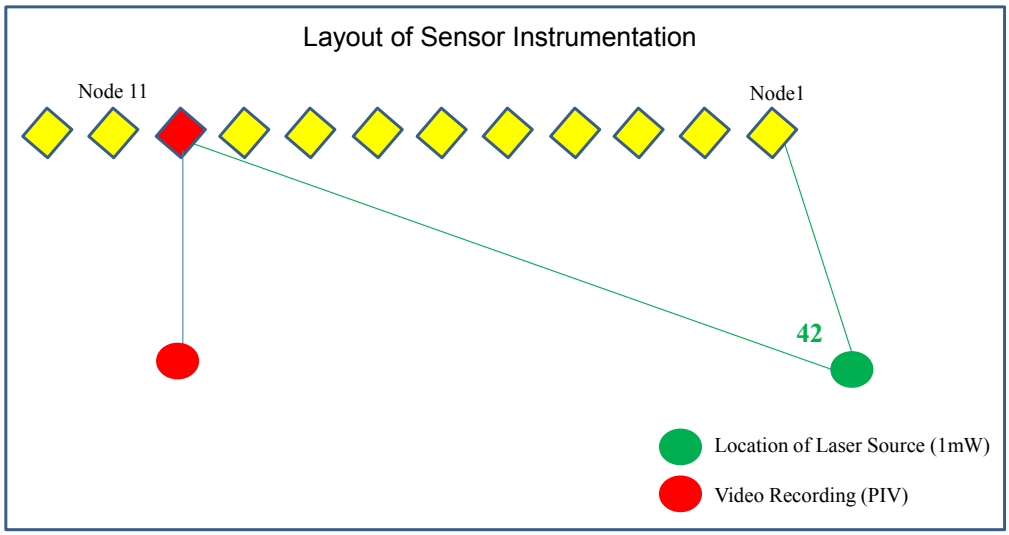

Figure 6-25: The installation layout of two systems (Video recording system and the laser measurement system)

Figure 6-26 (a), (b) and (c) show that either the laser source was moving somewhat as the train went past, or that the laser beam was moving away from the edge of the sensor so that it read slightly less on the downward movement: the maximum movement of the video recording system was 6.8 mm, 6.9 mm and 7 mm respectively for each case, whereas the maximum displacement of the laser measurement system was 6.3 mm, 6.9 mm and 6.3 mm, which results in a maximum discrepancy of 0.6 mm between the two systems. The laser sensor was the 10^{th} sensor (the third from the left), which was 10.8 m from the laser source and had a weak signal, even when the gain value was 184. The gain can be set within a range of 1 to 256, therefore it is a bit noisy, varying slightly after the train had passed.

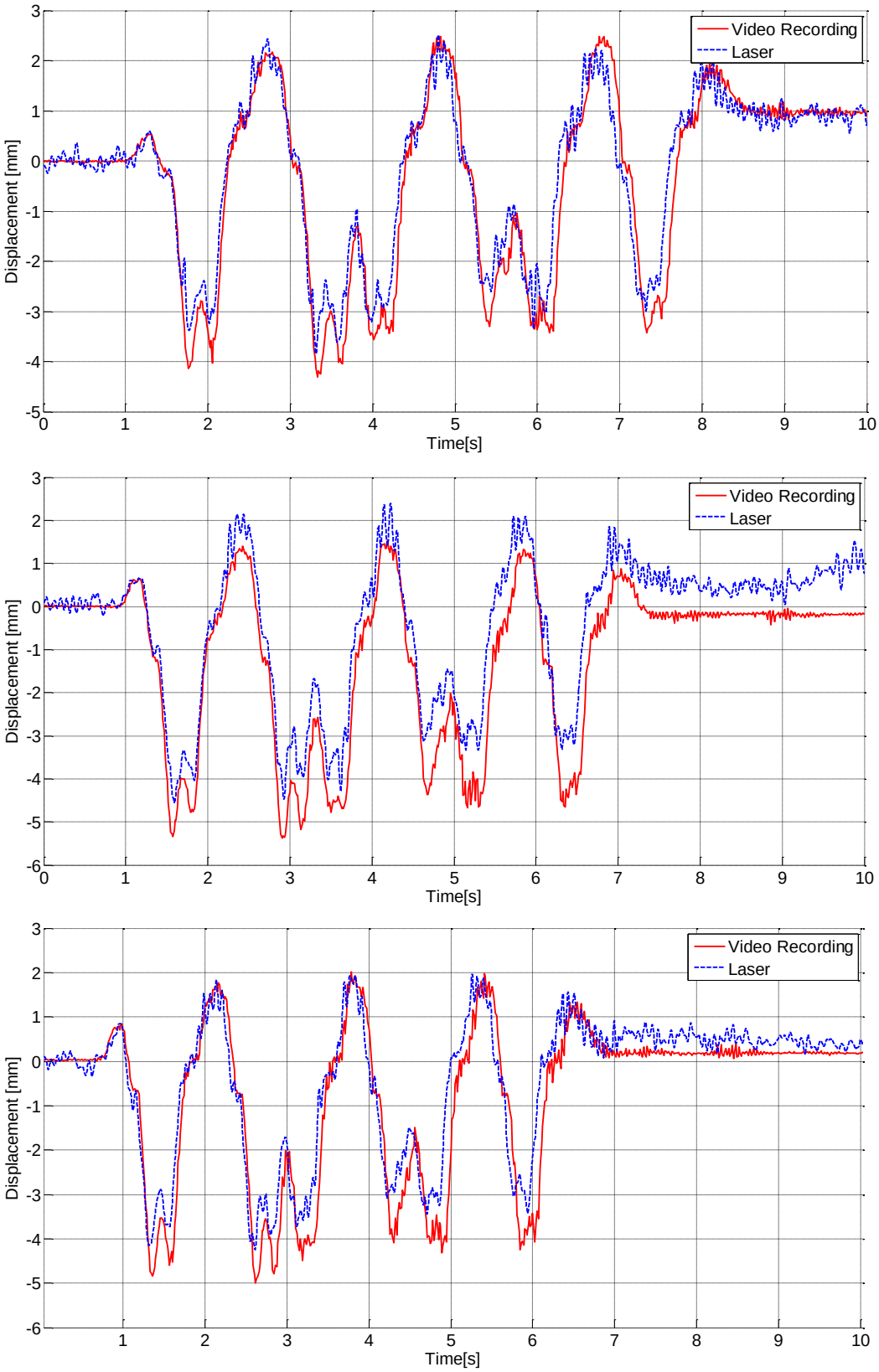

Figure 6-26: Comparison between laser and video recording system outputs at (a) 30 km/h (b) 34 km/h (c) 39 km/h

The following data result shows how one of the PIV results (see Figure 6-27) is missing a small section; the video recording probably malfunctioned.

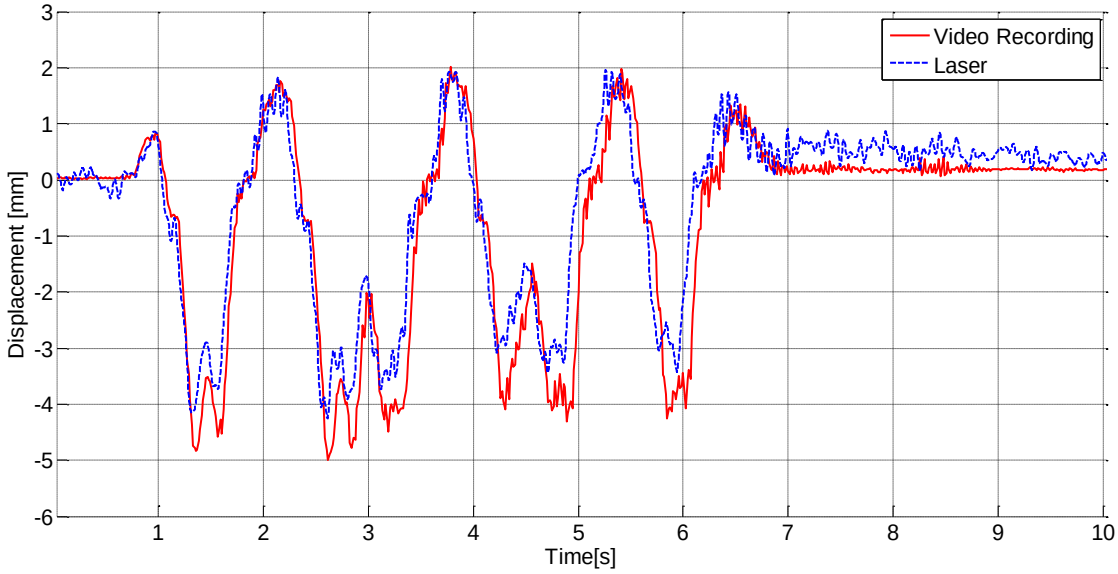

Figure 6-27: Issue of the video recording system dropping frames at t = 4 s

It is assumed that the camera dropped some frames as the fourth bogie went over the rail. The University of Southampton has a plan to test using a video camera which is capable of recording more frames per second (FPS) so that this error rate can be reduced for future tests (73 FPS is used in this test).

6.4.3 System Upgrades

6.4.3.1 Increasing the Level of Signal Strength to 10 mW

This trial was aimed at checking the feasibility of the measurement system at railway critical zones. The maximum speed during the trial was 39 km/h, so it was not meaningful to compare the geophone data to the data from the laser measurement system. The gain value was high, between 90 and 253; the controllable range is between 1 and 255. The data from the laser measurement system has been understated compared to the video recording system due to weak level of laser intensity. Therefore, in order to produce better data and to aim to measure multiple consecutive sleepers, possibly more than 12 so that the laser measurement system can be effective to the furthest node in the next trial, upgrading to a 10 mW laser source has been considered. It is expected that it would also get a better level of signal to ratio.

6.4.3.2 Consideration of a Gaussian Intensity

The remote line laser has a Gaussian intensity, therefore a better way of locating the laser source has been considered, by calculating the aperture angle of a line laser. It was 42° for the previous trial and a set up with less than 26° is now considered, as shown in Figure 6-28, so that the sensor placed furthest away from the laser source gets a stronger beam. This set up is expected to produce a better result at the next field trial.

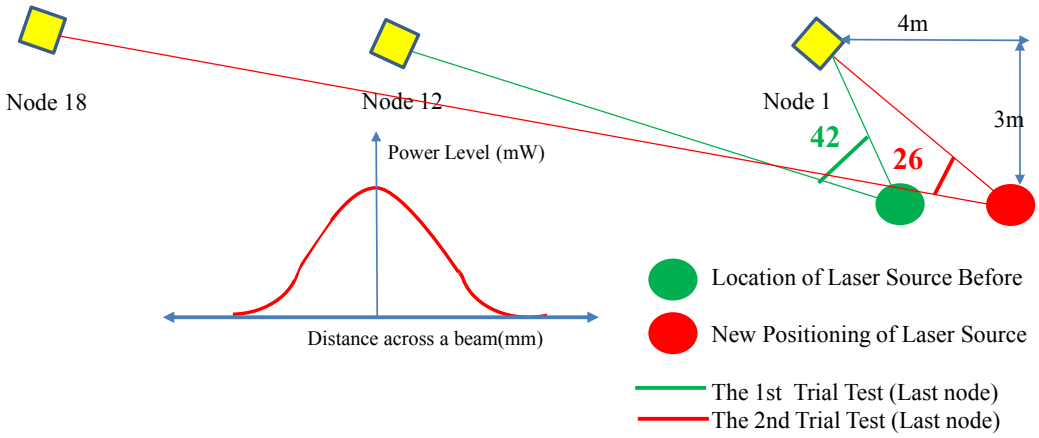

Figure 6-28: The new positioning of the laser source

6.4.3.3 Software Upgrades

Through the monitoring process, visualisation of laser strength has been additionally implemented in the software and Figure 6-29 shows the real time display of sleeper displacement for the field measurement.

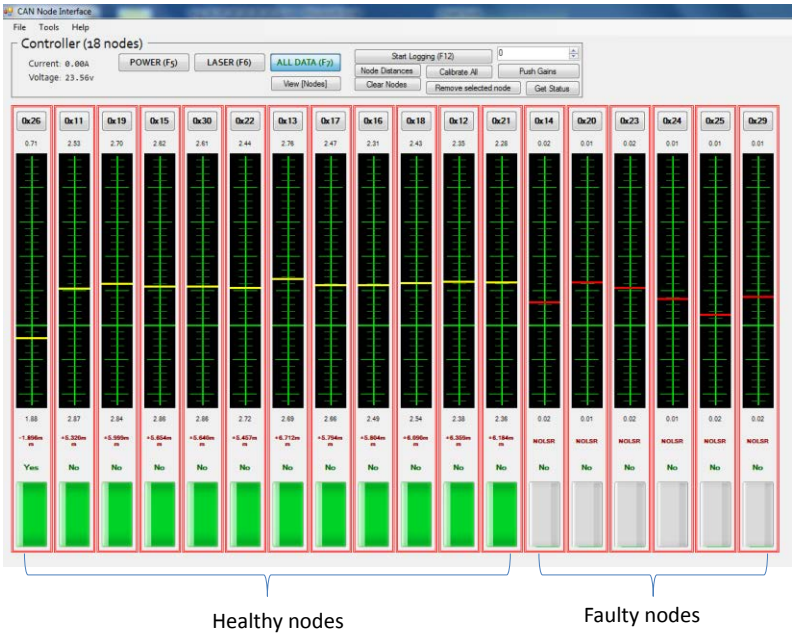

Figure 6-29: Screenshot of the software update to show signal strength (green bars)

The length of the green bar shows the signal strength received from the laser source, at the individual sensor nodes. Looking at the level of green bars helps to calibrate the gain value and align the angle of the sensor nodes. From the left on the screenshot, it shows twelve healthy sensor nodes and six faulty sensor nodes, due to an insufficient level of the laser source, caused by either the angle or distance from the laser source.

When the 24 mm PSD sensor was replaced by a 37 mm PSD sensor, the red laser source was replaced by an infrared laser, whose beam is invisible. Therefore, it was not so easy to set up the angle of the laser source on the tripod, i.e., it was not possible to ascertain that the laser source was directly facing each sensor node. In order to address this issue, the following screen (Figure 6-30) was implemented to help the alignment process of the laser source.

Figure 6-30: A screenshot of the software update to assist with the laser alignment and show the signal strength (Pink bar)

By looking at the relative position of each sensor node on the sleepers, the alignment of the laser source could be adjusted easily.

6.4.3.4 Hardware Improvements

One more issue was the instability of data transmission. The data transmission via a CAN bus was instable due to the large volume of data. In order to monitor more than 12 multiple nodes for the next trial, two PCAN-USB connectors were used to provide better data transmission, as described in Figure 6-31, which is upgraded from the previous schematic view (See, Figure 4-26). Each PCAN-USB is connected to 8-10 sensor nodes respectively. After upgrading, the system was able to operate up to 18 sensor nodes dependably. In addition, the build of an additional master node was considered, so the system has two master nodes, which control a 24 V power supply individually for each set of 9 nodes.

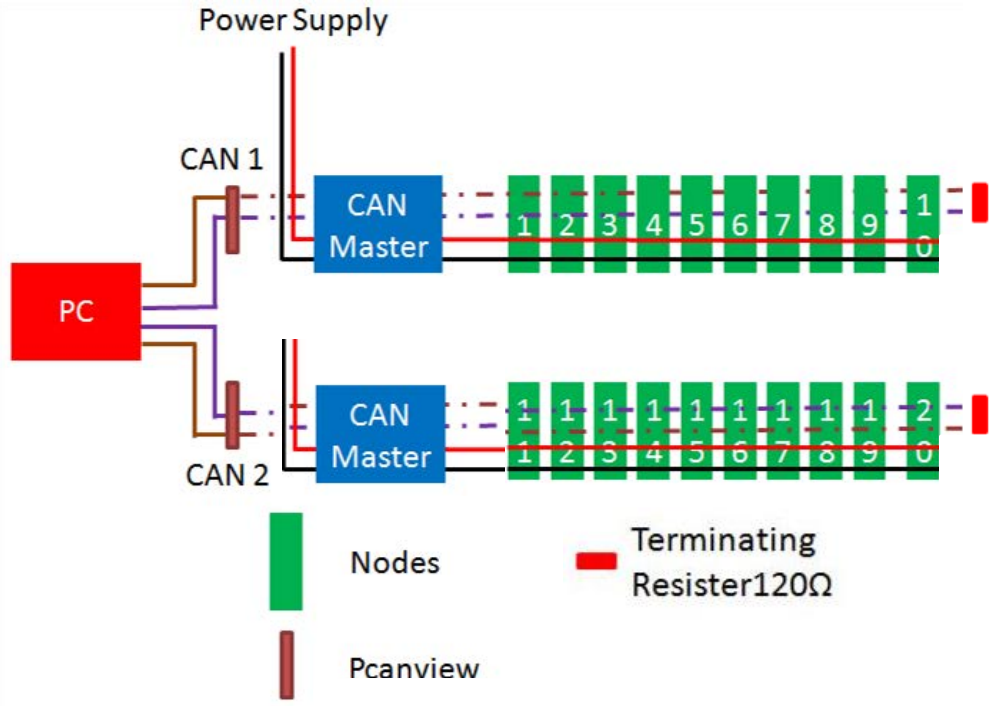

Figure 6-31: Schematic view of the CAN Bus connection with two PCAN-USB and two master nodes for deployed 12 + Nodes up to 18 nodes

6.5 Second Trial of Deflection Measurement

As previously discussed, the second field trial was conducted after planning to place the laser source in a different position, in order to address better the Gaussian effect and with the expectation of collecting reliable results thanks to the hardware improvements (two master nodes, two CAN-USB, 10 mW laser source) and a software upgrade, which was anticipated to allow aligning of the laser more easily and quickly towards the sensor nodes.

In summary, the aim of the second trial was to assess the performance of the newly developed laser based system, which had been enhanced by:

1) Improving the position of the laser source;
2) Using two master nodes to ensure robust data transmission;
3) Conducting a comparison test between the two sensors (geophone and laser system) at various speeds.

The setting up of the arrangements for the field test is described in the next section.

6.5.1 Description of Field Test Set-Up

Figure 6-32 : (a) Level crossing, June 2013, (b) Re-compacted ballast, concrete from level crossing, September 2014

Due to refurbishment work near to the switch on the test track at Long Marston, where the previous tests had taken place, the measurements were taken only on the approach section of the former level crossing area and the straight section of plain line track. As there has been track upgrade work, this section of track does not currently function as a level crossing; ballast is piled up adjacent to the rails and a concrete surface remains from the level crossing, as shown in Figure 6-32. The 18 sensor nodes were instrumented along the track, so that a track length of 13.44 m was used for the experimental site, as described in Figure 6-33, and six geophones were placed along the track and compared with the laser based system. The train moved from left to right as indicated in Figure 6-33.

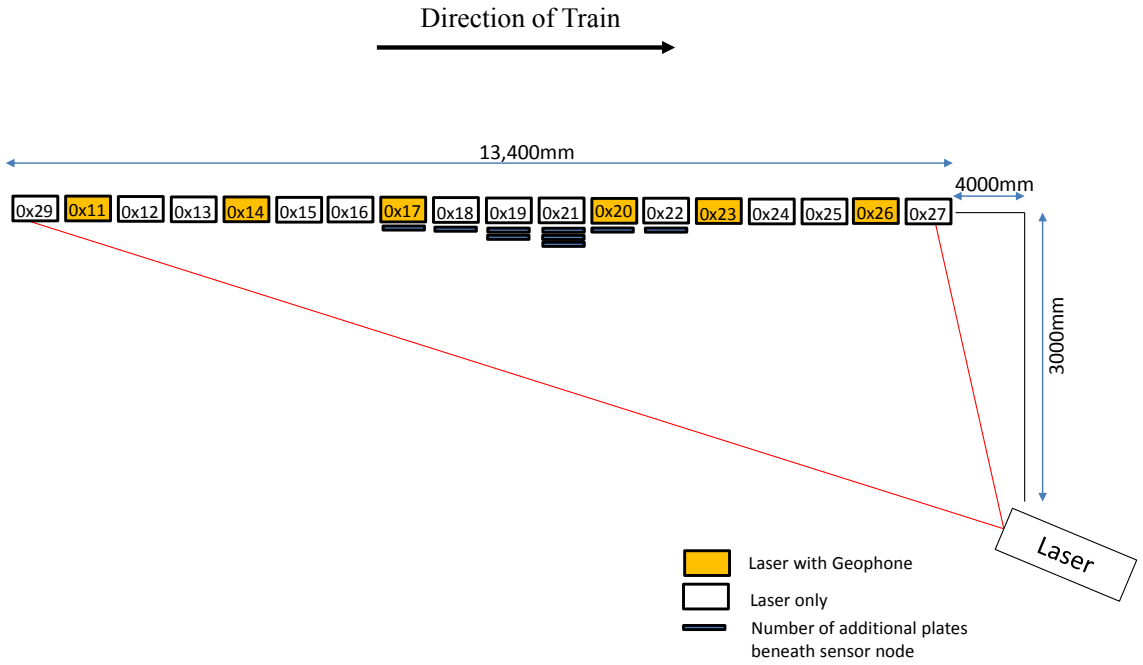

Figure 6-33: Schematic diagram of the sensor node instrumentation

Figure 6-34 : Photo of the field instrumentation of 18 sensor nodes

The distance between each sensor node, the node identification number and the value of gain are presented in Table 6-13.

Table 6-13: Detailed information on the set up of the sensor nodes

Node number (left-right)	Node id	Node between	Distance (mm)	Gain	Extra Plates	Geophone
node1(far left)	0x29	node1-2	810	10		
node2	0x11	node2-3	800	10		O
node3	0x12	node3-4	850	10		
node4	0x13	node4-5	820	8		
node5	0x14 (0x28)	node5-6	710	6		O
node6	0x15	node6-7	840	5		
node7	0x16	node7-8	840	5		
node8	0x17	node8-9	750	5	1	O
node9	0x18	node9-10	660	4	1	
node10	0x19	node10-11	680	4	2	
node11	0x21	node11-12	800	3	3	
node12	0x20	node12-13	830	3	1	O
node13	0x22	node13-14	770	2	1	
node14	0x23	node14-15	790	2		O
node15	0x24	node15-16	820	2		
node16	0x25	node16-17	890	2		
node17	0x26	node17-18	780	3		O
node18 (far right)	0x27		13440	3		

As shown in the table, it was found that the gain in signal strength is roughly proportional to the distance from the position of the laser source after calibration, so the furthest sensor nodes (nodes 1, 2 and 3) require the highest gain value, which is 10, whereas nodes 13-17 have smaller gain values.

Each sensor node had a cover to provide shade from direct sunlight, which can act as a source of interference, as shown in Figure 6-35.

Figure 6-35: Sunlight cover for each sensor node

When all 18 sensor nodes are connected via the CAN, the multiple connected nodes and each individual displacement are shown on screen, see Figure 6-34.

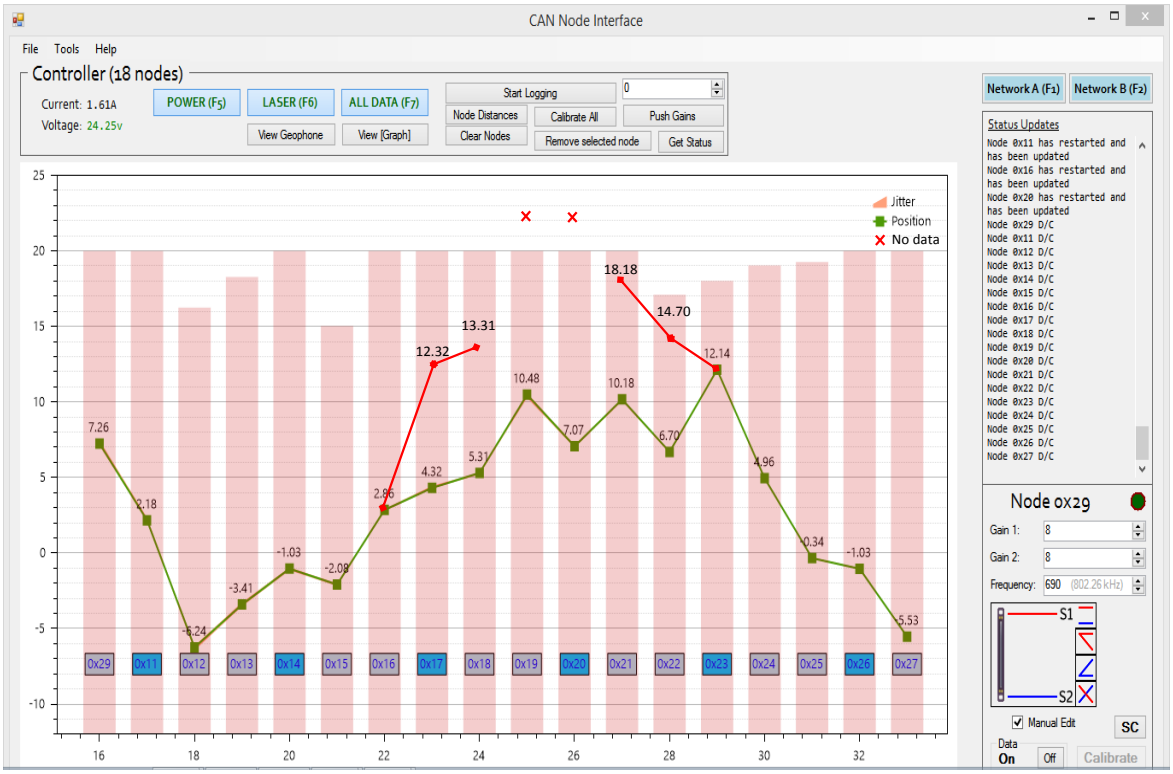

Figure 6-36: A snapshot of the status of 18 connected sensor nodes with six geophones (0x11, 0x14, 0x17, 0x20, 0x23 and 0x26)

The laser based measurement system can be ideal when the alignment of consecutive sleepers is in line. However, the vertical alignment of each sleeper was not equalised along the track, so some sleepers (0x17, 0x18, 0x19, 0x21, 0x20, 0x22), which are in the middle of the relevant section of track, are positioned lower than adjacent sleepers, as pointed out by the red line on . In order to align the sensor nodes on the sleepers for consistent alignment, one to three additional plates, equivalent to a height of 8 mm, were placed underneath the sensor nodes to lift up their position so that the line laser faces the laser within the range of the active area of the sensor, as shown in Figure 6-35.

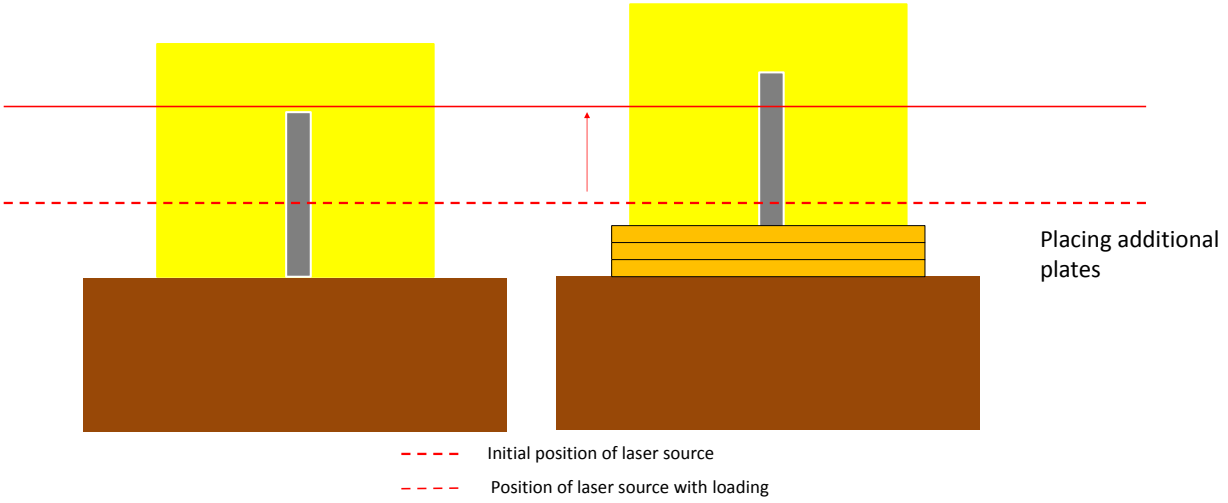

Figure 6-37 : The effect of placing additional plates under the sensor node

Another reason for aligning the sensor node as high as possible was that it gives sufficient allowance of the active area on the sensor to respond to the laser source. The sleepers normally move down during train passage, which means that the reference laser line goes up, as described in the diagram below.

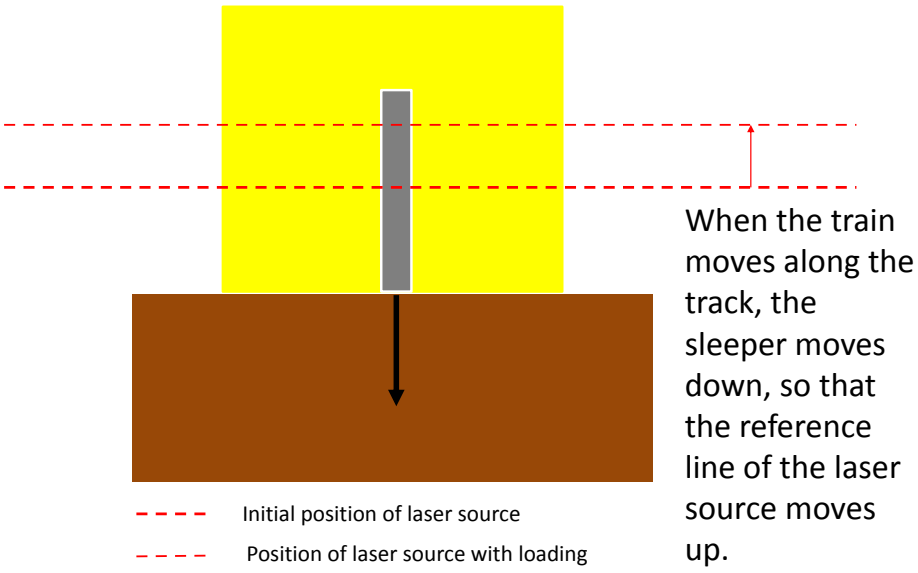

Figure 6-38: The movement of the reference line of the laser source

The vehicles used in this trial were a diesel railcar and a tanker, as described in Figure 6-37.

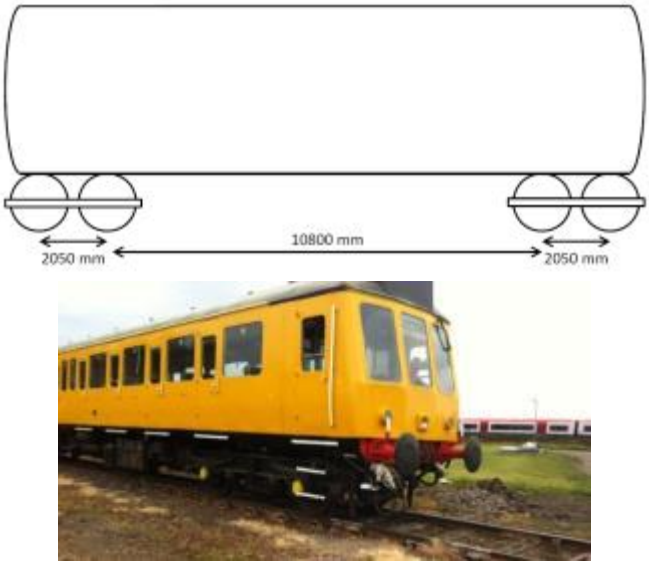

Figure 6-39: Dimensions of the running train

The train speed is calculated on the basis of one of the main frequencies which is generated by the distance between the second and third wheelsets and the time-deflection graph by its deflection. The example was calculated as shown in Figure 6-40.

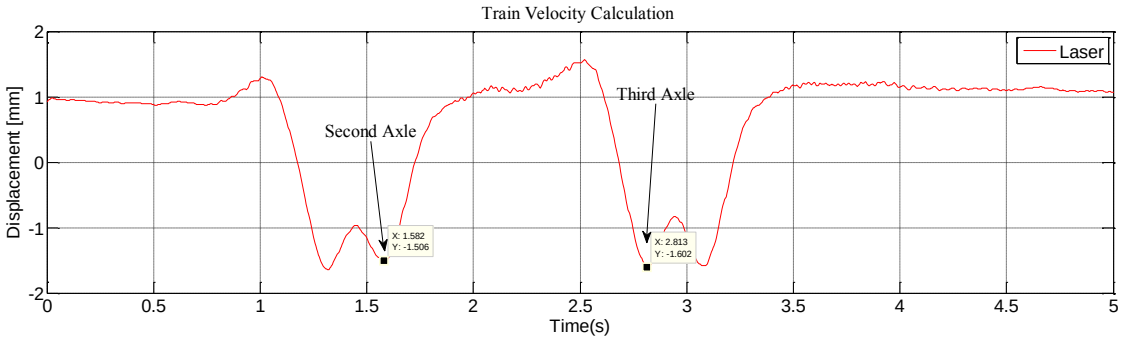

Figure 6-40 : Example of train velocity calculation

10.8 m / (2.813 s - 1.582 s) = 8.77 m/s = 31.572 km/h, 19.62 m/s

The data was collected whilst the train was running at between 7 km/h and 46 km/h, as shown in Table 6-14, and only forward (from left to right) running was allowed in this trial.

Table 6-14: Vehicle running schedule for the second trial

Run	Time	Speed (mph)	Speed (km/h)	Speed (m/s)	Direction	Notes
1	13:47	29	46	13	Forward	
2	13:58	29	46	13	Forward	
3	14:08	5	8	2	Forward	very low speed
4	14:20	10	16	5	Forward	

Run	Time	Speed	Speed (km/h)	Speed (m/s)	Direction	Notes
5	14:38	29	46	13	Forward	
6	14:59	20	32	9	Forward	
7	15:40	30	49	13.5	Forward	Only two sensors compared
8	15:52	20	32	9	Forward	

6.5.2 Data Processing for the Laser Measurement System

When data from each single sleeper is processed, the vertical displacement data contains similar patterns of noise, which is assumed to be caused by vibration of the laser source in Figure 6-41 (a). When the amplitude is scaled (Figure 6-41(b)) in order to see same pattern of movement for each node, the data at 0-1 s and 3-4.5 s shows that the amplitude of three nodes is exactly same, which is zoomed in Figure *6-42*.

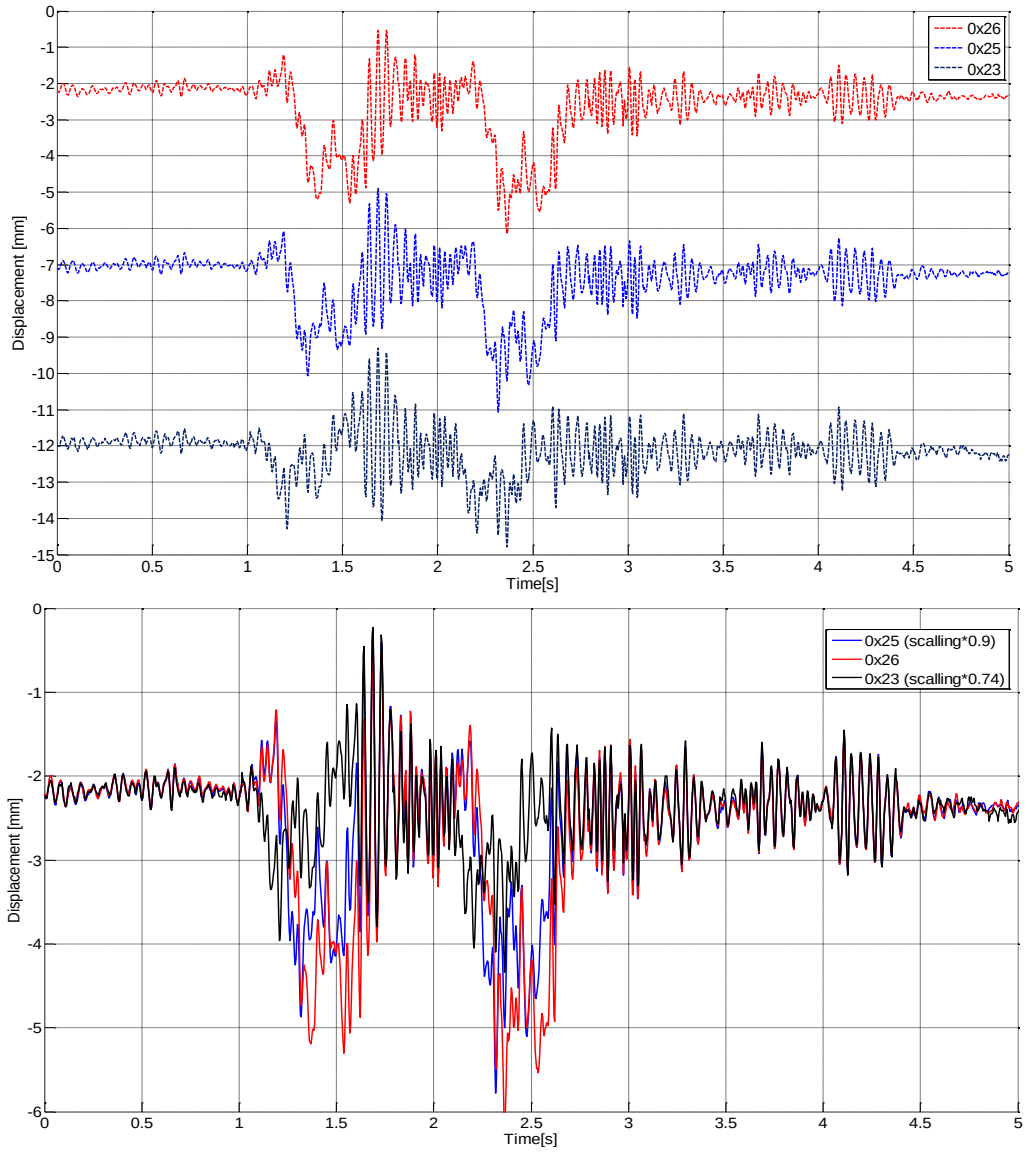

Figure 6-41: (a) raw data of three laser sensors and (b) data after scaling (46 km/h)

Therefore, this data is produced by the movement of the laser source rather than from the train rolling over the sleepers.

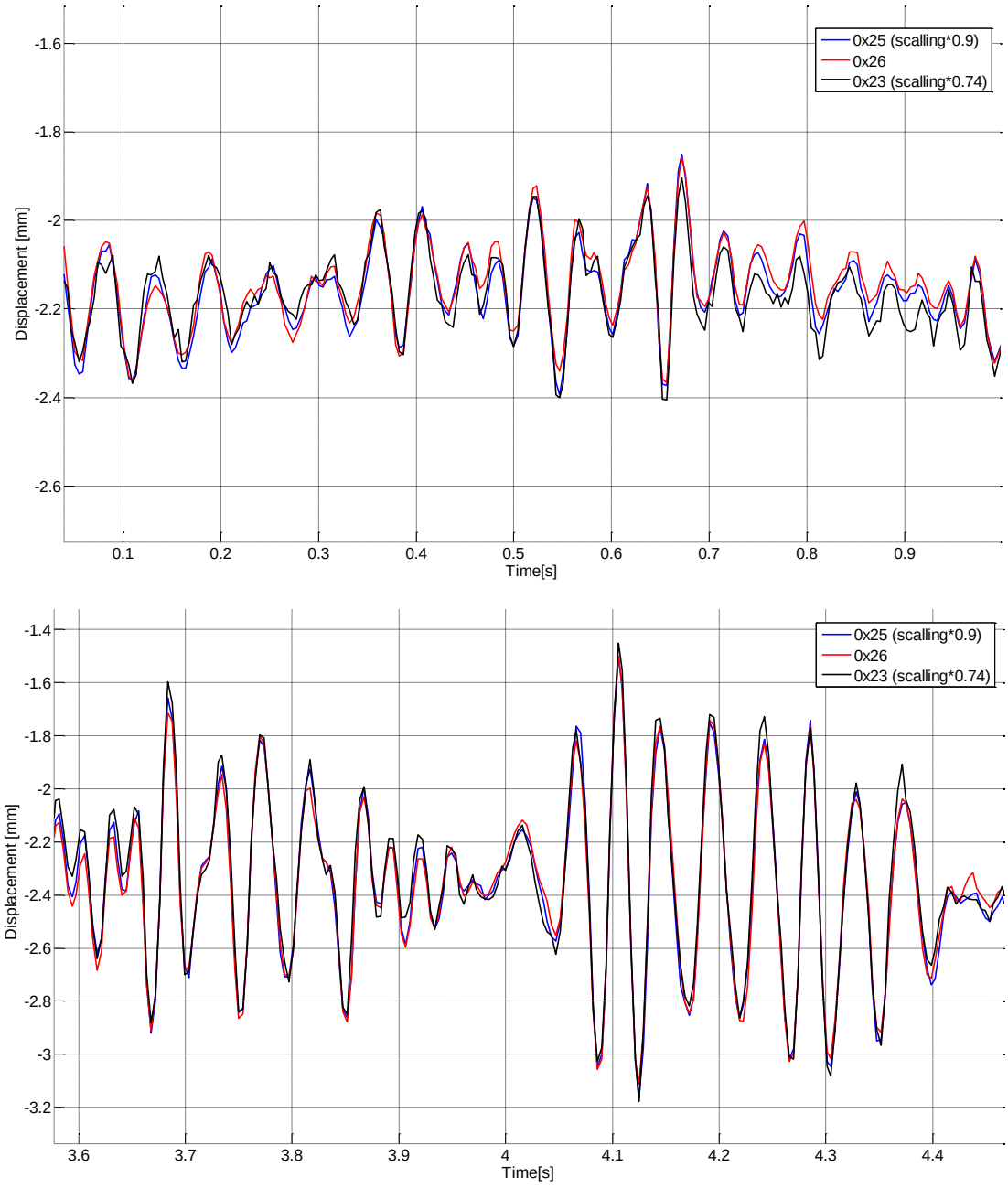

Figure 6-42: Zooming data between 0-1 s and 3.5-5 s

A Fast Fourier Transform (FFT) analysis was carried out as shown in Figure 6-43 (a) in order to find the major frequency due to train running and the frequency due to the noise (vibration). The FFT analysis shows that most of the noise is caused when the frequency is higher than 15 Hz. After scaling the displacement data (Figure 6-43 (b)), the relative amplitudes are very close to each other between the frequency of 15 to 40 Hz, whereas the major frequency is caused by the wheel rolling, which is around or less than 5 Hz. Therefore, the

laser data will be applied with a 15-18 Hz low pass filter (LF) and 6 Hz LF. The 1 Hz high pass filter was applied into the laser measurement data in order to achieve agreement between the two sensors, since the geophone has a built-in 1 Hz high pass filter.

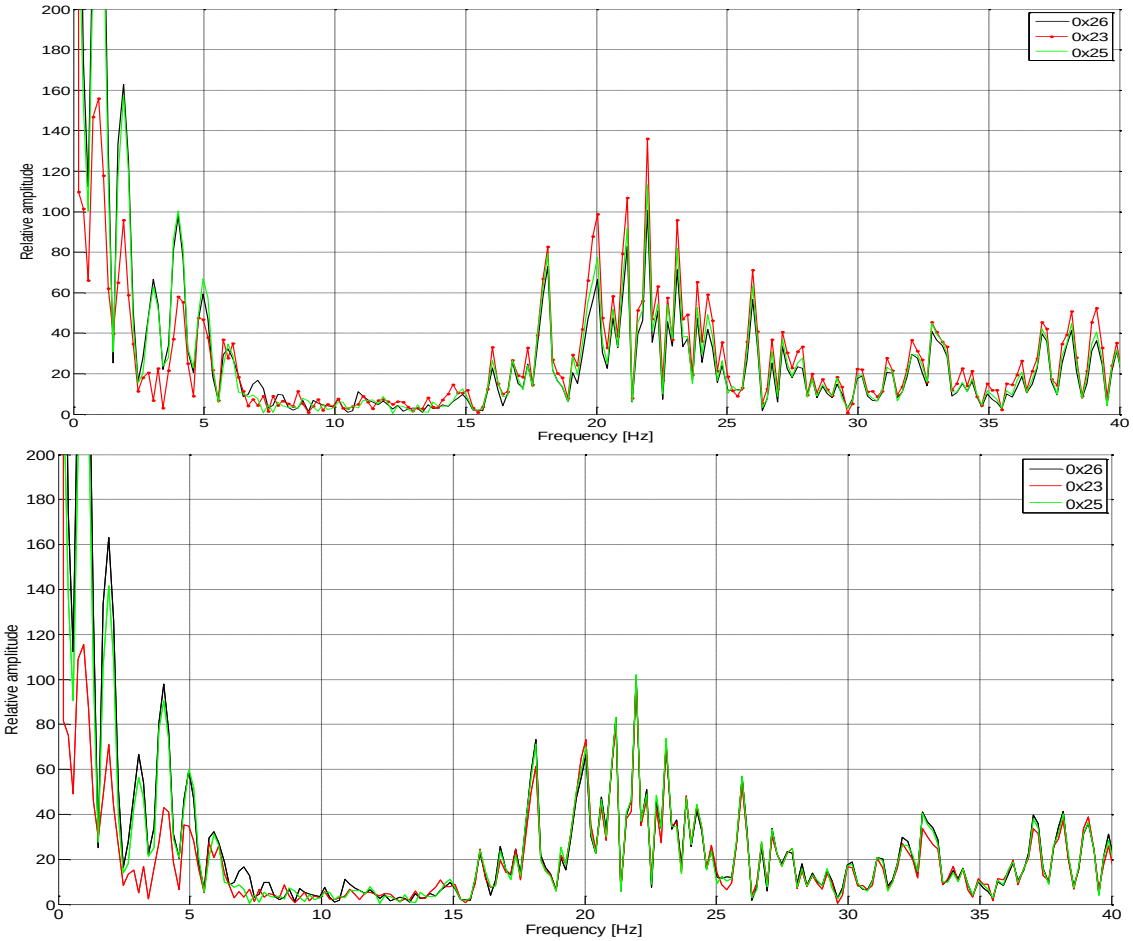

Figure 6-43: FFT analysis on (a) raw data and (b) after scaling the raw data

Therefore, 6, 15 and 18 Hz low pass filters have been applied to the laser data on sleeper number 17 (node number: 0x26), which is positioned second closest to the laser source while the train passes at 49 km/h, as shown in Figure 6-44(a). The data with the application of the 6 Hz low pass filter shows very good agreement as to the maximum displacement between the geophone data and the data of the laser measurement system, as shown in Figure 6-44 (b).

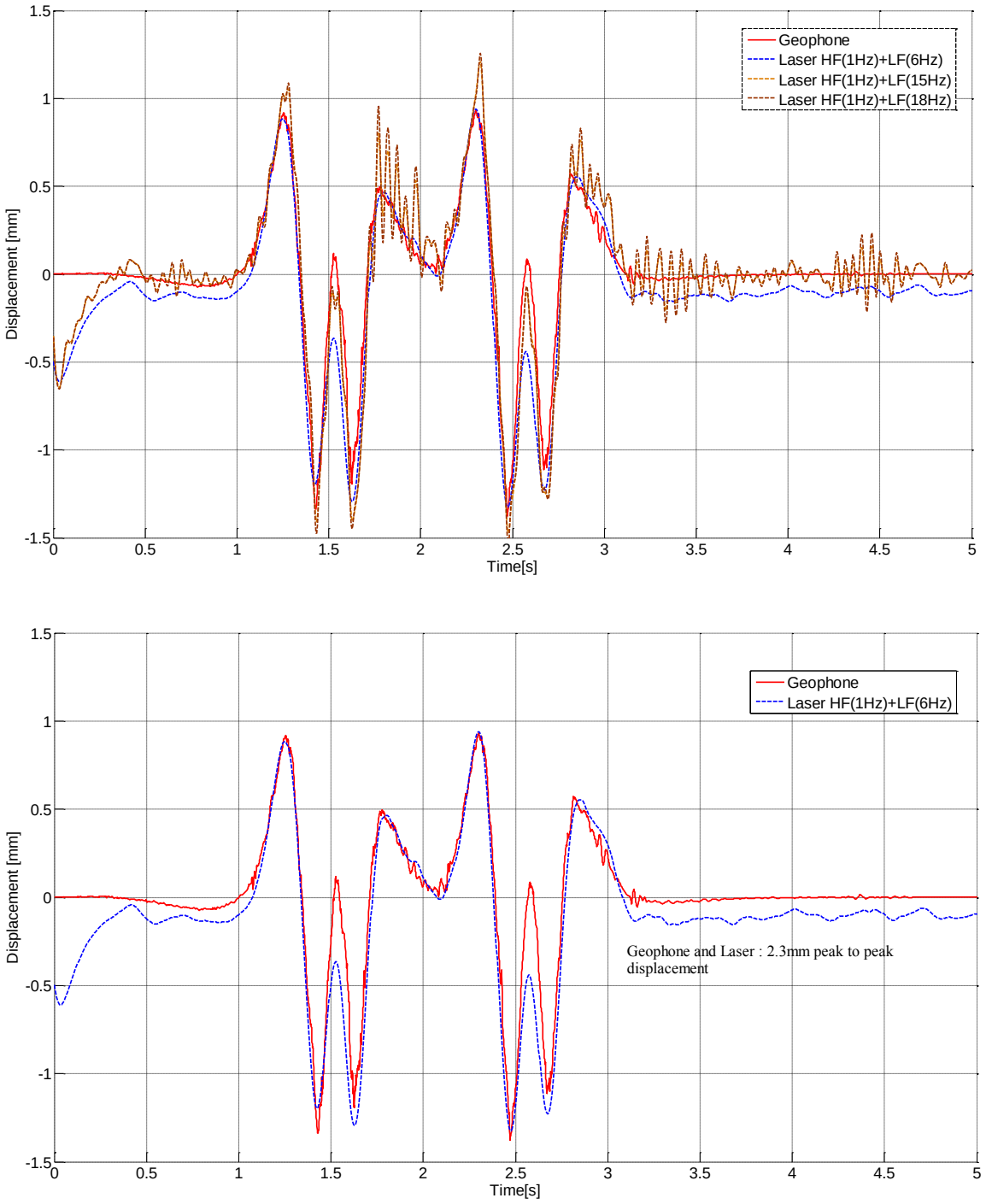

Figure 6-44: Data comparison *between the geophone (red) and the laser data (a) 6/15/18 LF (b) 6Hz LF applied for the laser data while the train is passing at 49 km/h*

The following graph shows the comparison data between the geophone and laser source while the train runs at 46 km/h. Figure 6-45 (a) shows the laser data has been distorted due to vibration of the laser source, so that a 6 Hz LF filter is applied, and it also shows that the data from the laser measurement system has good agreement with the geophone data,

within a 0.1 mm difference when the peak to peak is compared between the two measurement systems, as shown in Figure 6-45 (b).

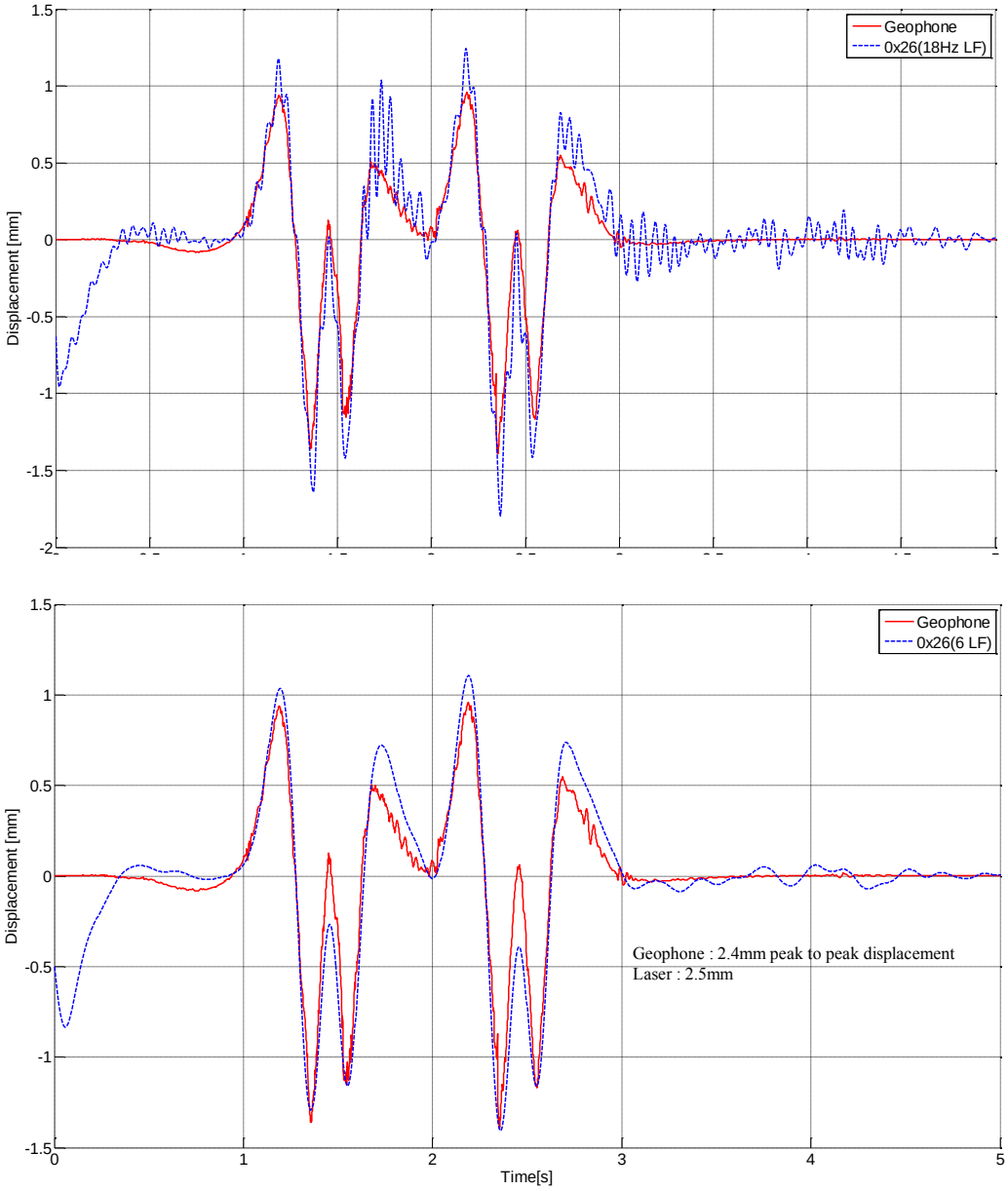

Figure 6-45 : Comparison of data produced while the train is passing at 46 km/h (a) 18 Hz LF applied (b) 6 Hz LF applied

Figure 6-44 and Figure 6-45 show that the agreement between the two sensors is good when the train's speed is close to 50 km/h while the bogie space is 10.8 m.

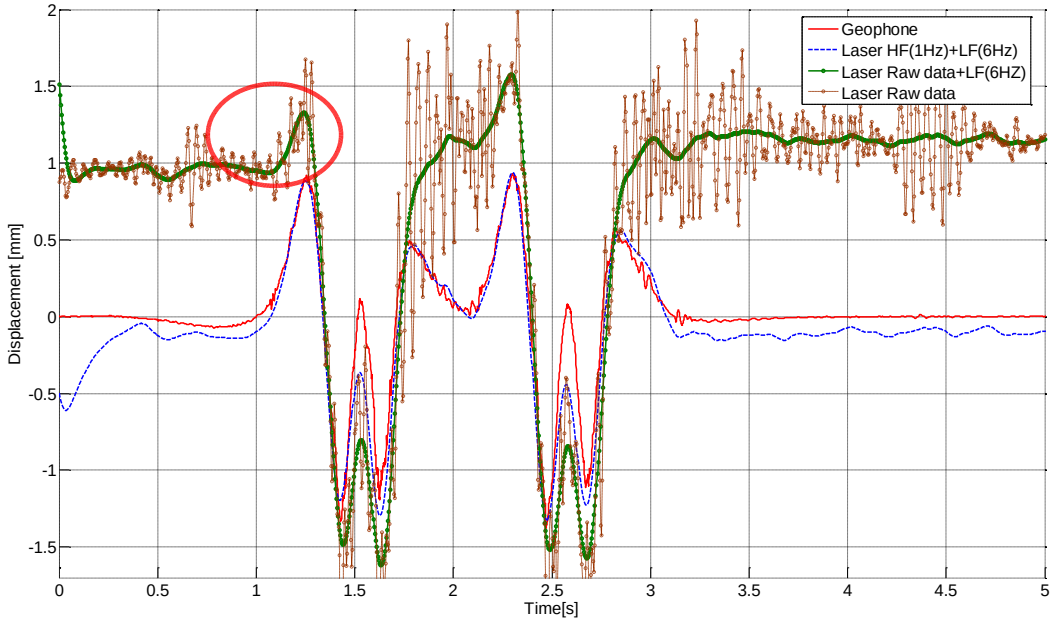

Figure 6-46: Realistic laser data without applying 1 Hz high-pass filter compared with geophone data

In summary, for the data agreement of the two sensors, the laser sensor data has been filtered by a 1 Hz high-pass filter and a 6 Hz zero-phasing filter has been applied in order to reduce phase distortion. Agreement has been achieved between the two data sets and the pattern is very similar. Peak to peak displacement has been agreed with 0.1 mm accuracy, which is verified by the test plan. However, there was a transient response error at the beginning of the filtered data, so it is not able to show the uplift in sleeper movement before the first wheel passed over the sleeper, pointed out with a red circle in Figure 6-46. The brown dotted line shows the data which is produced by applying 6 Hz low-pass filtering of the raw data, which is more realistic compared to the data from the geophone and the laser sensor, which applies a 1 Hz high-pass filter and LF. Therefore, the data from the laser measurement system shows a more realistic movement of the sleeper.

6.5.3 Test Results

6.5.3.1 Measurement System at Different Speeds

As found in Chapter 5, it is not reliable to get the data from the geophone when the frequency falls below 5 Hz. In addition, the data from the geophone is non-linear below a 10 Hz excitation frequency, as shown in Figure 3-20, therefore it is not straightforward to calculate the correct value of displacement data according to the excitation of frequency. In order to get the best value of displacement data from the two sensors, 1 Hz HF is not applied for data processing to the laser data in this section. It was found that the data where

the sensor node (0x22) is positioned at a distance of 8 m from the laser source, at 50 km/h shows good agreement. The peak to peak value is compared in Figure 6-47.

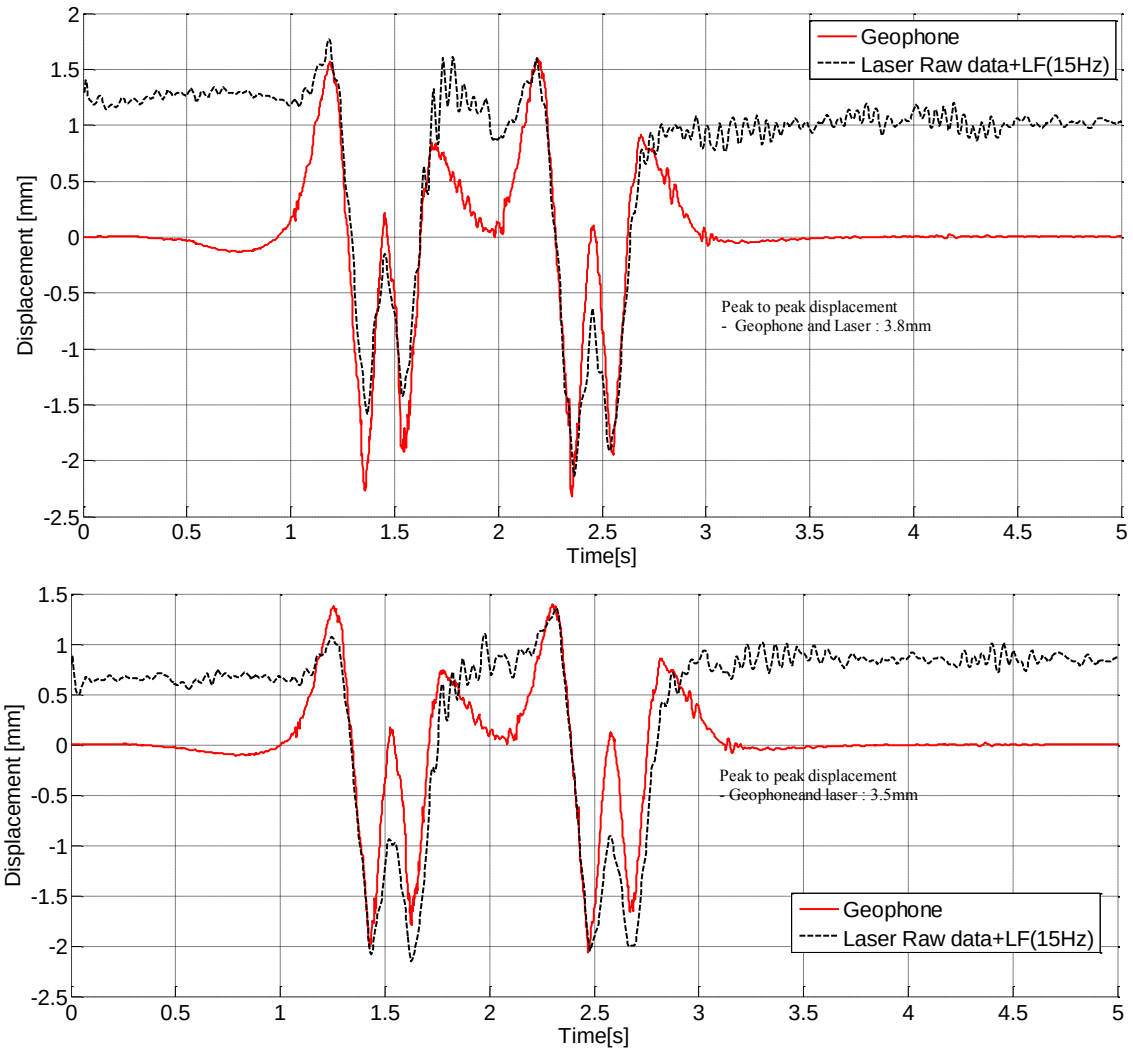

Figure 6-47: Comparison while the train is passing at 49 km/h and 46 km/h respectively

Figure 6-48 shows that the peak to peak is still similar when the difference between the two sensors is decreased to 0.2 mm while the train was running at 32 km/h. The data result should be divided into corresponding sensitivity values. The major frequency between the bogies is calculated as 0.8 Hz, which is below 1 Hz, and the sensitivity is 7 V/ms^{-1}. Therefore, the displacement between wheels which has high frequency (3.3 Hz) is over-calculated (pointed out by the black arrows on the graph), although the peak to peak displacement is similar.

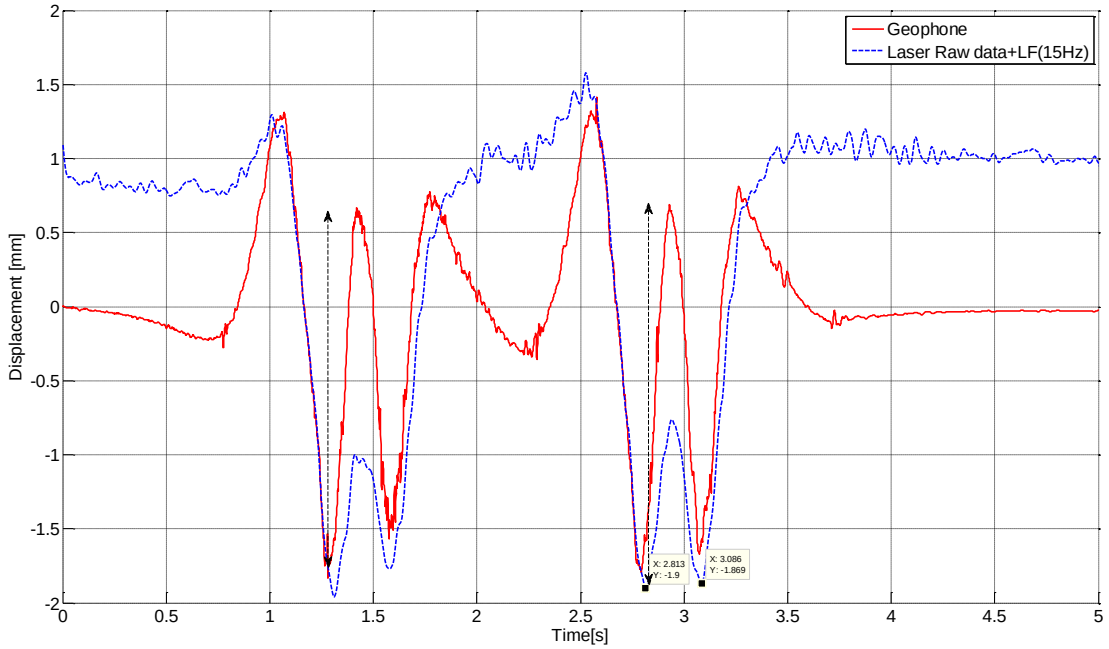

Figure 6-48: Comparison data while the train passing at 32 km/h

Figure 6-49 shows the comparison data while the train runs at 8 km/h; the data from the geophone is trying to centre to the zero so that the displacement is much smaller than the actual displacement due to the "zero" effect of the geophone. The main frequency at 8 km was 0.2 Hz between bogies and 0.8 Hz between wheels, far lower than 1 Hz, therefore it was not able to get peak to peak displacement at this low speed.

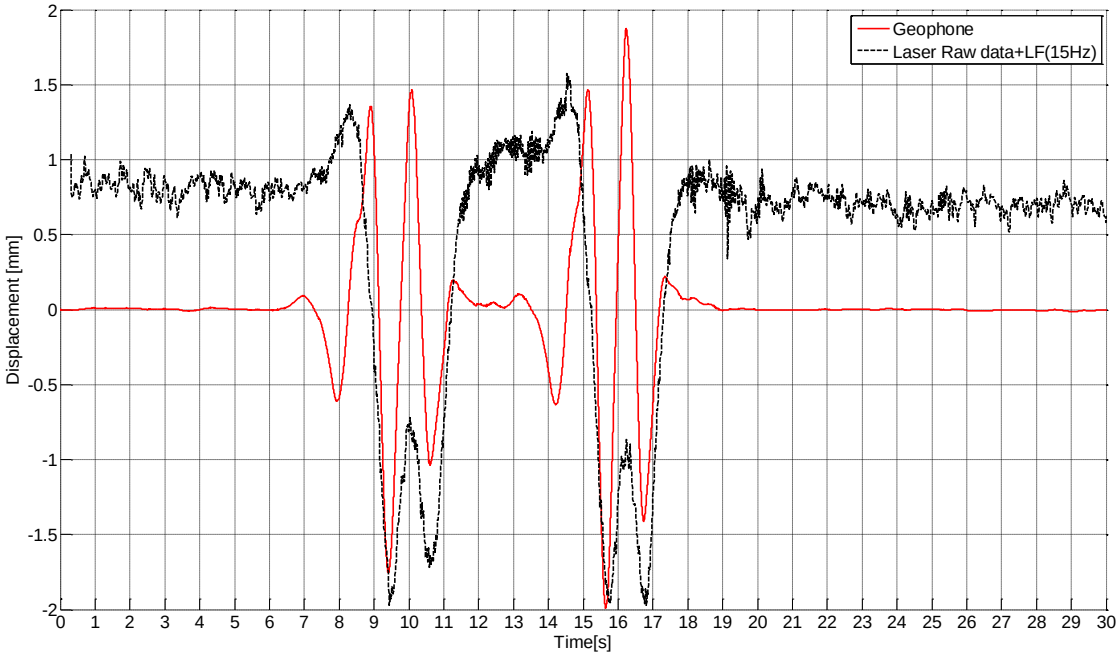

Figure 6-49: Comparison data while the train passes at 8 km/h

Table 6-15 summarises the results, which show the extent of agreement between the two sensors. While the train runs at speeds between 8 to 49 km/h, the maximum deflection of the geophone is 3.2 to 3.8 mm; the laser data shows 3.5-3.8 mm.

Table 6-15 : Maximum deflection corresponding to the variation in speeds

Velocity	Maximum Displacement (mm)		Difference(mm)
	Geophone	Laser sensor	
8 km/h	-	3.5	-
32 km/h	3.2	3.5	0.3
46 km/h	3.8	3.8	0
49 km/h	3.5	3.5	0

The analysed data and graphs show that the inconsistency in results between the two sensors is larger when the train speeds are lower.

6.5.3.2 Magnitude of Maximum Displacement at Different Train Speeds

The results for the maximum deflection of 18 sleepers collected in the field are shown in Figure 6-50.

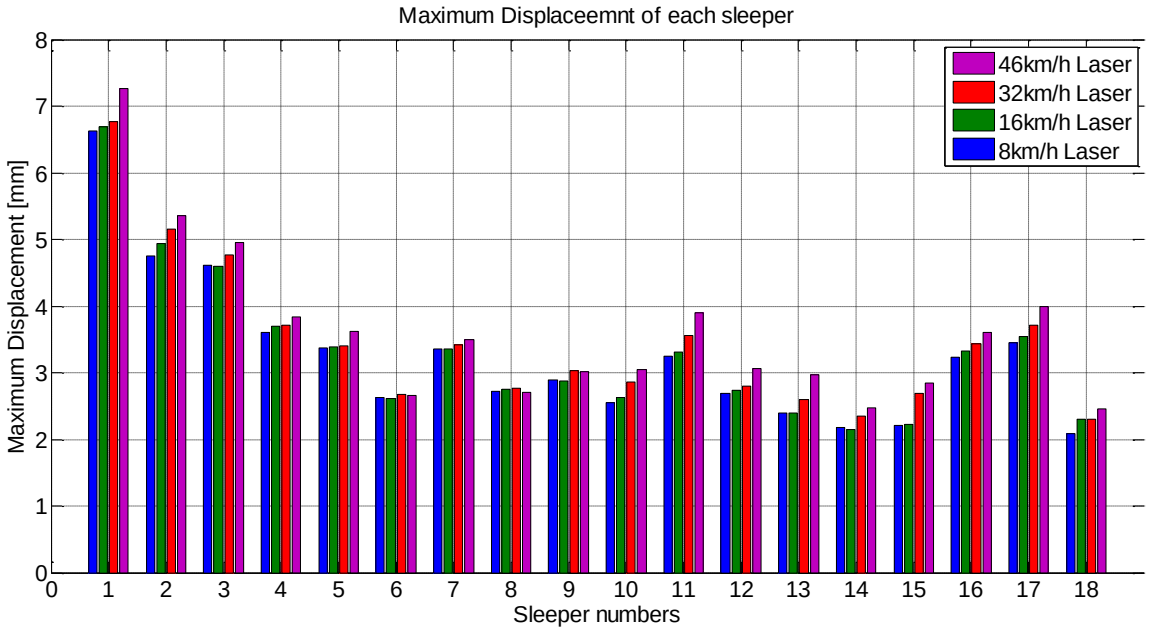

Figure 6-50 : Maximum displacement of each sleeper (laser measurement system)

Figure 6-50 shows the range of maximum vertical displacements, which is approximately 2 mm to 7 mm for each sleeper. The variation in deflection at low speed (8 km/h, 16 km/h and 32 km/h) is small, but the deflection is obviously large at 46 km/h.

The four sets of tests for the different train speeds are analysed in Table 6-16. The average deflection over 18 sleepers is 3.33 mm and the average stiffness is 13 kN/mm.

Table 6-16 : Data of Deflection and Stiffness over 18 sleepers

sleeper number	1	2	3	4	5	6	7	8	9	10	11	12	13	14	15	16	17	18	Avg
Average deflection (mm)	6.63	5.31	4.51	3.52	3.31	2.35	3.35	2.52	2.91	2.85	3.43	2.83	2.51	2.23	2.51	3.28	3.63	2.21	3.33
Stiffness(kN/mm)	6	7.5	8.83	11.3	12	16.9	11.9	15.8	13.7	14	11.6	14.1	15.9	17.9	15.9	12.1	11	18	13.02
Std																			3.43
VAR																			11.73

Geophones are only installed and measured over sleeper number 2, 5, 8, 12 and 17 to compare with data of the collected data from the laser measurement system. The data collected from geophones are plotted in Figure 6-51 in order to show the maximum vertical displacement data over six sleepers recorded by the geophones.

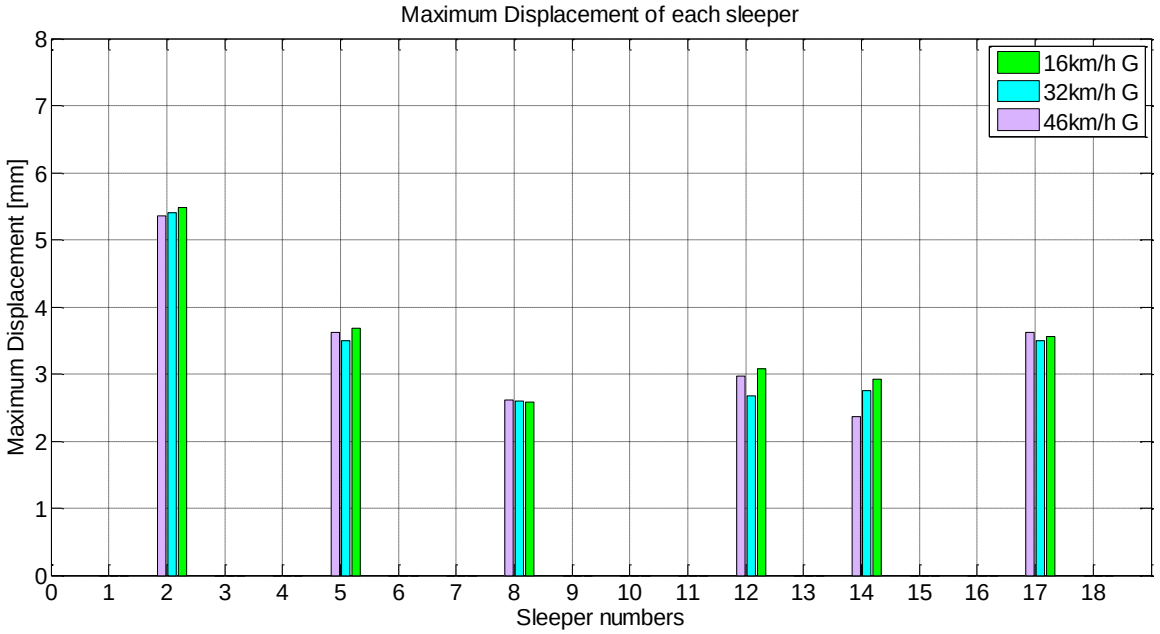

Figure 6-51 : Magnitude of maximum displacement of each sleeper (Geophones)

The overall maximum vertical measurement results from the two systems are summarized in order to give a comparison in the following graph (Figure 6-52). It was not straightforward to obtain the deflection data sets from the geophone when the train speed was lower. The geophone data when the train is running at 8 km/h is excluded from this graph. As mentioned in Section 6.5.3.1, this is due to the nature of the sensor, which is trying to centre to zero, and it also has a 1 Hz high pass filter.

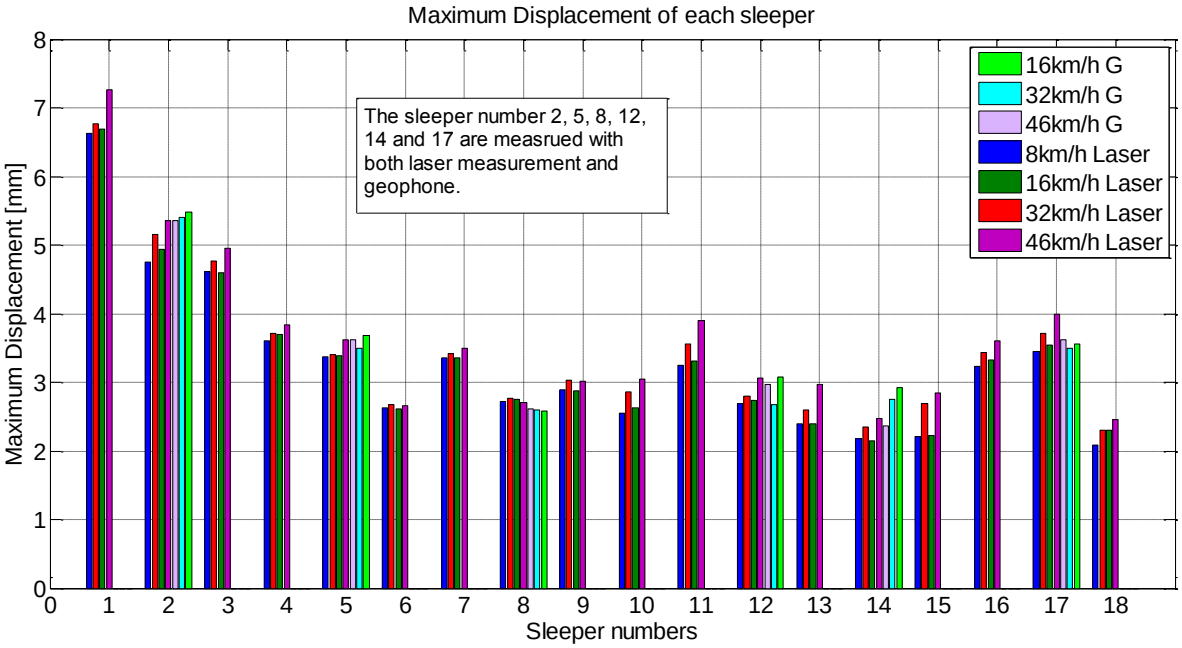

Figure 6-52 : Magnitude of maximum displacement of each sleeper at different speeds (Laser, Geophone)

However, when the train speed is closer to 50 km/h, the result from the geophone is closer to the data from the laser measurement system, as shown in the following graph.

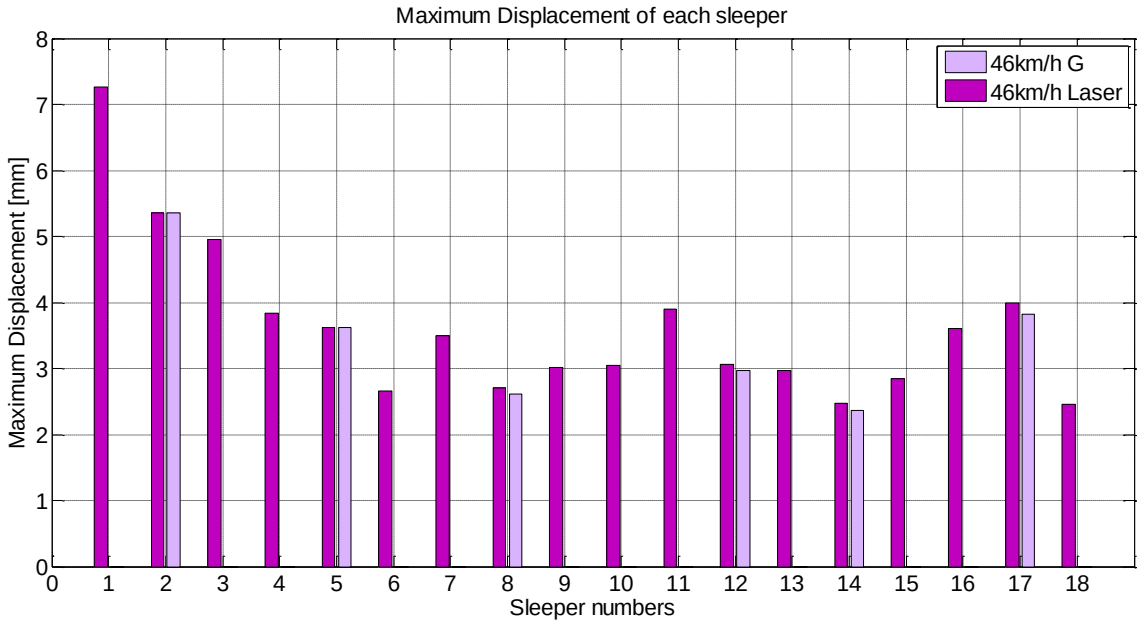

Figure 6-53: Comparison between two sensors over 18 sleepers for train speed 46 km/h

The data between the geophone and the laser agreed within a 0.1 mm tolerance.

6.5.4 Vibration of the Laser Source

The laser measurement system uses one reference line for monitoring multiple sleepers so that the vibration of the laser source can be detected by comparing the data of common patterns of sleeper movement. To improve the data distortion, attempts have been made to find the vibration of the laser source and remove it from the raw data. In the previous section, the data was processed by applying 6-18 Hz low pass filter after the FFT analysis. In this section, two different methods are approached, by making a comparison with the geophone data and using the versine concept (Iwnicki, 2006).

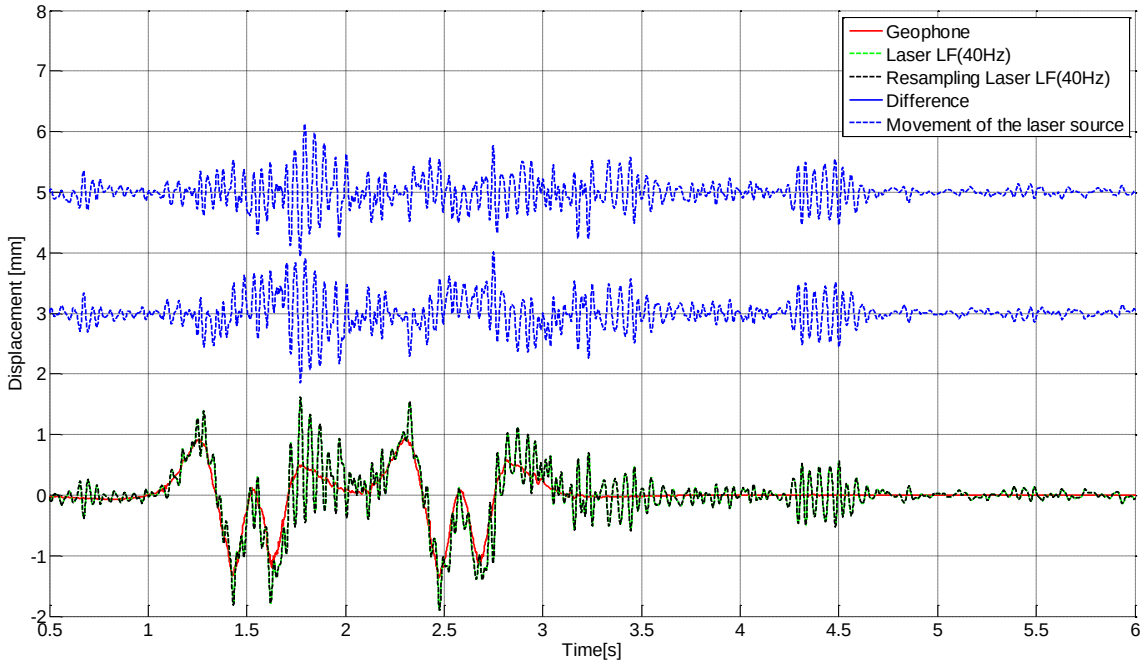

Figure 6-54: Vibration pattern of the laser source on sensor node 0x26

The first blue dotted line on the graph in Figure 6-54 presents the expected movement of the laser source, which is produced by a subtracted value between the geophone data and the laser data (0x26) and then applied to the 2 Hz high pass filter, so that the DC component is removed and the expected movement of the laser source is presented.

If this is a real vibration of the laser source, it should be possible to obtain this from the other comparison data, which was measured on different sleepers where the geophone and laser sensor were put together. From the following graph in Figure 6-55, the same pattern of vibration (green-0x23) was seen as compared to the expected vibration data (blue-0x26).

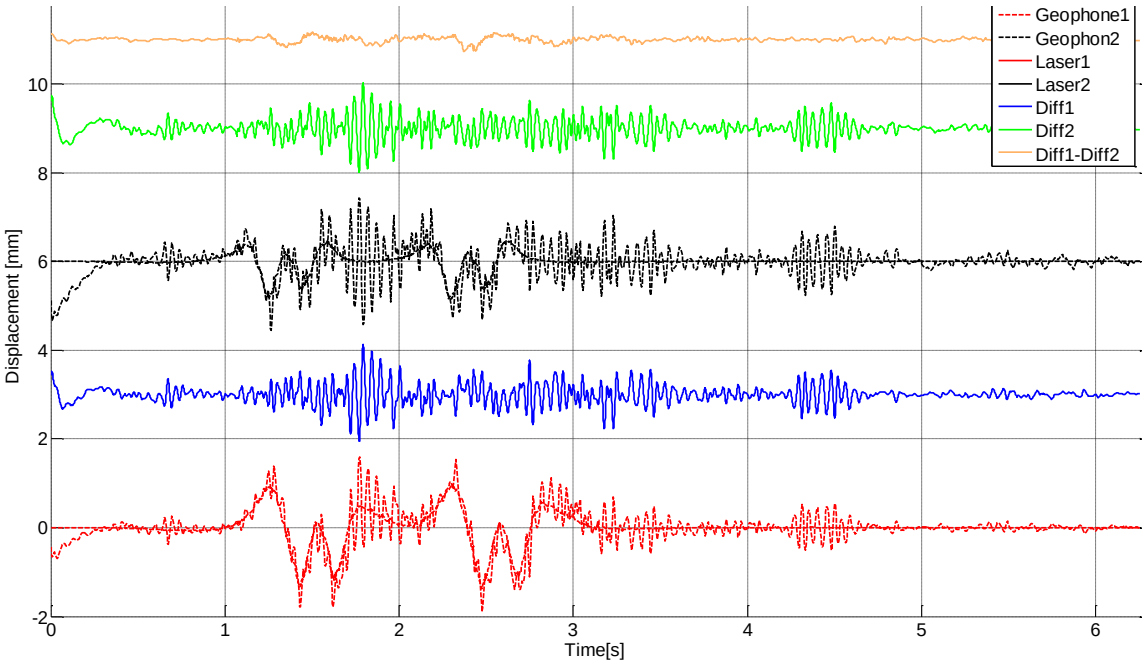

Figure 6-55: Vibration pattern of the laser source on sensor node 0x23, 0x26

In order to see the difference between Diff1 and Diff2, each relatively indicates the subtracted value between two sensors, the orange line is produced as shown in Figure 6-55 and the range is within 0.2 mm. When the laser data is subtracted by Diff1, which is assumed to be a vibration of the laser source, the second blue line shows the real laser displacement data. This following graph (Figure 6-56) shows data from the laser measurement of three different sensors (0x23, 0x25 and 0x26) after removing the vibration of the laser source.

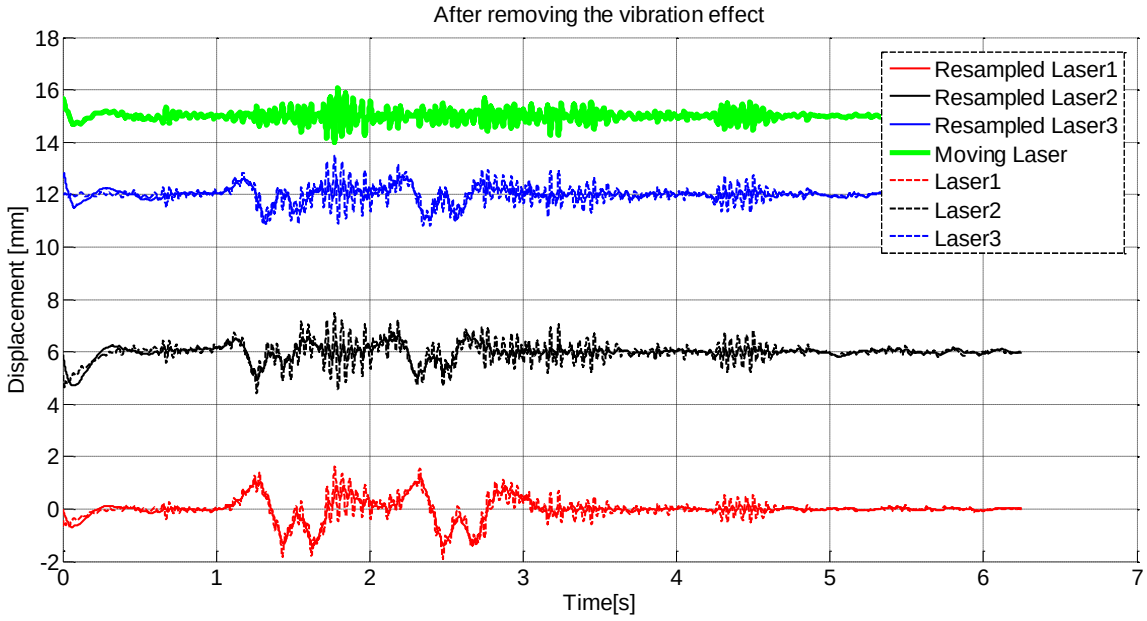

Figure 6-56: Real movement of sleepers excluding the vibration of the laser source

The following graph shows the movements of the four consecutive sleepers, as shown in Figure 6-57. In order to have an easier presentation of the displacement of four different sleepers during train passage, the reference line has been moved slightly up and down (i.e., the reference line was originally zero) so that the starting point on the y-axis is different.

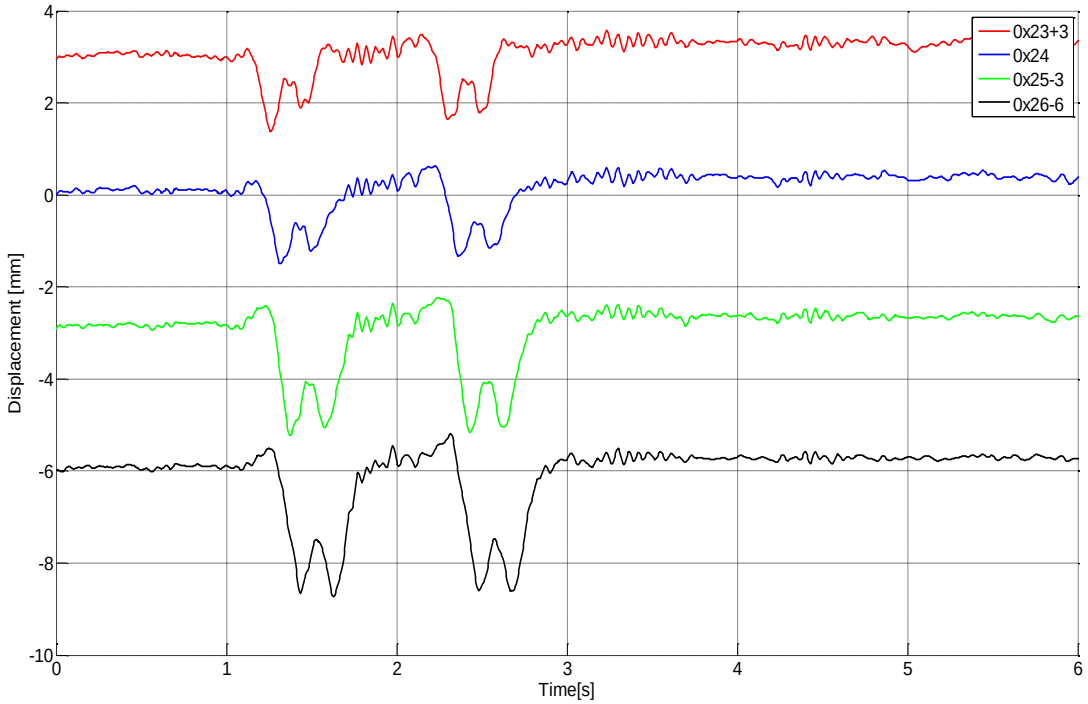

Figure 6-57: Four consecutive movements of sleepers (0x23, 0x24, 0x26 and 0x26)

As an additional way of removing the vibration of the laser source and showing the relative movement of sleepers, the concept of versine is applied. Versine is a common measurement to ascertain the straightness of railway track. In general, a versine is applied to the track geometry data of track recording vehicles in order to analse track irregularity over a certain length of track.

In theory, the bending of the rail motion can be detected across the three sleepers by averaging the displacement of the adjacent two sleepers, subtracting the displacement of middle sleeper which we are aiming to observe, as described in Figure 6-58.

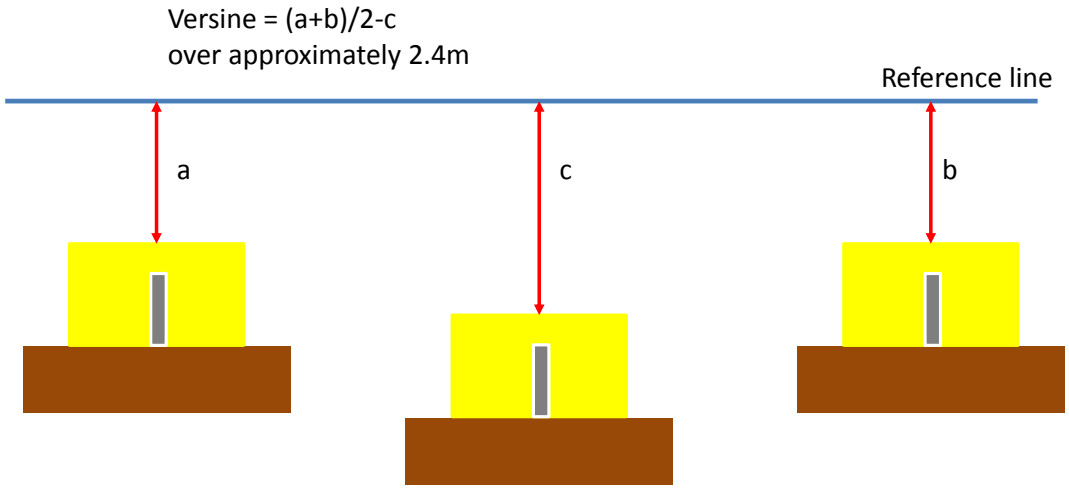

Figure 6-58: Application of the versine concept to remove the vibration effect

By obtaining the version data, it shows the relative displacement compared to the adjacent sleepers and it can possibly detect a voided sleeper by looking at the extent of the difference. As shown in Figure 6-59 (a), all solid lines show the sleeper displacement and dotted lines display the versine data of each sleeper, as shown in Figure 6-59(b).

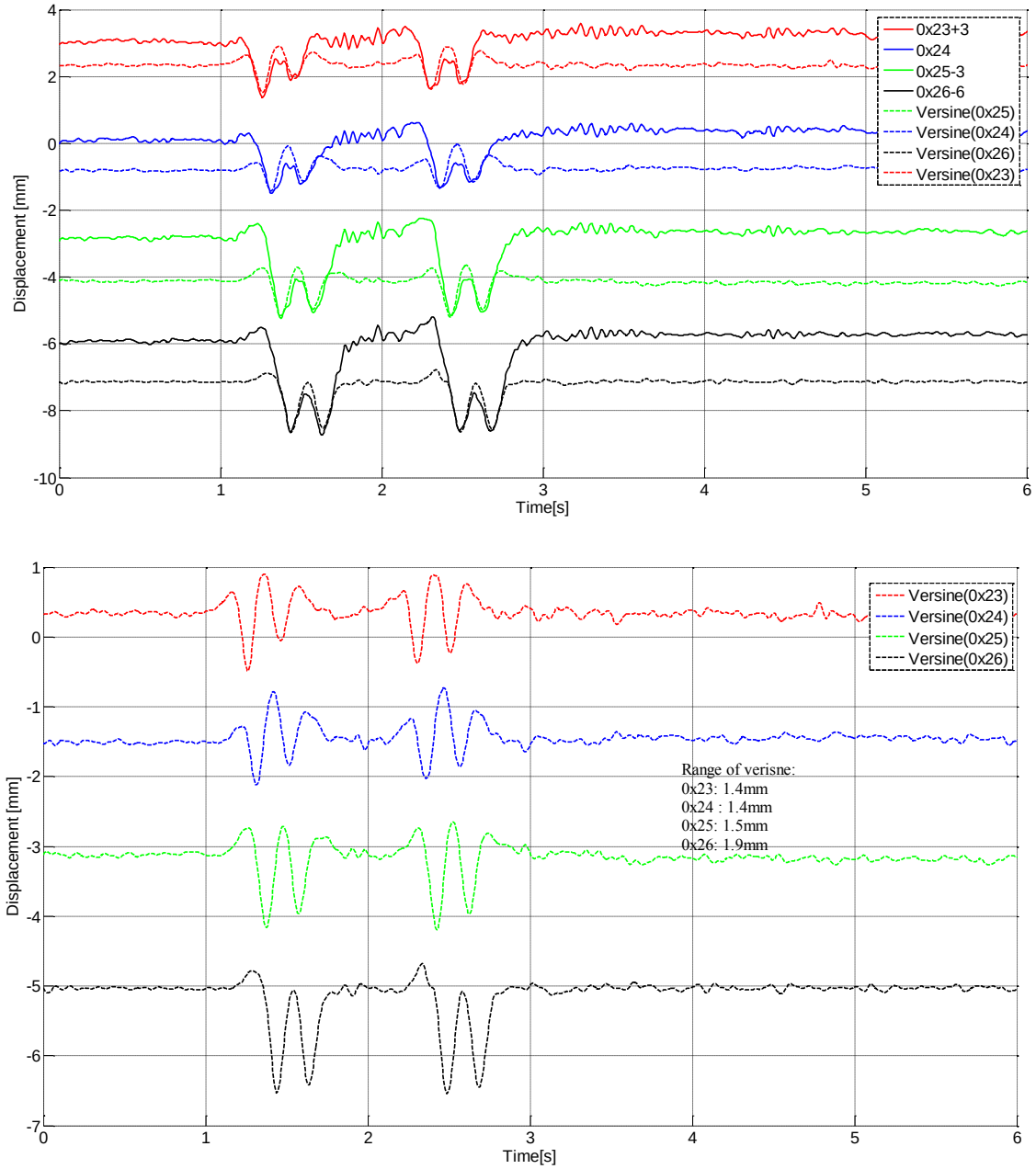

Figure 6-59: (a) Versine applied to four consecutive sleepers *and displacement data of each (b) Resulted versine of four sleepers*

6.5.5 Visualisation of Sleeper Movement during Passage of a Train

The data sets of the sensor nodes are plotted with the time domain on the x-axis and the magnitude of deflection (mm) on the y-axis, as set out in Figure 6-60. It shows the deflection response of individual sleepers to the vehicle travelling while the axle load is 39.8 kN. The individual movements of each sleeper are combined in Figure 6-60 (d).

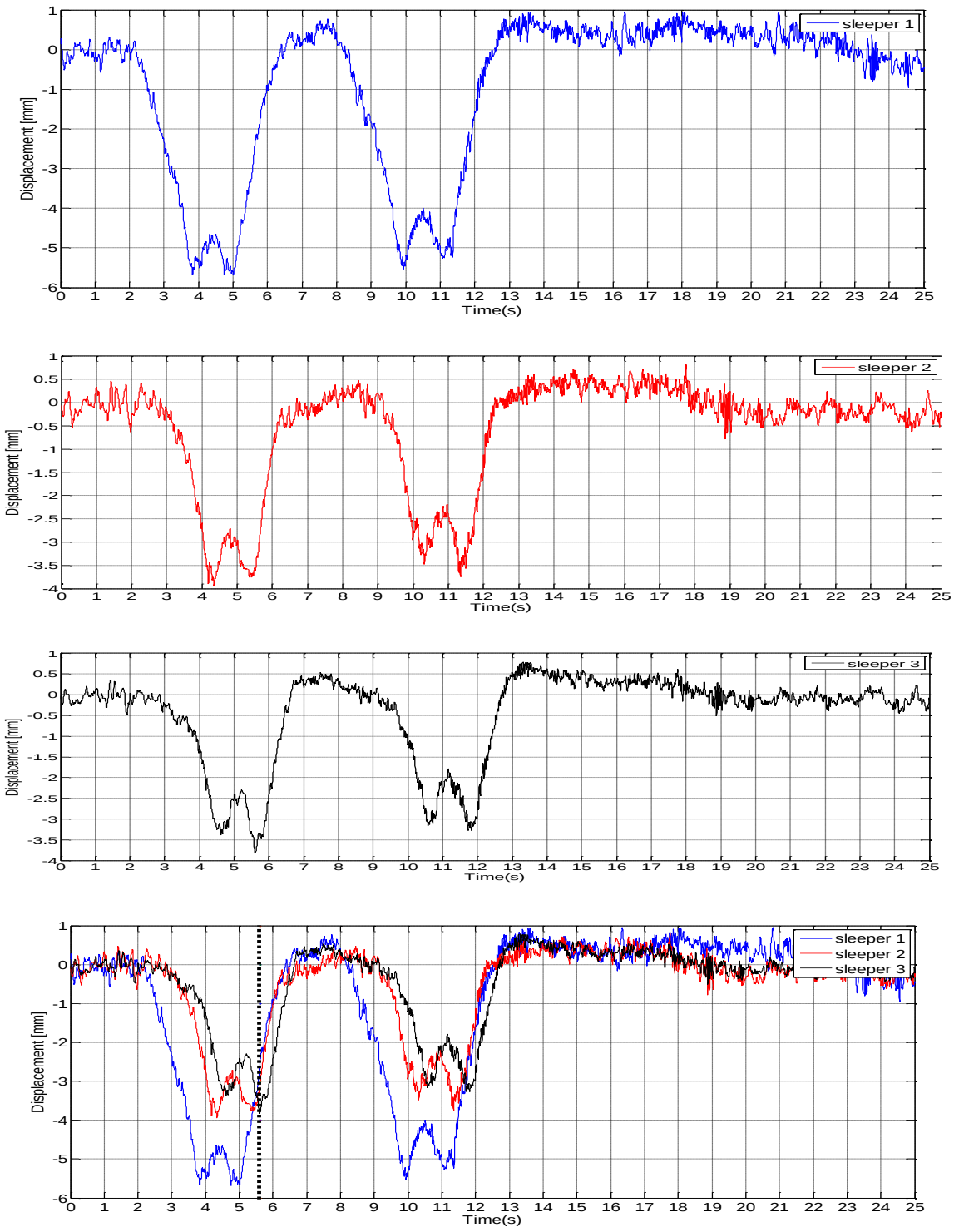

Figure 6-60: Example of data sets during train passage (a) sleeper 1 (b) sleeper 2 (c) sleeper 3 (d) Combination of the movement of three sleepers at t=5.6s

At 5.6 s, the first axle passed over sleeper 3 and the magnitude of displacement on the sleepers was 2.6 mm, 3.2 mm and 3.8 mm, respectively, across sleepers 1, 2 and 3. The displacement of sleeper 1 is greater than that of the other two, so it is not easy to observe the time that the axle is loading sleepers 2 and 3 in the graph (Figure 6-60 (d)).

In order to plot a continuous deflection curve that indicates the actual sleeper response during the train's passage, the individual sets of data were combined and visualised with Matlab, as shown in Figure 6-61. The mean values of the magnitude of deflection and stiffness over the 18 sleepers are 3.32 mm and 13.02 kN/mm respectively (Table 6-16) and the optimised displacement should be controlled within the 10% of variation in stiffness, 3.7 mm (Section 2.1.3- optimal track stiffness). Figure 6-61 shows the magnitude of displacement and the resulting stiffness while the first axle passes over sleeper 1 and subsequent sleepers. In Figure 6-61, diagram (a) is at the top, (b) in the middle and (c) at the bottom.

The wheelset is located directly above a sleeper for each of three times: (a) the first axle is above sleeper 1, (b) the first axle is above sleeper 2 and (c) the first axle is above sleeper 3 The stiffness is calculated based on the value of the axle load and the maximum displacement of each sleeper. The magnitude of displacement at sleeper 1 (Figure 6-61 (a)) is 5.75 mm for the downward movement and 0.8 mm for the upward movement and the resultant stiffness is 6.63 kN/mm. It is clear that the magnitude of sleeper deflection at sleeper 1 is outside the range on the graph. In addition, the slope of the deflection curve at sleeper 1 is very sharp, compared to Figure 6-61 (b) and Figure 6-61 (c), since the magnitude of displacement is greater than that of the other two sleepers.

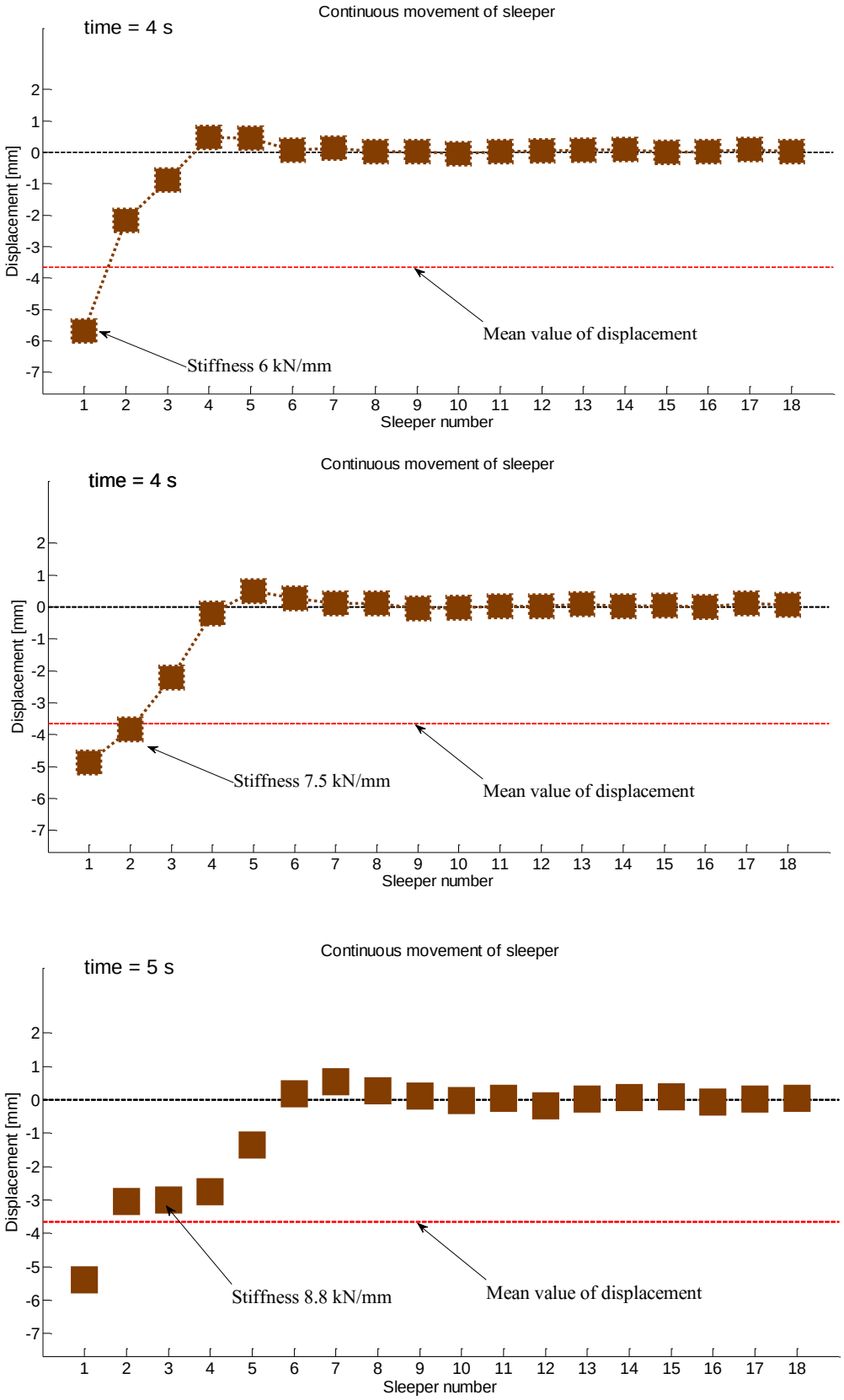

Figure 6-61: Visualised sleeper deflection curve

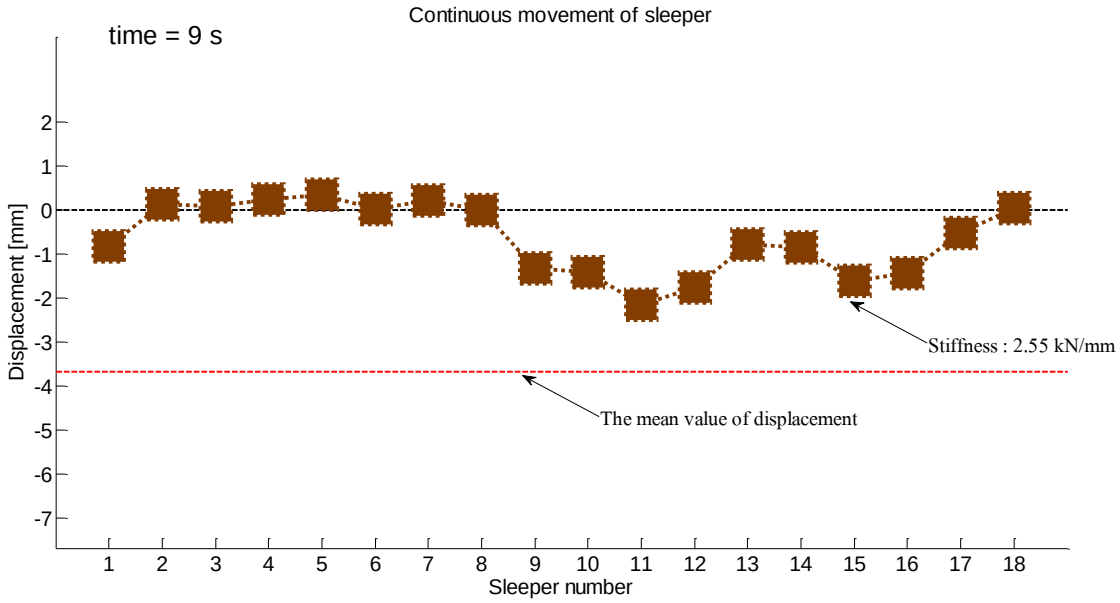

Figure 6-62: Section of track where the magnitudes of displacement are smaller while the first axle is on sleeper 15 and the second axle is over sleeper 11

The graph in Figure 6-62 indicates that the magnitudes displacements of sleepers 11 to 15 are smaller and the slope near sleeper 15 is much shallower than the slope at sleeper 1, shown in Figure 6-61 (a).

6.6 Discussion of Results and Further Analysis

The results of the continuous sleeper deflection measurement test over multiple sleepers demonstrate the benefit of the laser based measurement system in terms of its greater productivity, as it can measure up to 18 sleepers at the same time, with reasonable accuracy (0.1 mm). Measurements can be carried out while the track remains live, with no requirement for traffic closure. In addition, it can be used as an initial assessment tool for the subgrade condition. In this section, the author will discuss the influence of variations in train speed, loads, subgrade condition and different types of structures on the magnitude of displacement and the resulting stiffness.

6.6.1 Results of Field Trials and Theoretical Approach to Variation of Parameters

The theoretical deflection curve over 18 sleepers was calculated using Zimmermann's method, as discussed in Section 6.2, and maximum deflection varied between 1 mm and 7 mm, when the modulus of the subgrade reaction, C (N/mm^3), was 0.02, 0.05, 0.1 and 0.2 N/mm^3. This provided the link between the deflection and subgrade condition. The resulting stiffness is in a range of 3.3 N/mm to 39 N/mm (Table 6-3). In order to display the

actual response of the track, the magnitude of sleeper displacement was used as the measure. The deflection curve shown in Figure 6-63 is the comparison between the calculated magnitude of displacement and the actual response of the sleepers. Here, the magnitude of deflection of each sleeper is plotted with the wheelsets (loads) located directly above sleepers 1 (4th axle), 4 (3rd axle) and 17 (2nd axle). It indicates that C_1 under sleeper 1 is close to 0.02 N/mm^3 while C_4 and C_{17} under sleeper 4 and sleeper 17 are close to 0.05 N/mm^3, therefore, there is a sharp change in stiffness even over a very short section of track, for example, a significant difference is found in deflection between sleeper 1 and sleeper 4.

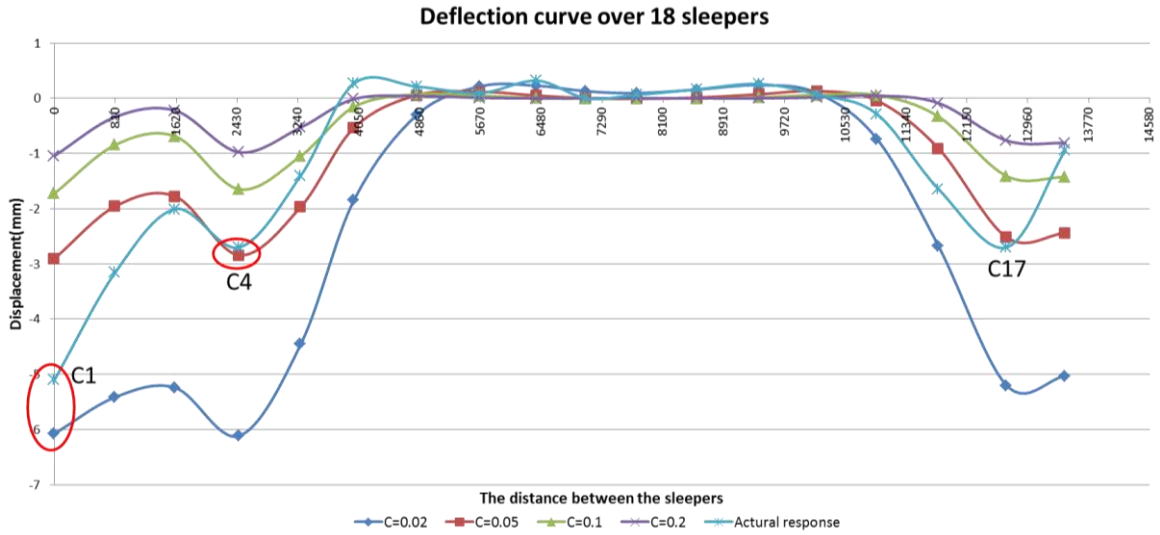

Figure 6-63: Comparison between the calculated deflection curves and the actual responses of the sleepers

The subgrade condition had been investigated using DCP tests, as described in Section 6.3 and provided approximate values of C (N/mm^3) for six locations (cribs between sleepers 13 to 19) by correlating between the DPI (mm/blow) and CBR (%) and between CBR (%) and the modulus of subgrade condition, Ks (N/mm^3). The Ks (N/mm^3) value from the DCP test can indicate the subgrade condition but it can also estimate the deflection curve by applying Zimmermann's method. The following graphs present the displacements of seven sleepers at speeds of 8, 16, 32 and 46 km while the first axle is passing over sleeper 1. While the real displacement data of sleeper 1 closely agrees with the theoretical deflection curve (Ks=0.052 N/mm^3 that resulted from the DCP test), in Figure 6-64 the displacement data of sleeper 2 closely agrees with the theoretical deflection curve (Ks=0.06 N/mm^3 that resulted from the DCP test) in Figure 6-65. In Figure 6-65, the comparison between the displacements of sleeper 2, sleeper 5 (red

circled) and the theoretical deflection curve (Ks=0.06 N/mm^3) indicates that the subgrade under sleeper 5 is softer than the subgrade under sleeper 2.

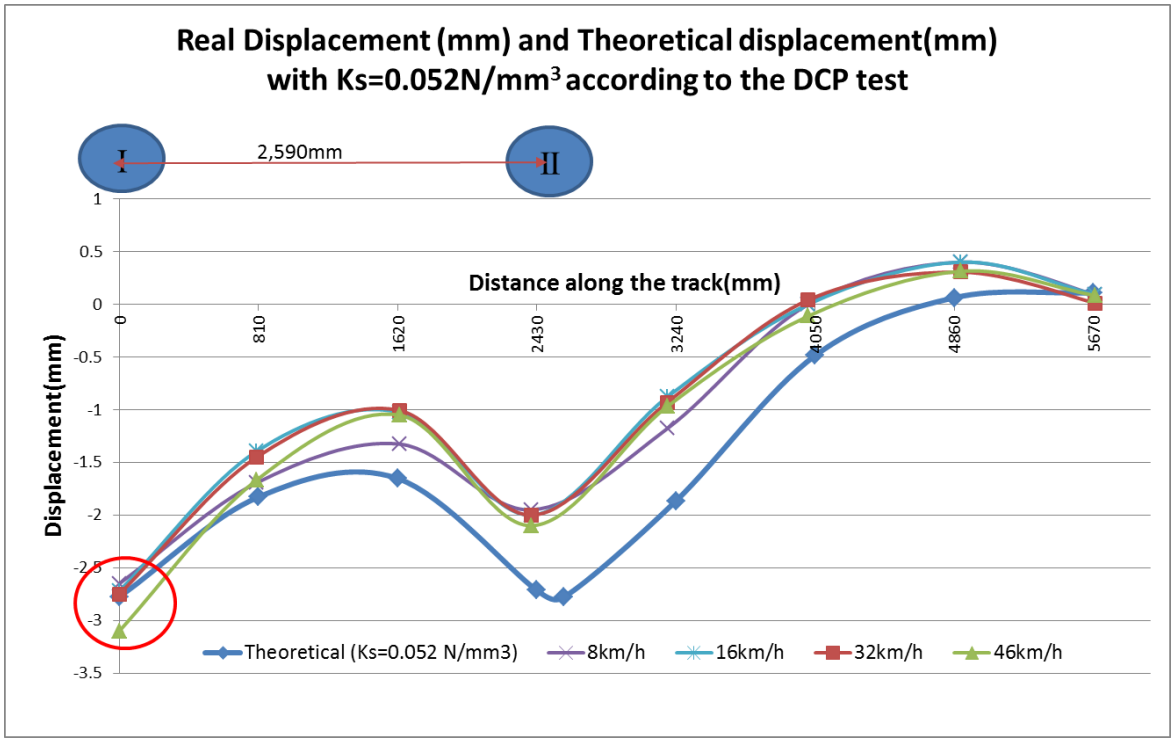

Figure 6-64: Actual response (mm) and theoretical deflection for sleeper 1 (Ks=0.052 N/mm^3)

In Figure 6-65, the theoretical deflection curve (Ks=0.06 N/mm^3) closely matches the displacement of sleeper 2 while the wheelset is running over sleeper 2 and sleeper 5. On the other hand, there is a 1 mm larger displacement under sleeper 5 compared to the theoretical deflection curve (Ks=0.06 N/mm^3).

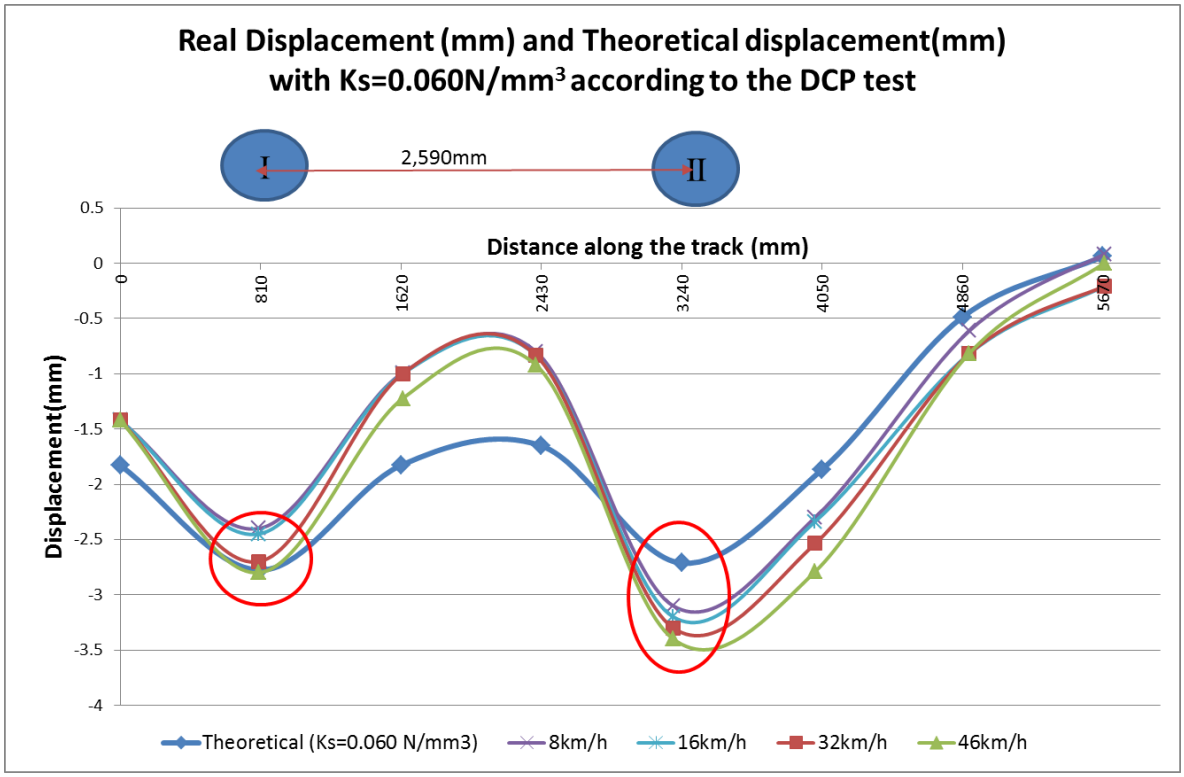

Figure 6-65: Actual response (mm) and theoretical deflection for sleeper 2 (Ks=0.06 N/mm³)

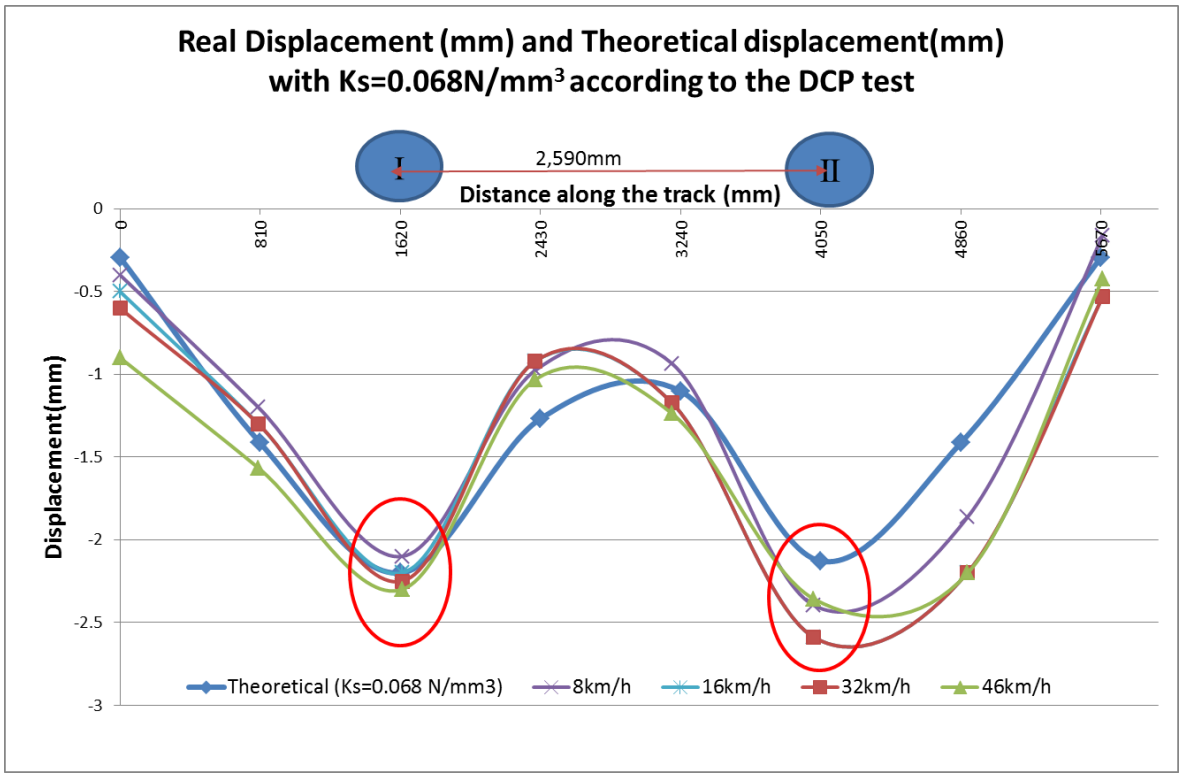

Figure 6-66: Actual response (mm) and theoretical deflection for sleeper 2 (Ks=0.072 N/mm³)

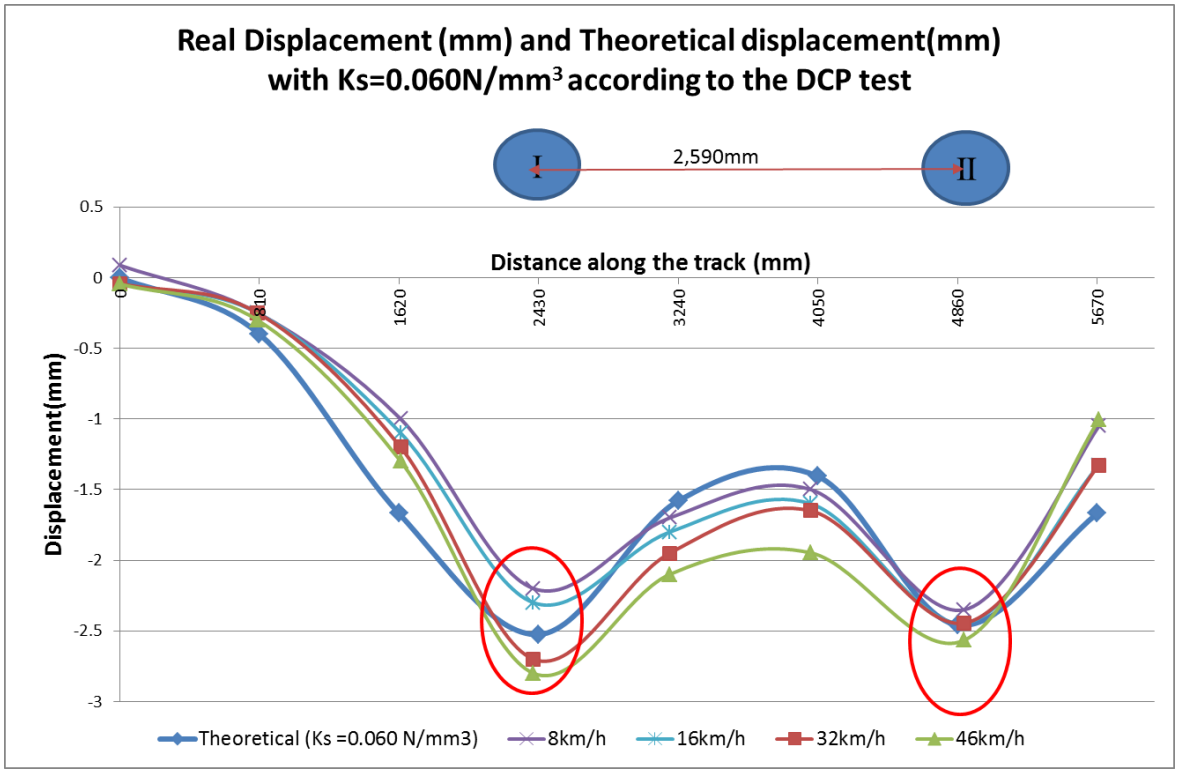

Figure 6-67: Actual response (mm) and theoretical deflection for sleeper 2 (Ks=0.060 N/mm^3)

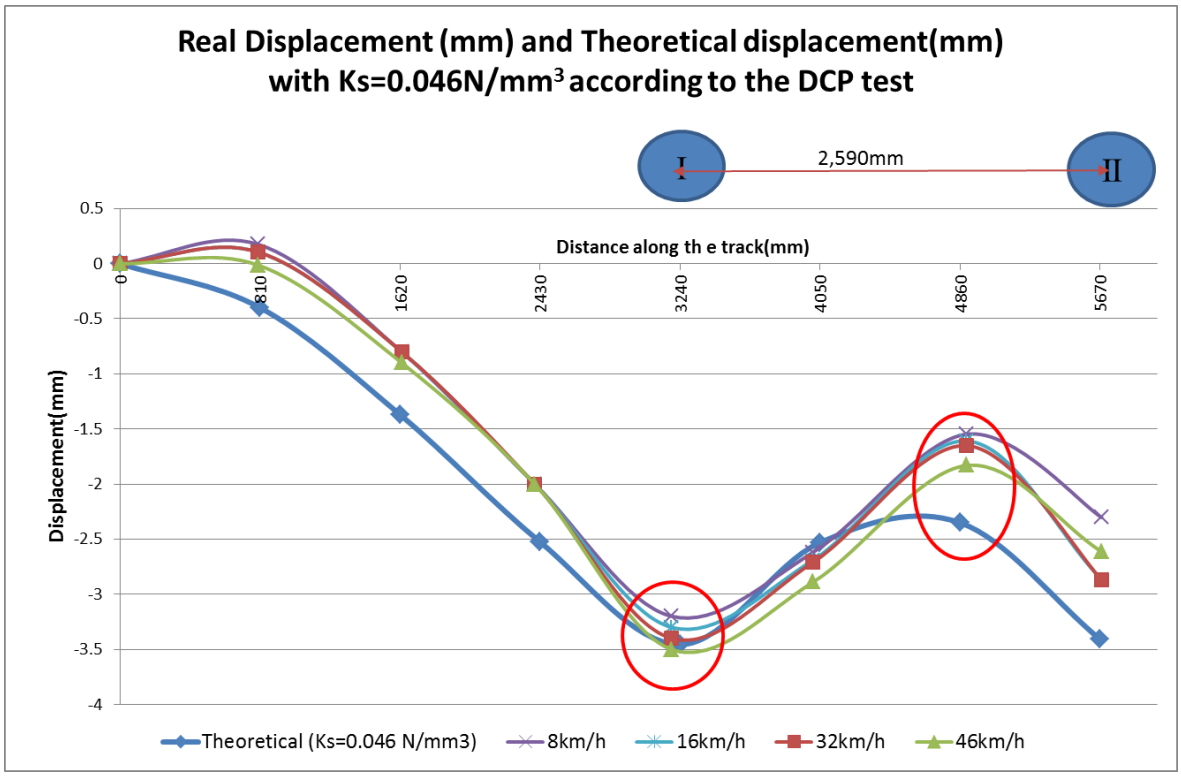

Figure 6-68 : Actual response (mm) and theoretical deflection for sleeper 2 (Ks=0.046 N/mm^3)

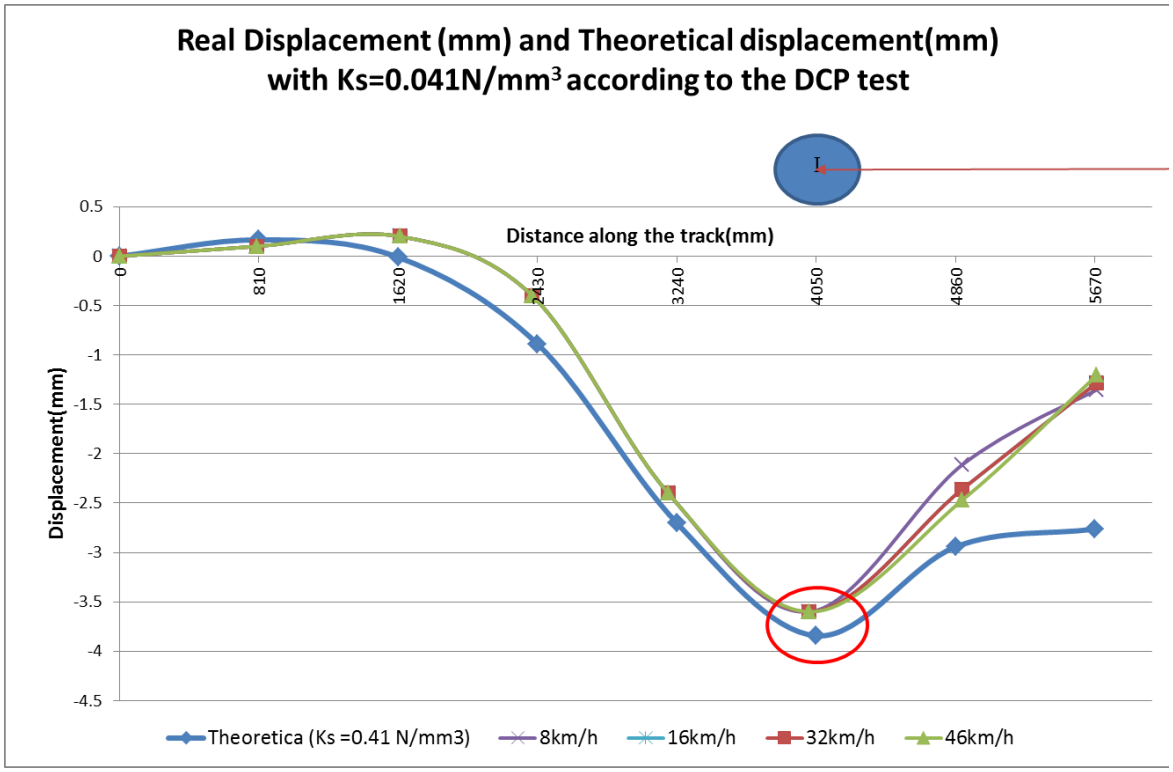

Figure 6-69: Actual response (mm) and theoretical deflection for sleeper 2 (Ks=0.041 N/mm^3)

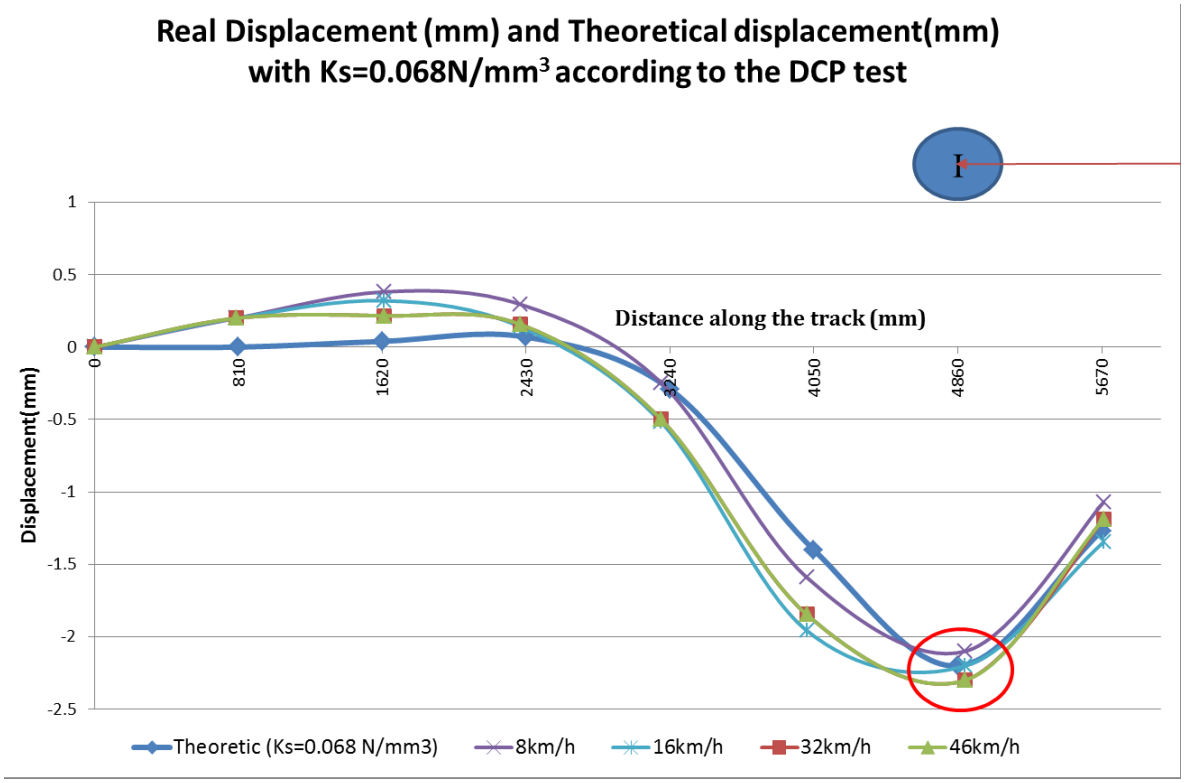

Figure 6-70: Actual response (mm) and theoretical deflection for sleeper 2 (Ks=0.068 N/mm^3)

In equation (7) in Section 2.1.1, that is $W_{max}=\frac{Q}{2CbL}$, the values Q, b and L are known and W_{max} is obtained from the laser measurement system. Thus, the estimated value of C can be established with equation (7). The maximum displacement data over 18 sleepers and the estimated subgrade condition have been plotted in Figure 6-71. The average value of the real displacement data at different speeds (Figure 6-64~Figure 6-70) is applied to Zimmermann's method (equation 7) and, therefore, the subgrade condition could be established across 18 sleepers, as shown in Figure 6-71. The variation in different subgrade conditions between 0.018 and 0.072 N/mm^3 results in the variation in the maximum displacement over the 18 sleepers. The range of the maximum displacement and resultant stiffness is between 2.21 mm and 6.63 mm, and 6 kN/mm and 18 kN/mm respectively.

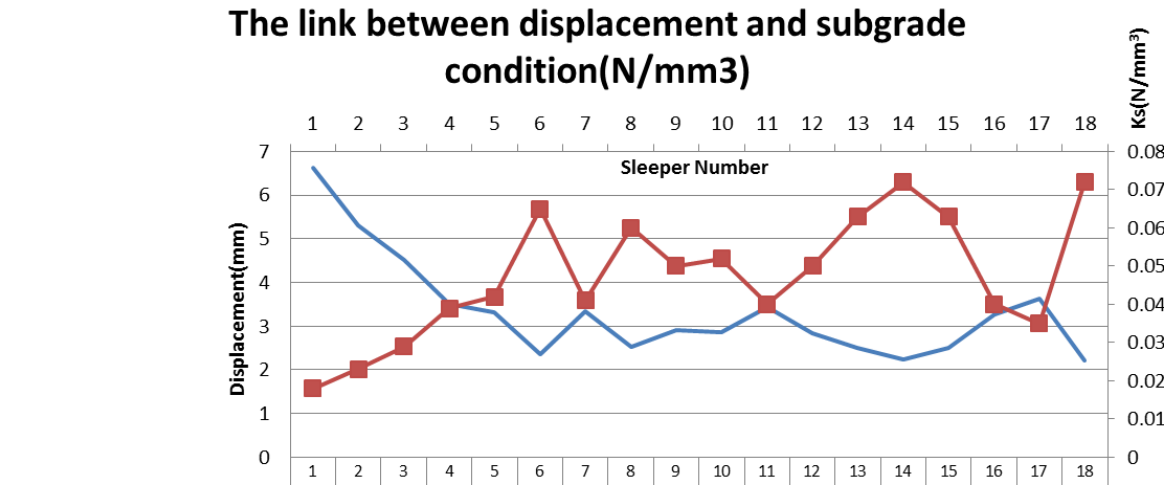

Figure 6-71: Relationship between the data for displacement and subgrade condition

The DCP test had been carried out in order to investigate the subgrade condition but it was also conducted to find the link between the displacement data and subgrade condition. In order to validate the estimated subgrade condition, the values of Ks (N/mm^3) under the seven sleepers, which are derived from the real displacement data, are compared to the result from the DCP test in Figure 6-72. Due to the labour intensive work involved and the available track access, the DCP test was only conducted at eight points, between the cribs. Then, the Ks value at each sleeper was calculated as the average of two points (Figure 6-11). The graph shows that there is a good agreement between the estimated Ks from Zimmermann's method and the Ks from the DCP test. Although these values are achieved by assuming DAF elements (Table 2-2), the pattern is very similar. At the test track in Long Marston, the track is not well

supported by the ballast, so only the subgrade condition could affect the magnitude of the sleeper displacement.

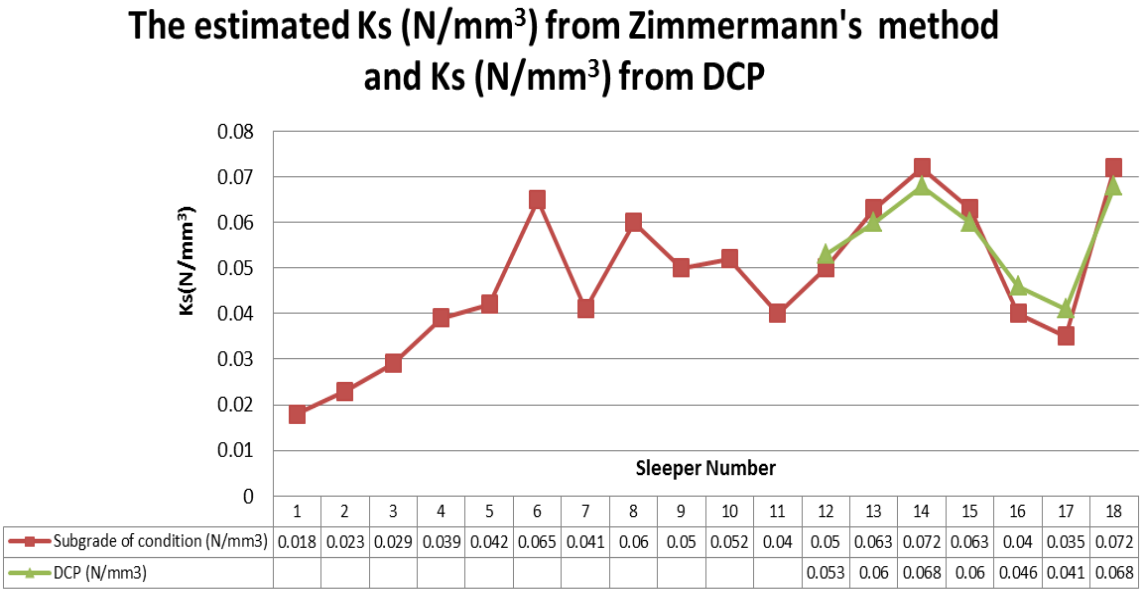

	1	2	3	4	5	6	7	8	9	10	11	12	13	14	15	16	17	18
Subgrade of condition (N/mm3)	0.018	0.023	0.029	0.039	0.042	0.065	0.041	0.06	0.05	0.052	0.04	0.05	0.063	0.072	0.063	0.04	0.035	0.072
DCP (N/mm3)												0.053	0.06	0.068	0.06	0.046	0.041	0.068

Figure 6-72: The estimated Ks (Zimmermann's theory) and Ks from DCP

In Section 1.1.2, it was found that track quality, which is defined as the track's ability to retain good geometry, is directly linked to the condition of subgrade. Figure 6-71 and Figure 6-72 show an agreement between the stiffness that resulted from the displacement and the modulus of the subgrade, which indicates the stiffness of the subgrade. Therefore, it indicates that the displacement data obtained from the laser measurement system over multiple sleepers can be used as an initial tool to assess the subgrade condition and can find the change in stiffness as shown in Figure 6-61 and Figure 6-62 in Section 6.5.5.

The theoretical displacement resulting from the variation in speed (60 km/h, 140 km/h and 200 km/h) in Figure 6-6 is clearly not found from the actual data, given that the test train speeds were 8 km/h, 16 km/h, 32 km/h and 46 km/h in Figure 6-50. However, the magnitude of displacement at 8 km/h and 46 km/h, where the permitted line speed was 50 km/h, shows a 0.5 mm difference under sleeper 1.

The effect of the variation in loads has been examined. Table 6-3 shows the theoretical displacement that resulted from the different axle loads (34.3 kN, 31.8 kN and 39.8 kN). While the subgrade condition is soft, heavier loads increase the displacement. For example, the variation in the loads results in 0.5-1.7 mm difference in displacement while the

subgrade condition, C, is between 0.02 and 0.2 N/mm^3. As shown in equation (1), stiffness results from the ratio between the load (N) and displacement (mm). In Figure 6-16, the actual response of the sleepers does not show the obvious effect of the load on displacement due to the fact that the displacement under the first wagon that is loaded half full with water is greater than the response when the power car passes over the sleeper. The load of the power car is heavier than the first wagon, but the displacement under the first wagon is greater than the displacement under the power car. This is because the fourth axle of the power car also has an effect on displacement under the first wagon.

In order to test the feasibility of using this novel laser based system to assess track performance at critical zones, measurements were taken over three different sections at the test track at Long Marston including a switch, a level crossing and plain line track in the initial set of tests. The stiffness of the track that is close to the level crossing was found to be 18 kN/mm, while the average stiffness at the switch and on plain line track is 9 kN/mm and 10 kN/mm respectively.

6.6.2 Effectiveness of the Laser Based Measurement System

There are different methods available to assess track quality and measure track stiffness, namely, by taking a measurement of vertical track displacement or vertical track velocity or running a specialised vehicle, such as the NMT or FWD. Track geometry measurement (e.g., using the NMT) provides an understanding of the functional condition of the track, however, the root causes of problems cannot be found by looking at track geometry data alone. The vertical data from the track geometry measurement vehicle during loaded or unloaded condition can provide an indication of voided sleepers or wet spots, which could possibly produce changes in track stiffness, however, the usefuleness of this information has not yet been demonstrated.

DCP is a relatively rapid in-situ measurement method to measure the strength of the trackbed layer at different depths. By measuring a penetration depth per blow, DCP provides the penetration index and this indicates soil density, moisture content and soil properties. Although DCP costs less than other disruptive methods, the procedure requires repeatedly dropping a hammer and extracting the DCP device by pumping the jack and is therefore quite labour intensive during measurement (Section 6.3).

While FWD systems are used extensively to investigate structural conditions for research purposes, for both railways and roads, they require a significant amount of track or road

occupancy due to their slow movement, which affects both train schedules and car users. A continuous deflection curve and change in stiffness curve (Figure 6-61 and Figure 6-62) cannot be achieved with the current FWD systems, since the geophone signals require further processing, especially at low speed.

The newly developed track stiffness measurement vehicle, a prototype development, enables monitoring at close to or actual line speed. However, each system has different pre-setup values and the operation speed is still limited, although it is higher than for FWD operation. Thus, finding a method of condition monitoring without traffic disturbance is significant for both railways and roads.

Therefore, this challenge required the development of an effective tool to measure changes in track stiffness over time, which is accurate and easy to use, without causing traffic disruption. The laser based measurement system was selected because of its effectiveness in terms of not absorbing track operational capacity and producing continuous deflection data. By producing continuous track deflection data over multiple sleepers it provided stiffness information that showed good agreement with the DCP result in Figure 6-71, thus indicating the subgrade condition. Therefore, it fulfils the aim of the research, which was stated as "to develop an innovative, productive and accurate means of measuring changes in track stiffness over time". As found from the comparative test between the geophone and laser based measurement systems in Section 6.5.3, the accuracy of the geophone is dependent on the dominant frequency during the passage of trains, which varies depending on the bogie spacing and train speed. The geophone data accuracy agrees with the laser measurement system to within 0.1 mm while the train speed is at 46 km/h, but the agreement is poor when the train speed is down to 8 km/h (Section 6.5.3).

From the concept of operation (Section 4.1.2), it was expected that the dynamic movement of each sleeper could be observed in real time with reasonable accuracy using a laser based sensor system. It was expected that the newly developed system could be applied to the critical zones where an initial assessment of change in track stiffness is required. It has been shown that the measurement system can provide a deflection curve by recording the deflection of each sleeper in real time, which can be saved to a computer in excel format.

Each time a train passes, the data can be collected continuously so that it enables sets of repetitive tests over the section of track, which is a strength of this measurement system. As the information obtained (Figure 6-61 and Figure 6-62) can be used find the change of

relative stiffness of each sleeper over time, especially where excessive changes in stiffness are expected, it can provide an estimate of the maintenance work required for the maintainers. After carrying out the maintenance work, the maintainer can check whether the maintenance or renewal was successful by re-measurement. The maximum length of observation with this system is 13 m and, therefore, this measurement system is able to monitor transition zones with a length of 4 m to 10 m (Kennedy et al., 2012) as demonstrated by producing the continuous deflection curve for the whole of the transition.

However, there are two major points for further work in this research. A 0.1 mm level of accuracy has only been achieved when the length of the monitored track is below 10 m. The influence of the vibration of the laser source can be removed by applying the FFT analysis and a versine concept. However, further work is required to improve the accuracy of the data. Comparing the DCP data and the calculated K_s value (N/mm^3) that results from the real displacement data, it shows that the variation in displacement over multiple sleepers is an indicated for the variation in subgrade condition. The stiffness of the ground under each sleeper is calculated based on the values of the maximum displacement of each sleeper and any abrupt change in stiffness is visible in the deflection curve. However, it would be useful to define a threshold value that can be applied to inform the maintainers automatically, if the limit is exceeded.

The test was conducted with trains running at a maximum speed of 11 m/s due to condition related speed restrictions at Long Marston. Under a real operation environment, the abrupt change in stiffness could have a greater effect on the performance of the track while running trains at high speed, so a high speed track might require more frequent monitoring. Therefore, further tests should be conducted on a high speed line in order to ascertain the system performance. As this system has been developed as a portable device, which is installed on a track when required, rather than permanent installation, the issue of track access should be considered further.

Overall, this approach overcomes some of the drawbacks of the measurement systems that are currently available, including the speed restrictions imposed by the trackside sensors, such as geophones, and considering productivity and price as below:

1. A laser based system can measure the displacement of multiple sleepers continuously and provides the continuous deflection curve that indicates the relative stiffness changes under each sleeper along a track;

2. The measurement system does not have an operation constraint for train running speed. Therefore, this system can measure the deflection of consecutive sleepers while trains run at low speed, capturing low and high frequency data. However, as discussed, it requires further testing to ensure the accuracy and reliability of the measurement system at high speed;
3. The cost is reasonable in terms of initial price for manufacture and labour cost during testing as compared in Table 6-17.

Table 6-17: Cost comparison between two sensors for the measurement of 18 nodes

Types		Unit cost	Number of nodes	Total Cost
Geophones		£383	18	**£6,894**
Laser Measurement System	PSD	£40	18	£720
	Node box	£80	18	£1,440
	All Components	£132	18	£2,376
	PCB	£20	18	£360
	Total	£272	18	**£4,896**

6.7 Summary for Chapter 6

In this chapter, the laser-based measurement system developed in Chapter 4 was further upgraded in order to build a more robust system. It was tested with up to 18 sensor nodes at the test track at Long Marston. Assessing the effectiveness of the laser based system in varying train speed conditions around 50 km/h or under has been proved by taking measurements at speeds as low as 8 km/h.

From the field trial that has been carried out, it is possible to conclude that a laser based measurement system can be effective when trains run over critical areas at low speed, being less than 50 km/h. One of the major advantages of this laser based measurement system is that the reference line is from the laser source, so that data showing the relative deflection of individual sleepers can be obtained.

When the train speed exceeds 50 km/h, which means that a linear output is achievable, measurement with the geophones can be more effective in places where the height of the sleepers is equal or where there is insufficient space to locate the laser source. In this case, an integrated system which combines the laser sensors with geophones could be a solution. This reduces the wire which is needed to connect individual geophones and the data-logger system, which is one of the drawbacks of using geophones for current research work.

It has been shown that the movement of 18 sensor nodes on consecutive sleepers can be observed continuously during a train passage. After the data processing, a video was made to visualise track performance, which provides an indication of the level of subgrade condition in this section.

However, it is expected that obtaining data from the laser measurement system with the current design will be limited with respect to its application at critical zones, since the laser source must be operated with line of sight propagation, due to the character of the measurement system.

The comparison test in the laboratory, which was conducted without vibration of the source, showed that there is a good agreement between the two sensors. However, the data from the field trial showed that the agreement between the two sensors for maximum deflection at a speed of 46 km/h was 0.1 - 0.5 mm. The error, which may have occurred due to ground borne vibration during train passages, has not been taken into account in this trial. Clearly, further research will be needed to find a method to reduce or remove the effects of vibration of the tripod so that it can take measurements to check the effectiveness of a laser-based system application for measurement during very high speed running.

7 Conclusions and Future Work

In this chapter, the main achievements are presented alongside the key findings. From that, the research conclusions are drawn. Then, the work done through the course of the research is reviewed to check whether it fulfils the research objective that was stated in Section 1.2. Lastly, the limitations of the work will be presented with the details of suggested future work and the recommendations for a practical system that can be implemented in mainline applications for commercialised stage implementation.

7.1 Main Achievements

In order to fill the gap in the existing systems for measuring track quality and to provide a rapid tool to assess track stiffness under multiple sleepers, the author studied the shortcomings of the existing systems and developed an advanced deflection measurement system that has been substantially improved when compared to an earlier laser based prototype system. The new system helps to assess the condition of the track substructure rapidly by measuring the deflection of sleepers.

7.1.1 Review of Shortcoming of Existing Track Stiffness Measurement System

In Chapter 3 the author reviewed the different existing methods to assess track quality by measuring track geometry, track deflection and track stiffness. The shortcomings and strength of each technique were discussed. In particular, the operational cost and the limited availability of track access for using FWDs and the shortcomings of current trackside sensors, such as accuracy and productivity, were found to be drawbacks. In order to overcome these challenges, the author decided to identify a rapid and highly reproducible method to obtain data to measure track deflection to address the urgent need to assess the subgrade condition in critical zones.

7.1.2 Innovative Approach to Developing a Multiple Sleeper Deflection Measurement system

Based on the existing system that showed the feasibility of measuring the deflection of multiple sleepers simultaneously, the author has developed a laser based system that includes substantial upgrades of the hardware and software (Section 4.2.1) in order to eliminate the shortcomings of the earlier prototype and to enhance its capability. In order to solve the challenges of using the previous system, such as the manual calibration and laser positioning work, a number of innovative upgrades have been introduced. The data from the multiple sleepers is automatically calibrated by a remote control function by

implementing a binary search based algorithm for the auto-calibration of the sensors. In the case of the previous system, the sensors had to be calibrated manually inside the sensor box that was mounted on the sleepers adjacent to the railway track. Since the new measurement system uses an infrared laser, while the previous system used a red laser, a new laser detection algorithm was implemented, as discussed in Section 4.2.2.3 and illustrated in Figure 4-20).

These upgrades are a significant achievement in terms of safety of practical track-side use and from the perspective of the system being user-friendly. By conducting comparative tests using three different methods, as discussed in Section 5.2 and Section 5.3 (geophone, commercial displacement sensor and Micro- Epsilon laser), the author verified the system against the functional requirements (Section 4.1.4) and found that the accuracy of the upgraded measurement system enables the error to be managed within 0.1 mm.

The following table shows how the new measurement system has been upgraded from the existing technology.

Table 7-1: Comparison between the pre-existing and advanced measurement system

	The prototype from 2007	The measurement system (2015)
General Installation	Three sensor boxes are placed over the sleeper and the displacement in (mm) of individual sleepers can be observed. A 24 mm long PSD sensor was used so it is limited to observing displacement up to 20 mm.	Multiple sensor boxes (up to 18) are installed on the sleepers and the deflection curve is observed and visualised continuously in real time. An adjustable sensor box was designed to align the sensor nodes; one of the ideas which could be developed to address this issue is to adopt a height adjustable sensor node similar to the first prototype and with an automatic function
Accuracy	It was not specified.	The accuracy was tested and managed within 0.1 mm.
Data communication	The cables between the sensor nodes on the sleepers and a computer have to be individually connected to three sensor nodes; therefore the cables require a space along the track.	A Controller Area Network (CAN) has been introduced. The sensor nodes and laptop are connected to a CAN bus so that multiple sensors communicate with the CAN. It can be operated at a distance, using a remote control with a high level of security.
Calibration	Manual calibration work has to be done inside the sensor box to adjust the analogue potentiometer and working on individual calibration near the trackside is not safe and takes more time.	An auto-calibration function with remote control is newly implemented using a binary search algorithm via a CAN bus.
Laser setting procedure	Laser setting procedure is not notified due to the small number of sensors and using red laser.	It has been found that the laser setting procedure is difficult due to the requirement for manual alignment of the laser source to the multiple sleepers, therefore a laser detection algorithm is being implemented.

7.1.3 Rapid Assessment of Track Subgrade Condition

From the results of the two trial studies conducted (Section 6.4 and Section 6.5), the author has demonstrated that there is a difference between the calculated deflection (Section 6.2) using the BOEF theory and the actual deflection. On the basis of the management requirement for monitoring the track subgrade, so as to ensure that the variations in the stiffness of the subgrade are less than 10% of the mean value of track stiffness (See Section 2.1.3), the author found the variations in the stiffness of the subgrade in some areas at Long Marston had not been managed well. For example, the maximum deflection of sleeper 3 has a difference of up to 4 mm compared to the adjacent sleeper, therefore the stiffness of the subgrade under this sleeper is 20% different compared to the mean value. The integration test between the deflection measurement test (Section 6.5) and the DCP test result (Section 6.3) demonstrated that there is a relationship between the results from the continuous deflection measurement, across multiple sleepers, and the strength of subgrade.

In Section 6.5.5, the deflection data was visualised to show the deflection curve over 18 sleepers and this type of visualisation ensures that the information about a change in the track stiffness over the short distance of the critical zones area can be used to assess the subgrade condition more rapidly if there is an area where it needs to be assessed promptly, a limitation to using other methods. In the visualised deflection curve (Section 6.5.5), the sharper angle indicates that the subgrade condition is poor and vice versa.

7.2 Agreement with Research Objective and System Requirements

In order to ensure that this research work has achieved what was set out at the beginning of the research, the objective of the research and the corresponding works have been reviewed as shown below:

7.2.1 Review the Concept of Track Stiffness, Transition Zones and the Relevant Theory

Chapter 2 provided a review of track stiffness being used in the railway industry. In order to estimate the theoretical deflection curve (Chapter 6), the BOEF theory and Zimmermann's calculation method were reviewed in Chapter 2. The research trend of track stiffness measurement at transition zones and the mechanism of a transition zone were also studied in order to support the field test in Chapter 6. Overall, the civil engineering background of the track structure and the performance of a transition zone have been reviewed.

7.2.2 Investigate and Evaluate the Current Techniques of Railway Trackbed Measurement Systems to Find the Strengths and Weaknesses

Chapter 3 provided a review of relevant current practices and techniques based on recent literature relating to the measurement of track geometry, track stiffness, track displacement and pavement stiffness. After comparing and discussing various methodologies to measure track quality, it concluded the establishment of the system requirements to build a trackside continuous measurement system.

7.2.3 Through the Analysis of the Necessary Functionalities and Characteristics Develop a Functional Specification of the Measurement Device

The whole development process of a laser-based deflection measurement system is described in Chapter 4. From the operation concept, that is multiple sensor nodes were built to measure the vertical deflection of multiple sleepers, system engineering has been adopted to develop the system.

7.2.4 Design and Construct a Measurement System in accordance with the Specification

The necessary functionalities have been developed from the system requirement and it developed further down to the design of the physical components and to validation of the measurement system. Before the validation of the development of the system, a laboratory based test was conducted to check if it fulfils the specification of the system. The laser-based system was tested by placing different depths of plates under the sensor node and taking measurements. In addition, it was tested comparatively with geophones and a commercial laser displacement sensor to find the level of accuracy in Chapter 5.

In order to ensure the stated requirements were reflected on the measurement system, individual requirements are reviewed with corresponding works in Table 7-2.

Table 7-2: Requirements validation

ID	Requirements Review
SR1	The measurement system must be a laser-based method: < In Chapter 4, the laser measurement system was developed with a 10 mW infrared and 37 mm PSD sensor used for the system.
SR2	The measurement system shall monitor the condition of track continuously while a train passes the transition zones: < By development of a robust firmware system for stability during the measurement and a stabilised CAN network, enabling continuous measurement.

ID	Requirements Review
SR3	The system shall quantify the amount of track displacement so that it gives specific evidence to help maintenance decisions: < In Section 6.3.5, the continuous movement of sleepers can be observed through the data visualisation**.**
SR4	The system shall be practically tested in both adjacent railway track and in the lab: < The robustness of the system has been considered, especially water proofing of the sensor node box and cable connections.
SR5	The laser based system should be comparatively tested with one of the existing systems: < The laser based system (Section 5.2.2) and the commercialised laser sensor (Section 5.2.3) have been comparatively tested with the geophone in the lab. In the field trial, one of sleepers was measured with a video recording system (Section 6.2) and 18 sleeper were observed with the geophone together.
SR6	The power for the system shall be sufficient for it to be operated either for the laboratory based or field based test: < For the first trial, the generator was used and a 15 Ah battery capacity was sufficient to supply the power for a one day trial (1.5A for 10 hours).
SR7	Data shall be obtained during measurement and easily read in the right format: < Displacement data is stored in the PC with an excel format.
SR8	The required level of accuracy of measurement shall be managed within the error of 0.1 mm. The level of accuracy shall be demonstrated considering two elements of accuracy that are repeatability and reproducibility. < The 0.1mm accuracy was achieved in the lab test discussed in Chapter 5. The accuracy was lower than required in the field trial, so that further work is required, which will be discussed in Section 7.3. In order to prove repeatability and reproducibility of the measurement system, the lab based dynamic load frame system would be better to use. Reproducibility can be ensured by a number of users. However, it has not been conducted in this research due to time limitations. Repeatability has been tested by a number of tests at the same speed. However, it was not easy to achieve the same operating train speed repetitively.
SR9	The system shall not cause any harm or pose any risk to users. (Since it is a laser based system, which was concluded in Chapter 3, the power level of the laser will be considered with regard to health and safety matters): < In Section 4.3.2, the power intensity of the laser was tested and the laser was classified as Class One, which does not require safety countermeasures to protect users.
SR10	The system shall not disturb train operations, e.g., it shall not require track occupancy during measurement: < The dimensions of the system give clearance to the track, so that the train can run on the track and the measurement system can perform under normal traffic conditions.
SR11	The system should be remote controlled: < The functions of power on and off and calibration are controlled by the C# software, implemented in Section 4.2.2.
SR12	The measurement system should be easy and simple to install and remove so that the process takes less than two hours: < Although the alignment of laser beam takes some time, the total time for setting up takes less than one and a half hours.
SR13	The measurement system should be as light as possible to carry: < The whole system can be carried with two crafts.
SR14	The market price must be reasonably affordable and competitive compared to other measurement systems. It should be priced at a similar level as current practices, or lower. < The prices between the two sensor systems are similar, relatively £6,894 (Geophone) and £4,896 (Laser measurement system), based on an 18 sleeper measurement system. < The labour cost for manufacturing the laser sensor node and the cost of the data logger for the

ID	Requirements Review
	geophone is excluded. Therefore, the laser based system is affordable on the basis of the measurement of 18 sleepers at once.

7.2.5 Validate the Measurement System by Carrying out Field Tests

The measurement system was implemented along 18 consecutive sleepers and measurements were taken during train passages at the test track facility at Long Marston. A video recording system and geophones were used to validate the data from the laser measurement system. In addition, the theoretical calculations and data from the DCPT have been analysed to validate the measurement system.

7.2.6 Analyse the Effectiveness of the Measurement System and Draw Conclusions

The effectiveness of the system has been discussed in Section 6.6.2. In addition, the limits of the measurement system and future work to overcome the constraints of the system will be discussed in Section 7.4.

7.3 Conclusions

The main findings of the research are concluded below.

7.3.1 Strength of Laser Based Sleeper Deflection Measurement System

The quality of a section of track has been defined as its ability to retain good geometry and it is closely linked to the design and condition of the trackbed and the foundation. In Britain, track geometry data is being collected to give an indication of track quality on a regular basis from periodic measurement systems such as NMT. There is the potential to detect a voided sleeper by using the load and unloaded data but this has not yet been proven to be a reliable approach. Stiffness is an important parameter that indicates the condition of the substructure. The FWD is a standard method to measure track stiffness but the substantial cost of travelling and operation is one of the main drawbacks which prevents this system from being used as a means of rapid measurement. Since other measurement systems also have their own drawbacks, in order to fill this gap, the laser based measurement system has been significantly upgraded from the earlier prototype. The major findings related to the advanced laser-based measurement system are concluded as below.

(1) The feasibility of measuring the behaviour of multiple sleepers was demonstrated with the earlier system in a test that measured three sleepers at East Leake in 2008.

However, limitations and shortcomings of the initial laser prototype have been found in this research and have been.addressed in the design of the new system;

(2) In order to deal with the weaknesses of the earlier laser sensor prototype, significant upgrades have been required, including the implementation of an auto-calibration function with remote control and an easier laser detection function which enables sleeper deflection monitoring in a user-friendly and safe manner. The improvements have largely overcome the challenges of the earlier prototype;
(3) Based on the measuring principle of using a line laser, displacement data can be extracted from the data that has been affected by the vibration of the laser source. The real sleeper movement has been extracted by using the data from the different sleeper sensors since it is produced by the vibration of the laser source;
(4) The data from the laser measurement system has been shown to agree with the video recording system and geophone to within 0.1 mm over a 10 m distance from the laser source, which would mean that the accuracy can be ensured to measure 16 sleepers where the sleeper space is 600 mm;
(5) Due to the nature of the geophone sensor, it loses lower frequency data and it requires further data processing, whereas the laser is capable of monitoring lower frequencies. In order to overcome the limitations of the geophone and obtain reliable displacement data, the laser measurement system was upgraded to measure multiple sleepers at once in this research.

7.3.2 Measurement of Change in Displacement and Stiffness

Variation in track stiffness over the transition zone should be managed to improve the performance of railway track in terms of passenger comfort and safe and economic track-train interaction. In order to monitor the change in stiffness, a measurement system has been developed using an infrared laser that can show the relative stiffness of up to 18 sleepers. Two field trials were conducted on the test track at Long Marston. The major conclusions of the field trials are summarised as follows.

(1) In an area which requires a rapid assessment of the stiffness change over a limited distance, the laser based measurement system is able to provide information on the relative stiffness by measuring the continuous deflection curve during train passage. The continuous deflection curve provides an indication of the change in stiffness;
(2) The variation in operational conditions such as maximum train speed, mass, different types of structure and the effect of stiffness have been examined, but the maximum train speed in the trial was low at 40 km/h, so the variation in displacement due to the effect of train speed could not be demonstrated.
(3) The variation in stiffness change was found to be different from the theoretical deflection and stiffness data due to the subgrade condition;
(4) In order to prove the effectiveness of the system at various speeds, a further test up to the speed of 300 km/h is required.

7.3.3 Assessment of the Substructure Condition

A DCP test has been completed over 7 sections in order to investigate the subgrade condition and to find the Ks value of Zimmerman's theory. Agreement has been observed between the subgrade condition result from the DCP test and the calculated K value from the real displacement measurement. Therefore, the case study also demonstrated the links between the stiffness and strength of track subgrade by looking at the deflection data and DCP test data. The major conclusions are as follows.

(1) The result of the comparative analysis between the deflection measurement system using the laser based technique and the DCP method indicates that the there is a clear relationship between the stiffness and the strength of the substructure;
(2) The DCP test is known as a tool to assess the substructure condition involving relatively little labour intensive work. However, it requires track occupancy during the measurement and extracting the DCP by pumping the jack takes nearly 10 minutes for each measurement point.
(3) The case study also demonstrated that measurement of the stiffness under multiple sleepers contributes more to a rapid method for an initial assessment of substructure condition than a sleeper by sleeper assessment.

7.4 Limitations and Future Work

The measurement system has been designed to be able to assess changes in stiffness by measuring the sleeper displacement with a high level of accuracy rapidly. Along the track, an abrupt change in displacement from one sleeper to the adjacent sleeper can be found with the laser-based measurement system for and initial assessment in a straightforward manner. Although there is agreement between the actual response of the sleeper and data from the DCP, it would be useful to collect additionally the data from the standardised methods such as FWD and NMT. The location of the test facility at Long Marston and the operational cost did not allow data collection with these methods. In addition, it is not sufficient to look into the fundamental reason for an abrupt change in stiffness, so a diagnostic function with a high level of accuracy will be required when the collected data is to be used for maintenance planning. Therefore, further detailed investigation is required in order to find the root cause of problems such as unsupported and hanging sleepers, e.g., further measurement by GPR or ABS. In addition, only vertical displacement has been measured in this research, and taking a measurement of dynamic load is outside the scope of this work, therefore, there is further work required in order to get an accurate value for track stiffness.

The site used for this study was on a test track, which was safe for the placement of the measurement system. It has been demonstrated in the thesis that a laser based system has the potential to be applied to monitor critical zones, including transition zones. However, the current design is limited in that it cannot be installed in all possible critical zones (e.g., on a steep embankment or shallow tunnel) on a railway. In order to take a measurement with this laser based system in all different types of critical zones, which have been operating with regular train services, the design for the sensor node box and cable connection must be considered for easier and simpler installation so that it can be practically applied for monitoring all critical zones in mainlines. In addition, further field tests are required to see the performance of the laser measurement system at higher train speeds. The key improvements to ensure commercial operation would be wireless operation, compact size, battery life and reducing the installation cost, including labour intensity and possession requirements for installation. In particular, it was a time consuming process to align the sensor nodes; one of the ideas which could be developed to tackle this issue is to adopt a height adjustable sensor node similar to the first prototype and with an automatic function.

One more issue is the level of accuracy, see Table 4-1, SR 8. The aim was to develop a measurement system which has a 0.1 mm level of accuracy. This was achieved when the distance between the sensor nodes and laser source was 8 to 10 m, so that the intensity of the laser source is sufficient (see Section 4.3.2 and Section 6.5.3.1). However, the level of accuracy is decreased due to the fact that the laser beam widens when the distance is greater. A way of improving the system accuracy shall be considered for further applications. One method is to use multiple laser sources, whereby each laser source produces a different frequency modulation to the laser sensor nodes, so that the individual sensor node can receive the nearest laser source using a bandpass filter, which is instrumented in the sensor nodes, overlooking the laser source which has less strength. This approach will be useful to measure the displacement of sleepers at areas where there are different heights of sleepers (where the alignment of sleepers is too different to use one laser source) or curves on a track, as described in Figure 7-1.

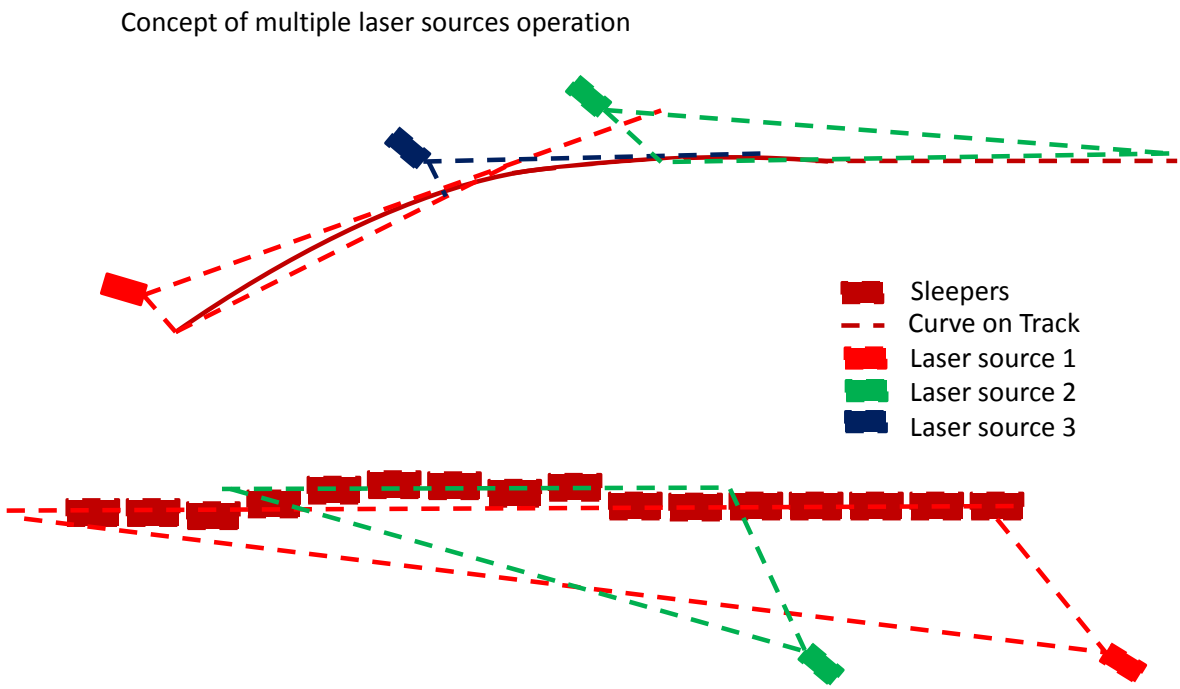

Figure 7-1: Concept of multiple laser source operation (plan view and side elevation)

Errors also arose due to the motion of the laser source (See Section 6.5.4), which distorted the measurement data and caused inaccuracy of the measurement system. A better understanding of the vibration of the laser beam may allow the system performance to be improved. If the motion of the laser source could be estimated, it could be extracted from the measured data, which would enable more accurate data to be presented. A sensor in the laser box could be used to monitor the motion of the laser source and compensate the data to improve the accuracy of the system.

The state estimation method, using a Kalman filter (KF), which has been widely applied as an algorithm for data processing of object tracking (Kleeman, 1995), (Li *et al*., 2007), (Weston *et al*., 2007b) can estimate the laser beam position by its rocking and rolling motion. The process of the KF takes two steps repetitively; prediction and measurement. In the first step, the current state of the laser beam position will be predicted and the measurement data will be collected and then new position will updated compared to the prediction data in the second step.

The input of the system shall be the noisy measurement of the laser beam displacement of multiple PSD sensors and white noise. The output of the system shall be the position of the laser beam. The development of a KF algorithm could help to detect the vibration of the laser source so that it may increase the accuracy of the measurement data.

Appendix A Publications

The following shows the papers that have been published during the course of the PhD research for this thesis:

Kim, H., Saade, L., Weston, P., *et al*. (2014) Measuring the deflection of a sequence of sleepers at a transition zone. The 6th IET RCM conference. 2014. pp. 1–6

Kim, H., Weston, P., Roberts, C., *et al*. (2011) Trackside measurement at railway critical zones using sensors and vehicle-borne instrumentation. The 5th IET Conference on Railway Condition Monitoring and Non-Destructive Testing (RCM 2011)

Appendix B Theoretical Defleciton Curves (BOEF theory)

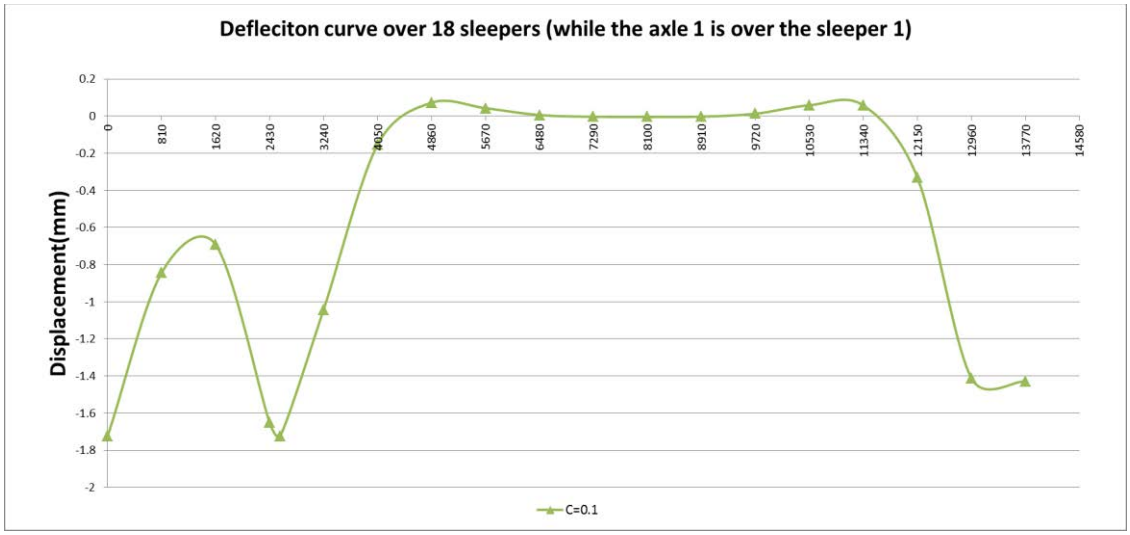

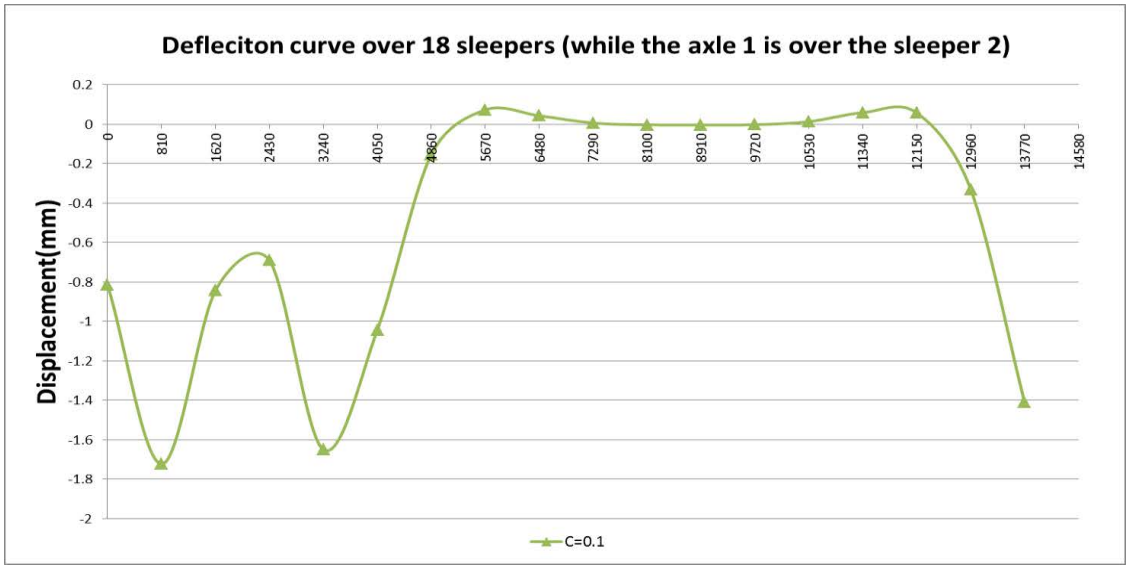

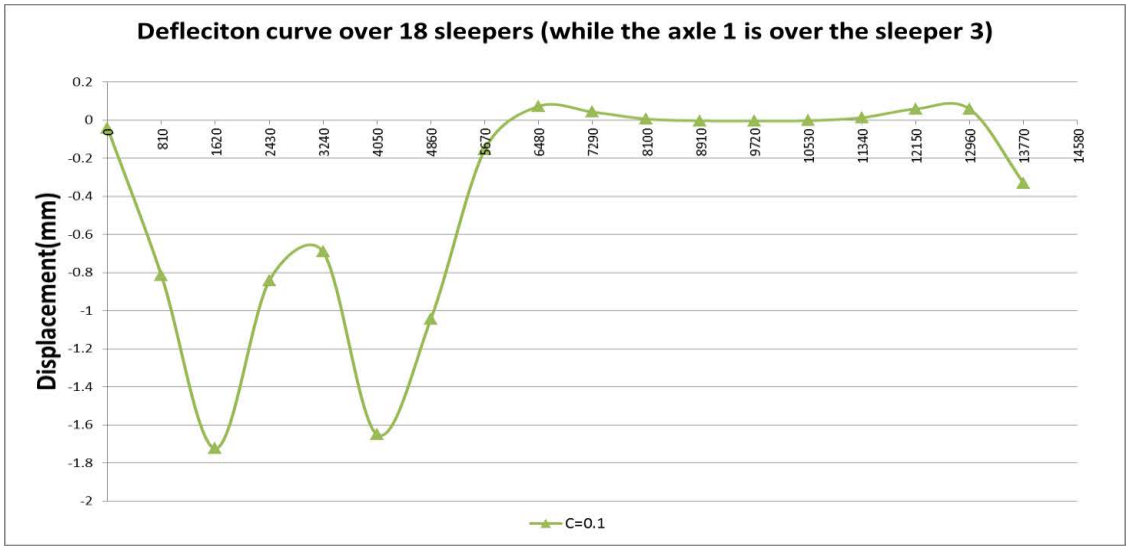

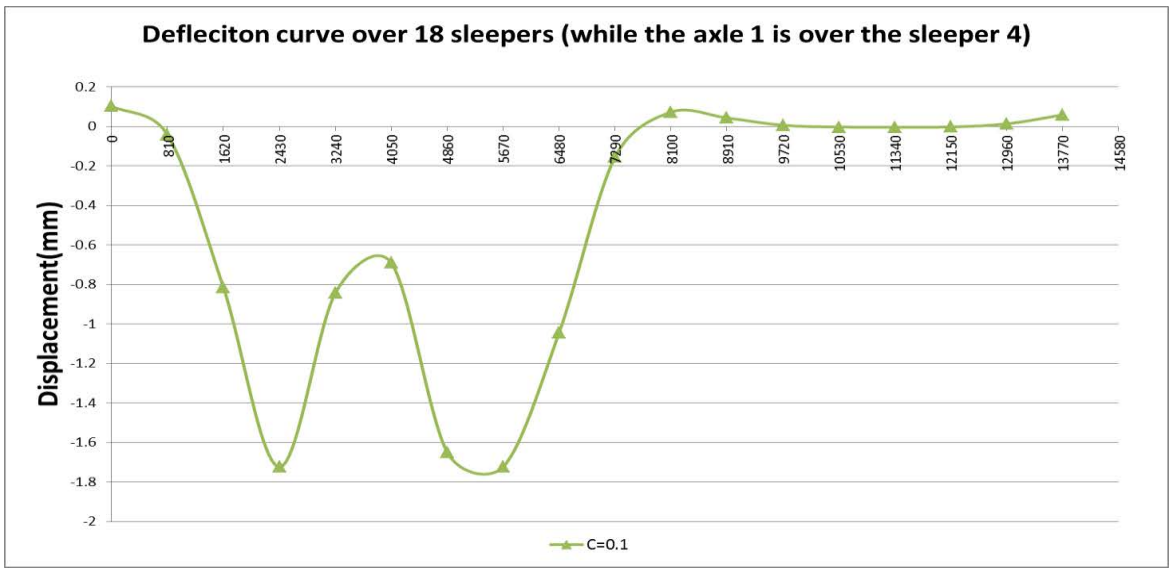
Defleciton curve over 18 sleepers (while the axle 1 is over the sleeper 4)
Displacement(mm)
0.2
0
-0.2
-0.4
-0.6
-0.8
-1
-1.2
-1.4
-1.6
-1.8
-2
0
810
1620
2430
3240
4050
4860
5670
6480
7290
8100
8910
9720
10530
11340
12150
12960
13770
14580
C=0.1

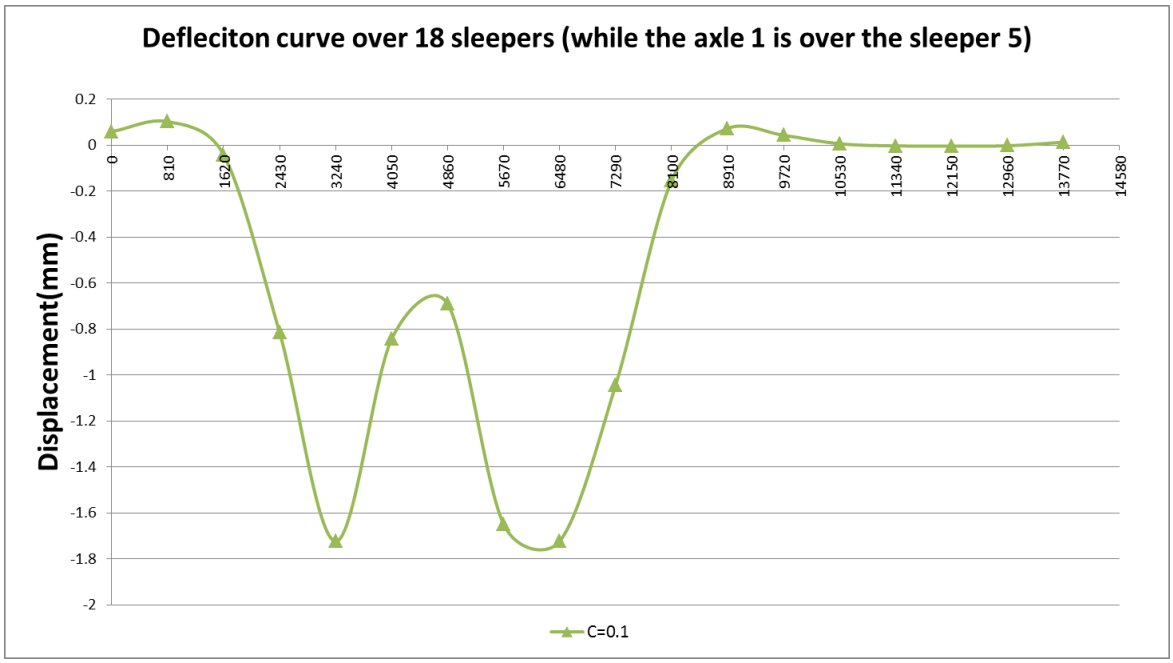
Defleciton curve over 18 sleepers (while the axle 1 is over the sleeper 5)
Displacement(mm)
0.2
0
-0.2
-0.4
-0.6
-0.8
-1
-1.2
-1.4
-1.6
-1.8
-2
0
810
1620
2430
3240
4050
4860
5670
6480
7290
8100
8910
9720
10530
11340
12150
12960
13770
14580
C=0.1

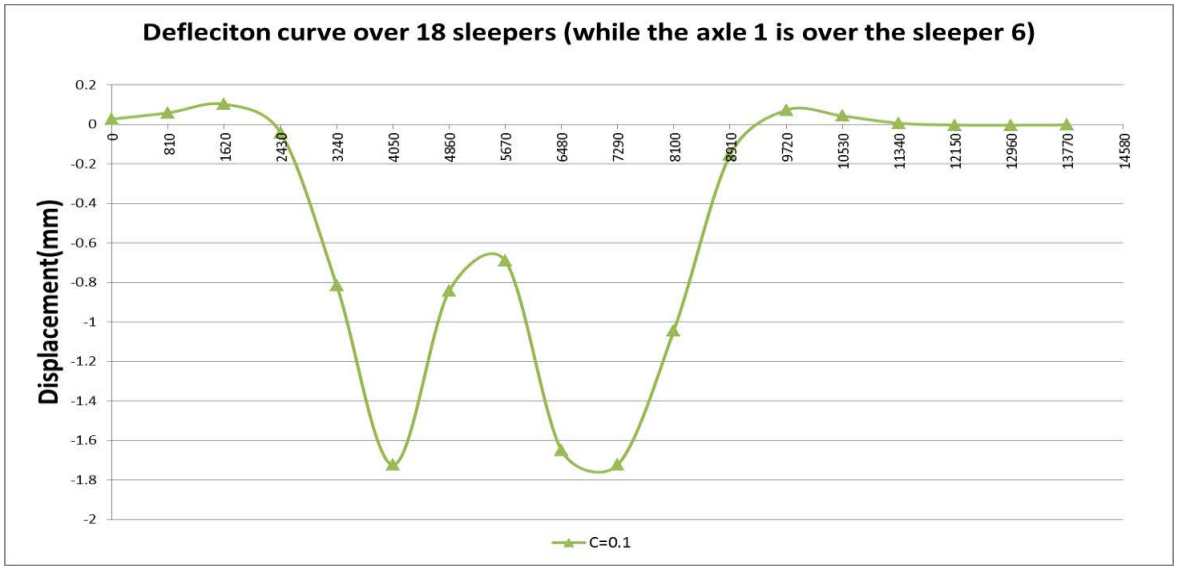
Defleciton curve over 18 sleepers (while the axle 1 is over the sleeper 6)
Displacement(mm)
0.2
0
-0.2
-0.4
-0.6
-0.8
-1
-1.2
-1.4
-1.6
-1.8
-2
0
810
1620
2430
3240
4050
4860
5670
6480
7290
8100
8910
9720
10530
11340
12150
12960
13770
14580
C=0.1

Appendix C DCPT data for six locations

Test site	Sleeper11-12				Test site	Sleeper12-13			
Blows (no)	Readings	DPI (mm/blow)	Accu depth (mm)	Estimated CBR(%)	Blows (no)	Readings	DPI (mm/blow)	Accu depth (mm)	Estimated CBR(%)
initial posi	90		0	0.0	initial posi	90		0	0.0
1	130	5	-5	47.6	1	130	20	-20	10.1
2	160	5	-10	47.6	2	160	20	-40	10.1
3	190	20	-30	10.1	3	190	20	-60	10.1
4	210	20	-50	10.1	4	210	20	-80	10.1
5	235	20	-70	10.1	5	235	20	-100	10.1
6	250	20	-90	10.1	6	250	20	-120	10.1
7	270	20	-110	10.1	7	270	20	-140	10.1
8	290	20	-130	10.1	8	290	20	-160	10.1
9	310	20	-150	10.1	9	310	20	-180	10.1
		-					-		
22	690	50	-740	3.6	22	690	50	-770	3.6
23	710	50	-790	3.6	23	710	50	-820	3.6
24	320	50	-840	3.6	24	320	50	-870	3.6
25	340	50	-890	3.6	25	340	50	-920	3.6
26	350	50	-940	3.6	26	350	50	-970	3.6
27	370	50	-990	3.6	27	370	10	-980	21.9
28	384	50	-1040	3.6	28	384	10	-990	21.9
29	397	20	-1060	10.1	29	397	10	-1000	21.9
30	412	20	-1080	10.1	30	412	10	-1010	21.9
31	427	20	-1100	10.1	31	427	10	-1020	21.9
32	440	20	-1120	10.1	32	440	10	-1030	21.9
33	452	20	-1140	10.1	33	452	10	-1040	21.9
34	465	20	-1160	10.1	34	465	10	-1050	21.9
35	479	20	-1180	10.1	35	479	10	-1060	21.9
36	489	20	-1200	10.1	36	489	10	-1070	21.9
37	499	20	-1220	10.1	37	499	10	-1080	21.9
38	509	20	-1240	10.1	38	509	10	-1090	21.9
39	519	20	-1260	10.1	39	519	10	-1100	21.9
40	529	20	-1280	10.1	40	529	10	-1110	21.9
41	539	20	-1300	10.1	41	539	10	-1120	21.9
42	549	10	-1310	21.9	42	549	10	-1130	21.9
43	559	10	-1320	21.9	43	559	10	-1140	21.9
44	569	10	-1330	21.9	44	569	10	-1150	21.9
45	579	10	-1340	21.9	45	579	10	-1160	21.9
46	589	10	-1350	21.9	46	589	10	-1170	21.9
47	599	10	-1360	21.9	47	599	10	-1180	21.9
		-					-		
61	738	5	-1445	47.6	61	738	10	-1320	21.9
62	746	5	-1450	47.6	62	746	10	-1330	21.9
63	752	5	-1455	47.6	63	752	10	-1340	21.9
64	760	5	-1460	47.6					
65	769	5	-1465	47.6				CBR(%)	13.1
66	777	5	-1470	47.6				Ks(N/mm^3)	0.056
67	786	5	-1475	47.6					
68	793	5	-1480	47.6					
69	800	5	-1485	47.6		sleeper 12	0.052		
			CBR(%)	9.07					
			Ks(N/mm^3)	0.048					

Test site	Sleeper12-13				Test site	Sleeper13-14			
Blows (no)	Readings	DPI (mm/blow)	Accu depth (mm)	Estimated CBR(%)	Blows (no)	Readings	DPI (mm/blow)	Accu depth (mm)	Estimated CBR(%)
initial posi	90		0	0.0	initial posi	90		0	0.0
1	130	20	-20	10.1	1	130	5	-5	47.6
2	160	20	-40	10.1	2	160	5	-10	47.6
3	190	20	-60	10.1	3	190	5	-15	47.6
4	210	20	-80	10.1	4	210	5	-20	47.6
5	235	20	-100	10.1	5	235	5	-25	47.6
6	250	20	-120	10.1	6	250	5	-30	47.6
7	270	20	-140	10.1	7	270	5	-35	47.6
8	290	20	-160	10.1	8	290	5	-40	47.6
9	310	20	-180	10.1	9	310	5	-45	47.6
10	330	20	-200	10.1	10	330	5	-50	47.6
		-					-		
26	350	50	-970	3.6	26	350	80	-955	2.1
27	370	10	-980	21.9	27	370	80	-1035	2.1
28	384	10	-990	21.9	28	384	50	-1085	3.6
29	397	10	-1000	21.9	29	397	50	-1135	3.6
30	412	10	-1010	21.9	30	412	50	-1185	3.6
31	427	10	-1020	21.9	31	427	5	-1190	47.6
32	440	10	-1030	21.9	32	440	5	-1195	47.6
33	452	10	-1040	21.9	33	452	5	-1200	47.6
		-					-		
42	549	10	-1130	21.9	42	549	5	-1245	47.6
43	559	10	-1140	21.9	43	559	5	-1250	47.6
44	569	10	-1150	21.9	44	569	5	-1255	47.6
45	579	10	-1160	21.9	45	579	5	-1260	47.6
46	589	10	-1170	21.9	46	589	5	-1265	47.6
		-					-		
59	721	10	-1300	21.9	59	721	5	-1330	47.6
60	729	10	-1310	21.9	60	729	5	-1335	47.6
61	738	10	-1320	21.9	61	738	5	-1340	47.6
62	746	10	-1330	21.9	62	746	5	-1345	47.6
63	752	10	-1340	21.9	63	752	5	-1350	47.6
					64	760	5	-1355	47.6
			CBR(%)	13.1	65	769	5	-1360	47.6
							-		
					91	915	5	-1492	47.6
					92	920	5	-1497	47.6
					93	925	5	-1502	47.6
					94	930	4	-1506	61.1
					95	935	5	-1511	47.6
					96	940	5	-1516	47.6
					Sleeper 13	0.06		CBR(%)	18.8
								Ks(N/mm	0.068

Test site	Sleeper13-14				Test site	Sleeper14-15			
Blows (no)	Readings	DPI (mm/blow)	Accu depth (mm)	Estimated CBR(%)	Blows (no)	Readings	DPI (mm/blow)	Accu depth (mm)	Estimated CBR(%)
initial posi	90		0	0.0	initial positi	120		0	0.0
1	130	5	-5	47.6	1	140	20	-20	10.1
2	160	5	-10	47.6	2	170	30	-50	6.4
3	190	5	-15	47.6	3	200	30	-80	6.4
4	210	5	-20	47.6	4	220	20	-100	10.1
5	235	5	-25	47.6	5	240	20	-120	10.1
6	250	5	-30	47.6	6	255	15	-135	13.9
7	270	5	-35	47.6	7	270	15	-150	13.9
8	290	5	-40	47.6	8	285	15	-165	13.9
9	310	5	-45	47.6	9	305	20	-185	10.1
		-					-		
27	370	80	-1035	2.1	27	1055	20	-935	10.1
28	384	50	-1085	3.6	28	1065	10	-945	21.9
29	397	50	-1135	3.6	29	1075	10	-955	21.9
30	412	50	-1185	3.6	30	1085	10	-965	21.9
31	427	5	-1190	47.6	31	1095	10	-975	21.9
32	440	5	-1195	47.6	32	200	10	-985	21.9
33	452	5	-1200	47.6	33	210	10	-995	21.9
34	465	5	-1205	47.6	34	220	10	-1005	21.9
35	479	5	-1210	47.6	35	230	10	-1015	21.9
36	489	5	-1215	47.6	36	240	10	-1025	21.9
37	499	5	-1220	47.6	37	250	10	-1035	21.9
38	509	5	-1225	47.6	38	260	10	-1045	21.9
39	519	5	-1230	47.6	39	270	10	-1055	21.9
40	529	5	-1235	47.6	40	278	8	-1063	28.1
		-					-		
53	657	5	-1300	47.6	53	364	6	-1149	38.8
54	669	5	-1305	47.6	54	370	6	-1155	38.8
55	681	5	-1310	47.6	55	375	5	-1160	47.6
56	691	5	-1315	47.6	56	380	5	-1165	47.6
57	701	5	-1320	47.6	57	385	5	-1170	47.6
58	711	5	-1325	47.6	58	390	5	-1175	47.6
59	721	5	-1330	47.6	59	395	5	-1180	47.6
94	930	4	-1506	61.1	94	571	5	-1356	47.6
95	935	5	-1511	47.6	95	576	5	-1361	47.6
96	940	5	-1516	47.6	96	581	5	-1366	47.6
					97	586	5	-1371	47.6
			CBR(%)	18.8	98	591	5	-1376	47.6
			Ks(N/mm	0.068	99	596	5	-1381	47.6
					100	601	5	-1386	47.6
					101	606	5	-1391	47.6
					102	611	5	-1396	47.6
		-					-		
					111	656	5	-1441	47.6
					112	661	5	-1446	47.6
					113	666	5	-1451	47.6
					114	671	5	-1456	47.6
					sleeper 14	0.068		CBR(%)	19.6
								Ks(N/mm^3)	0.07

Test site	Sleeper14-15				Test site		Sleeper15-16		
Blows (no)	Readings	DPI (mm/blow)	Accu depth (mm)	Estimated CBR(%)	Blows (no)	Readings	DPI (mm/blow)	Accu depth (mm)	Estimated CBR(%)
initial positi	120		0	0.0	initial positi	100		0	
1	140	20	-20	10.1	1	120	20	-20	10.1
2	170	30	-50	6.4	2	140	20	-40	10.1
3	200	30	-80	6.4	3	160	20	-60	10.1
4	220	20	-100	10.1	4	180	20	-80	10.1
5	240	20	-120	10.1	5	200	20	-100	10.1
6	255	15	-135	13.9	6	220	20	-120	10.1
7	270	15	-150	13.9	7	240	20	-140	10.1
8	285	15	-165	13.9	8	260	20	-160	10.1
9	305	20	-185	10.1	9	280	20	-180	10.1
10	325	20	-205	10.1	10	300	20	-200	10.1
		-					-		
37	250	10	-1035	21.9	37	453	10	-1151	21.9
38	260	10	-1045	21.9	38	463	10	-1161	21.9
39	270	10	-1055	21.9	39	473	10	-1171	21.9
40	278	8	-1063	28.1	40	478	5	-1176	47.6
41	286	8	-1071	28.1	41	483	5	-1181	47.6
42	294	8	-1079	28.1	42	488	5	-1186	47.6
43	302	8	-1087	28.1	43	493	5	-1191	47.6
44	310	8	-1095	28.1	44	498	5	-1196	47.6
45	316	6	-1101	38.8	45	503	5	-1201	47.6
46	322	6	-1107	38.8	46	508	5	-1206	47.6
47	328	6	-1113	38.8	47	513	5	-1211	47.6
48	334	6	-1119	38.8	48	518	5	-1216	47.6
49	340	6	-1125	38.8	49	523	5	-1221	47.6
50	346	6	-1131	38.8	50	528	5	-1226	47.6
51	352	6	-1137	38.8	51	533	5	-1231	47.6
52	358	6	-1143	38.8	52	538	5	-1236	47.6
53	364	6	-1149	38.8	53	543	5	-1241	47.6
54	370	6	-1155	38.8	54	548	5	-1246	47.6
55	375	5	-1160	47.6	55	553	5	-1251	47.6
56	380	5	-1165	47.6	56	558	5	-1256	47.6
57	385	5	-1170	47.6	57	563	5	-1261	47.6
58	390	5	-1175	47.6	58	568	5	-1266	47.6
		-					-		
105	626	5	-1411	47.6	105	803	5	-1501	47.6
106	631	5	-1416	47.6	106	808	5	-1506	47.6
107	636	5	-1421	47.6	107	813	5	-1511	47.6
108	641	5	-1426	47.6					
109	646	5	-1431	47.6				CBR(%)	12.3
110	651	5	-1436	47.6				Ks(N/mm	0.055
111	656	5	-1441	47.6					
112	661	5	-1446	47.6	sleeper 15	0.06			
113	666	5	-1451	47.6					
114	671	5	-1456	47.6					
			CBR(%)	19.6					
			Ks(N/mm^3	0.07					

Test site		Sleeper15-16			Test site	Sleeper16-17			
Blows (no)	Readings	DPI (mm/blow)	Accu depth (mm)	Estimated CBR(%)	Blows (no)	Readings	DPI (mm/blow)	Accu depth (mm)	Estimated CBR(%)
initial positi	100		0		initial posi	100		0	
1	120	20	-20	10.1	1	135	50	-50	3.6
2	140	20	-40	10.1	2	170	50	-100	3.6
3	160	20	-60	10.1	3	195	50	-150	3.6
4	180	20	-80	10.1	4	220	50	-200	3.6
5	200	20	-100	10.1	5	240	50	-250	3.6
6	220	20	-120	10.1	6	265	50	-300	3.6
7	240	20	-140	10.1	7	285	80	-380	2.1
8	260	20	-160	10.1	8	305	80	-460	2.1
9	280	20	-180	10.1	9	325	90	-550	1.9
10	300	20	-200	10.1	10	340	100	-650	1.7
11	360	60	-260	2.9	11	355	100	-750	1.7
12	420	60	-320	2.9	12	390	100	-850	1.7
13	480	60	-380	2.9	13	410	100	-950	1.7
14	540	60	-440	2.9	14	440	100	-1050	1.7
15	600	60	-500	2.9	15	500	80	-1130	2.1
16	660	60	-560	2.9	16	575	80	-1210	2.1
17	740	80	-640	2.1	17	600	80	-1290	2.1
18	820	80	-720	2.1	18	635	80	-1370	2.1
		-					-		
38	463	10	-1161	21.9	38	505	5	-1605	47.6
39	473	10	-1171	21.9	39	512	5	-1610	47.6
		-					-		
54	548	5	-1246	47.6	54	651	5	-1685	47.6
55	553	5	-1251	47.6	55	665	5	-1690	47.550337
56	558	5	-1256	47.6	56	681	5	-1695	47.6
57	563	5	-1261	47.6					
58	568	5	-1266	47.6	sleeper 16	0.046			
59	573	5	-1271	47.6				CBR(%)	2.5
60	578	5	-1276	47.6				Ks(N/mm^3)	0.037
61	583	5	-1281	47.6					
		-					-		
100	778	5	-1476	47.6					
101	783	5	-1481	47.6					
102	788	5	-1486	47.6					
103	793	5	-1491	47.6					
104	798	5	-1496	47.6					
105	803	5	-1501	47.6					
106	808	5	-1506	47.6					
107	813	5	-1511	47.6					
			CBR(%)	12.3					
			Ks(N/mm	0.055					

Test site		Sleeper15-16			Test site	Sleeper16-17			
Blows (no)	Readings	DPI (mm/blow)	Accu depth (mm)	Estimated CBR(%)	Blows (no)	Readings	DPI (mm/blow)	Accu depth (mm)	Estimated CBR(%)
initial positi	100		0		initial posi	100		0	
1	120	20	-20	10.1	1	135	50	-50	3.6
2	140	20	-40	10.1	2	170	50	-100	3.6
3	160	20	-60	10.1	3	195	50	-150	3.6
4	180	20	-80	10.1	4	220	50	-200	3.6
5	200	20	-100	10.1	5	240	50	-250	3.6
6	220	20	-120	10.1	6	265	50	-300	3.6
7	240	20	-140	10.1	7	285	80	-380	2.1
8	260	20	-160	10.1	8	305	80	-460	2.1
9	280	20	-180	10.1	9	325	90	-550	1.9
10	300	20	-200	10.1	10	340	100	-650	1.7
11	360	60	-260	2.9	11	355	100	-750	1.7
12	420	60	-320	2.9	12	390	100	-850	1.7
13	480	60	-380	2.9	13	410	100	-950	1.7
14	540	60	-440	2.9	14	440	100	-1050	1.7
15	600	60	-500	2.9	15	500	80	-1130	2.1
16	660	60	-560	2.9	16	575	80	-1210	2.1
17	740	80	-640	2.1	17	600	80	-1290	2.1
18	820	80	-720	2.1	18	635	80	-1370	2.1
		-					-		
38	463	10	-1161	21.9	38	505	5	-1605	47.6
39	473	10	-1171	21.9	39	512	5	-1610	47.6
		-					-		
54	548	5	-1246	47.6	54	651	5	-1685	47.6
55	553	5	-1251	47.6	55	665	5	-1690	47.550337
56	558	5	-1256	47.6	56	681	5	-1695	47.6
57	563	5	-1261	47.6					
58	568	5	-1266	47.6	sleeper 16	0.046			
59	573	5	-1271	47.6				CBR(%)	2.5
60	578	5	-1276	47.6				Ks(N/mm^3)	0.037
61	583	5	-1281	47.6					
		-					-		
100	778	5	-1476	47.6					
101	783	5	-1481	47.6					
102	788	5	-1486	47.6					
103	793	5	-1491	47.6					
104	798	5	-1496	47.6					
105	803	5	-1501	47.6					
106	808	5	-1506	47.6					
107	813	5	-1511	47.6					
			CBR(%)	12.3					
			Ks(N/mm	0.055					

Test site	Sleeper16-17				Test site	Sleeper17-18			
Blows (no)	Readings	DPI (mm/blow)	Accu depth (mm)	Estimated CBR(%)	Blows (no)	Readings	DPI (mm/blow)	Accu depth (mm)	Estimated CBR(%)
initial po	100		0		initial posi	150		0	0.0
1	135	50	-50	3.6	1	190	40	-40	4.6
2	170	50	-100	3.6	2	220	30	-70	6.4
3	195	50	-150	3.6	3	250	30	-100	6.4
4	220	50	-200	3.6	4	280	30	-130	6.4
5	240	50	-250	3.6	5	330	50	-180	3.6
6	265	50	-300	3.6	6	420	90	-270	1.9
7	285	80	-380	2.1	7	490	70	-340	2.5
8	305	80	-460	2.1	8	550	60	-400	2.9
9	325	90	-550	1.9	9	600	50	-450	3.6
10	340	100	-650	1.7	10	630	30	-480	6.4
11	355	100	-750	1.7	11	665	35	-515	5.4
12	390	100	-850	1.7	12	690	25	-540	7.8
13	410	100	-950	1.7	13	720	30	-570	6.4
14	440	100	-1050	1.7	14	750	30	-600	6.4
15	500	80	-1130	2.1	15	780	30	-630	6.4
16	575	80	-1210	2.1	16	0	30	-660	6.4
17	600	80	-1290	2.1	17	30	30	-690	6.4
18	635	80	-1370	2.1	18	50	20	-710	10.1
		-					-		
36	490	5	-1595	47.6	36	512	25	-1172	7.8
		-					-		
54	651	5	-1685	47.6	54	737	10	-1397	21.9
55	665	5	-1690	47.550337	55	747	10	-1407	21.9
56	681	5	-1695	47.6	56	757	10	-1417	21.9
					57	767	10	-1427	21.9
					58	787	20	-1447	10.1
			CBR(%)	2.5					
			Ks(N/mm^3)	0.037				CBR(%)	6.5
								Ks(N/mm	0.044
					sleeper 17	0.041			

Test site	Sleeper17-18				Test site	Sleeper18-19			
Blows (no)	Readings	DPI (mm/blow)	Accu depth (mm)	Estimated CBR(%)	Blows (no)	Readings	DPI (mm/blow)	Accu depth (mm)	Estimated CBR(%)
initial pc	150		0	0.0	initial posi	110		0	
1	190	40	-40	4.6	1	150	40	-40	4.6
2	220	30	-70	6.4	2	185	35	-75	5.4
3	250	30	-100	6.4	3	215	30	-105	6.4
4	280	30	-130	6.4	4	240	25	-130	7.8
5	330	50	-180	3.6	5	270	30	-160	6.4
6	420	90	-270	1.9	6	290	20	-180	10.1
7	490	70	-340	2.5	7	315	25	-205	7.8
8	550	60	-400	2.9	8	355	40	-245	4.6
9	600	50	-450	3.6	9	430	75	-320	2.3
10	630	30	-480	6.4	10	480	50	-370	3.6
		-							
36	512	25	-1172	7.8	36	655	10	-900	21.9
55	747	10	-1407	21.9	55	770	5	-1015	47.6
56	757	10	-1417	21.9	56	775	5	-1020	47.6
57	767	10	-1427	21.9	57	780	5	-1025	47.6
58	787	20	-1447	10.1	58	785	5	-1030	47.6
					59	793	8	-1038	28.1
			CBR(%)	6.5	60	798	5	-1043	47.6
			Ks(N/mm	0.044	61	808	5	-1048	47.6
					62	813	5	-1053	47.6
					83	918	5	-1158	47.6
					84	923	5	-1163	47.6
					85	928	5	-1168	47.6
		-							
					100	1003	5	-1243	47.6
					101	1008	5	-1248	47.6
				Sleeper 18	0.068				
								CBR(%)	30.8
								Ks(N/mr	0.092

8 References

Arnold, G., Salt, G., Stevens, D., et al. (2009) **Compliance testing using the Falling Weight Deflectometer for pavement construction, rehabilitation and area-wide treatments - NZ Transport Agency research report 381**. NZ Transport Agency, New Zealand

Berggren, E. (2009) **Railway Track Stiffness Dynamic measurements and Evaluation for Efficient Maintenance**

Berggren, E., Hosseingholian, M., Saussine, G., et al. (2006) **Methods of track stiffness measurement**. TIP-CT-2006-031415

Berggren, E.G. (2010) Efficient track maintenance: methodology for combined analysis of condition data. **Proceedings of the Institution of Mechanical Engineers, Part F: Journal of Rail and Rapid Transit** [online], 224 (5): 353–360. Available from: http://pif.sagepub.com/lookup/doi/10.1243/09544097JRRT354 [Accessed 29 March 2012]

Bowness, D., Lock, A.C., Powrie, W., et al. (2007) Monitoring the dynamic displacements of railway track. **Proceedings of the Institution of Mechanical Engineers Part F Journal of Rail and Rapid Transit** [online], 221 (1): 13–22. Available from: http://dx.doi.org/10.1243/0954409JRRT51

BSI (2008) **Railway applications — Track — Track geometry quality —Part 1 : Chracterisaion of track geometry**., 3

Burrow M., Priest, J.A., Ghataora, G.., et al. (2007) **Track subgrade performance and monitoring**. In **2007**. In Railway Engineering - 9th International Conference and Exhibition, London, UK, 20 - 21 Jun 2007.

Burrow, M., Teixeira, P.F., Dahlberg, T., et al. (2010) **Track stiffness considerations for high speed railway lines In Railway Transportation: Policies, Technology and Perspectives**. Nova Scien.

CEDEX/ADIF (2009) Study of variation of vertical stiffness in transition zone. **Technical Report, Innotrack**

Coelho, B., Hoelscher, P., Priest, J., et al. (2011) An assessment of transition zone performance. **Proceedings of the Institution of Mechanical Engineers, Part F, Journal of Rail and Rapid Transit**

Coelho, B., Priest, J.A., Holscher, P., et al. (2009) **Monitoring of transition zones in railways - ePrints Soton**. [online]. Available from: http://eprints.soton.ac.uk/73930/

Colorado, P., Read, D. and Li, D. (2006) Design of Track Transitions. **Research Results Digest 79**, (October)

Ekberg, A. and Paulsson, B. (2010) **Innotrack Concluding Technical Report (UIC)**. (Innotrack project - Madrid- Barcelona)

Eriksen, A., Venables, B., Gascoyne, J., et al. (2006) **Benefits of high speed GPR to manage trackbed assets and renewal strategies**., (June): 3–7

Esveld, C. (2001) **Modern Railway Track, Second Edition**. Delft Univ. Koninklijke van de Garde BV

Ferne, B., Langdale, P., Round, N., et al. (2009) Development of the UK highways agency traffic speed deflectometer. **Proceedings of the 8th International Conference**

Gmbh, R.B. (1991) **CAN Specification (Version 2.0)**. , Robert Bosch GmbH, Postfach 30 02 40, D-70442 Stuttgart

H.Sullivan, R. (2015) **User guide to the dynamic cone penetrometer, Mn Road (Office of Minesota Road Research)**

Hakim, B. (2013) Trackbed evaluation and design using FWD Deflections as performance indicators. **7th European FWD Users Group**, (June): URS Infrastructure&Enviroment

Hamamatsu (2011) **One-dimensional PSD Datasheet**. [online]. Available from: http://www.hamamatsu.com/jp/en/product/category/3100/4010/4155/S3270/index.html

Hendry, M., Barbour, L. and Hughes, D. a. (2010) Track displacement and energy loss in a railway embankment. **Proceedings of the ICE - Geotechnical Engineering** [online], 163 (1): 3–12. Available from: http://www.icevirtuallibrary.com/content/article/10.1680/geng.2010.163.1.3 [Accessed 26 March 2014]

Hosseingholian, M., Froumentin, M. and Levacher, D. (2009) Continous Method to Measure Track Stiffness (A new tool for inspection of rail infrastructure). **World Applied Sciences Journal 6(5)**, pp. 579–589

Hunt, G. (2005) Review of the effect of track stiffness on track performance. **Technical Report, Rail Safety & Standards Board (RSSB), Research Project T372**

Iwnicki, S. (2006) **Handbook of Railway Vehicle Dynamics**. CRC Press

Iwnicki, S. and Dahlberg, T. (2006) **Handbook of Railway Vehicle Dynamics** Iwnicki, S. (ed.). [online], p. 154. Available from: http://www.crcnetbase.com/doi/book/10.1201/9781420004892

Jenkins, M. (2009) Geometric and absolute calibration of the English highways agency traffic speed deflectometer. **Transport Research Laboratory**, (1): 1–11

Kaewunruen, S. (2014) Monitoring structural deterioration of railway turnout systems via dynamic wheel/rail interaction. **Case Studies in Nondestructive Testing and Evaluation** [online]. Available from: http://linkinghub.elsevier.com/retrieve/pii/S2214657114000069 [Accessed 16 April 2014]

Kang, Y.-S., Na, S.-H., Shin, J., et al. (2002) “Experimental and Analysis Study on Transition Area Between Bridge and Earthwork.” In **Korean railway conference**. **2002**

Kang, Y.S., Yang, S.C., Lee, H.S., et al. (2006) A Study of Track and Train Dynamic Behavior of Transition Zone Between Concrete Slab Track and Ballasted Track. **Korean railway conference**

Kennedy, J., Medero, G.M., Banimahd, M., et al. (2012) Behaviour of train–track interaction in stiffness transitions. **Proceedings of the ICE - Transport** [online]. 165 (3) pp. 205–214. Available from: http://www.icevirtuallibrary.com/content/article/10.1680/tran.10.00030

Kim, H., Saade, L., Weston, P., et al. (2014) “Measuring the deflection of a sequence of sleepers at a transition zone.” In **The 6th IET RCM conference**. **2014**. The Institution of Engineering and Technology. pp. 1–6

Kim, H., Weston, P., Roberts, C., et al. (2011) “Trackside measurement at railway critical zones using sensors and vehicle-borne instrumentation.” In **5th IET Conference on Railway Condition Monitoring and Non-Destructive Testing**. **2011** [online]. IET. pp. 4A3–4A3. Available from: http://digital-library.theiet.org/content/conferences/10.1049/cp.2011.0595

Kleeman, L. (1995) **Understanding and Applying Kalman Filtering**. Monash University, Clayton, Austrailia

Lee, I.L.S. and Kang, S.L.T. (2010) “Evaluation of Deformation Characteristics for Bridge/Earthwork Transition Reinforcement Methods Considering Moving Load.” In **Korean railway conference**. **2010**. pp. 298–303

Lee, J., Choi, C. and Lee, I. (2005) “Experimental study on the Variation of Stiffness Transition Zone between Earthwork and Tunnel.” In **Korean railway conference**. **2005**

Li, D., Otter, D. and Carr, G. (2010) Railway bridge approaches under heavy axle load traffic: problems, causes, and remedies. **Proceedings of the Institution of Mechanical Engineers, Part F: Journal of Rail and Rapid Transit** [online], 224 (5): 383–390. Available from: http://journals.pepublishing.com/openurl.asp?genre=article&id=doi:10.1243/09544097JRRT345 [Accessed 22 November 2010]

Li, D., Thompson, R. and Semih, K. (2004) **Update of TTCI’s Research in Track Condition Testing and Inspection**. Pueblo, CO 81001

Li, M.X.D. and Berggren, E.G. (2010) A study of the effect of global track stiffness and its variations on track performance: simulation and measurement. **Proceedings of the Institution of Mechanical Engineers, Part F: Journal of Rail and Rapid Transit** [online], 224 (5): 375–382. Available from: http://pif.sagepub.com/lookup/doi/10.1243/09544097JRRT361 [Accessed 29 March 2012]

Li, P., Goodall, R., Weston, P., et al. (2007) Estimation of railway vehicle suspension parameters for condition monitoring. **Control Engineering Practice** [online], 15 (1): 43–55. Available from: http://linkinghub.elsevier.com/retrieve/pii/S0967066106000463 [Accessed 17 November 2010]

LoÂpez, P., Teixeira, P.F. and Robuste, F. (2004) High speed and track deterioration : the role of vertical stiffness of the track. **Rail and Rapid Transit**, 218: 31–40

Lu, S. (2008) **Real-time vertical track deflection mesurement system**. The Graduate College at the University of Nebraska

Michas, G. (2012) **Slab Track Systems for High-Speed Railways**. Royal Institute of Technology(KTH), Division of Highway and Railway Engineering

Molenaar, A. (2006) PART VI Structural Evaluation and Strengthening of Flexible Pavements Using Deflection Measurements and Visual Condition Surveys Structural Design of Pavements. **Delft University of Technology**

N.F. Doyle (1980) "Railway Track Design - A reveiw of current practice." In **BHP Melbourne Research Laboratories, Australian Goverment Publishing Service CANBERRA, ISBN: 0642 05014 7e**.

Nielsen, J., Berggren, E., Lolgen, T., et al. (2013) **Overview of Methods for Measurement of Track Irregularities Important for Ground-Borne Vibration**

Norman, C., Farritor, S., Arnold, R., et al. (2004) **Preliminary design of a system to measure track modulus from a moving railcar**. University of Nebraska - Lincoln

Paixao, A., Fortunato, E. and Calcada, R. (2013) Design and construction of backfills for railway track transition zones. **Proceedings of the Institution of Mechanical Engineers, Part F: Journal of Rail and Rapid Transit** [online]. Available from: http://pif.sagepub.com/lookup/doi/10.1177/0954409713499016 [Accessed 15 April 2014]

Le Pen, L., Watson, G., Powrie, W., et al. (2014) The behaviour of railway level crossings: Insights through field monitoring. **Transportation Geotechnics** [online]. Available from: http://linkinghub.elsevier.com/retrieve/pii/S2214391214000130 [Accessed 11 September 2014]

Priest, J. a., Powrie, W., Grabe, P.J., et al. (2010) Measurements of transient ground movements below a ballasted railway line. **Géotechnique** [online], 60 (9): 667–677. Available from: http://www.icevirtuallibrary.com/content/article/10.1680/geot.7.00172 [Accessed 31 December 2010]

Priest, J.A. and Powrie, W. (2009) Determination of dynamic track modulus from measurement of track velocity during train passage. **Journal of Geotechnical and Geoenvironmental Engineering** [online], 135 (11): 1732–1740. Available from: http://dx.doi.org/10.1061/(ASCE)GT.1943-5606.0000130

Puzavac, L., POPOVIĆ, Z. and LAZAREVIĆ, L. (2012) Influence of Track Stiffness on Track Behaivor under Vertical Load. **Traffic Infrastructure Review**, 24 (5): 405–412

Robinet, A., Hosseingholian, M., Quibel, A., et al. (2008) **Track stiffness assessment**

Si, A.N.S. (2000) **Position-Sensitive devices and sensor systems for optical tracking and displacement sensing applications**. Oulu University, Finland

Silmon, J. a and Roberts, C. (2010) Improving railway switch system reliability with innovative condition monitoring algorithms. **Proceedings of the Institution of Mechanical Engineers, Part F: Journal of Rail and Rapid Transit** [online], 224 (4): 293–302. Available from: http://pif.sagepub.com/lookup/doi/10.1243/09544097JRRT313 [Accessed 29 March 2012]

Silvast, M., Nurmikolu, A., Wiljanen, B., et al. (2010) An inspection of railway ballast quality using ground penetrating radar in Finland. **Proceedings of the Institution of Mechanical Engineers, Part F: Journal of Rail and Rapid Transit** [online], 224 (5): 345–351. Available from: http://journals.pepublishing.com/openurl.asp?genre=article&id=doi:10.1243/09544097JRRT367 [Accessed 22 November 2010]

Sorge, S. (2008) **Development of an Innovative Ground Penetrating Radar System for Fast and Efficient Monitoring of Rail Track Substructure Conditions**., pp. 1–13

Wan, C., Markine.V.L, Shevsov.I.Y, et al. (2013) **Improvement of Train-Track Interaction in Turnout by Optimising the Shape of Crossing Nose**. In **2013**. 23rd International Symposium on Dynamics of Vehicles on Roads and Tracks, Qingdao, China, 19-23 August 2013. pp. 1–9

Ward, C.P., Weston, P.F., Stewart, E.J.C., et al. (2010) Condition monitoring opportunities using vehicle-based sensors. **Proceedings of the Institution of Mechanical Engineers, Part F: Journal of Rail and Rapid Transit**, 1 (-1): 1–17

Weston, P., Ling, C., Goodman, C., et al. (2007a) Monitoring lateral track irregularity from in-service railway vehicles. **Proceedings of the Institution of Mechanical Engineers, Part F: Journal of Rail and Rapid Transit** [online], 221 (1): 89–100. Available from: http://journals.pepublishing.com/openurl.asp?genre=article&id=doi:10.1243/0954409JRRT64 [Accessed 12 November 2010]

Weston, P., Ling, C., Roberts, C., et al. (2007b) Monitoring vertical track irregularity from in-service railway vehicles. **Proceedings of the Institution of Mechanical Engineers, Part F: Journal of Rail and Rapid Transit** [online], 221 (1): 75–88. Available from: http://journals.pepublishing.com/openurl.asp?genre=article&id=doi:10.1243/0954409JRRT65 [Accessed 12 November 2010]

Xin, T., Kumar, U. and Gao, L. (2014) **Dynamic design of track transition between two different slab tracks**

Yang, L. a., Powrie, W. and Priest, J. a. (2009) Dynamic Stress Analysis of a Ballasted Railway Track Bed during Train Passage. **Journal of Geotechnical and Geoenvironmental Engineering** [online], 135 (5): 680. Available from: http://link.aip.org/link/JGGEFK/v135/i5/p680/s1&Agg=doi

Zoeteman, A. (2001) **Life cycle cost analysis for managing rail infrastructure**.

Zong, N., Wexler, D. and Dhanasekar, M. (2013) Structural and Material Characterisation of Insulated Rail Joints. **Electronic Journal of Structural Engineering**, 13 (1): 75–87